Functional characterization of anion channels of the SLAC/SLAH family in *Arabidopsis thaliana*

Memoria que presenta

la Licenciada en Biología **Paloma Cubero Font**

para optar al título de Doctora en Biología

por la Universidad de Sevilla

Sevilla 2017

Functional characterization of anion channels of the SLAC/SLAH family in *Arabidopsis thaliana*

Visado en Sevilla, a 23 de junio de 2017

EL DIRECTOR

Dr. D. José Manuel Colmenero Flores
Científico titular del CSIC
Instituto de Recursos Naturales y Agrobiología de Sevilla (IRNAS)

EL TUTOR

Dr. D. Francisco Javier Cejudo Fernández
Catedrático de la Universidad de Sevilla
Universidad de Sevilla - Instituto de Bioquímica Vegetal y Fotosíntesis (IBVF, CSIC)

Memoria que presenta
la Licenciada en Biología Paloma Cubero Font
para optar al título de Doctora en Biología
por la Universidad de Sevilla

DOCTOR D. JOSÉ ENRIQUE FERNÁNDEZ LUQUE, DIRECTOR DEL INSTITUTO DE RECURSOS NATURALES Y AGROBIOLOGÍA DE SEVILLA (IRNAS) DEL CONSEJO SUPERIOR DE INVESTIGACIONES CIENTÍFICAS (CSIC)

CERTIFICA: Que la presente Memoria de Investigación titulada "Functional characterization of anion channels of the SLAC/SLAH family in *Arabidopsis thaliana* ", presentada por la Licenciada en Biología Paloma Cubero Font para optar al grado de Doctora en Biología, ha sido realizada en el Departamento de Biotecnología Vegetal, bajo la dirección del Dr. José Manuel Colmenero Flores, reuniendo todas las condiciones exigidas a los trabajos de Tesis Doctorales.

En Sevilla, a 23 de junio de 2017.

Dr. José Enrique Fernández Luque

El presente trabajo se ha realizado en el marco de los proyectos AGL2009-08339 y AGL2015-71386-R pertenecientes al Plan Nacional de Investigación y Desarrollo (PNIDI 2008-2011), y al Plan Estatal de Investigación Científica e Innovación (PEICTI 2013-2016), respectivamente, así como del Proyecto CSIC-2015-40E108 de la Agencia Estatal CSIC, con la ayuda de una Beca Predoctoral JAE-PREDOC financiada por el Consejo Superior de Investigaciones Científicas (CSIC), así como con una Ayuda para Facilitar la Movilidad de Investigadores en Formación del Programa JAE-PREDOC del CSIC, y una Beca de Investigación para Doctorandos y Jóvenes Científicos financiada por el Servicio Alemán de Intercambio Académico (DAAD).

The results obtained during the development of this thesis have been presented in national and international scientific congresses and have led to a publication.

SCIENTIFIC PUBLICATIONS

Cubero-Font P, Maierhofer T, Jaslan J, Rosales MA, Espartero J, Díaz-Rueda P, Müller HM, Hürter AL, Al-Rasheid KAS, Marten I, Hedrich R, Colmenero-Flores JM, Geiger D (2016) Silent S-Type anion channel subunit SLAH1 gates SLAH3 open for chloride root-to-shoot translocation. *Current Biology* 26, 2213–2220.

CONTRIBUTIONS TO MEETINGS AND SYMPOSIUMS

Franco JD Brumós, Rosales MA, Vázquez A, Cubero-Font P**,** Rivero CM, Talón M, Colmenero-Flores JM (2012) Homeostasis de Cl^- y regulación del balance hídrico en plantas. *V Reunión Nacional de la Red Española de Estrés Abiótico de las Plantas***.** Murcia, Spain. Oral presentation.

Cubero-Font P**,** Rosales MA, Díaz Rueda P, Franco-Navarro JD, Espartero J, Colmenero-Flores JM (2014) Functional characterization of the root anion channels SLAH1 and SLAH4: involvement in Cl^- and NO_3^- nutrition and interaction with abiotic stress. *XII Reunión de Biología Molecular de Plantas*. Cartagena, Murcia, Spain. Abstract book, 234–235. Poster.

Cubero-Font P**,** Espartero J, Maierhofer T, Rosales MA, Díaz-Rueda P, Hedrich R, Geiger D, Colmenero-Flores JM (2016) Characterization of a root anion channel that plays a pivotal role in plant chloride nutrition. *XVI Simposio Hispano-Luso de Nutrición Mineral de las Plantas*. San Pedro del Pinatar, Murcia, Spain. Abstract book, 9–10. Oral presentation.

Cubero-Font P**,** Franco-Navarro JD, Rosales MA, Espartero J, Colmenero-Flores JM (2016) Differential regulation of Chloride *vs*. Nitrate transport in plants: biological relevance and molecular mechanisms. *RED DE EXCELENCIA de Transportadores Na y K (KNaTS).* Málaga, Spain. Oral presentation.

Cubero-Font P, Barrera Gavira JM, Díaz-Rueda P, Colmenero-Flores JM (2017) Canales aniónicos SLAH2 y SLAH4. *RED DE EXCELENCIA de Transportadores Na y K (KNaTS).* Madrid, Spain. Oral presentation.

Franco-Navarro JD, Cubero-Font P, Rosales MA, Día-Rueda P, Espartero J, Geiger D, Colmenero-Flores JM (2017) Chloride as multifunctional beneficial ion: Biological functions and regulation. *XXII Reunión de la Sociedad Española de Fisiología Vegetal (SEFV), XV Spanish-Portuguese Congress of Plant Physyology*. Barcelona (Spain). Poster.

ACKNOWLEDGEMENT

First and foremost, I would like to express my gratitude to my thesis director Dr. José Manuel Colmenero Flores (Chema) for his constant guidance throughout these years and for his dedication at any time of the day, at any day of the week all over the year.

I truly appreciate the determined support of Prof. Dr. Dietmar Geiger from the Institute for Molecular Plant Physiology and Biophysics (University of Würzburg) during my stay at his Institute. I keep in mind the memory of the first successful measurement of anion currents in SLAH1-SLAH3 complex. I am really grateful for his supervision and the opportunity to collaborate in his laboratory. I would also like to thank Dr. Tobias Maierhofer from the same Institute for his training in electrophysiology and continuous guidance.

I would like to express my thankfulness to Prof. Dr. Francisco Ramos Morales from the University of Sevilla (US) for his kindness and availability every time I needed his help and to Prof. Dr. Francisco Javier Cejudo from the Institute of Plant Biochemistry and Photosynthesis (IBVF; CSIC/US) for his support and advice.

Finally, I would like to thank the *Spanish National Research Council* (CSIC), which offered me the funds to accomplish my PhD studies at the Institute of Natural Resources and Agrobiology of Seville (IRNAS, Seville, Spain). I also would like to express my sincere gratitude to the German Academic Exchange Service (DAAD) for awarding me with the Research Grant for Doctoral Candidates and Young Academics and Scientists at the Institute for Molecular Plant Physiology and Biophysics (University of Würzburg, Würzburg, Germany).

Gracias a mis compañeros de laboratorio, empezando por Sofía que, aunque compartimos relativamente poco tiempo, lo disfruté muchísimo. A JuanD le agradezco ser tan servicial, su alegría y todos los buenos ratos en el laboratorio e invernadero, a Carlos sus chistes malos con su buena intención de hacernos reír y a Pablo por verlo todo siempre tan sencillo. Gracias a Kino por su buen humor y por transmitirlo con canciones, pareados, chistes... A Pilar y a Mara por amenizar los encuentros fuera del laboratorio, a Leti por su gran corazón y a Miriam por dedicarme siempre un rato cuando nos encontramos. Quisiera agradecerle a Alberto todos esos ratos de risa floja imparable tan divertidos; pero, sobre todo, le agradezco enormemente a Fran su compañerismo, amistad, disponibilidad, ayuda, atención… Con su llegada mejoró el laboratorio en todos los aspectos.

Me gustaría expresar también mi agradecimiento a mis amigas y compañeras de trabajo: a Marina por todos los momentos que compartimos, que tanto nos hacen disfrutar. Conocerla en Ecuador fue lo mejor de aquel viaje. Quiero agradecerle a mi gran compañera de oficina Elena el cambio que supuso su amistad en estos años de tesis. Desde que dejó su silla vacía la he echado mucho de menos por su alegría, dulzura y bondad. A Jara le agradezco especialmente todas las risas y esos almuerzos tan amenos al aire libre. Muchas gracias a las chicas del fondo de la segunda planta: Marta, Irene, Sara, Ana… ¡Cuánto se puede disfrutar comiendo y limpiándose los dientes! Y a mi querida Ángela me gustaría agradecerle su amabilidad, sus detalles y todo el cariño que siempre me ha transmitido, incluso desde la distancia.

Le estoy sinceramente agradecida a Raúl por todos sus consejos, que siempre me han resultado tan prácticos. Espero seguir disfrutando tanto de su sabiduría como de su sentido del

humor. Asimismo, quiero darle las gracias a Pili por animar el ambiente de trabajo con bromas y risas, a José María por sus acertijos y actividades para fomentar la atención y por esas originales celebraciones de cumpleaños junto a Elena, Marta y José Ramón. A la gente del laboratorio de la tercera planta del departamento de Biotecnología Vegetal (Zaida, Anna, Paula, Belén, Fran, Javi), aunque ya no estén allí, les agradezco la ayuda y el compañerismo dentro y fuera del laboratorio.

Muchas gracias de corazón a todos los que pertenecen y han pasado por el grupo de Riego y Ecofisiología de Cultivos, en el que realmente empecé: José Enrique, Antonio Díaz, Torres, Alfonso, Celia, Antonio Montero, Vicky, Carmen, Virginia, Rafa, Adrián, María Dolores, Saray, Sheren, Bárbara… He disfrutado mucho con ellos, hasta quitando las malas hierbas, y espero seguir haciéndolo en cada uno de nuestros encuentros.

Gracias al pequeño grupo fusionado que creamos cuando empecé en el laboratorio de Chema entre la gente de éste (incluyendo a Sofy, Migue, Pablo y Alberto) y la del laboratorio de Heike (Marta, María, Marina, Lorena y Marta la cordobesa) por los momentos tan necesarios de desconexión laboral.

Me gustaría darle las gracias a todas esas personas del IRNAS que han hecho que con un simple encuentro por las instalaciones cambie mi estado de ánimo favorablemente: David y José Manuel de portería, Antonio de mantenimiento, Mª Ángeles y Mercedes del servicio de limpieza, Luisa, Mª Luz y Paqui de gerencia, María, JosAn, José María de la Rosa, Valme, Isa, Julia, Rocío, Chona, Jesús Cambrollé, Carmen Trigo, Celia Jiménez, Andrés, Pepijn, Esteban, Maite, Rosa, José Luis, Marta Gil, Pablo, José Manuel, Gabriela, Manuel…, y especialmente le agradezco a Alicia el cariño que me ha transmitido siempre y su alegría permanente.

Quiero agradecerles a algunas de las personas que han pasado por el IRNAS la huella que han dejado en mí. A Silvia su cercanía, amistad y todo lo que eso conlleva, a Graciele su amabilidad y tener siempre una sonrisa en la cara, a Rita por toda su alegría y por el mejor cumpleaños de mi vida y a Vincent por el intercambio de idiomas con el que ambos adquirimos mayor fluidez.

También me gustaría expresar mi gratitud a la gente del laboratorio de Fisiología Vegetal del Departamento de Biología Vegetal y Ecología de la Facultad de Biología (US), donde me inicié en el mundo de la investigación, por el buen trato que siempre me han dado. En especial, le agradezco a la Dr. Sofía García-Mauriño su firme apoyo, y a Isa y Cire su positividad y buenas recomendaciones. Además, me gustaría darle las gracias a Irene del Departamento de Microbiología de la Facultad de Biología (US) por su alegría, ánimos y consejos.

I big thank you to everyone from Geiger's lab: Sönke, Jenny, Julia, Meli, Nadin, Möritz, Michael…, especially to Anna-Lena and Christof for their help, friendship, laughs, talks, time… And thanks to the other people working in Botanik-I that I met during my stay in Germany: Hanna, Lena, Antonella, Maris, Katha, Justyna, Dawid, Ayla, Natalia, Jens, Bea, Alicija, Martin… and particularly to Sarah and Karimi for their happiness and for being so open.

Franca, herzlichen Dank für alles: deine Fröhlichkeit, deine Zuneigung, deine Hilfe, das super Zusammenleben! Ich bedanke mich bei deinen Eltern für die tolle Zeit. Agnes, Hani und Evi: danke schön auch!

Gracias a todos mis compañeros y profesoras del Instituto Cultural Alemán (Anna, Angelika, Miriam, Lysann, Elena, Mercedes, Arabia, Carmen, Toñi, Andrea, Eleanor, Noelia…) por esas buenas horas de aprendizaje que han hecho que tres horas de alemán un viernes sean más llevaderas. Además, le agradezco francamente a mi maestra de Taichi Dª Mª Carmen López su vocación, la

energía que transmite y su sabiduría. Ha sido un placer compartir sus clases con Begoña, Reyes, Bea, Manoli, Isabel, Inma, Carlos, Rosa, Miguel Ángel, Concha, Manuela…

Quiero agradecerles también a mis amigas todas las experiencias compartidas durante mis años de doctorado. A Lucía, que fue mi sol en Alemania en los meses en que éste no salió, por su alegría, simpatía, cariño y tantos buenos momentos que disfrutamos y seguimos compartiendo. A mi amiga Isis por todas las veces que ha venido a comer conmigo a Reina Mercedes para compartir un ratito y, sobre todo, por su sincera amistad. A mi amiga de la infancia Mª Ángeles por tenerme siempre presente y por hacer que, junto a su estupenda pareja, nuestros encuentros estén repletos de risas constantes. A Hanah le agradezco su forma de ser, la correspondencia a lo largo de estos años y que siempre que nos vemos reina el buen humor.

A mi madre y a mi padre les doy las gracias por su confianza, apoyo y amor inquebrantables y a mi querido hermano Ernesto le agradezco, además, su visita a Würzburg en 2014 por esos momentos inolvidables que tanto me alegra recordar.

Quisiera agradecerles a todos mis familiares y demás allegados que siempre tengan tan buena disposición para reír y disfrutar del tiempo que compartimos. Eso siempre viene bien, sobre todo para desconectar y disminuir el estrés. A mi abuela Clara le quiero dar las gracias por su cálida sonrisa, y a mi tía-abuela Julia por la energía y felicidad que siempre transmite, que no aminora con los años, y eso que ya está rozando el siglo.

Finalmente, y no por ello menos importante, le agradezco profundamente a mi queridísimo Javi, mi ideal compañero de vida, su alegría diaria, sus bromas, su buen humor, sus constantes detalles y su apoyo incondicional desde que nos conocemos, que hace que siempre me sienta bien y tenga una sonrisa en la cara.

“I’ve learned that people will forget what you said,
people will forget what you did,
but people will never forget how you made them feel”

Maya Angelou (1928–2014)

ABSTRACT

Optimal growth of plants requires the synchronic supply of both chloride (Cl^-) and nitrate (NO_3^-) molecules (Franco-Navarro *et al*., 2016a), but salt stress causes excessive accumulation of Cl^- in the leaves, which can produce ionic toxicity, especially in Cl^--sensitive crops such as citrus and grapevine. Both Cl^- and NO_3^-, which can be transported through the same or different plasma membrane (PM) transporters, are incorporated into the root symplast through the combined action of active (influx) and passive (efflux) PM transporters. Influx of both anions is governed by high- and low-affinity symporters, not identified so far (Babourina *et al.*, 1998b; Britto and Kronzucker, 2006; Felle, 1994; Wang *et al*., 2012), while their release from cells is a passive transport mechanism mediated by unknown channels (Roberts, 2006; White and Broadley 2001).

Uptake of nutrients is followed by their retention in the root or their load into the xylem for root-to-shoot transport. Chloride loading into root xylem vessels is a key mechanism regulating shoot Cl^- accumulation (Brumós *et al*., 2010; Gong *et al.,* 2011; Tregeagle *et al.,* 2010) and it is expected that xylem loading of NO_3^- and Cl^- has to be tightly regulated for maintaining an appropriate balance between both anions. This mechanism is highly likely to be electrochemically passive and hence facilitated by PM anion channels, not characterized at the molecular level so far (Gilliham and Tester, 2005; Köhler and Raschke, 2000; Köhler *et al.*, 2002). Channels regulating xylem translocation of electrolytes like potassium and Cl^- are negatively regulated by abiotic stress and abscisic acid (ABA; Cram and Pitman, 1972; Pitman, 1977; Pitman and Wellfare, 1978; Pitman *et al*., 1974).

We propose that anion channels are key regulators of Cl^- nutrition and salt tolerance in plants, and we hypothesize that according to the environmental conditions (e.g. salinity and water deficit), ABA-mediated regulation of channel activity modulates the degree of Cl^- inclusion/exclusion in plants. However, genes encoding for anion channels involved in these processes, as well as the molecular mechanisms underlying the appropriate balance between NO_3^- and Cl^- in plants, remain elusive.

In this work, the root-expressing *AtSLAH1* and *AtSLAH4* genes of *Arabidopsis thaliana* plants, which encode slow (S)-type anion channels of the SLAC/SLAH family, have been characterized and their biological roles have been described. Single mutant lines disrupted in these genes show developmental alterations, whose manifestation depended on the Cl^- dose applied in the culture medium, thus providing evidence of an interaction between Cl^- nutrition and the function of both SLAH1 and SLAH4 channels. Furthermore, the single mutant *slah1-2* accumulates less Cl^- in the shoot, whereas the mutant *slah4-2* exhibits the opposite phenotype, proving that SLAH1 and SLAH4 channels participate in Cl^- homeostasis at the whole plant level.

In xylem sap samples obtained from *slah1-2* mutant plants, the Cl^-, but not the NO_3^- content, is reduced by 50%. In the root, *AtSLAH1* expression specifically localizes to cells facing xylem vessels (xylem-pole pericycle), where this gene is co-expressed with *AtSLAH3*, other member of the SLAC/SLAH family. Studies with single *slah3* and double *slah1-slah3* mutant lines indicate that a concerted activity of both SLAH1 and SLAH3 channels is required for adequate regulation of Cl^- translocation into root xylem vessels. While functional expression of SLAH1 in

Xenopus oocytes remains electrically silent, it is shown that SLAH1 and SLAH3 physically interact when co-expressed, proving that the vascular S-type anion channel can be arranged as a SLAH1/SLAH3 heteromer. To conduct NO_3^- and Cl^- anions in oocytes, SLAH3 requires extracellular NO_3^- and Ca^{2+}-dependent kinases (Geiger *et al.*, 2011; Maierhofer *et al.*, 2014a; Scherzer *et al.*, 2012). In the absence of these regulatory components, macroscopic currents could only be measured when SLAH3 was co-expressed with SLAH1. These results, together with that obtained from the co-expression of SLAH1 and SLAH3 heteromers containing alternatively a wild-type subunit together with a mutant interacting partner unable to conduct anions, prove that, rather than the addition of a SLAH1 intrinsic Cl^- conductance, the activity of the heteromer is a consequence of a modification of the electrical properties of SLAH3. Moreover, SLAH1 substitutes for kinase and NO_3^--dependent activation of SLAH3, increasing seven times the Cl^- conductance of the SLAH1/SLAH3 heteromer compared to the SLAH3/SLAH3 homomer.

Abiotic stress, including water deficit and salinity, strongly down-regulates *AtSLAH1* expression through an ABA-dependent manner. We propose that SLAH1 functions like a molecular switch that regulates Cl^- translocation according to environmental cues. Under optimal conditions, actively growing plants require the coordinated translocation of both Cl^- and NO_3^- nutrients by the SLAH1/SLAH3 heteromer, whereas abiotic stress favours the SLAH3 homomerization by a strongly reduction of SLAH1 synthesis, greatly reducing thus root-to-shoot Cl^- translocation.

In addition, *AtSLAH4* is expressed in epidermal and cortical cells of the root. The loss of SLAH4 function leads to higher accumulation of Cl^- in the shoot, demonstrating that SLAH4 control net Cl^- uptake through the regulation of Cl^- release to the root/soil interface. In contrast to *AtSLAH1*, *AtSLAH4* expression is developmentally down-regulated during early seedling establishment, indicating that optimal plant growth requires high Cl^- uptake after germination and during the first days of plant growth. Subsequently, proper Cl^- homeostasis requires the SLAH4 function for optimizing the adequate balance between root Cl^- uptake and release, mainly during late developmental stages and senescence.

Finally, *AtSLAH1* is also actively expressed in flower organs like the anther filament and the stigmatic papillae, where the requirement of SLAH1 activity for optimal production of seeds has been proved.

RESUMEN

El crecimiento óptimo de las plantas requiere el aporte sincronizado de cloruro (Cl^-) y nitrato (NO_3^- ; Franco-Navarro y col., 2016a), pero el estrés salino causa la acumulación excesiva de Cl^- en órganos aéreos, lo que puede producir toxicidad iónica, especialmente en cultivos sensibles como los cítricos y la vid. La toma neta de ambos aniones en el simplasto de la raíz resulta del equilibrio entre la entrada activa y la salida pasiva llevada a cabo por transportadores de membrana plasmática (MP), que pueden ser compartidos por ambos aniones. La entrada de Cl^- y NO_3^- está regida por transportadores activos de alta y baja afinidad, no identificados aún (Babourina y col*.,* 1998b; Britto y Kronzucker, 2006; Felle 1994; Wang *et al*., 2012), mientras que su salida de las células es un mecanismo de transporte pasivo mediado por canales aniónicos desconocidos (Roberts, 2006; White y Broadley 2001).

Tras su adquisición, los nutrientes se retienen en la raíz o se transportan a la parte aérea a través del xilema. La translocación de Cl^- al xilema es un mecanismo clave en la regulación de la acumulación de este anión en la parte aérea (Brumós y col., 2010; Gong y col*.,* 2011; Tregeagle y col*.,* 2010). Para mantener un equilibrio adecuado entre ambos aniones, la translocación de NO_3^- y Cl^- al xilema debe estar adecuadamente regulada, probablemente a través de procesos electroquímicamente pasivos facilitados por canales aniónicos de MP aún no caracterizados a nivel molecular (Gilliham y Tester, 2005; Köhler y Raschke, 2000; Köhler y col., 2002). Los canales que regulan la translocación al xilema de electrolitos como potasio o Cl^-, son regulados negativamente por estrés hídrico y el ácido abcísico (ABA; Cram y Pitman, 1972; Pitman, 1977; Pitman y Wellfare, 1978; Pitman y col., 1974).

Proponemos que los canales aniónicos son reguladores clave de la nutrición por Cl^- y de la tolerancia a la salinidad en las plantas, y que la regulación de la actividad de los canales mediada por ABA modula el grado de inclusión/exclusión de Cl^- en las plantas en función de las condiciones ambientales (por ejemplo, el déficit hídrico y la salinidad). Sin embargo, aún no se conocen los genes que codifican los canales aniónicos implicados en estos procesos, así como tampoco los mecanismos moleculares responsables del correcto equilibrio entre NO_3^- y Cl^- en las plantas.

En este trabajo hemos caracterizado los genes *AtSLAH1* y *AtSLAH4* que se expresan en la raíz de *Arabidopsis thaliana* y que codifican canales aniónicos de tipo lento de la familia SLAC/SLAH, y hemos descrito su función biológica. Las líneas mutantes simples interrumpidas en estos genes muestran alteraciones en el desarrollo, cuya manifestación depende de la dosis de Cl^- aplicada en el medio de cultivo, proporcionando así evidencia de una interacción entre la nutrición por Cl^- y la función de los canales SLAH1 y SLAH4. Además, el mutante *slah1-2* acumula menos Cl^- en la parte aérea, mientras que el mutante *slah4-2* muestra un fenotipo opuesto, probando que los canales SLAH1 y SLAH4 participan en la homeostasis de Cl^- a nivel de la planta completa.

En las muestras de savia del xilema obtenidas de las plantas mutantes *slah1-2*, el contenido de Cl^-, pero no el de NO_3^-, se reduce un 50%. En la raíz, la expresión de *AtSLAH1* se localiza específicamente en las células del periciclo adyacentes a los vasos del xilema, donde este gen se coexpresa con *AtSLAH3*, otro miembro de la familia SLAC/SLAH. Los estudios con las

líneas de mutantes *slah3* y con la doble mutante *slah1-slah3* indican que la regulación correcta de la translocación de Cl^- al xilema de la raíz requiere la actividad conjunta de ambos canales. Mientras que la expresión funcional de SLAH1 en ovocitos de *Xenopus* no genera corrientes eléctricas, se muestra que SLAH1 y SLAH3 interaccionan físicamente cuando se coexpresan, probando que ambos canales pueden organizarse como heterómeros. SLAH3 requiere NO_3^- extracelular y quinasas dependientes de Ca^{2+} para transportar NO_3^- y Cl^- en ovocitos (Geiger *et al.*, 2011; Maierhofer *et al.*, 2014a; Scherzer *et al.*, 2012). En ausencia de estos factores de regulación, cuando SLAH3 se coexpresó con SLAH1 se registraron corrientes macroscópicas. Estos resultados, junto con los obtenidos de la coexpresión de heterómeros SLAH1 y SLAH3 que contenían alternativamente la subunidad de uno de ellos silvestre y la del otro con una mutación puntual que impedía conducir aniones, prueban que la actividad del heterómero es consecuencia de la modificación de las propiedades eléctricas de SLAH3, en lugar de la adición de una conductancia de Cl^- intrínseca de SLAH1. Además, SLAH1 sustituye la activación de SLAH3 dependiente de quinasa y NO_3^-, aumentando siete veces la conductancia por Cl^- en el heterómero SLAH1/SLAH3 respecto al homómero SLAH3/SLAH3.

El estrés abiótico (déficit hídrico y salinidad) reduce fuertemente la expresión de *AtSLAH1* a través de un mecanismo regulatorio mediado por ABA. Proponemos que SLAH1 funciona como un interruptor molecular que regula la translocación de Cl^- al xilema en función de las condiciones ambientales. En situaciones favorables, las plantas crecen activamente y necesitan la translocación simultánea de Cl^- y NO_3^- a través del heterómero SLAH1/SLAH3, mientras que el estrés abiótico favorece la homomerización de SLAH3 debido a la reducción de la síntesis de SLAH1, limitando fuertemente el transporte de Cl^- desde la raíz a la parte aérea.

Por otra parte, *AtSLAH4* se expresa en las células de la epidermis y del córtex de la raíz. La pérdida de función de SLAH4 conlleva a una mayor acumulación de Cl^- en la parte aérea de la planta, demostrando que SLAH4 controla la entrada neta de Cl^- en la raíz mediante la regulación de la liberación de Cl^- al medio exterior. A diferencia de *AtSLAH1*, la expresión de *AtSLAH4* está regulada por el desarrollo y está anulada en los primeros días de crecimiento, indicando que el desarrollo óptimo de la planta requiere una alta absorción de Cl^- tras la germinación y durante los primeros días del establecimiento de la plántula. Posteriormente, la correcta homeostasis de Cl^- requiere la actividad de SLAH4 para optimizar el equilibrio entre la entrada y salida de Cl^- en la raíz, principalmente durante las etapas tardías del desarrollo y la senescencia.

Finalmente, *AtSLAH1* también se expresa activamente en órganos florales como el filamento de la antera y en las papilas del estigma, donde la actividad de SLAH1 es necesaria para la producción óptima de semillas.

LIST OF ABBREVIATIONS

A	Ampere
ABA	Abscisic Acid
ABC	ATP-Binding Cassette
ABI1/2	ABA Insensitive 1 or 2
ABRE	ABA-Response Elements
AKT1	*Arabidopsis* K^+ Transporter 1
Ala	Alanine
ALMT	Aluminum activated Malate Transporter
Arg	Arginine
Asn	Asparagine
Asp	Aspartic acid
At	*Arabidopsis thaliana*
A. thaliana	*Arabidopsis thaliana*
***At*rbohF**	Respiratory Burst Oxidase Homologue F
A. tumefaciens	*Agrobacterium tumefaciens*
BiFC	Bimolecular Fluorescence Complementation
BLAST	Basic Local Alignment Search Tool
BNS	Basal Nutrient Solution
bp	Base Pair
BS	Basal Solution
bZIP	Basic leucine Zipper
Ca^{2+}	Calcium
$CaCl_2$	Calcium Chloride
$Ca(NO_3)_2$	Calcium Nitrate
$CaSO_4$	Calcium Sulfate
CBL	Calcineurin-B-Like protein
Cc	*Citrus clementina*
CC	Companion Cell
CCC	Cation Chloride Cotransporter
cDNA	Complementary DNA
CFU	Colony Forming Units
CIPK	CBL-Interacting Protein Kinase
Cl^-	Chloride
CLC	Chloride Channel
Col	Columbia
CPK	Calcium-dependent Protein Kinase
cRNA	Complementary RNA
CT	Carboxilo Terminal
cv	Cultivar
ºC	Degree Centigrade/Celsius
d	Day
das	Days After Sowing
DDT	Dithiothreitol
DEPC	Diethyl pyrocarbonate
DIDS	4,4'-diisothiocyanatostilbene-2,2'-disulfonic acid
DM	Dry matter
Dm	*Dionaea muscipula*
DNA	Deoxyribonucleic Acid
dNTP	deoxynucleotide Triphosphate
dsDNA	Double-Stranded DNA
DW	Dry Weight

3D	Three-dimensional
ΔE_n	Nerst potential
E_{Cl}	Chloride diffusion potential
E. coli	*Escherichia coli*
EDTA	Ethylenediaminetetraacetic acid
e.g.	For example
eIF4A1	Eukaryotic translation Initiation Factor 4A1
E_m	Membrane potential
etc	et cetera
F	Fardays constant
F^-	Fluoride
Fig.	Figure
Figs.	Figures
FW	Fresh Weight
g	Gramme
× *g*	Units of times gravity
GFP	Green Fluorescent Protein
Gly	Glycine
GORK	Guard cell Outward Rectifying K^+ channel
GUS	β-Glucuronidase
h	Hour
H^+	Protons
HAB1/2	Homology to ABI1 or ABI2
HCO_3^-	Carbonate
HI	Harvest Index
HiTehA	*Haemophilus influenza*
HNO_3	Nitric acid
H_2O_2	Hydrogen peroxide
H_2SO_4	Sulphuric acid
I	Electrical current (ampere)
IAA	Indole-3-acetic acid
i.e.	That is
I_{inst}	Instantaneous Currents
IJPB	Institut Jean-Pierre Bourgin
IM	Infiltration Medium
IP_3	Inositol-3-Phosphate
I_{SS}	Steady State Currents
I_T	Instantaneous Currents
I_{tail}	Tail streams
IVT	*In Vitro* Transcription
IVT-PCR	*in vitro* PCR
K	Degree Kelvin
K^+	Potassium
KAT1/2	K^+ channel in *Arabidopsis thaliana* 1/2
Kb	Kilobase
KCl	Potassium Chloride
$K_3Fe(CN)_6$	Potassium ferricyanide
$K_4Fe(CN)_6$	Potassium ferrocyanide
KH_2PO_4	Potassium dihydrogen Phosphate
KNO_3	Potassium Nitrate
KO	Knockout
K_2SO_4	Potassium Sulfate

l	Litre
$LaCl_3$	Lanthanum Chloride
LB	Luria-Bertani
Le	*Lycopersicon esculentum*
LEA-M	Late-Embryogenesis Abundant
Leu	Leucine
LiCl	Lithium Chloride
m	Metre
M	Molar
MA^{2-}	Malate
MAE	MOPS-Sodium Acetate-EDTA
MES	4-Morpholineethanesulfonic acid
mg	Milligramme
$MgCl_2$	Magnesium Chloride
$Mg(NO_3)_2$	Magnesium Nitrate
$MgSO_4$	Magnesium Sulfate
min	Minute
ml	Millilitre
mM	Millimolar
$MnCl_2$	Manganese Chloride
MOPS	4-Morpholino Propanesulfonic acid
MPa	Megapascal
mRNA	Messenger RNA
MS	Murashige and Skoog medium
Ms	Millisecond
MscS	Small-conductance Mechanosensitive channel
Mt	*Medicago trunculata*
mV	Millivolt
N	Nitrogen
nA	nanoampere
Na^+	Sodium
NaCl	Sodium Chloride
NADPH	Reduced Nicotinamide Adenine Dinucleotide Phosphate
$NaNO_3$	Sodium Nitrate
NaOH	Sodium Hidroxide
NASC	Nottingham Arabidopsis Stock Centre
NAXT1	Nitrate Excretion Transporter 1
NCBI	National Center for Biotechnology Information
NH_3	Ammonia
NH_4^+	Ammonium
NH_4Ac	Ammonium Acetate
NHX1	Na^+/H^+ exchanger 1
NKCC	$Na^+:K^+:Cl^-$ Cotransporter
NO	Nitric Oxide
NO_3^-	Nitrate
NPF	Nitrate Transporter 1/Peptide Transporter
NRT1/PTR	Nitrate Transporter 1/Peptide Transporter
NRT1-2	Nitrate Transporter 1-2
nt	Nucleotide
NT	Amino Terminal
N. tabacum	*Nicotiana tabacum*
NTP	Nucleotide Triphosphate
OD	Optical Density
Os	*Oryza sativa*
O. sativa	*Oryza sativa*
OST1	Open Stomata 1, SnRK2.6

P	Permeability
PA	Phosphatidic Acid
PAR	Photosynthetically-Active Radiation
PBS	Phosphate buffered saline
PCR	Polymerase Chain Reaction
PEG	Poly Ethylene Glycol
Pfu polymerase	DNA polymerase isolated from *Pyrococcus furiosus*
pH	Potential of Hydrogen
Phe	Phenylalanine
PIP3	Phosphatidyl-Inositol-3-Phosphate
PLC	Phospholipase C
PLDα_1	Phoshpholipase Dα_1
PM	Plasma Membrane
P_O	Open Probability
Pp	*Physcomitrella patens*
PP2C	Protein Phosphatases type 2C
PSII	Photosystem II
PTR	Peptide Transporter
Ptt	*Populus tremula x P. tremuloides*
PYR	Pyrabactin Resistance
PYL	PYR1 Like
PZ	4-Phenylazobenzyl- oxycarbonyl-L-prolyl-L-leucyl-glycyl-L-prolyl-D-arginine
qPCR	Quantitative real time PCR
QUAC	Quick Anion Channel
R	Universal gas constant
RCAR	Regulatory Component of ABA Receptor
Rel. P_O	Relative Open Probability
RH	Relative Humidity
RNA	Ribonucleic Acid
ROS	Reactive Oxygen Species
rpm	Revolutions Per Minute
RT-PCR	Reverse Transcriptase PCR
R-Type	Rapidly activated anion channel
s	Second
Sb	*Solanum bicolor*
SDS	Sodium Dodecyl Sulfate
SE	Sieve Element
Ser	Serine
SKOR	Stelar K^+ Outwardly-Rectifying
SLAC	Slow Anion Channel
SLAC1	Slow Anion Channel-Associated 1
SLAH1-4	SLAC1-Homolog 1-4
SnRK2	Sucrose non-fermenting-1 Related protein Kinase type-2
SO_4^-	Sulphate
SOB	Super Optimal Broth
SOC	Super Optimal broth with Catabolite repression
Spp.	Species
S-Type	Slowly activated anion channel
SV	Slow Vacuolar channel
T	Absolute temperature
TAE	Tris Acetate-EDTA buffer
Taq polymerase	DNA polymerase isolated from *Thermus aquaticus*
t-DNA	Transfer DNA by *A. tumefaciens*
T-DNA	Transfer DNA by mutagenesis

TDT	Tellurite-resistance/C4-dicarboxylate
TE	Tris-EDTA
TEVC	Two-Electrode Voltage Clamp
TM	Transmembrane
TPK1	Two-Pore K^+ channel 1
tRNA	Transfer RNA
U	Enzyme Unit
USER	Uracil-Specific Excision Reagent
UTR	Untranslated Region
V	Volt
$V_{½}$	Half-maximal activation potential
Val	Valine
V_c	Voltage of command signal
VDAC	Voltage-Dependent Anion Channels
V_H	Holding potential
V_{rev}	Reversal Potentials
VK	Vacuolar K^+ channels
V_m	Membrane potential
vs.	*versus*
Vv	*Vitis vinifera*
Ws	Wassilewskija
WT	Wild-type
X-IRAC	Xylem Inward Rectifying Anion Channel
X. laevis	*Xenopus laevis*
X-QUAC	Xylem Quickly activating Anion Conductance
X-SLAC	Xylem Slowly activating Anion Conductance
YEP	Yeast Extract Peptone
YFP	Yellow Fluorescent Protein
µA	Microampere
µg	Microgramme
µE	Microeinstein
µl	Microlitre
µm	Micrometre
µM	Micromolar

LIST OF FIGURES

LIST OF TABLES

TABLE OF CONTENTS

INTRODUCTION

1. INTRODUCTION

1.1. CHLORIDE AS A NUTRIENT

Physiological events in plant metabolism are directly or somewhat associated with the mineral elements. Therefore the attempt to understand the molecular mechanisms behind their transport has great importance in terms of basic and applied plant sciences.

1.1.1. Chloride is an essential micronutrient for plants

Chloride (Cl^-) is an essential micronutrient for higher plants (Broyer *et al*., 1954; Johnson *et al*., 1957; Whitehead, 1985), involved in the regulation of important cellular functions like enzyme activities, membrane potentials, pH gradients and electrical excitability (Marschner, 1995; Teakle and Tyerman, 2010; White and Broadley, 2001; Xu *et al*., 2000).

As an essential micronutrient, Cl^- is involved in the stabilization of the water splitting system at the oxidizing site of photosystem II (PSII) in the chloroplast and in the regulation of enzyme activities such as the asparagine synthethase, amylases, and the proton-pumping ATPase at the tonoplast (Churchill and Sze, 1984; Kusunoki, 2007). Important Cl^- functions are also related to the electrical charge balance of essential cations such as potassium (K^+) and protons (H^+), playing main roles in the stabilization of the electric potential of cell membranes and the regulation of pH gradients (Broadley *et al*., 2012b; Hänsch and Mendel, 2009; White and Broadley, 2001; Xu *et al*., 2000).

In addition, Cl^- is a major osmotically active solute in the vacuole involved in both turgor and osmoregulation processes, such as stomatal movement (section 1.5.2.2) and the activity of motor cells controlling nastic movements, like the seismonastic leaf movement of *Mimosa pudica* (section 1.4.3; Broadley *et al*., 2012b; Flowers, 1988; Hänsch and Mendel, 2009; Marschner, 1995; White and Broadley, 2001).

The tissue Cl^- concentration at which deficiency symptoms are observed varies between about 0–1 to 5–7 mg g^{-1} Dry Weight (DW), around 0.3 mg g^{-1} DW in most glycophyte plants (Zu *et* al., 2000). Typical symptoms of Cl^- deficiency include curling of leaflets, reduction of leaf growth, bronzing and wilting of leaves, as a consequence of chlorosis and necrosis (Ozanne *et al*., 1957; Smith *et al*., 1987; White and Broadley, 2001). Moreover, roots become stunted and the development of lateral roots is suppressed and fruits are decreased in number and size (White and Broadley, 2001). Furthermore, Schwenke and colleagues (2015) showed that Cl^- deficiency also delayed flowering and reduced plant biomass, grain size and grain yield in most durum and bread wheat varieties trialled.

Nevertheless, Cl^- deficiency rarely occurs in normal conditions because the biochemical requirement of plants for Cl^- is very low and the Cl^- concentrations in soil after rain, irrigation and pollution are usually enough (Chen *et al*., 2010; White and Broadley, 2001). It becomes a limiting factor for plant growth in areas of high precipitation far from the sea (Fixen, 1987; Xu *et al*., 2000). Its value as fertiliser was recognised in the mid-1800s when sodium chloride (NaCl) was applied to stiffen barley straw in England (Schwenke *et al*., 2015). Researchers have reported inconsistent yield responses to the application of Cl^- fertiliser in winter cereals grown

on soils where tests indicated a likely response (Díaz-Zorita *et al*., 2004; Fixen *et al.,* 1986; Freeman *et al*., 2006; Grant *et al*., 2001). The response to Cl^- fertilizers is higher in plant species with a high Cl^- requirement such as kiwifruit (Buwalda and Smith, 1991; Smith *et al.*, 1987) and palm trees (Braconnier and d'Auzac, 1990). In addition, Cl^- in macronutrient fertilizers was found to partially control a number of diseases in different crop species (Fixen, 1993).

1.1.2. Chloride as a beneficial macronutrient

Although classified as a micronutrient, our research group has compiled abundant information indicating that Cl^- is a multifunctional beneficial macronutrient. Under moderate external Cl^- in the soil medium (3–5 mM), plants accumulate Cl^- to levels of 2–20 mg g^{-1} DW that are typical of the content of a macronutrient (Broadley *et al.*, 2012b; Brumós *et al*., 2010; Franco-Navarro *et al*., 2016a; Marschner, 1995; Xu *et al*., 2000), specifically stimulating plant growth and leaf cell expansion, improving tissue water balance and water relations at the whole plant level (Franco-Navarro *et al*., 2016a; Raven, 2017). In addition, macronutrient levels of Cl^- are specifically required to allow optimal seedling establishment, to enhance water-use and nitrate-use efficiency, to increase drought tolerance, and to improve mesophyll diffusion conductance to CO_2 (Franco-Navarro *et al.*, 2012; Franco-Navarro *et al.*, 2016b; Franco-Navarro *et al.*, 2016c).

Under non-saline conditions Cl^- uptake via the symplastic pathway is an electrogenic $Cl^-/2H^+$ symport mechanism, which requires metabolic energy (Beilby and Walker, 1981; Britto and Kronzucker, 2006; Felle, 1994; Sanders, 1980; White and Broadley, 2001). Its uptake should implicate regulatory mechanisms since Cl^- accumulation to macronutrient concentration requires a considerable use of energy (Brumós *et al*., 2010).

1.2. CHLORIDE IN THE AGRICULTURE AND ITS INTERACTION WITH NITRATE

Chloride concern in the agriculture is related in most of the cases to its toxicity and also to its antagonism effect in nitrate (NO_3^-) uptake and accumulation. But Cl^- sensitivity varies extensively within plant species and the inhibition of NO_3^- uptake by Cl^- is determined also by the plant species, as well as the NO_3^- and Cl^- concentrations in the medium. However, according to the results of our research group, Cl^- toxicity thresholds have been underestimated and the antagonistic effect of Cl^- on the transport and assimilation of NO_3^- in higher plants has probably been overestimated (Franco-Navarro *et al*., manuscript in preparation).

1.2.1. Chloride in the agriculture

The negative effects of high Cl^- concentrations in the soil and in irrigation water on crop production are observed in coastal, arid, and semiarid areas, where freshwater sources are often scarce and the available groundwater is saline (Xu *et al.*, 2000).

Sensitivity to high Cl^- concentrations varies widely between plant species and cultivars. Generally, most nonwoody crops tolerate high levels of Cl^-, whereas many woody plant species and beans are susceptible to Cl^- toxicity (Maas, 1986). There are agricultural crops tolerant to high levels of soil Cl^-, as corn (Parker *et al.,* 1985). Sugar beet is the crop with the greatest tolerance to Cl^-, that may contain up to 50.8 mg g^{-1} Cl^- in the leaves (Zhou and Zhang, 1992).

Whereas another crops are sensitive to Cl^-, like the chinese cabbage (Yin *et al*., 1989) and the soybean (Parker *et al.,* 1983). The least sensitive plants are large seeded beans**,** squash, barley, maize and buckwheat (White and Broadley, 2001).

According to the literature (reviewed in Xu *et al*., 2000), the critical toxicity concentration is about 4–7 and 15–50 mg g^{-1} for Cl^--sensitive and Cl^--tolerant plant species, respectively.

The data in our laboratory indicate that these toxicity thresholds should be modified. On the one side, in the presence of 5 mM Cl^- *Nicotiana tabacum* accumulates 40–50 mg g^{-1} Cl^- in the leaves (Franco-Navarro *et al*., 2016a). According to Xu *et al*. (2000), this is the critical toxicity level of Cl^--tolerant species. The so-called Cl^--sensitive Citrus varieties Carrizo citrange and rough lemmon, treated for 30 weeks with 4.5 mM Cl^-, showed no visible symptoms of stress with leaf accumulation values of 30–35 mg g^{-1} Cl^-, also typical of a supposed tolerant specie (Walker *et al.*, 1982; Brumós *et. al*., 2010). On the other side, our group has measured values of 5–15 mg g^{-1} Cl^- content in different plant species growing with very low amounts of Cl^- (75 mM) during seedling establishment (Franco-Navarro *et al*., manuscript in preparation). According to the aforementioned ionic toxicity thresholds, these values correspond to the critical toxicity level of Cl^--sensitive species. It seems therefore that: (1) the role of Cl^- as a multifunctional beneficial macronutrient have yet to be adequately established; (2) the type of treatment and the developmental state of the plant are parameters that must be taken into account to define chloride toxicity and tolerance thresholds.

1.2.2. Chloride and nitrate interaction

Both NO_3^- and Cl^- are essential for plant growth and the most abundant anions in plants tissues. In addition to Cl^-, NO_3^- represents the major counterion for K^+ and also plays an essential role in plant cellular osmoregulation and membrane potential control (Franco-Navarro *et al*., 2016a; Marschner, 1995; White and Broadley, 2001). These anions can be transported through the same or different proteins since they are monovalent anions with a similar ionic radius.

The macronutrient NO_3^- is the major source of nitrogen (N) for protein and nucleic acid metabolism and, after water, the main limiting factor for growth of terrestrial plants (Marschner, 1995). Uptake of sufficient N from the environment serves as a key process for plants to successfully grow and develop (Wang *et al.*, 2012). Nevertheless the availability of N is often a limiting factor in plant growth and crop productivity, but the application of N fertilizers to counteract N deficiencies can have detrimental economic and environmental effects. Plant roots can effectively absorb certain forms of N in the soil, including organic (amino acids) and inorganic molecules, such as NH_4^+ and NO_3^-. Nitrate is the most common form in which N is assimilated by the plant, indicating that NO_3^- uptake and allocation are key factors in efficient N utilization (Wang *et al.*, 2012).

As other nutrients like phosphate or ammonium (NH_4^+), NO_3^- participates in the regulation of lateral roots development and architecture, leaf development, flowering induction and seed dormancy (Alboresi *et al*., 2005; Chiu *et al*., 2004; Drew *et al*., 1973; Drew and Saker, 1975; Krouk *et al*., 2010b; Marin *et al*., 2011; Remans *et al*., 2006; Ruffel *et al*., 2011, 2014, 2016; Walch-Liu *et al*., 2006).

Besides its role as a nutrient, NO_3^- is also a signal molecule, which is involved in the control of many physiological processes, plant growth and crop yield (Crawford, 1995; Krapp *et al.*, 2014; Vidal *et al.*, 2014). As a signal molecule, NO_3^- can induce the expression of a number of genes implicated in NO_3^- transport and assimilation (Bi *et al*., 2007; Krouk *et al*., 2011; Medici and Krouk, 2014; Wang *et al*., 2000; 2003, 2004).

The form in which N is taken up by a plant (NH_4^+ or NO_3^-) affects the sensitivity of the plant to Cl^- salt stress (Xu *et al*., 2000). The antagonism between NO_3^- and Cl^- uptake was demonstrated in many agronomic crops, such as avocado (Bar *et al.*, 1997; Wiesman, 1995), barley (Glass and Siddiqi, 1985; Smith, 1973), broccoli (Liu and Shelp, 1996), citrus (Bañuls *et al.*, 1990, 1997; Bar *et al.*, 1997; Cerezo *et al.*, 1997; Chapman and Liebig, 1940), kiwifruit (Smith *et al.*, 1987), melon and lettuce (Feigin, 1985; Wei *et al*., 1989), peanut (Leidi *et al.*, 1992; Wang *et al.*, 1989), potato (James *et al.*, 1970), strawberry (Wang *et al.*, 1989), tobacco (Fuqua *et al.*, 1976), tomato (Feigin *et al.*, 1987; Kafkafi *et al.*, 1982; Zabala, 1984) and wheat (Silberbush and Lips, 1991; Wang *et al.*, 1989).

It is well established that the presence of NO_3^- in soils can mitigate the toxic effect of excessive Cl^-, apparently due to the suppressive effect that NO_3^- has on Cl^- fluxes into the plant, and on Cl^- accumulation in plant tissues (Adler and Wilcox, 1995; Bar *et al.*, 1997; Glass and Siddiqi, 1985; Kafkafi *et al.*, 1982). Increasing concentrations of NO_3^- decrease Cl^- concentrations in plants in a linear fashion (Xu *et al*., 2000). The competition of NO_3^- *versus* Cl^- was found to be stronger in salt-sensitive plants, such as peanut, than in salt-tolerant plants, like cotton (Leidi *et al.*, 1992).

Less clear is the inhibition of NO_3^- uptake by Cl^-, which has been reported to depend on the plant species and the concentrations of both NO_3^- and Cl^- in the uptake medium (Cerezo *et al*., 1997). Our research group has shown that under a moderate Cl^- treatment (5mM Cl^-), resulting macronutrient Cl^- accumulation (40–50 mg g^{-1} Cl^-) promote optimal NO_3^--use efficiency. Probably, plants under sub-optimal Cl^- nutrition require compartmentalization of NO_3^- for maintaining adequate osmoregulatory capacity, reducing NO_3^- availability for N assimilation (Franco-Navarro *et al.*, 2016b).

A variety of NO_3^- transporters have evolved in the plant kingdom with different localizations and functions: uptake of NO_3^- by roots, long-distance transport in the xylem and phloem, regulation of NO_3^- content in seeds, and transport into the vacuole for storage (Dechorgnat *et al*., 2011; Forde, 2000; Hechenberger *et al*., 1996; Orsel *et al.*, 2002; Tsay *et al.*, 2007; Wang *et al*., 2012). In *Arabidopsis* four transporter families are involved in these functions: the low-affinity nitrate transporter 1/peptide transporter (NRT1/PTR) family, recently named NPF (Lerán *et al.*, 2014), the high affinity nitrate transporter 2 (NRT2) family transporters (Krapp *et al.*, 2014; Orsel *et al.*, 2002), the chloride channel (CLC) family (Barbier-Brygoo *et al*., 2011), and the slow anion channel-associated homologues (SLAC/SLAH) family (Negi *et al.,* 2008). Several of these transporters also play versatile roles in NO_3^- sensing, plant development, pathogen defense, and stress response (Krapp, 2015; Krapp *et al*., 2014; Krouk *et al*., 2010a**;** Noguero and Lacombe, 2016; Roeselfma *et al*., 2012; Wang *et al*., 2012). However, these transporter families are not exclusive for NO_3^- and in many cases also transport Cl^-. Altogether these four families contain 73 genes, but only 35 have been characterized in detail and, among these, 24 encode NO_3^- transporters (Krapp *et al.*, 2014).

On a worldwide basis Cl^- deficiency rarely occurs in normal conditions, and the bigger concern about this anion is due to its toxicity.

1.3. CHLORIDE TOXICITY UNDER SALT STRESS

The saline areas of the world consist of salt marshes of the temperate zones, mangrove swamps of the subtropics and tropics, and their interior salt marshes adjacent to salt lakes. Saline soils are abundant in semiarid and arid regions, where the amount of rainfall is insufficient for substantial leaching. In addition, salinity problems occur in nonirrigated croplands and pastures as a result of evaporation and transpiration of saline underground water or due to salt input from rainfall (Marschner, 1995).

Soil salinity is a major abiotic stress that adversely affects crop quality and productivity (Munns, 2002; Munns and Tester, 2008; Roy *et al.*, 2014). And this problem is increasing due to irrigation, improper drainage, seawater in coastal areas, and salt accumulation in arid and semi-arid regions (Rengasamy, 2010).

Saline soils are characterized by toxic levels of chlorides and sulphates of sodium (Na^+). Salinity restricts plant growth as it causes nutritional constraints by decreasing uptake of phosphorus, K^+, NO_3^- and calcium (Ca^{2+}), ion cytotoxicity and osmotic stress, leading to metabolic imbalances and oxidative stress, and thereby decreasing the yield and quality of crops (Alscher *et al.*, 1997; Hirt and Shinozaki, 2004; Munns, 2002; Munns and Tester, 2008; Munns *et al.*, 2006; Rengasamy, 2010; Roy *et al.*, 2014).

According to plant growth response in saline soils, species can be grouped into four categories: (1) halophytes (defined as the native flora of saline soils), which can be subdivided further into species whose growth is stimulated (e.g. *Sueda maritima*, *Atriplex numnmlaria*) and species whose growth is little affected by 200 mM Cl^- (e.g. *Atriplex hastata*, *Spartina spp.*, sugar beet); (2) non-halophytes (glycophytes) whose growth is reduced substantially by 100 mM Cl^-, which can be additionally subdivided into tolerant (e.g. *Festuca rubris*, *Puccinella peisonis*, cotton, barley), intermediate (e.g. tomatoes) and sensitive (e.g. beans, soybeans) species; and (3) very salt-sensitive non-halophytes (e.g. citrus and woody plant species). Many important cereal, vegetable and fruit crops are susceptible to Cl^- toxicity during cultivation (White and Broadley, 2001).

Considering that salinity is a common feature of arid and semiarid lands, plants have evolved mechanisms to tolerate it through the adequate control of several process mediated by membrane transporters (Fig. 1.1): (1) regulation of influx into cells, (2) control over long distance transport, and (3) compartmentalization at both cellular and tissue levels (Blumwald, 2000; Flowers and Colmer, 2008).

Considering that NaCl is the most soluble and widespread salt, it is not surprising that all plants have evolved mechanisms to regulate its accumulation and to select against it in favour of other nutrients commonly present in low concentrations, such as K^+ and NO_3^- (Munns and Tester, 2008).

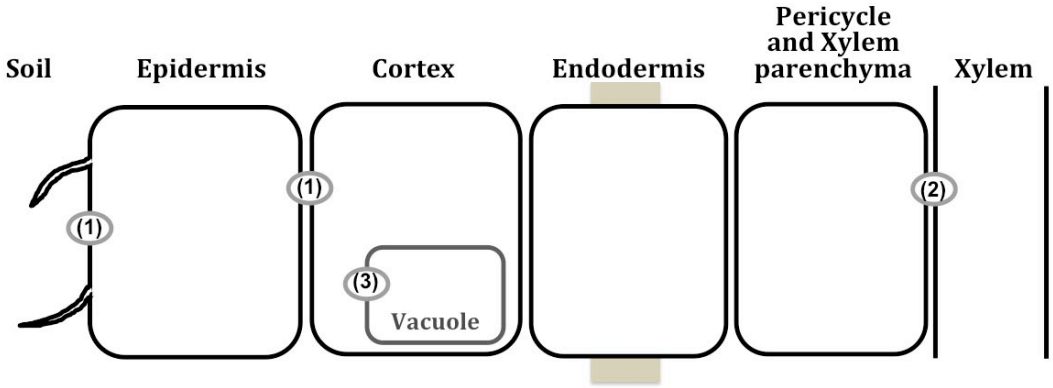

Figure 1.1. Salt tolerance mechanisms in plants regulated by membrane transporters. (1) Ion uptake control into cells. (2) Ion movement control over long distance transport. (3) Regulation of the compartmentalization at cellular level.

As mentioned earlier, there are two main components to salinity stress in plants: an initial osmotic stress in response to the increase in external osmotic pressure and a subsequent accumulation of toxic ions, which negatively affects cellular metabolism (Munns and Tester, 2008; Munns *et al*., 2006). The osmotic component of salinity is caused by excess inorganic ions, such as Na^+ and Cl^-, in the environment that decrease the osmotic potential of the soil solution and hence water uptake by the root. Therefore, uptake of abundantly available Na^+ and Cl^- offers a comparatively cheap way to lower the tissue-osmotic potential (Brini and Masmoudi, 2012). To avoid the risk of ion toxicity associated with this strategy, Na^+ and Cl^- are generally compartmentalized at the cellular and intracellular level, especially in the vacuole (section 1.4.4) and in less sensitive tissues to avoid toxic concentrations within the cytoplasm, especially in mesophyll cells in the leaf (Munns and Tester, 2008; Roy *et al*., 2014). Concurrently, adjustment of the cytoplasmic compartment is achieved via production of compatible osmolytes such as proline, mannitol, sorbitol, and glycine betaine (Brini and Masmoudi, 2012). The glycine betaine additionally acts as antioxidant and thus detoxifies reactive oxygen species (ROS). Nevertheless, when plants are growing in high salt concentrations, an adequate sequestration of ions in the vacuole can become a limiting factor, especially in the case of glycophytes.

Under salinity, plants can accumulate excessive amount of Na^+ in the cytosol, which negatively affects many aspects of cellular physiology. The most abundant inorganic cation in the plant cytosol is K^+. The physicochemical similarities between Na^+ and K^+ lead to a competition at transport and catalytic sites that usually bind the essential cation K^+ and maintaining a high cytosolic K^+/Na^+ ratio is believed to improve salt tolerance (Maathuis and Antmann, 1999; Zhu, 2001).

Similarly to the selectivity between Na^+ and K^+ to maintain favourable K^+/Na^+ ratios, a parallel situation has been proposed for Cl^- with respect to the macronutrient NO_3^-, considering that Cl^- and NO_3^- compete for membrane transport mechanisms. These anions can be transported through the same or different proteins since they are monovalent anions with a similar ionic radius (Li *et al.*, 2016). However, contrary to K^+, Na^+ and Cl^-, NO_3^- is assimilated in plant anabolic processes. In addition, plant NO_3^- concentrations strongly varies along different developmental stages, e.g. vegetative *versus* reproductive stages, indicating that NO_3^-/ Cl^- ratios might not be an adequate predictor of Cl^- toxicity under salt stress conditions (Colmenero-Flores JM, personal communication).

Given that Cl^- loading into root xylem vessels is a key mechanism regulating shoot Cl^- accumulation (Brumós *et al*., 2010; Gong *et al.,* 2011; Tregeagle *et al.,* 2010), xylem loading of NO_3^- and Cl^- has to be tightly regulated to maintain an appropriate balance between both anions. Taken into account that the thermodynamics of anion transport, release of Cl^- and NO_3^- into the root xylem is highly likely to be electrochemically passive and therefore facilitated by plasma membrane anion channels that are not yet identified.

Both Na^+ and Cl^- are toxic to plants at high concentrations, but it has been proposed that Cl^--sensitive species can control Na^+ transport better than Cl^-. Under salt stress conditions, Cl^--sensitive, frequently woody perennial plants exhibit toxicity symptoms to Cl^-, rather than to Na^+, accumulation. This difference may arise because Na^+ is accumulated so effectively in woody roots and stems that little amounts reach the leaves. Thus Cl^-, which continues passing to the leaves, becomes the more significant toxic component of the saline solution (Munns and Tester, 2008; Teakle and Tyerman, 2010; White and Broadley, 2001). But this statement does not imply that Cl^- is more metabolically toxic than Na^+, rather that these species are better excluding Na^+ from the leaf blades than Cl^- (Munns and Tester, 2008). Therefore, many economically valuable species in which Na^+ is predominantly retained in the roots and stems, Cl^- is considered more toxic because this ion is accumulated to high levels in shoot tissues, negatively impacting on essential processes such as photosynthesis (Brini and Masmoudi, 2012) and leading to the disturbance of growth and productivity (Geilfus *et al*., 2015; Munns, 2001; Teakle and Tyerman, 2010). This phenomenon has been mainly described in fruit tree species that are routinely grown on Cl^--excluding rootstocks like citrus (Maas, 1993; Storey and Walker, 1999; Tadeo *et al*., 2008), stone fruit trees (Bernstein *et al.*, 1956), grapevine (Antcliff *et al*., 1983) and avocado (Bar *et al.,* 1997). But, Cl^- excess is also harmful to a number of herbaceous species, including economically important cereals and vegetables as soybean (Abel, 1969), wheat (Bernal *et al.*, 1974) and barley (Greenway and Munns, 1980).

In citrus, the evidence for the detrimental effect of Cl^- is mostly supported by the association between genetic differences in the rate of Cl^- accumulation in leaves and the plant salinity tolerance (Cole, 1985; Moya *et al*., 2003; Romero-Aranda *et al*., 1998; Storey and Walker, 1999). According to this information, Bañuls and Primo-Millo (1992) showed that NaCl and potassium chloride (KCl) stress had similar toxicities, while sodium nitrate ($NaNO_3$) resulted less harmful. Higher correlations between shoot Cl^- accumulation, than between Na^+ accumulation, and defoliation were found using different rootstock combinations and different chloride salts (Bañuls and Primo-Millo, 1995; Brumós *et al*., 2009). Photosynthesis and growth disturbances were also highly correlated with leaf Cl^- growth (Romero-Aranda *et al*., 1998; Brumós *et al.*, 2009). A gradient of toxicity (KCl>NaCl>$CaCl_2$) that did not correlate with the presence of the toxic cation Na^+ was found when salinity damage was quantified in terms of dry weight loss (Romero-Aranda *et al*., 1998) or in terms of global gene expression (Brumós *et al.*, 2009).

Improving salt exclusion from the shoot is one resource for enhancing plant salinity tolerance (Apse and Blumwald, 2007; Guan *et al.*, 2014; Horie *et al*., 2009; Munns and Tester, 2008; Munns *et al*., 2012). Given that Cl^- tolerant citrus rootstocks apparently possess more efficient root mechanism for Cl^- exclusion than sensitive ones (Fernández-Ballester *et al*. 2003; Moya *et al*. 2002; Storey and Walker 1999), Brumós and colleagues (2010) studied Cl^- excluder and includer citrus rootstocks under non-salinized conditions in order to delimit specific Cl^- transport activities in the symplastic pathway, Cl^- uptake, translocation and distribution. They

conclusively observed that different citrus rootstock species actively transport Cl^- to the shoot regardless of their ability to exclude it under salinity stress, these rootstocks modulate Cl^- uptake according to nutrient availability and the regulation of root-to-shoot Cl^- transport appears to be the main factor determining the degree of Cl^- exclusion. Based on these results, they proposed a model in citrus for the regulation of Cl^- uptake and transport through the symplastic pathway (Fig. 1.2).

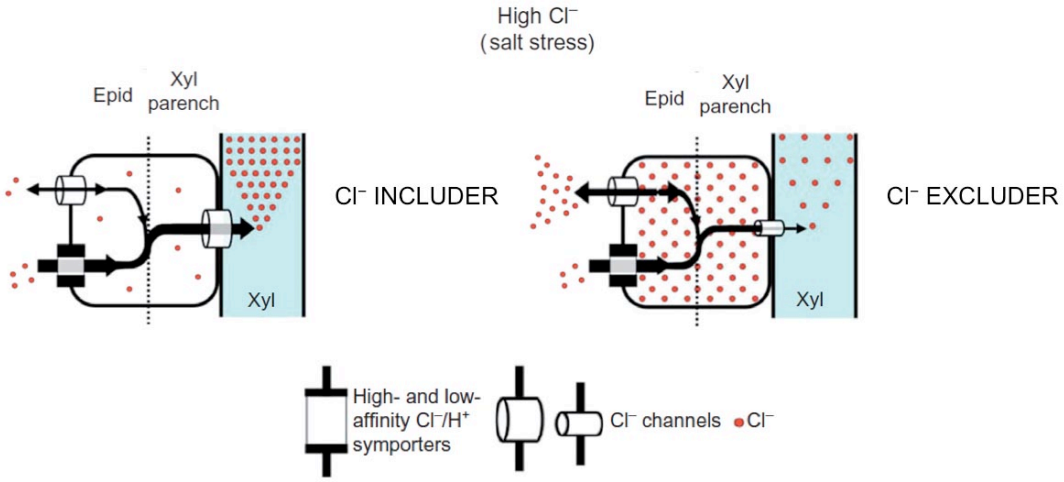

Figure 1.2. Proposed model for the symplastic regulation of chloride (Cl^-) homeostasis in the root of a Cl^- includer and a Cl^- excluder rootstock. Under high Cl^- concentration, anion channels from epidermal cells can mediate Cl^- influx. Cl^- xylem translocation is restricted in the salt-tolerant rootstock (Cl^- excluder), but not in the sensitive one (Cl^- includer). Epid, epidermal cells; Xyl parench, xylem parenchyma cells; Xyl, xylem vessel. Modified from Brumós *et al.*, 2010.

The fact that salt-tolerant genotypes translocate a lower amount of Cl^- from the roost to the shoot compared to salt-sensitive genotypes (Brumós *et al.*, 2010; Läuchi *et al.*, 2008; Moya *et al.*, 2003; Teakle and Tyerman, 2010) indicates that membrane transport proteins at the sites of xylem loading contribute to plant salinity tolerance via selective Cl^- exclusion.

Franco-Navarro and colleagues (2016a) have recently reported that under non-saline conditions Cl^- is actively taken up and accumulated into leaf tissues of citrus plants through symplastically regulated transport mechanisms, indicating that citrus (and probably other glycophyte plants) handle Cl^- homeostasis similarly to a macronutrient such as K^+, rather than a toxic ion such as Na^+. In addition, as mentioned before, Cl^- does not appear to be a typical micronutrient since the actual Cl^- concentration in plants, in the range of 2–20 mg g^{-1} DW (Broadley *et al.*, 2012b; Brumós *et al.*, 2010; Franco-Navarro *et al.*, 2016a; Xu *et al.*, 2000), is 10–100 times higher than the concentration required as an essential micronutrient. This is a relevant fact considering that all other mineral micronutrients (B, Cu, Fe, Mn, Mo, Ni, and Zn) are present at much lower concentrations in plant tissues (10^{-4}–10^{-1} mg g^{-1} DW) and their accumulation to higher levels results in plant toxicity (Hänsch and Mendel, 2009).

It is well established that uptake, efflux, translocation, and compartmentalization of toxic ions (mainly Na^+ and Cl^-) provide important bases for salinity tolerance in plants, and hence, a potential pathway to improve crops. However, a lack of understanding regarding the molecular entities and complex interactions of the responsible Cl^- membrane transport proteins has hindered progress in this respect.

1.4. CHLORIDE AND NITRATE ACQUISITION AND DISTRIBUTION

The identification of proteins and genes that are responsible for the transport of Cl^- is a basic requirement for the understanding of Cl^- uptake and distribution in the plant.

In plants, several transporter families have been reported to participate in anion transport, thereby in Cl^- transport. These anion transporters include the slow anion channel-associated 1 (SLAC1) protein, aluminum activated malate transporter (ALMT) family, anion/H^+ antiporters, ATP-binding cassette (ABC) transporter family, voltage-dependent Cl^- channels (CLC), cation-Cl^--cotransporters (CCC), voltage-dependent anion channels (VDAC), nitrate transporter 1/peptide transporter (NRT1/PTR) family (NPF), and MscS-like mechanosensitive channels (Teakle and Tyerman, 2010).

Between these Cl^- transporter families, only CCC and CLC have been shown to be important for Cl^- homeostasis under high salinity in *Arabidopsis* (Colmenero-Flores *et al.*, 2007, Jossier *et al.,* 2010; Nguyen *et al.*, 2016). In addition, some other channels such as stretch-activated anion channels, slowly activated anion channels (S-type) and rapidly activated anion channels (R-type) were also shown to be involved in Cl^- ion efflux in plasma membranes of guard cells (White and Broadley, 2001).

Although the pathways for Cl^- entry and movement within the plant have been biochemically characterized, their molecular determinants are poorly defined (Henderson *et al.*, 2014; Teakle and Tyerman, 2010).

1.4.1. Root acquisition

Higher plants take up mineral nutrients from the soil solution via the roots and they have to be channelled toward the root xylem vessels for distribution within the plant body (Fig. 1.3).

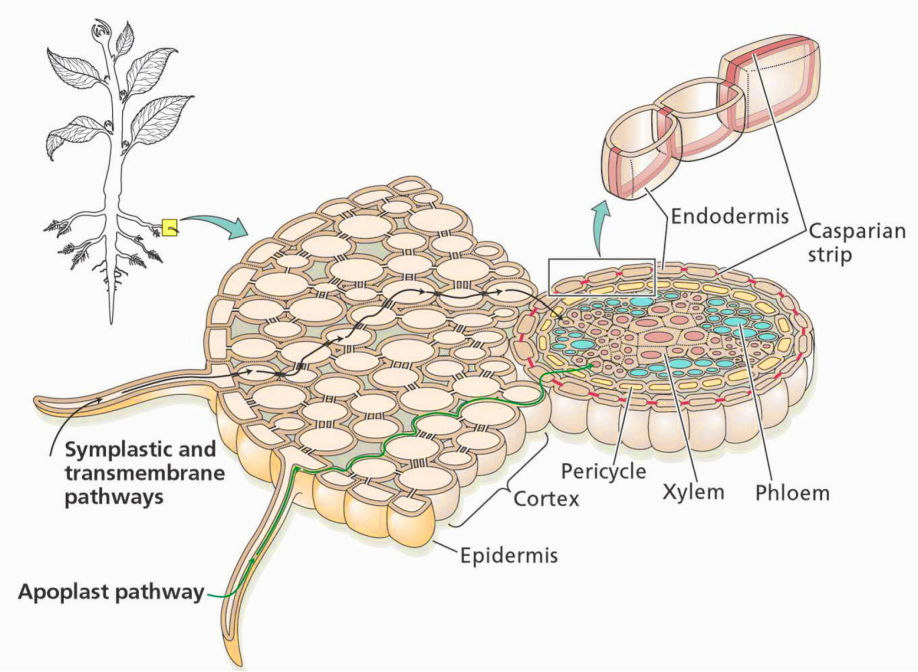

Figure 1.3. Root pathways for nutrients and water uptake. In the symplastic pathway, ions travel between cells through plasmodesmata. In the apoplast pathway, ions move through the cell wall without crossing any membranes, but this way is blocked at the endodermis by the Casparian strip. Obtained from Taiz and Zeiger, 2002.

The plasma membrane of epidermal and cortical cells contains H^+/Cl^- symport activity, which drives Cl^- uptake, and several Cl^- channels that facilitate Cl^- fluxes into and out of the root cell (White and Broadley, 2001). There are two pathways by which anions might reach the xylem, the symplastic (cytoplasmic) and the apoplastic (extracellular) pathway (Fig. 1.3).

The ion transport across the root until the xylem is regulated and influenced by the ion concentrations in the root cell, which influences the membrane potential (V_m), and the carriers, pumps or channels contained within the membrane (Clarkson, 1993). All living cells exhibit a membrane potential due to asymmetric ion fluxes between the inside and outside of a cell. The free-running membrane potential of a plant cell is typically dominated by two parallel potential differences, the ion (j) diffusion potential (E_j) and the pump potential (E_P). The pump potential is generated by the activity of a H^+-ATPase situated within the plasma membrane. Protons are pumped out of the root, driving the cytosol negative with respect to the outside. The Nerst equation ($E_i - E_o$) indicates whether ions will move passively into or out of the cell:

$$E_i - E_o = \frac{RT}{z_j F} \ln \frac{P_j[j^-]_i}{P_j[j^-]_o}$$

where R is the gas constant, T is the absolute temperature, Z_j is the valence of the ion (j) in question, F is the Farday's constant, P is the permeability coefficient of the individual ion and $[j^-]$ is the concentrations of the ions outside (o) or inside (i) the cell.

This can be simplified for a monovalent ion such as Cl^-, with a negative charge, under standard conditions as the diffusion potential:

$$E_{Cl} = 59.1 \log \frac{[Cl^-]_i}{[Cl^-]_o}$$

When Cl^- is taken up against its electrochemical potential difference, the equilibrium potential for Cl^- (E_{Cl}) is usually quite positive because Cl^- is a negatively charged molecule and therefore requires active transport through the plasma membrane under non-saline conditions (White and Broadley, 2001), using the force of protons moving back into the root, via a cotransport protein, which facilitates Cl^- entry with two H^+ (Babourina *et al.,* 1998b; Britto and Kronzucker, 2006; Epstein, 1972; Felle, 1994; Glass *et al*., 1992; Lee, 1982; Sanders, 1980).

Passive influx can only occur when the membrane potential becomes more positive than the equilibrium potential for the anion, a situation that can occur when the external concentration of the anion is high relative to the internal concentration or when membrane potential is depolarized, two situations that take place under salt shock. Sodium entry to the cytoplasm would depolarize the membrane potential (Cakirlar and Bowling, 1981; Blumwald *et al.*, 2000**;** Schachtman *et al*., 1991), which could drive the membrane potential positive of the equilibrium potential for Cl^-. The passive entry of Cl^- could initially prevent excessive depolarization by clamping the membrane potential at the equilibrium potential for Cl^-, provided this is reasonably negative. Thereby, under high Cl^- concentrations in the soil, like high soil salinity (NaCl), Cl^- may enter the cell passively via ion channels, because the equilibrium potential for Cl^- is negative of the membrane potential of the cortical or epidermal cells, allowing passive Cl^- influx (Cram, 1973; Binzel *et al*., 1988; Skerrett and Tyerman, 1994), particularly if

the entry of Na^+ depolarizes the membrane potential. But after the cytoplasmic Cl^- concentration has stabilized at higher levels, influx would have to be active.

During radial transport towards the conducting xylem vessels, ions have to enter the cytoplasm across the plasma membranes of the root cells at the endodermis because of the hydrophobic suberin and lignin deposits in the radial and transverse walls of the endodermis (the Casparian strip). This deposits inhibit the flow of water, and hence of ions, travelling in the apoplast. Subsequently, ions travel from cell to cell through plasmodesmatal connections towards the xylem and are exported across the plasma membrane of cells within the stele (Fig. 1.4). To get to the shoot, ions have to enter the extracellular space of the stele, which is connected to the xylem vessels. Thus, Cl^- ions movement across the root implies at least two processes catalysed by Cl^- transporters in the plasma membrane, which could control the selectivity and magnitude of Cl^- fluxes to the shoot.

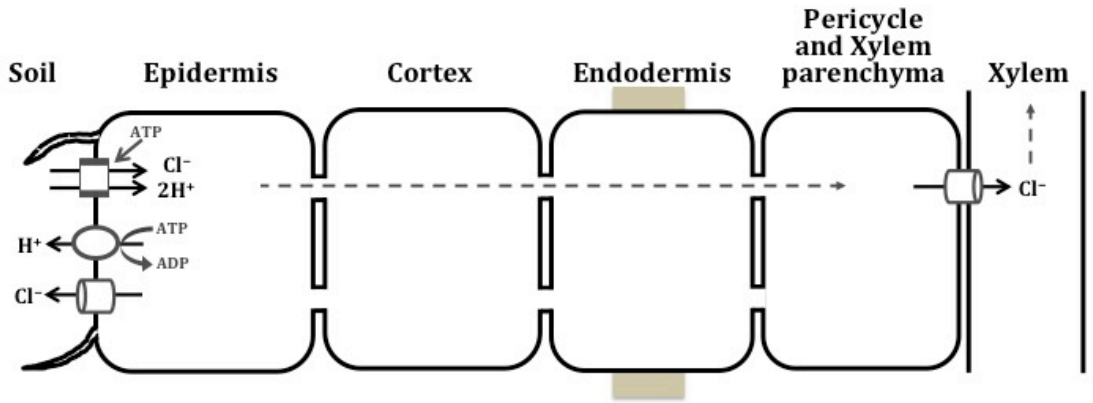

Figure 1.4. Chloride (Cl^-) uptake from the soil and loading to the shoot under non-nutrient stressed conditions. Ions movement between cells in the root from the soil to the xylem vessels implies at least two plasma membrane transport mechanisms.

Nevertheless, Cl^- uptake under non-saline conditions occurs primarily via the symplastic pathway and is regulated according to nutrient availability (Brumós *et al.,* 2010; Pitman, 1982), as a result of the combined activities of influx (active) and efflux (passive) plasma membrane transporters (Fig. 1.4; Britto and Kronzucker, 2006). Chloride influx is governed by high- and low-affinity $Cl^-/2H^+$ symport activities, requiring metabolic energy (Babourina *et al.*, 1998; Britto and Kronzucker, 2006; Epstein, 1972; Felle 1994; Lee, 1982; Wang *et al*., 2012; White and Broadley, 2001). As mentioned before, Cl^- release from the cell occurs through anion efflux channels (Roberts, 2006; White and Broadley 2001), which have been proposed to make a considerable contribution to the resultant net Cl^- uptake at plasma membrane potentials more negative than − 50 mV (Babourina *et al.,* 1998).

Similarly to Cl^-, the inward transport of NO_3^- across the plasma membrane occurs against a steep electrochemical potential gradient because the negatively charged NO_3^- ion has to overcome both the negative plasma membrane potential as well as an uphill concentration gradient. Therefore NO_3^- influx requires metabolic energy, like Cl^- uptake, and is an electrogenic $NO_3^-/2H^+$ symport mechanism.

The *Arabidopsis NRT1.1* gene (also known as *CHL1* and recently named as *At*NPF6.3; Léran *et al.*, 2014) belongs to the low-affinity NO_3^- transporter NRT1 family, recently named NRT/PTR family (NPF). Exceptionally in the NPF family, *NRT1.1* encodes a dual-affinity NO_3^- transporter that contributes to both low- and high-affinity uptake in roots of *Arabidopsis*

seedlings (Liu *et al.*, 1999; Touraine and Glass, 1997; Tsay *et al.*, 1993). Both high and low affinity NO_3^- transport activities depend upon phosphorylation/dephosphorylation by the CBL-interacting protein kinase CIPK23 at a threonine residue (T101; Liu and Tsay, 2003) and are mediated by low NO_3^- conditions (Ho *et al.*, 2009). This gene is inducible and is expressed preferentially at the epidermis of the root tip, in lateral root primordial and in the cortex and endoderm of upper root parts (Huang *et al.*, 1996). In addition it is also located in proliferating regions of shoots (like young leaves) and in guard cells (Guo *et al.*, 2003). The NRT1.1 active transporter is also involved in the activation of NO_3^--related genes (Ho *et al.*, 2009), the signalling network for regulation of root development (Ho and Tsay, 2010) and auxin transport (Krouk *et al.*, 2010b), contributing to the growth of nascent organs (Guo *et al.*, 2001) and playing an important role in stomatal opening, essentially when Cl^- is not available (Guo *et al.*, 2013).

In addition, the low-affinity transporter NRT1.2 (recently named *At*NPF4.6; Lerán *et al.*, 2014) expression occurs in the root tip, root hairs and epidermis of mature root parts and it is also involved in NO_3^- uptake from the soil into roots and is responsible for the constitutive low-affinity NO_3^- uptake capacity of roots being expressed even in the absence of NO_3^- (Huang *et al.*, 1999; Tsay *et al.*, 1993). NRT1.2 has been recently shown to mediate cellular ABA uptake and it could be involved in stomatal aperture regulation by ABA influx at the site of ABA biosynthesis (Kanno *et al.*, 2012).

The high affinity NRT2 family member *NRT2.1*, expressed in the epidermis, cortex and endodermis of mature root parts in *Arabidopsis*, together with NRT2.2, is involved in high-affinity NO_3^- uptake using a H^+ gradient as a driving force to transport NO_3^- from the soil into plant cells and their gene expression is transiently increased by N starvation (Filleur *et al.*, 2001; Li *et al.*, 2007; Little *et al.*, 2005; Nazoa *et al.*, 2003; Orsel *et al.*, 2004).

While the low- and high-affinity uptake of NO_3^- from the soil through H^+-coupled NO_3^- carriers of the NPF and NRT2 families is well understood, the molecular mechanism of Cl^- uptake remains elusive.

1.4.2. Xylem translocation

After mineral nutrients arrive to the root stele, they have to be translocated to the xylem vessels to be distributed within the shoot.

Living xylem parenchyma and pericycle cells control the anion composition of the sap flow between root and shoot (Köhler *et al.*, 2002; Köhler and Raschke, 2000; Lin *et al.*, 2008). In contrast, xylem vessels represent dead cells and thus water and nutrients transported within the xylem move extracellularly (through the apoplast). The physical structure of the root dictates that ions have to enter the cytoplasm of the cells surrounding the xylem before they can enter the apoplast of the xylem. Thus, nutrients such as NO_3^- and Cl^- have to be released across the plasma membrane of xylem parenchyma cells into xylem vessels.

The negative plasma membrane potential of plant cells (up to −250 mV) and the outward-directed NO_3^- and Cl^- concentration gradients suggest that NO_3^- and Cl^- entry into the xylem vessels is facilitated by anion efflux channels at plasma membrane potentials more negative than –50 mV (Babourina *et al.,* 1998; Glass and Siddiqi, 1995; Roberts, 2006; White and Broadley, 2001). Due to the measured ion concentrations in root cytoplasm and xylem, the loading of Cl^- into the root xylem is highly likely to be electrochemically passive, following the

electrochemical potential gradient for Cl^-, and it is thus likely to be facilitated by plasma membrane anion channels or carriers (Henderson *et al*., 2014; Kollist *et al.,* 2011; Munns and Tester, 2008; Roberts, 2006; Teakle and Tyerman, 2010; White and Broadley, 2001).

The release of NO_3^- from xylem parenchyma across the plasma membrane into the xylem vessels was in part assigned to H^+-coupled NO_3^- carriers. One of them is the *At*NRT1.5 (recently named as *At*NPF7.3; Léran *et al.*, 2014), a low-affinity H^+/NO_3^- symporter member of the NPF family in *Arabidopsis*, which is expressed in pericycle cells surrounding the protoxylem (Lin *et al*., 2008). In addition, another member of the NPF family, *At*NPF2.3, is also expressed at the plasma membrane of root pericycle cells. This transporter has a strong selectivity for NO_3^- and contributes to its translocation into the xylem under salt stress (Taochy *et al.*, 2015).

However, the molecular determinants of long-distance Cl^- transport in plants and how it is regulated in response to salinity stress are still largely unknown (Henderson *et al.*, 2014; Teakle and Tyerman, 2010). Some candidate proteins have been proposed to retrieve Cl^- from the xylem, such as the cation-chloride-cotransporter (CCC; section 1.4.4.2) proteins which affect root-to-shoot distribution of Cl^- and Na^+ in *A. thaliana* (Colmenero-Flores *et al*., 2007), but its localization at the Golgi/*trans*-Golgi network and its strong implication on plant development question its direct involvement in Cl^- xylem translocation (Henderson *et al*., 2015; Teakle and Tyerman, 2010).

It has been recently shown that the anion channel *At*NPF2.4, a member of the NPF at the plasma membrane of the root stele, is involved in Cl^- loading into the xylem in *Arabidopsis*, regulating its accumulation in the shoot in response to salt stress by the rapidly down-regulation of the gene. When it was expressed in *Xenopus laevis* oocytes, this channel catalysed Cl^- efflux at membrane potentials equivalent to those in the stele (–100 mV; Li *et al.*, 2016).

A transcriptional comparison between the roots of good and poor Cl^--excluding grapevine rootstocks suggested further candidate genes for this multigenic trait including aluminum activated malate transporters (ALMT; section 1.4.4.3), Cl^- channels (CLC; section 1.4.4.1) and their putative activating kinases (Henderson *et al*., 2014). But anion channels involved in root-to-shoot Cl^- transport remain to be identified and functionally characterized at a molecular level.

Patch clamp studies have identified several types of anion conductances in protoplasts of root xylem parenchyma cells of barley (*Hordeum vulgare*; Köhler and Raschke, 2000) and maize (*Zea mays*; Gilliham and Tester, 2005): an inward rectifying anion channel (X-IRAC), which is activated by cellular hyperpolarization, a slowly activating anion conductance (X-SLAC), which has slow activating/deactivating kinetics, and a quickly activating anion conductance (X-QUAC), which has quick activating/deactivating kinetics (Fig. 1.5). All of them were shown to be NO_3^- and Cl^- permeable and X-SLAC conductance was also permeable to malate (MA^{2-}). These conductances may thus represent the gates for anion release into the xylem (Roberts, 2006).

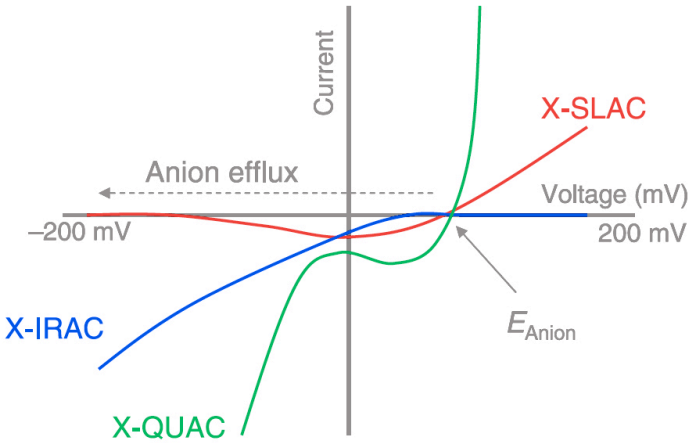

Figure 1.5. Representative current-voltage curves for the three plasma membrane anion conductances from barley xylem parenchyma cells. X-SLAC, slowly activating anion conductance; X-QUAC, quickly activating anion conductance; X-IRAC, inwardly rectifying anion conductance. E_{ANION}, Equilibrium potential for the permeant anion. Obtained from Roberts, 2006.

Moreover, Gilliham and Tester (2005) showed that X-IRAC and X-QUAC are differentially regulated by water stress and Köhler and colleagues (2002) demonstrated that apoplastic NO_3^- modifies the voltage dependent gating of X-QUAC. The anion channel inhibitor 4,4'-diisothiocyanatostilbene-2,2'-disulfonic acid (DIDS) significantly reduced xylem loading in barley seedlings, indicating that anion channels contribute to the release of anions into xylem vessels (Köhler *et al.*, 2002; Schroeder *et al.*, 1993).

To maintain an appropriate balance between the major anions NO_3^- and Cl^- in the root-to-shoot translocation process, xylem loading has to be tightly regulated. In response to salt stress, plants restrict the translocation of Cl^- into the shoot by Cl^- exclusion from the xylem vessels in the root. Nevertheless, the molecular nature of transporters loading the xylem with Cl^- and the regulatory mechanism leading to an appropriate balance between NO_3^- and Cl^- in the xylem sap remain elusive.

1.4.3. Redistribution via the phloem

During the growth of a plant, Cl^- is translocated from the root to the shoot via the xylem and is redistributed between tissues via the phloem. Long-distance transport in the phloem takes place in living cells, the sieve tubes (Fig. 1.6). The sieve element (SE)/companion cell (CC) complex is the functional unit of sieve tubes in angiosperms. Whereas the SE is almost dead, the CC is full of activity (Van Bel, 2003). The highly specialized SEs accommodate a mass flow of phloem sap, which is always directed from sugar producing regions (the sources) to sugar consuming regions (the sinks). For mineral nutrients, the main sites for phloem loading are located in the stem and leaves as components of either mineral nutrient supply to growth sinks (shoot apices, fruits, roots) or of nutrient recycling (Marschner, 1995). The driving force for phloem transport of loading solutes at the source and its unloading at the sink is thought to result in a gradient of osmotic potential along the phloem tubes (Liesche and Schulz, 2013). The resulting gradient in turgor pressure gives rise to the movement of water and solutes (mass flow as great as 1 m h^{-1}) toward the sink (Oparka and Turgeon, 1999; Patrick, 1997; Sjölund, 1997).

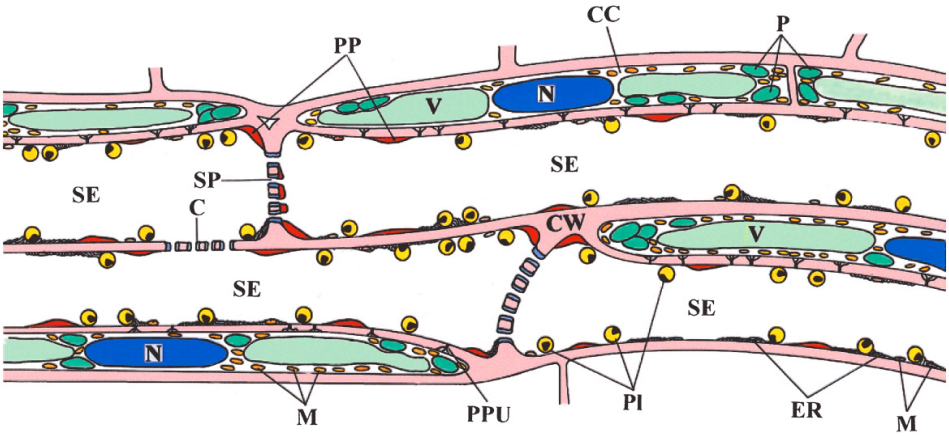

Figure 1.6. Structure of the sieve elements (SEs) in *Vicia faba* with companion cells (CCs). SEs and CCs are connected through numerous pore/plasmodesma units (PPUs). Sieve-element plastids (Pl), mitochondria (M), and endoplasmic reticulum stacks (ER) are partially positioned and evenly distributed along the SE plasma membrane, whereas parietal proteins (PPs) are locally aggregated. PPs and ER are sometimes located on the sieve plates (SPs) or at the margins of the sieve pores, but do not impede mass flow. C, callose; CW, cell wall; N, nucleus; P, plastids; V, vacuole. Modified from Van Bel, 2003.

Phloem transport has a role in cycling of mineral elements. Potassium is the major cation in the phloem and stimulates sugar loading into the phloem sap (Giaquinta, 1980; Peel and Rogers, 1982). Within the phloem, Cl^- is relatively mobile (Lessani and Marschner, 1978) and its recirculation (defined as the ratio of phloem/xylem nutrient fluxes) is about 20% in a number of plants with the phloem Cl^- concentration positively correlating with the Cl^- solution in which plants are grown (White and Broadley, 2001). In the phloem sap, Cl^- concentration may be in the order of 120 mM and seems to play a role in phloem loading and unloading of sugars, for example in the osmoregulation in the specialized motor leaf organs, pulvini**,** of *Mimosa pudica* during the very fast seismonastic leaf movement (Fig. 1.7). This movement is thought to result from sudden Cl^-, K^+ and sugars unloading from the phloem into the extensor apoplast. The increase of osmotic potential promotes water efflux from cells (Fromm and Eschrich, 1989; Moran, 2007). The osmotic strength for the leaf movement is powered by a plasma membrane H^+-ATPase, which drives KCl and water fluxes. The movement results from different volume and turgor changes in the two oppositely positioned parts in the pulvinus (Moran, 2007).

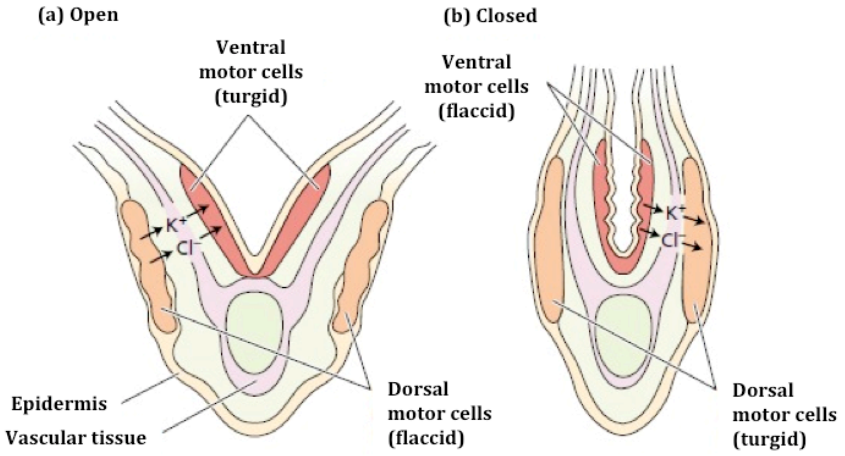

Figure 1.7. Cross section of *Mimosa pudica* leaves. (a) Leaf in an open position. **(b)** Leaf in a folded state. Obtained from Taiz and Zeiger, 2002.

Leaves are sink for NO_3^- during the vegetative growth stage meanwhile assimilated N compounds are remobilized for reuse in the developing seeds during senescence (Xu *et al*., 2012). Nitrogen can be also recycled from older (senescent) leaves to sustain the growth of younger developing tissues. Although NO_3^- is mostly transported by xylem, phloem transport has been proposed for local NO_3^- redistribution in the root (Wang and Tsay, 2011) and for NO_3^- remobilization from older leaves to N-demanding tissues, mostly under conditions of N starvation (Fan *et al*., 2009; Kiba *et al*., 2012).

The plasma membrane low affinity NO_3^- transporter NRT1.7 (recently named as *At*NPF2.13; Léran *et al.*, 2014), which belongs to the NPF family, is localized in the phloem SE/CC complex and is involved in NO_3^- excess movement from older leaves into developing tissues (Fan *et al*., 2009). In addition, another NPF member called *AtNRT1.9* (recently named as *At*NPF2.9; Léran *et al.*, 2014) is expressed in phloem CC of roots and is involved in local NO_3^- redistribution in the root (Wang and Tsay, 2011). Furthermore, the high affinity NRT2.4 transporter from the NRT2 family, is expressed in phloem-associated cells and is involved in the delivery of NO_3^- into the phloem for remobilization under conditions of N starvation (Kiba *et al*., 2012).

As mentioned above, to mitigate the damaging effects of salinity, the movement of toxic ions across cellular membranes is tightly regulated. At the whole-plant level, plants restrict shoot ion accumulation by controlling net ion uptake and xylem loading (Britto *et al*., 2004; Brumós *et al*., 2010; Craig Plett and Møller, 2010; Møller and Tester, 2007; Teakle and Tyerman, 2010). But according to Davenport and colleagues (2007) and Munns (2002), recirculation of ions to the roots via the phloem does not significantly contribute to the reduction of Na^+ and Cl^- levels in leaf tissue.

Nowadays, different NO_3^- transporters involved in NO_3^- redistribution within the plant have been identified at the phloem in *Arabidopsis*, but the identification of membrane transport proteins involved in Cl^- allocation though the phloem remains unexplored so far.

1.4.4. Vacuolar compartmentalization and transport into other organelles

Ion channels reside on intracellular membranes to regulate various organellar and cellular functions (Stael *et al.*, 2012; Zampese and Pizzo, 2012). Over 80% of transport processes occur inside the cells, but the mechanisms of ion flux across intracellular membranes (the endoplasmic reticulum, Golgi apparatus, endosomes, lysosomes, mitochondria, chloroplasts, and vacuoles) are difficult to investigate and remain poorly understood.

The large central vacuole serves as a storage reservoir that accumulates and releases ions as well as metabolites according to demands. The physical and functional plasticity of the vacuole enables plants to efficiently use energy and nutrients and maintain optimal physiological conditions in the cytosol. Vacuolar storage capacity regulates intracellular ion homeostasis but also influences whole-plant ion accumulation and distribution (Baetz *et al.*, 2016). Plant vacuoles store high concentrations of Ca^{2+} and Na^+ (Peiter, 2011), with Cl^- acting as a major counteranion and osmotically active solute involved in both turgor and osmoregulation processes (Marschner, 1995).

In addition, vacuolar ion uptake is crucial to confer cellular tolerance during long-term salinity and also to modulate shoot ion accumulation and whole-plant ion distribution during

early phases of salinity (Baetz *et al.*, 2016). During salinity the sequestration of Na^+ and Cl^- ions into the vacuole is crucial to maintain optimal metabolic conditions in the cytosol and mitigate cellular damage. Several transport proteins localized at the tonoplast have been suggested to facilitate intracellular ion distribution and thereby regulate cellular ion homeostasis (Martinoia *et al*., 2007, 2012). However, only few transporters involved in vacuolar ion uptake during salinity have been studied.

Some transporter families are related with anion flux across intracellular membranes in *Arabidopsis*, such as the chloride channel (CLC), the cation-chloride-cotransporter (CCC) and the aluminum-activated malate transporter (ALMT) families.

1.4.4.1. The CLC family

Since the vacuole is moderately positive with reference to the cytoplasm, part of the vacuolar Cl^- sequestration could proceed through ion channels. Several voltage-gated anion channels of the chloride channel (CLC) family (Fig. 1.8) have been located in the tonoplast of various species. Phylogenetic and functional analyses have shown that plant *CLC* genes encode anion channels and active $(NO_3^-/Cl^-)/H^+$ antiporters, localized in endosomal compartments (Chen, 2005; Lv *et al*., 2009; Zifarelli and Pusch, 2010).

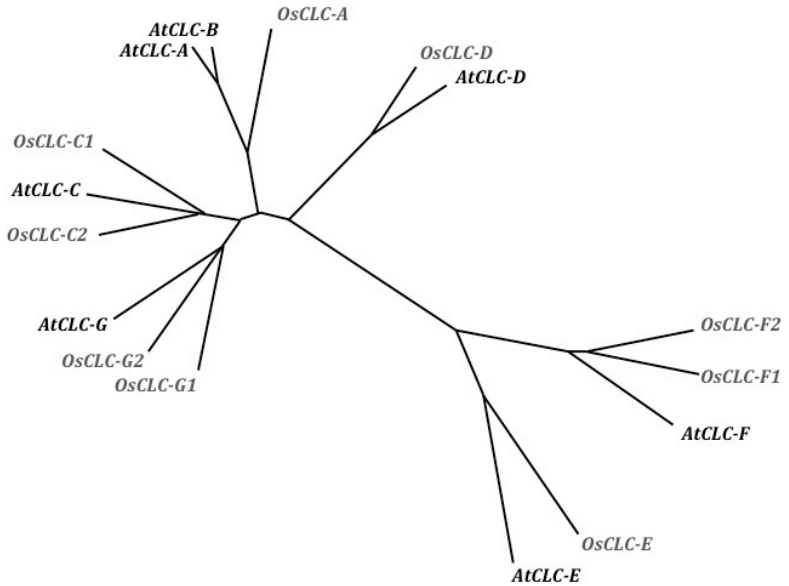

Figure 1.8. Phylogenetic tree of the CLC family from *Arabidopsis thaliana* (*At*) and *Oriza sativa* (*Os*). Obtained from Von der Fecht *et al.*, 2010.

Seven CLC members have been identified in the *Arabidopsis* genome (Isayenkov *et al.*, 2010) and all of them are expressed in vascular tissues in both roots and shoots (De Angeli *et al.*, 2007; Isayenkov *et al*., 2010; Lv *et al*., 2009; Zifarelli and Pusch, 2010).

The studies on the subcellular localizations of *At*CLCs have illuminated intracellular anion transport mechanisms in plant cells. In 2006 the *At*CLCa transporter was characterized as a $2Anion^-/H^+$ exchanger that drives the uptake of anions into vacuoles of *Arabidopsis* mesophyll and guard cells (Fig. 1.9; De Angeli *et al*., 2006; Wege *et al.*, 2016). *At*CLCa is permeable to Cl^- and NO_3^-, transporting NO_3^- more selectively than Cl^- (De Angeli *et al*., 2006; Wege *et al.*, 2010). *Arabidopsis clca* knockout mutants provide evidence that CLCa functions in NO_3^- accumulation into vacuoles in *A. thaliana* (Geelen *et al*., 2000). Furthermore, it was shown that a very steep

NO_3^- gradient is maintained in plants accumulating NO_3^- as N reserve (Wege *et al.*, 2014). Interestingly, *At*CLCa plays a dual role in guard cells, accumulating anions in the vacuole during stomata opening in response to light and releasing anions from the vacuole during ABA-induced stomata closure. The direction of NO_3^- flux is established by its phosphorylation status carried out by the kinase OST1 (Open Stomata 1; also named SnRK2.6) on its N-terminal domain (Wege *et al.*, 2014).

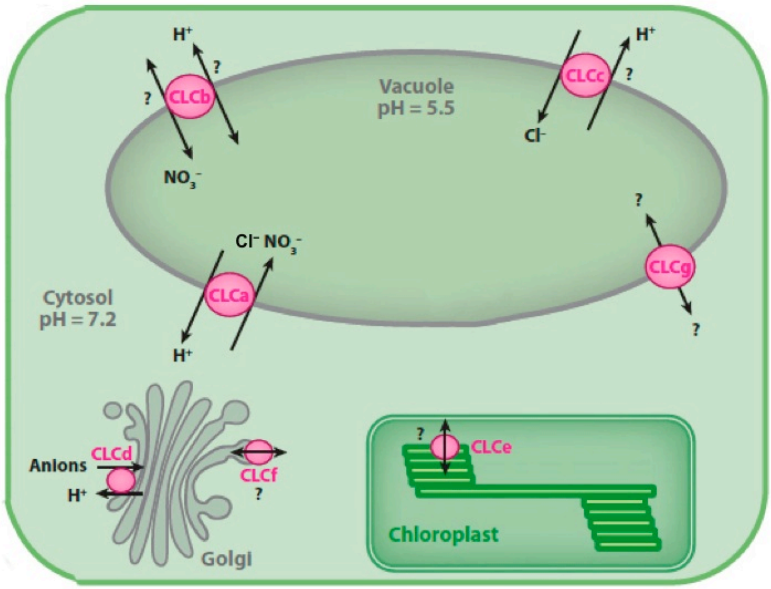

Figure 1.9. Subcellular localization of CLC family members in *Arabidopsis thaliana*. *At*CLCa-c and *At*CLCg are located in the tonoplast, *At*CLCd and *At*CLCf are present at the plasma membrane of the Golgi vesicles, and *At*CLCe is localized in the thylakoid membranes. Modified from Barbier-Brygoo *et al*., 2011.

AtCLCb is expressed in roots, shoots and in filaments and petals in the flower (Von der Fecht-Bartenbach *et al.*, 2010). The CLCb transporter functions also as a NO_3^-/H^+ antiporter like CLCa. Both channels have a higher selectivity for NO_3^- over Cl^- and are important for anion accumulation inside the vacuole (Fig. 1.9; De Angeli *et al.*, 2006; Geelen *et al.*, 2000; Von der Fecht-Bartenbach *et al.*, 2010). However, given that no phenotype of CLCb was reported, the physiological role of CLCb remains elusive (Martinoia *et al.,* 2012).

A a single amino acid substitution can change the selectivity from NO_3^- to Cl^- (Bergsdorf *et al.*, 2009), raising the possibility that other members of the CLC family might actually be Cl^-/H^+ antiporters. Indeed, *At*CLCc, which is localized at the tonoplast (Fig. 1.9) and expressed in guard cells, pollen grains and in the root (Jossier *et al.*, 2010), is involved in the accumulation of Cl^- into the vacuole. T-DNA insertion mutants in *CLCc* presented lower Cl^- vacuolar contents, and this fact correlated with the impaired light-induced stomatal opening and ABA-induced stomatal closure showed by these mutants (Jossier *et al.*, 2010). In addition, the *clcc* knockout mutants were found to be more sensitive to salt stress than the wild type, and hence it was suggested that CLCc contributes to the detoxification of the cytosol by sequestrating Cl^- into the vacuole (Jossier *et al.*, 2010).

AtCLCg, the closest homolog to *AtCLCc*, is also expressed at the tonoplast (Fig. 1.9), like *CLCa*, *CLCb* and *CLCc* (Marmagne *et al.*, 2007; Nguyen *et al.*, 2016) and is strongly expressed in mesophyll cells, but also in epidermal cells, hydathodes and phloem within the leaf (Nguyen *et al.*, 2016). As CLCc, CLCg has a physiological role in plants during salt stress and both genes act in the same pathway through reciprocal control of their expression (Nguyen *et al.*, 2016).

*At*CLCd was localized to the Golgi apparatus (Fig. 1.9) and is involved in pH regulation in the *trans*-Golgi system (Von der Fecht-Bartenbach *et al*., 2007). *At*CLCf also reside in the Golgi membranes, specifically al the *cis*-Golgi (Fig. 1.9; Marmagne *et al*., 2007). And *At*CLCe is targeted to the thylakoid membranes (Marmagne *et al*., 2007) and to the chloroplast (Fig. 1.9; Teardo et al., 2005). The outer envelope membrane of the chloroplast is considered to be permeable to most ions and metabolites. In contrast, the inner envelope membrane and the thylakoids harbour numerous selective ion and metabolite transport pathways, allowing regulation of optimal metabolic activities and of signaling within this organelle (Eisenhut *et al.*, 2015; Finazzi *et al.*, 2015; Weber and Linka, 2011). CLCe and CLCf are predicted to function as channels rather than transporters based on their amino acid sequences, in particular by substitution of a conserved glutamic acid, implicated in Cl^-/H^+ antiporter activity (Zifarelli and Pusch, 2010).

1.4.4.2. The CCC family

*At*CCC, a member of the cation-chloride-cotransporter (CCC) family in *Arabidopsis*, is a Na^+:K^+:Cl^- cotransporter (NKCC) localized at the plasma membrane of the *trans*-Golgi system involved in plant development and ion homeostasis (Colmenero-Flores *et al*., 2007; Groen *et al*., 2014; Henderson *et al*., 2015). Given that *At*CCC affects root-to-shoot distribution of Cl^- and Na^+ in *A. thaliana* and that promoter GUS fusions of *AtCCC in planta* displayed strong expression in the vasculature at the xylem/symplast boundary (Colmenero-Flores *et al*., 2007), it was proposed to retrieve Cl^- from the xylem. But its localization at the Golgi/*trans*-Golgi network and its strong implication on plant development suggested a function in the Golgi network that impacts plant development and indirectly influences the ability of plants to tolerate high salinity. Probably the CCC family functions as NKCC but further studies to clarify its function in plants should be done.

1.4.4.3. The ALMT family

The ALMT (aluminum-activated malate transporter) protein family is specific to plants (Xu *et al*., 2015) and encodes channels able to mediate anion fluxes across cellular membranes (Barbier-Brygoo *et al*., 2011). The ALMT protein family is constituted of fourteen members in *Arabidopsis* (Hoekenga *et al*., 2006) and the phylogenetic tree is characterized by the presence of three main branches (Fig. 1.10; Kovermann *et al.*, 2007). Recent results show that in clade II, ALMT4, ALMT5, ALMT6 and ALMT9 are localized at the tonoplast, indicating that clade II may consist of vacuolar ALMTs (Martinoia *et al*., 2012). Furthermore, ALMT6 and ALMT9 mediate anion fluxes directed to the vacuolar lumen, i.e., inward-rectifying currents (De Angeli *et al.*, 2013; Kovermann *et al*., 2007; Meyer *et al*., 2011).

The MA^{2-} permeable channel *At*ALMT4 was recently known to be targeted to the vacuolar membrane, and the corresponding gene is highly expressed in leaves and roots. The *atalmt4* knockout mutants exhibited an impairment of drought tolerance compared to wild-type plants (Zhang, 2013), but its function has not been precisely determined so far.

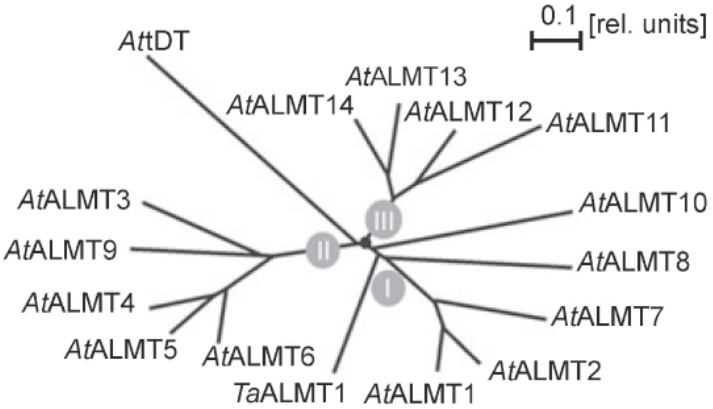

Fig 1.10. *Arabidopsis thaliana* ALMT family phylogenetic tree. The *At*ALMT dendogram presents three main groups. Branch lengths are proportional to the level of interfered evolutionary change and are given in relative units. *Att*DT, *Arabidopsis thaliana* tonoplast dicarboxylate transporter; *Ta*ALMT1, *Triticum aestivum* aluminum-activated malate transporter 1. Obtained from Kovermann *et al*., 2007.

ALMT6 was found to be expressed in *Arabidopsis* guard cells where it was localized to the tonoplast (Meyer *et al*., 2011). It is a hyperpolarization-activated channel permeable to MA^{2-} and fumarate, which is present in guard cells in large quantities. This channel transport MA^{2-} into the vacuole in a Ca^{2+}- and pH-dependent manner (Meyer *et al.*, 2011). A detailed electrophysiological analysis revealed that vacuolar pH and cytosolic malate regulate the threshold of activation of *At*ALMT6-mediated currents. The interplay of these two parameters determines whether *At*ALMT6 functions as a MA^{2-} influx or efflux channel (Meyer *et al.*, 2011).

ALMT9 resides in the vacuolar membrane of mesophyll and guard cells and it is also localized in both shoots and roots. This channel is permeable to MA^{2-} and Cl^-, whereby its physiological function is linked to the Cl^- conductivity (De Angeli *et al*., 2013; Kovermann *et al*., 2007). Differently from ALMT6, ALMT9 is not regulated by cytosolic Ca^{2+} (De Angeli *et al*., 2013). ALMT9-mediated Cl^- currents across the tonoplast are activated by physiological concentrations of cytosolic MA^{2-}, and mesophyll vacuoles of *almt9* knockout mutants lacking the vacuolar channel exhibit lower overall Cl^- currents (De Angeli *et al.,* 2013). Moreover, *ALMT9* channel mediating influx of Cl^- ions into vacuoles is essential for stomatal opening, given that *almt9* plants have reduced Cl^- uptake into vacuoles of guard cells resulting in impaired light-dependent stomatal opening and reduced wilting during drought stress. Recently, Baetz and colleagues (2016) showed that ALMT9 is highly expressed in the vasculature of shoots and roots and is somehow involved in the regulation of long-distance transport of Cl^- and Na^+.

Summarizing, a plenty of metabolite and ion transport systems are found in plastids. Nowadays the protein families that are related with Cl^- transport across the plasma membrane of the vacuole, Golgi apparatus and chloroplasts in *Arabidopsis* are the chloride channel (CLC), the cation-chloride-cotransporter (CCC) and the aluminum-activated malate transporter (ALMT) families (Fig. 1.11). Among these families, the protein channels localized to the tonoplast (ALMT4, ALMT6, ALMT9, CLCa-c and CLCg) regulate Cl^- vacuolar sequestration, encouraging Cl^- homeostasis regulation. But further investigations to better understand their regulation mechanisms and to identify new Cl^- transporters should be done.

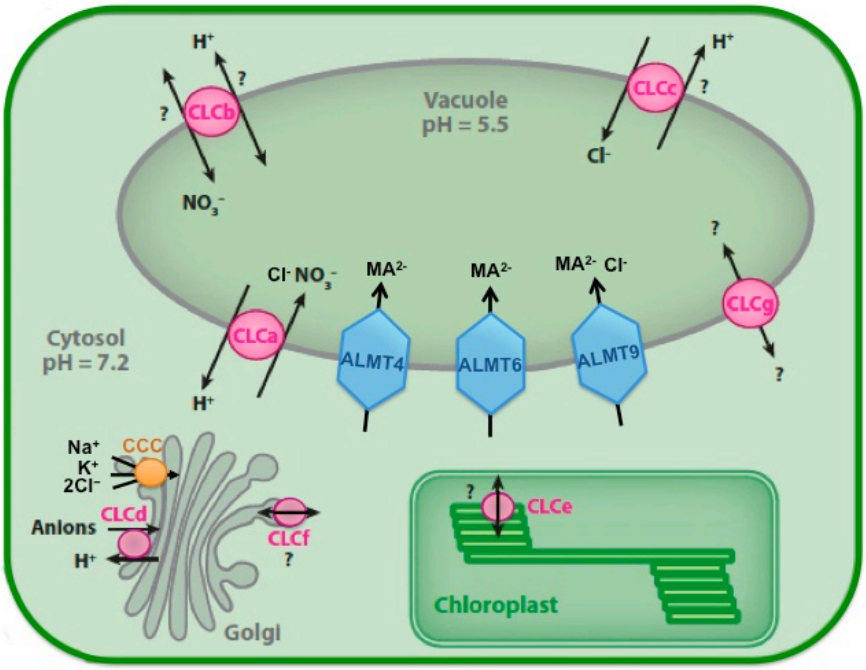

Figure 1.11. Ion channels at intracellular membranes in *Arabidopsis thaliana*. CLCa-c, CLCg and ALMT9 are located in the vacuolar membrane. CLCd and CCC are localized at the *trans*-Golgi network and CLCf is also present at the plasma membrane of the Golgi, specifically al the *cis*-Golgi. And CLCe is located in the chloroplast. Modified from Barbier-Brygoo *et al.*, 2011.

1.5. PLASMA MEMBRANE PROTEINS

Depending on the thermodynamics, plasma membrane proteins that mediate the transport of solutes across biological membranes can be classified in active and passive transporters (Gadsby, 2009).

Active transporters catalyse molecules translocation across cellular membranes against their electrochemical gradient, activity that requires energy input. These transporters can be divided according to their energy source in primary and secondary active transporters (Gadsby, 2009). On the one side, primary active transporters can be energized by ATP hydrolysis (ATP-powered pumps), light and redox reactions that are coupled by the protein to the movement of molecules uphill the electrochemical gradient, like H^+-ATPases (Gadsby, 2009). On the other side, secondary active transporters (carrier proteins) use the electrochemical gradient of a chemical species as an energy source and couple the downhill flux of this species to the movement of a second species against its electrochemical gradient. Thus, the activity of secondary active transporters is not directly driven by ATP hydrolysis but relies on the presence of electrochemical gradients of solutes across cell membranes that are generated and maintained by primary transporters. In higher plant cells, the energy exploited by secondary active transporters is generated by the gradient of H^+ across cellular membranes. Carriers move solutes across membrane by selective binging and significant conformational change. Furthermore, secondary active transporter can be classified into symporters and antiporters. While the symporters transport two substrates in the same direction across the membrane, the antiporters transport the substrates in opposite directions (Gadsby, 2009).

Passive transporters allow the fluxes of molecules across membranes along their electrochemical gradient and are dissipative transport systems. Ion channels are a specific

category of passive transporters. They are integral membrane proteins that form selective aqueous pores through which anions are rapidly transported across cell membranes. Ion channels switch between open and closed states according to the factors that control their gating. When an ion channel is open, massive ion fluxes occur according to their electrochemical gradients. Ion movement across a membrane through ion channels can be measured directly using electrophysiological techniques, as two-electrode voltage clamp (TEVC). The ion channels selectivity depends on the specific interaction between the permeating ionic species and the permeation pore of the channel (Dutzler *et al*., 2002, 2003; Yamashita *et al*., 2005; Zhou *et al*., 2001). Based on their selectivity characteristics, ion channels are traditionally divided into anion and cation channels. In order to fulfil their biological function, their activity is tightly regulated by different parameters such as the membrane potential, ligands, hormones, light and posttranslational modifications like protein phosphorylation (Hille, 2001).

Anion channels are present in all plant membranes, where they are key to a wide spectrum of physiological functions in plants, such as turgor regulation, membrane voltage stabilization, pH regulation, signal propagation, toxic metal tolerance and nutrient acquisition (Barbier-Brygoo *et al*, 2011; Roberts, 2006; Roelfsema *et al,* 2012). Furthermore, plasma membrane channels are responsible for short and long distance net anions fluxes.

1.5.1. Anion channels in plants

Plant anion channels can be broadly classified on the basis of their voltage dependence into depolarization- and hyperpolarization-activated channels and channels activated by light or membrane stretch.

Depolarization-activated anion channels can be subdivided further according to their kinetics and gating properties into Rapid type (R-type), Slow type (S-type), and outwardly rectifying anion channels (Schroeder, 1995; White and Broadly, 2001).

R-type and S-type channels differ in the velocity of their voltage-dependent activation and deactivation and both display the lowest degree of activity at negative membrane potentials (Vm < −150 mV), but are activated when the plasma membrane becomes more positive (depolarizes). The speed of R-type channel activation is approximately 1000 times faster than activation of S-type channels (5–50 ms for R-type *versus* 5–50 s for S-type channels; Kolb *et al.*, 1995; Linder and Raschke, 1992).

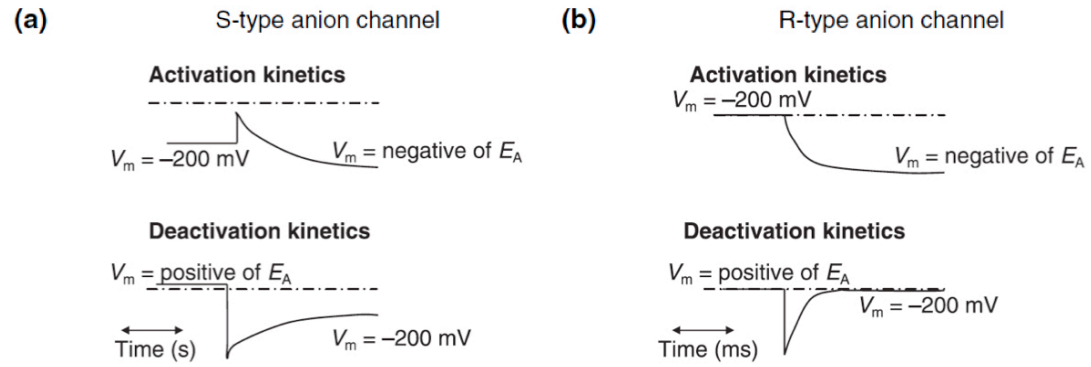

Figure 1.12. Schematic representation of whole-cell activation and deactivation currents for (a) S-type currents and (b) R-type currents. The dashed line represents zero current. E_A, equilibrium potential for the permeant anion; V_m, membrane potential. Obtained from Roberts, 2006.

R-type channels, which display pronounced voltage dependence, are inactive at hyperpolarized membrane potentials but progressively activate upon depolarization (Fig. 1.12 b; Hedrich and Marten, 1993; Kolb *et al.*, 1995). In contrast, S-type channels are only weakly voltage dependent (Fig. 1.12 a). The voltage dependent gating of both anion channel types is strongly modulated by the external anion activity (Dietrich and Hedrich, 1998; Geiger *et al.*, 2009b, 2011; Hedrich and Marten, 1993; Hedrich *et al.*, 1994; Lohse and Hedrich, 1995; Maierhofer *et al.*, 2014b).

The difference between the anion channel types becomes obvious when cells are exposed to a gradual change in membrane potential (from −160 mV to +80 mV) within seconds (voltage ramp; Fig. 1.13). S-type channels facilitate inward (negative) currents (anion efflux) at −160 mV that decrease at more positive potentials and eventually the current reverses the direction (anion influx; Fig. 1.13 a). The current–voltage relation for R-type channels is similar, except for small currents at strongly negative potentials because of fast channel deactivation at these voltages (Fig. 1.13 b; Hedrich and Marten, 1993; Kolb *et al.*, 1995). The R-type channels have a maximum activity at approximately −50 mV and they are rapidly deactivated by hyperpolarization of the plasma membrane.

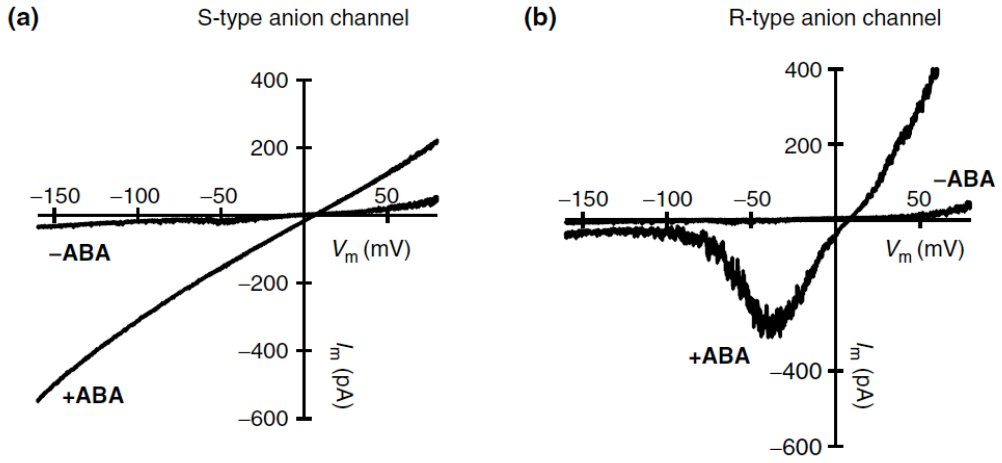

Figure 1.13. Current-voltage relationships of (a) S-type and (b) R-type anion channels in *Vicia faba* guard cell protoplasts in the absence and presence of ABA. The activities of these two types of anion channels are stimulated by the presence of ABA. The S-type anion channel presents a nearly linear current-voltage relationship, indicating weak voltage dependence, whereas the R-type anion channel shows a strong deactivation at membrane potential more negative than −100 mV. ABA, abscisic acid; I_m, current; V_m, voltage across the membrane. Obtained from Roelfsema *et al.*, 2012

Being permeable to the common anions MA^{2-}, NO_3^- and Cl^-, the R-type channel has the peculiarity to be highly permeable also to sulphate. However, S-type channels are highly selective for NO_3^- but they are also permeable, in a lesser extent, to Cl^- (Geiger *et al.*, 2009b, 2011; Schmidt and Schroeder, 1994).

R-type and S -type channels coexist in the plasma membrane of several cell types and their physiological role was elucidated in guard cells using electrophysiological approaches, where R- and S-type channels were respectively named QUAC (for quick anion channel) and SLAC (for slow anion channel). These channels are involved in the early steps of stomatal closure in response to the drought hormone abscisic acid (ABA; section 1.5.2.2; Barbier-Brygoo *et al.*, 2011; Dreyer *et al.,* 2012).

In 2008 the molecular nature of the guard cell slow anion channel was uncovered and the gene encoding for this transporter was named *SLAC1* (section 1.5.1.2; Negi *et al.*, 2008; Saji *et al.*, 2008; Vahisalu *et al.*, 2008), whereas the R-type channel is encoded by *ALMT12*, a member of the aluminum-activated malate transporter family (Meyer *et al.*, 2010; Sasaki *et al*., 2010).

1.5.1.1. The R-type channel ALMT12

The first gene encoding a R-type channel or QUAC was identified in a screen for guard cell localized members of the ALMT channel family (section 1.4.4.3).

The aluminum-activated malate transporter (ALMT) family participates in Cl^- and MA^{2-} transport (De Angeli *et al.*, 2013; Kovermann *et al.,* 2007; Sasaki *et al*. 2004), in addition to play key roles in the aluminium resistance response, where plants release organic acids, including MA^{2-} and citrate from their roots, to chelate free aluminium in acidic soils (Kochian *et al*., 2004; Ma *et al*., 2001; Sasaki *et al*. 2004).

ALMT12 (also named *QUAC1*), which belongs to clade III of the ALMT family (Fig. 1.10; Kovermann *et al.*, 2007), is expressed basically in guard cells but also in the mesophyll of *Arabidopsis*. ALMT12 is located at the plasma membrane and shows a MA^{2-}-dependent R-type channel activity (Meyer *et al.*, 2010). T-DNA insertion mutants of *AtALMT12* were impaired in stomatal closure in response to darkness, CO_2, ABA and Ca^{2+} (Meyer *et al*., 2010; Sasaki *et al*., 2010). This channel is permeable to Cl^-, NO_3^-, MA^{2-} and sulphate, suggesting a role in anion release from guard cells during stomatal closure (Meyer *et al*., 2010; Sasaki *et al*., 2010).

Nowadays, *At*ALMT12 is the major component of the ABA-activated R-type anion current and is regulated by protein phosphorylation (Meyer *et al*., 2010). A bimolecular fluorescence complementation (BiFC) assay confirmed that OST1 and ALMT12 exhibit a direct protein-protein interaction and that the ALMT12-mediated current was activated by OST1 when they were heterologously coexpressed in *Xenopus* oocytes. This protein-protein interaction results in the OST1-mediated phosphorylation of ALMT12 and its consequently activation (Imes *et al.*, 2013).

Interestingly, *ALMT12* expression was also found in pollen grains (Gutermuth *et al*., 2013) and in root stelar cells, similarly to *ALMT9* (section 1.4.4.3; Sasaki *et al*., 2010). Therefore, it is a good candidate for being a channel that catalyses Cl^- xylem loading, although its role in this process has not been yet examined.

1.5.1.2. The S-type anion channel family SLAC/SLAH

1.5.1.2.1. The SLAC/SLAH family in *Arabidopsis*

The NO_3^- and Cl^- conductance of xylem parenchyma cells registered by early patch clamp studies are reminiscent to electrical characteristics of anion channels from the SLAC/SLAH (slow-type) family (Negi *et al*., 2008; Vahisalu *et al*., 2008).

In *Arabidopsis*, this family of S-type anion channels consists of five members (Fig. 1.14; Brumós *et al*., 2010; Negi *et al*., 2008). The phylogenetic tree of the SLAC protein family is characterized by the presence of two main branches that separate the *Arabidopsis* guard cell anion channel SLAC1 and SLAH2 (SLAC1 homolog 2) and SLAH3 (SLAC1 homolog 3) proteins

from the highly homologous family members SLAH1 and SLAH4 (Brumós *et al.*, 2010; Dreyer *et al.*, 2012; Zheng *et al.*, 2015).

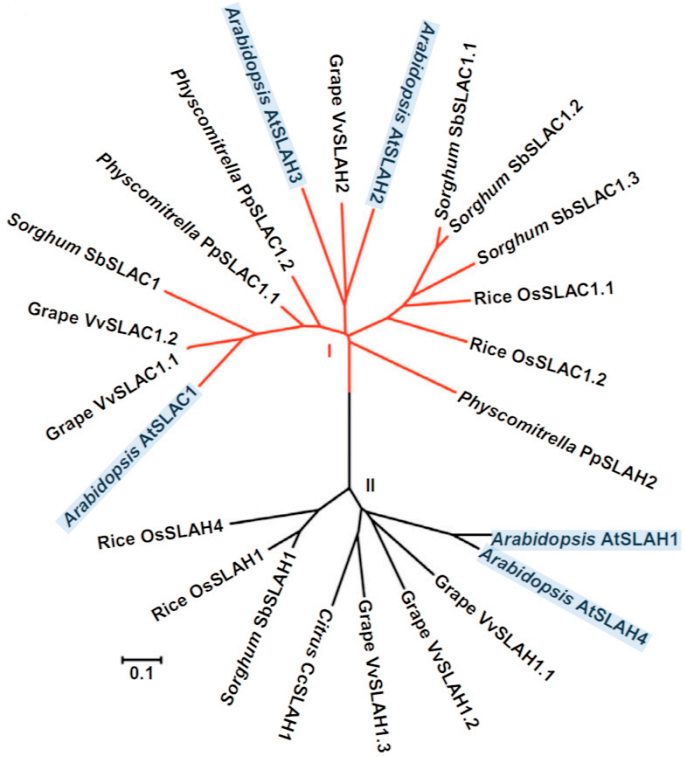

Figure 1.14. SLAC/SLAH family phylogenetic tree from different species. *Arabidopsis thaliana* genes are highlight in blue. Modified from Brumós *et al.*, 2010.

1.5.1.2.2. *SLAC/SLAH* gene expression and protein localization

In vegetative organs, *AtSLAC1* gene expression is limited to guard cells, present in photosynthetic tissues (Fig. 1.15; Geiger *et al.*, 2011; Negi *et al.*, 2008; Zheng *et al.*, 2015). *SLAH3* is also expressed in guard cells (Fig. 1.15; Geiger *et al.*, 2011; Zheng *et al.*, 2015) and, together with SLAC1, both proteins represent the anion release pathway required for stomatal closure in response to ABA (Geiger *et al.*, 2009b, 2011).

Moreover, *SLAH3* is also expressed in mesophyll cells (Fig. 1.15; Demir *et al.*, 2013; Geiger *et al.*, 2011), in pollen grains and in pollen tubes within the pistil of *Arabidopsis* (Gutermuth *et al.*, 2013).

Nevertheless, all SLAC1-homologous genes, included SLAH3, exhibit significant gene expression in the root (Fig. 1.15; Maierhofer *et al.*, 2014b; Negi *et al.*, 2008; Zheng *et al.*, 2015). *AtSLAH2*, the closest homologue of SLAH3 (Dreyer *et al.*, 2012), is expressed in the root stele (Fig. 1.15; Maierhofer *et al.*, 2014b; Negi *et al.*, 2008; Zheng *et al.*, 2015).

Expression patterns observed with the β-Glucuronidase (GUS) reporter gene driven by *SLAH1* or *SLAH4* gene promoters suggest that both are also expressed in the root vascular cylinder (Fig. 1.15; Negi *et al.*, 2008; Zheng *et al.*, 2015).

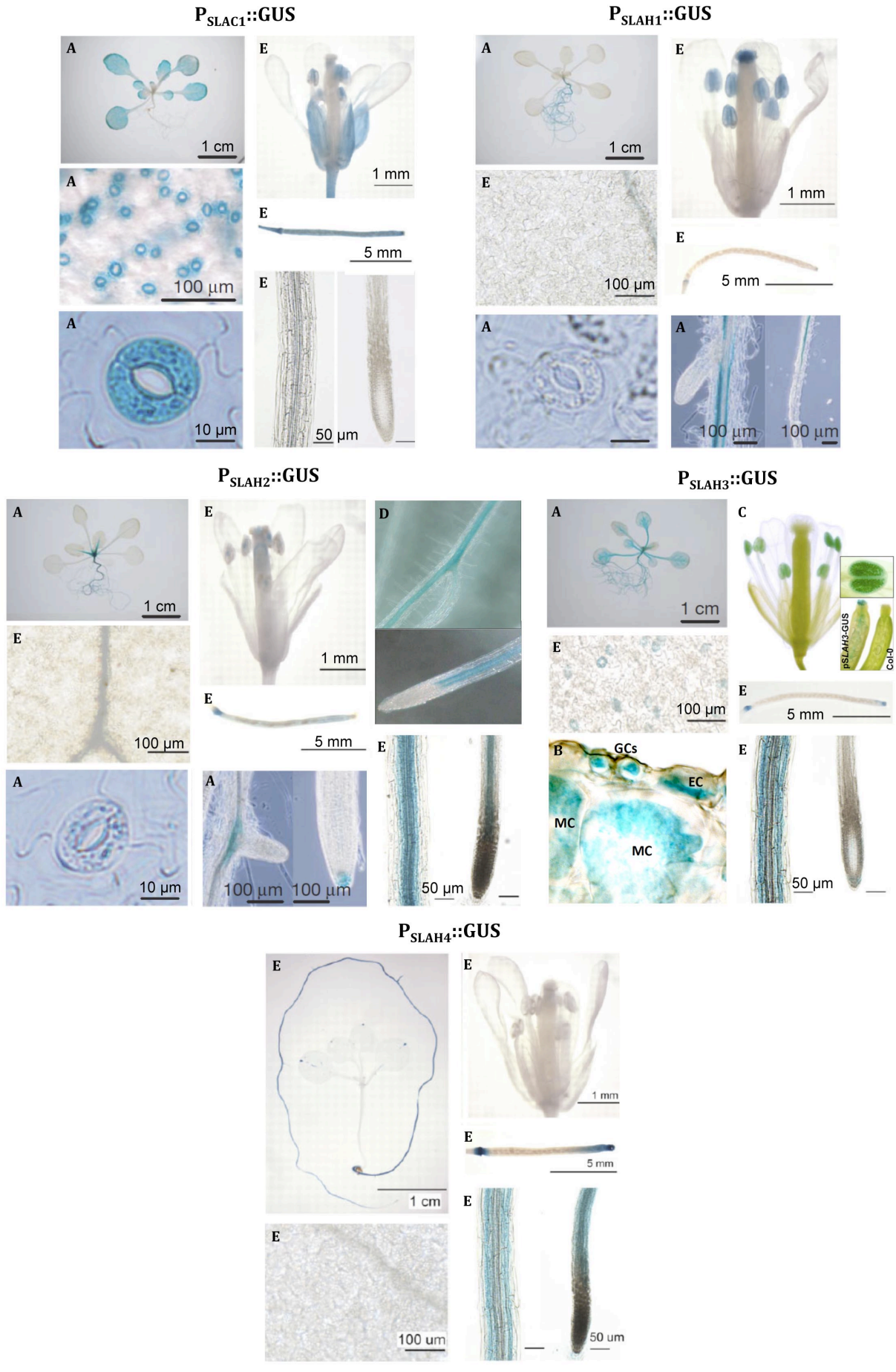
P SLAC1 ::GUS
P SLAH1 ::GUS
P SLAH2 ::GUS
P SLAH3 ::GUS
P SLAH4 ::GUS
A
E
D
B
C
1 cm
1 mm
5 mm
100 µm
10 µm
50 µm
GCs
EC
MC
pSLAH3-GUS
Col-0

Figure 1.15. Localization of SLAC/SLAH genes expression. Histochemical β-Glucuronidase (GUS) staining of transgenic plants expressing the GUS reporter gene under the control of the SLAC/SLAH gene promoters. *AtSLAC1* is expressed mainly in guard cells. Expression of *AtSLAH1* gene occurred in the vascular system of roots. *AtSLAH2* is expressed in the root. *AtSLAH3* expression was confined to guard cells, mesophyll cells, pollen grains, pollen tubes in the flower and roots. Expression of *AtSLAH4* gene was localized basically in the root. EC, epidermal cell; GCs, guard cells; MC, mesophyll cell. Modified from different works. Letter correspond to the literature reference: A, Negi *et al*., 2008; B, Geiger *et al*., 2011; C, Gutermuth *et al*., 2013; D, Maierhofer *et al*., 2014b; E, Zheng *et al*., 2015.

SLAC1 channel was located in the plasma membrane (Fig. 1.16; Negi *et al*., 2008; Vahisalu *et al*., 2008), as well as their homologues SLAH1, SLAH2 and SLAH3 (Fig. 1.16; Negi *et al*., 2008). SLAH4 protein localization has not been confirmed yet.

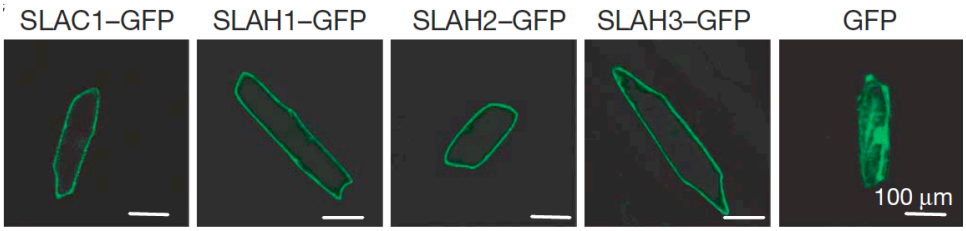

Figure 1.16. Plasma membrane localization of SLAC/SLAH proteins. Transient expression of green fluorescent protein (GFP) fluorescence regulated by SLAC/SLAH gene promoters in onion localizes the plasma membrane as the subcellular localization of these channels. Obtained from Negi *et al*., 2008.

1.5.1.2.3. Structure and functional characterization

Regarding the gene structure of the *Arabidopsis* SLAC/SLAH protein family, the most outstanding feature distinguishing both phylogenetic groups is the lack of the 5' Exon in *SLAH1* and *SLAH4* genes, encoding for long cytosolic N-terminal moieties (Fig. 1.17; Chen *et al*., 2010; Dreyer *et al*., 2012; Negi *et al*., 2008). In SLAC1 and SLAH3 channels, this protein domain contains the phosphorylation sites regulating ABA activation in guard cells (Fig. 1.17; Geiger *et al*., 2009b, 2010, 2011; Lee *et al*., 2009; Maierhofer *et al*., 2014a). The C-terminal moiety of SLAC1 is also a regulated phosphorylation site (Geiger *et al*., 2009b; Lee *et al*., 2009). In addition, *SLAH1* and *SLAH4* genes contain shorter C-terminal domains at the 3' Exon (Fig. 1.17; Chen *et al*., 2010; Dreyer *et al*., 2012; Negi *et al*., 2008; Vahisalu *et al*., 2010).

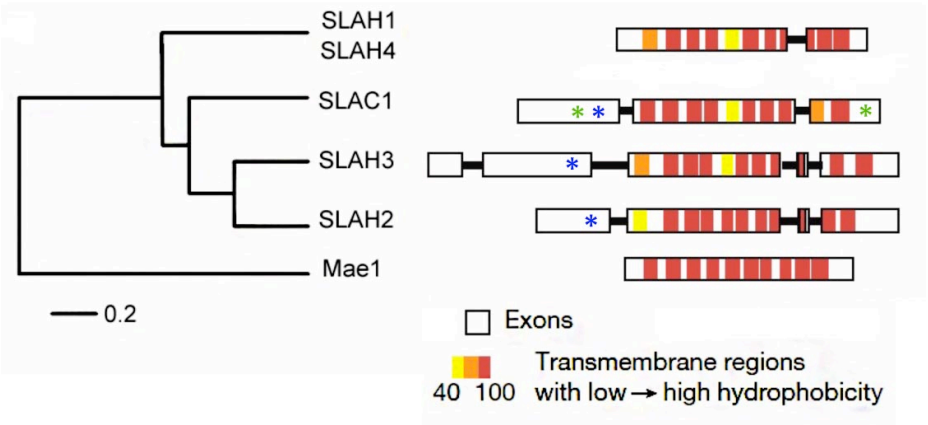

Figure 1.17. SLAC/SLAH genes genomic structure. Blue asterisks indicate CPKs phosphorylation sites and green asterisks indicate OST1 phosphorylation sites. Mae1, member of the C4-docarboxylate (TDT) transporter family in *Schizosaccharomyces pombe*. Modified from Negi *et al*., 2008.

Concerning the SLAC/SLAH channel topology, SLAC1 shares homology to the tellurite-resistance/C4-dicarboxylate (TDT) transporters expressed in bacteria, archaea, and fungi. Using as a template the crystal structure of HiTehA channel, a member of this family from *Haemophilus influenza*, a molecular model of the three-dimensional structure of the SLAC1 channel was calculated (Fig. 1.18; Chen *et al.*, 2010). SLAC1 channels are trimers composed of quasi-symmetrical subunits (Fig. 1.18 b). Each subunit has 10 transmembrane (TM) helices (Fig. 1.18 a) arranged from helical hairpin pairs to form an inner five-helix TM pore (Fig. 1.18 b) with a central conserved phenylalanine (Phe) residue (F450) located on TM9 that represents the anion gate and blocks the pore (Fig. 1.18 a, c; Chen *et al.*, 2010; Dreyer *et al.*, 2012). Indeed, mutation of the pore Phe by replacing this residue by alanine (F450A) led to a constitutively open anion conductance in SLAC1, even in the absence of functional kinases (Chen *et al.*, 2010). This residue is conserved in the entire SLAC/SLAH protein family (Chen *et al.*, 2010; Dreyer *et al.*, 2012).

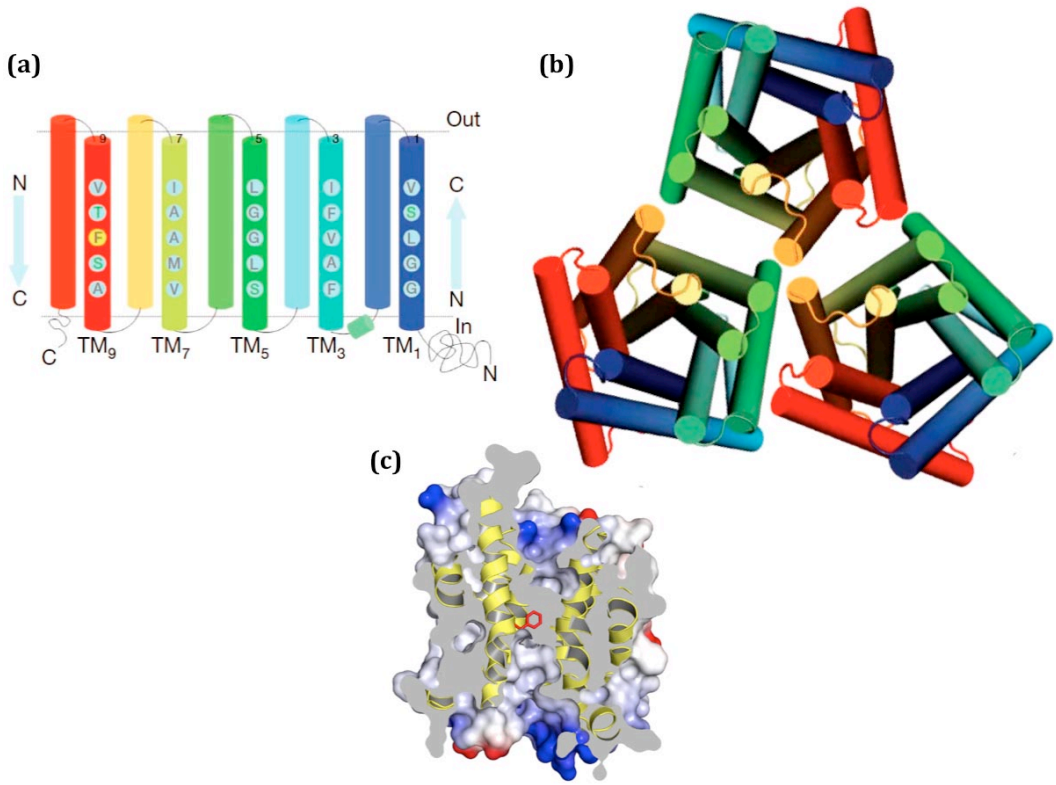

Figure 1.18. Homology model for *At*SLAC1 channel. (a) Rolled-open structure of the channel spectrally coloured from blue at its N terminus to red at its C terminus. The channel has ten transmembrane (TM) regions. The yellow background highlights the conserved phenylalanine (F). **(b)** Three channel modules assemble into a trimeric structure. **(c)** Cross-section through the channel homology model with the electrostatic potential shown on the external surface of the molecular envelope. The side chain of the phenylalanine (red) is shown on the backbone ribbon (yellow). Modified from Chen *et al.*, 2010.

In addition, the SLAH2 three-dimensional (3D) homology model was also generated based on the crystal structure of Hi-TehA (Maierhofer *et al.*, 2014b). The conserved side chain of the gating Phe in SLAH2 (F402) was located in the middle of the pore, as described previously for SLAC1 (Chen *et al.*, 2010), and mutation of this Phe by replacing this residue by alanine (F402A) also led to a open channel conductivity that no longer requires activation by protein kinase, although the presence of extracellular NO_3^- was still required (Maierhofer *et al.*, 2014b).

So far, only SLAC1, SLAH2 and SLAH3 anion channels have been partially characterized in *Arabidopsis thaliana* and/or in heterologous *Xenopus* oocyte expression system (Brandt *et al.*,

2012; Demir *et al.*, 2013; Geiger *et al.*, 2009b, 2010, 2011; Lee *et al.*, 2009; Maierhofer *et al.*, 2014a, 2014b).

These SLAC/SLAH family channels are regulated by distinct protein kinases (Brandt *et al.*, 2012; Geiger *et al.*, 2009b, 2010, 2011; Lee *et al.*, 2009; Maierhofer *et al.*, 2014a, 2014b; Scherzer *et al.*, 2012).

SLAC1 is activated by phosphorylation through the protein kinase OST1 (also named SnRK2.6; Fig. 1.19; Geiger *et al.*, 2009b; Lee *et al.*, 2009) from the Snf–1 related protein kinase type-2 (SnRK2) family and, together with SLAH3, by Ca^{2+}-dependent kinases from the calcium-dependent protein kinase (CPK**;** Figs. 1.19 and 1.20) family and the CBL-interacting protein kinase (CIPK) family (combined with its interacting calcineurin B–like (CBL) calcium sensor) at its N-terminal domain (Fig. 1.20; Geiger *et al.*, 2010, Maierhofer *et al.*, 2014a; Scherzer *et al.*, 2012).

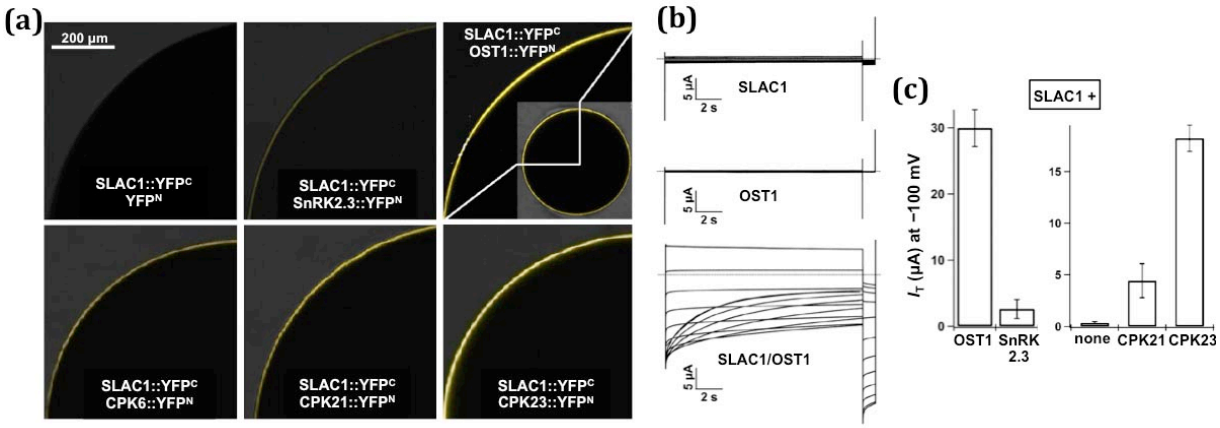

Figure 1.19. Regulation of SLAC1 activity by different kinases. (a) Bimolecular fluorescence complementation (BiFC) experiments in *Xenopus* oocytes identified interacting proteins with SLAC1. Pictures show a quarter of an optical slice of an oocyte and depict fluorescence in the plasma membrane. The coinjected plasmids combinations are indicated in the figure. BiFC assays revealed that SLAC1 physically interacts with SnRK2.3, OST1 (SnRK2.6), CPK6, CPK21 and CPK23. **(b)** Whole-oocyte current recordings in standard bath solution (30 mM Cl^-, pH 5.6) upon 15 s voltage pulses ranging from +40 to −180 mV in 20 mV decrements followed by a 3 s voltage pulse to −120 mV. The holding potential was 0 mV. No current responses of oocytes expressing SLAC1 or OST1 alone were recorded. Only coexpression of SLAC1 together with OST1 resulted in macroscopic anion currents slowly deactivating at negative membrane potentials. **(c)** SLAC1 Instantaneous currents (I_T) following a preactivation voltage pulse at −100 mV in standard bath solution. OST1 coexpression with SLAC1 resulted in the largest anion currents. SLAC1 expression alone (indicated as none) did not result in macroscopic anion currents. YFP^C, C-terminal half of the YFP fused to the protein; YFP^N, N-terminal half of the YFP fused to the protein. Modified from Geiger *et al.*, 2009b, 2010.

SLAC1 plays an essential role in stomatal closure in response to CO_2, ABA, ozone, darkness, humidity reduction, Ca^{2+}, hydrogen peroxide (H_2O_2), and nitric oxide (NO; Negi *et al.*, 2008; Vahisalu *et al.*, 2008). SLAH3 is also involved in stomatal closure upon drought stress (section 1.5.2.2.2; Geiger *et al.*, 2011)

In addition to its phosphorylation, SLAH3 requires the presence of extra-cellular NO_3^- to gate S-type channel open (Fig. 1.20 b; Geiger *et al.*, 2011; Maierhofer *et al.*, 2014a). Nitrate shifts the voltage dependent gate of SLAH3 to the resting potential of guard cells and thereby activates SLAH3. Nitrate thus functions as a substrate as well as a gate opener of SLAH3 (Geiger *et al.*, 2011). Both SLAC1 and SLAH3 channels differ in their biophysical properties, although both are

permeable to NO_3^- and Cl^-. In comparison to SLAC1, SLAH3 exhibits a higher preference for NO_3^-, being the permeability $P(NO_3^-)/P(Cl^-)$ ratio of 10 for SLAC1 (Geiger *et al.*, 2009b) and of 20 for SLAH3 (Geiger *et al.*, 2011).

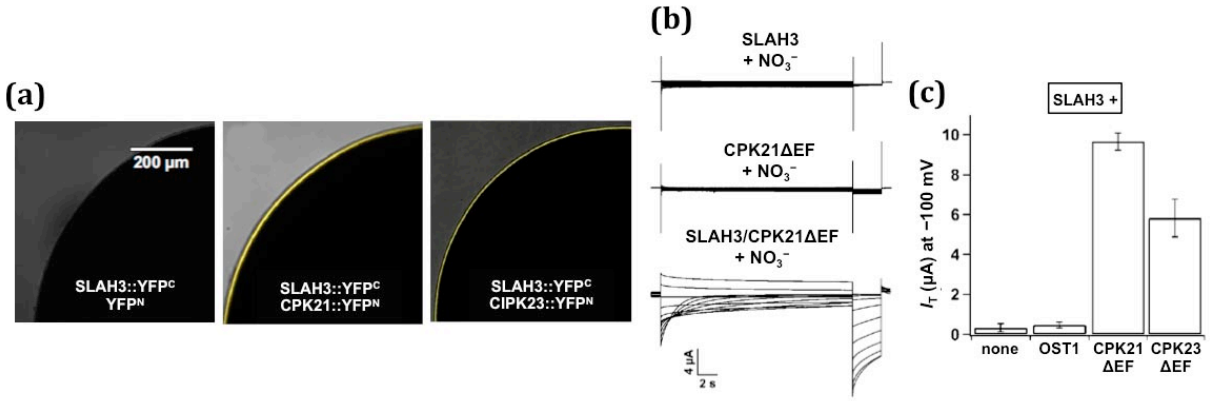

Figure 1.20. Regulation of SLAH3 activity by different protein kinases. (a) BiFC-based interaction of SLAH3 and its regulatory components in *Xenopus* oocytes. Pictures show a quarter of an optical slice of an oocyte and depict fluorescence in the plasma membrane. The coinjected plasmids combinations are indicated in the figure. BiFC experiments revealed that SLAH3 physically interacts with CPK21 and CIPK23. **(b)** Whole-oocyte current recordings in standard bath solution (3 mM NO_3^-, pH 7.5) upon 20 s voltage pulses ranging from +40 to −180 mV in 20 mV decrements followed by a 3 s voltage pulse to −120 mV. The holding potential was 0 mV. No current responses of oocytes expressing SLAH3 or CPK21ΔEF alone were recorded. Coexpression of SLAH3 together with CPK21ΔEF resulted in macroscopic anion currents slowly deactivating at negative membrane potentials in the presence of NO_3^- only. **(c)** Instantaneous currents (I_T) recorded at −100 mV of oocytes expressing SLAH3 in the presence of OST1, CPK21ΔEF and CPK23ΔEF in NO_3^--based buffer. SLAH3 expression alone (indicated as none) did not result in macroscopic anion currents. CPK21ΔEF and CPK23ΔEF are truncated CPKs variant lacking a junction and Ca^{2+}-binding domain, which renders these kinases Ca^{2+}-independent and constitutively active to avoid the influence of different kinase-specific Ca^{2+} sensitivities on SLAH3 activation. YFP^C, C-terminal half of the YFP fused to the protein; YFP^N, N-terminal half of the YFP fused to the protein. Modified from Geiger *et al.*, 2011 and Maierhofer *et al.*, 2014a.

Upon ABA activation, SLAC1 and SLAH3 release NO_3^- and Cl^- in a concerted action in the plasma membrane of guard cells (section 1.5.2.2.2; Geiger *et al.*, 2011; Negi *et al.*, 2008; Vahisalu *et al.*, 2008).

Besides its localization in guard cells, *SLAH3* was also shown to be expressed in the root (Negi *et al.*, 2008; Zheng *et al.*, 2015), where it was recently shown that plays a role in NO_3^--dependent alleviation of NH_4^+ toxicity (Zheng *et al.*, 2015).

Similar to SLAH3, SLAH2 for becoming active requires phosphorylation at its N-terminal domain by a Ca^{2+}-dependent kinase for channel priming and the presence of NO_3^- in the extracellular space to gate open (Fig. 1.21). Unlike SLAC1 and SLAH3, which are permeable to NO_3^- and Cl^-, SLAH2 is strictly NO_3^- selective, considering that it has a permeability $P(NO_3^-)/P(Cl^-)$ratio of 82.4 (Maierhofer *et al.*, 2014b).

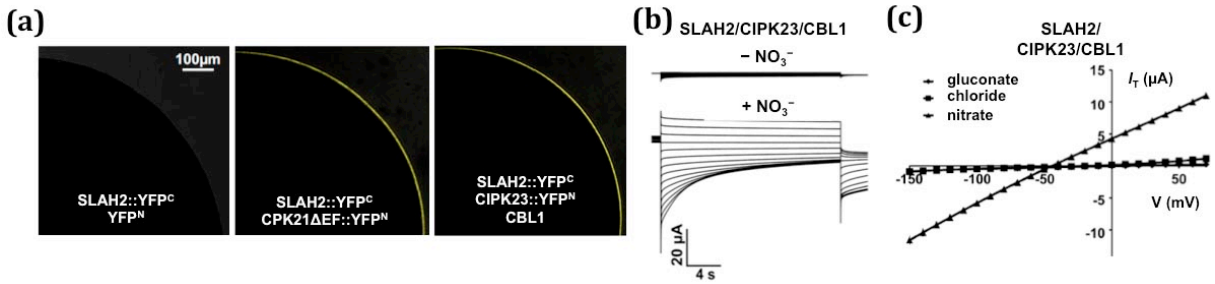

Figure 1.21. Regulation of SLAH2 activity by different kinases. (a) BiFC experiments in *Xenopus* oocytes identified interacting proteins with SLAH2. Pictures show a quarter of an optical slice of an oocyte and depict fluorescence in the plasma membrane. The coinjected plasmids combinations are indicated in the figure. BiFC assays revealed that SLAH2 physically interacts with CPK21 and CIPK23. **(b)** Whole-oocyte current recordings in the presence or absence of 30 mM $NaNO_3^-$ upon 20 s voltage pulses ranging from +40 to −180 mV in 20 mV decrements followed by a 3 s voltage pulse to −120 mV. The holding potential was 0 mV. Cooexpression of SLAH2 together with CIPK23/CBL1 in oocytes resulted in macroscopic anion currents in the presence of external NO_3^- only. The currents slowly deactivated at negative membrane potentials. **(c)** Instantaneous currents (I_T) of oocytes in standard buffers containing different anions (gluconate, chloride or nitrate) plotted against the applied voltage. Nitrate was required in the extracellular bath solution for ion conduction. CPK21ΔEF, truncated CPK variant lacking a junction and Ca^{2+}-binding domain, which renders this kinase Ca^{2+}-independent and constitutively active to avoid the influence of different kinase-specific Ca^{2+} sensitivities on SLAH2 activation. YFP^C, C-terminal half of the YFP fused to the protein; YFP^N, N-terminal half of the YFP fused to the protein. Modified from Maierhofer *et al.*, 2014b.

Interestingly when expressed in *slac1-2* loss-of-function mutant under the control of the SLAC1 promoter, SLAH1 was capable to rescue the SLAC1 stomatal phenotype (Negi *et al.*, 2008), suggesting that this S-type channel isoform might carry SLAC1-like anion transport properties. However, the physiological role of SLAH1 and SLAH4 *in planta* and their functional characterization in heterologous expression system remain unexplored so far.

1.5.2. Hormonal regulation and signal transduction by ABA

There are similarities between xylem loading and stomatal closure, considering that both are mechanisms that implicate ion efflux and are regulated by ABA. However, whereas ABA triggers SLAC1 and SLAH3 channel activation (opening) in guard cells, the stress phytohormone negatively regulates ion channel activities implicated in root-to-shoot translocation of Cl^- (Gilliham and Tester, 2005). This indicates that the regulation of Cl^- ion efflux from cells surrounding the xylem and stomatal guard cell is opposite, suggesting the possibility that different signalling elements are involved in both processes

1.5.2.1. ABA inhibits salt translocation into the xylem

While little is known about the genes and proteins responsible for Cl^- loading into the root xylem apoplast, more is known about the biological processes involved. ABA was shown to significantly inhibit xylem loading of Cl^-, as well as K^+, while having a limited effect on the initial uptake of these ions from the external medium (Cram and Pitman, 1972; Pitman, 1977; Pitman and Wellfare, 1978; Pitman *et al.*, 1974). Therefore, abiotic stress leads to a reduced delivery of both Cl^- and K^+ ions to the shoot and their accumulation in the root (Cram and Pitman, 1972; Pitman, 1977; Pitman *et al.*, 1974). The inhibition of ion transport following water stress by ABA could facilitate the observed increases in the osmotic potential, sustaining root growth.

Two *Arabidopsis* root K^+ channels, AKT1 and the stelar K^+ outwardly-rectifying channel SKOR, have been identified as being involved in K^+ uptake from the soil solution and K^+ release into the xylem sap, respectively (Gaymard *et al*., 1998; Hirsch *et al*., 1998; Lagarde *et al*., 1996; Xu *et al*., 2006). While SKOR is down-regulated by ABA at both transcriptional and posttranslational level (Gaymard *et al*., 1998; Roberts, 1998; Roberts and Snowman, 2000), the *AKT1* expression in the root cortex was unaffected by this hormone (Roberts and Snowman, 2000).

In addition, the root stele NO_3^- transporter *AtNRT1.5* (*At*NPF7.3) gene expression is decreased in response to salt stress, decreasing NO_3^- translocation to shoot (Taochy *et al.*, 2015).

The *AtNPF2.4* gene, which encodes for a transporter possibly involved in Cl^- delivery into xylem vessels, was also down-regulated by salt and ABA treatment (Li *et al.*, 2016).

Therefore, down-regulation of genes expressed in vascular tissues following ABA application, water deficit or salt exposure can be used as a framework to identify proteins that regulate Cl^- loading into the root xylem.

1.5.2.2. ABA triggers salt efflux from guard cells

In response to external or internal stimuli, including light, humidity, Ozone or CO_2 concentration, phytohormones, drought and long-distance signals from the root, turgor changes within guard cells promote stomatal movement to regulate the uptake of CO_2 and the transpirational water loss from leaves (Assmann and Shimazaki, 1999; Hetherington and Woodward, 2003; Raschkle, 1987; Roelfsema and Hedrich, 2005; Schroeder *et al*., 2001b).

Stomatal opening and closure are regulated through the changes in guard cells turgor, which are the consequence of osmolyte concentration changes within the cytosol (Fischer, 1968; Pandey *et al.*, 2007). Solute influx and efflux take place through plasma and vacuolar membrane ion channels and transporters, given that there are not plasmodesmata within mature guard cells (Kim *et al*., 2010; Pandey *et al*., 2007; Wille and Lucas, 1984). The major active solutes involved in these processes are K^+, Cl^-, MA^{2-}, NO_3^- and other metabolites like sugars (Humble and Raschke 1971; MacRobbie and Lettau 1980; Poffenroth *et al.,* 1992; Talbort and Zeiger, 1998). Considering that osmolytes and water are accumulated in the vacuole, all fluxes are coupled between the tonoplast and the plasma membrane (Belin *et al.*, 2010; Ward *et al.*, 1995).

1.5.2.2.1. Stomatal opening

Guard cells keep a cytoplasmic pH of 7.5−7.8, at which the H^+-ATPase presents a low activity. Stomatal opening is initiated by the activation of the membrane H^+-ATPases by blue light, red light or auxins (Fig. 1.22; Assmann *et al*., 1985; Schroeder *et al.*, 2001; Shimazaki *et al*., 1986). The H^+-ATPases cause a hyperpolarization of the plasma membrane potential through the H^+ efflux from the cytoplasm to the apoplast (Assmann *et al*., 1985; Kinoshita and Shimazaki, 1999; Shimazaki *et al*., 1986, 2007).

This hyperpolarization activates inward rectifying K^+ channels, such as KAT1 (K^+ channel in *Arabidopsis thaliana* 1) and KAT2 (K^+ channel in *Arabidopsis thaliana* 2), which induce the passive influx of K^+ from the apoplast to the cytoplasm (Fig. 1.22; Lebaudy *et al*., 2007; Pilot *et al*., 2001; Wang and Wu, 2013). During stomatal opening, guard cells accumulate Cl^-, NO_3^- and

MA^{2-} as counterions of K^+ (Van Kirk and Raschke, 1978). Presumably Cl^- and NO_3^- enter into the cell by symport with apoplastic H^+, given the outward-directed anion gradient and the negative membrane potential of plant cells (Dietrich *et al.*, 2001; Roelfsema and Hedrich, 2005). For example, the NO_3^-/H^+ symporter *At*NRT1.1 (also known as CHL1 and recently named as *At*NPF6.3; Léran *et al.*, 2014) mediates NO_3^- influx from the apoplast to the cytoplasm (Fig. 1.22; Guo *et al.*, 2003; Tsay *et al.*, 1993).

In guard cells, K^+ is accumulated in the vacuole by H^+/K^+ antiporters, and anions can be transported into vacuoles through low-affinity anion channels and H^+/anion exchange mechanisms. The vacuolar antiporter K^+/H^+ *At*NHX1 plays an important role in K^+ uptake into the vacuole (Fig. 1.22; Barragán *et al.*, 2012; Leidi *et al.*, 2010; Shi and Zhu, 2002). The Cl^- channels CLCa and CLCc play a key role in stomatal function, in the stomatal opening as well as in the stomatal closure. On the one side, CLCa drives the uptake of Cl^- and NO_3^- into the vacuole during stomata opening (Fig. 1.22; Wege *et al.*, 2014). On the other side, light-induced stomatal opening was impaired in *AtCLCc* T-DNA mutants (Jossier *et al.*, 2010), indicating that CLCc participates in vacuolar Cl^- compartmentalization during stomatal opening.

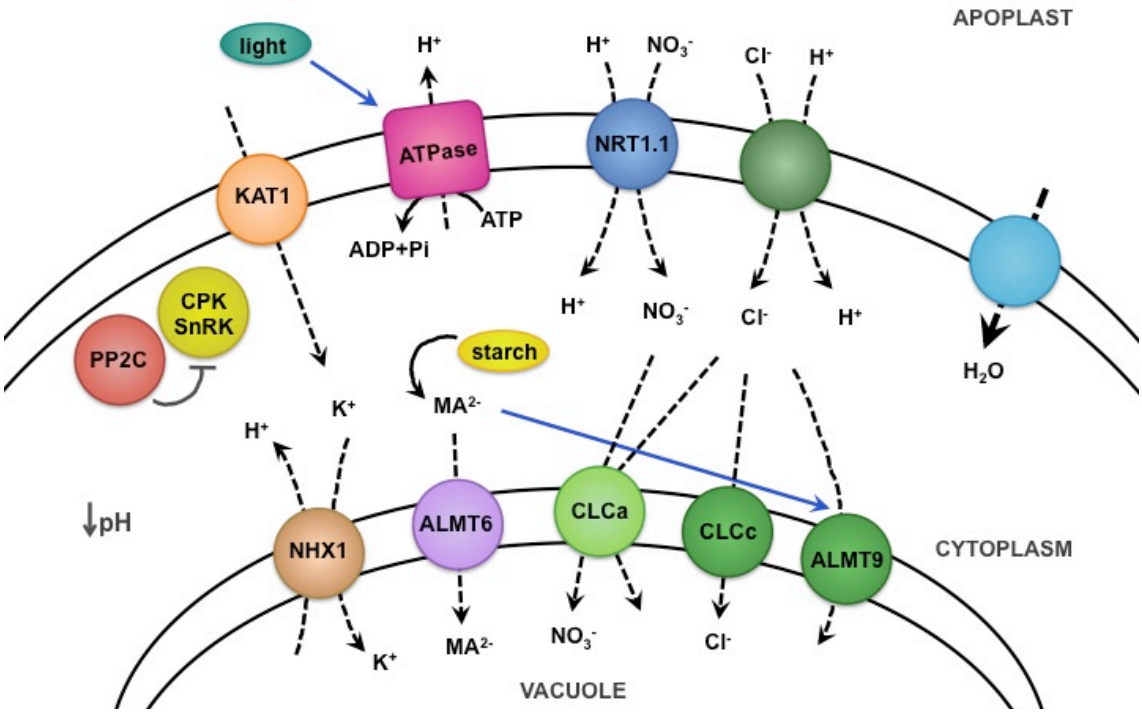

Figure 1.22. Guard cell signaling during stomatal opening. Blue arrows indicate activation or positive interactions between the factors. Grey arrows indicate inhibition. Dashed arrows indicate ion movement. ALMT, aluminum-activated malate transporter; CLC, chloride channel; CPK, Ca^{2+}-dependent protein kinase; KAT1, K^+ channel in *Arabidopsis thaliana* 1; NHX1, Na^+/H^+ exchanger 1; NRT1.1, nitrate transporter 1; PP2C, protein phosphatase 2C; SnRK, Snf–1 related protein kinase.

Taken into account that the R-type channel ALMT6 is activated by hyperpolarization and that vacuolar pH and cytosolic MA^{2-} regulate its activation threshold (Meyer *et al.*, 2011), ALMT6 will be probably induced, and subsequently MA^{2-} transport into the vacuole will take place (Fig. 1.22). Similarly, physiological concentrations of cytosolic MA^{2-} activate ALMT9, which is known to mediate Cl^- currents across the tonoplast directed to the vacuolar lumen (Fig. 1.22; De Angeli *et al.*, 2013).

Rise of K^+, Cl^- and NO_3^-, together with the production of MA^{2-} from osmotically inactive starch, increase the osmotic potential (Fischer, 1968). This process decreases the water

potential, driving water into the cells that increase their turgor pressure, thus leading to the swelling of guard cells and to the concomitant aperture of the stomata.

During stomatal opening the type-2C protein phosphatase (PP2C) ABI1, ABI2 and HAB1 interact with different protein kinases, such as OST1, SnRK2.2, SnRK2.3, CPK3, CPK6, CPK21 and CPK23, supressing their activity by dephosphorylation (Fig. 1.22; Fujii *et al.*, 2009; Imes *et al.*, 2013; Scherzer *et al.*, 2012; Umezawa *et al.*, 2009; Vlad *et al.*, 2009). In addition, ABI1 also interacts and desphosphorilates the N-termini of SLAC1 channel (Maierhofer *et al.*, 2014a).

As a consequence of CPK and SnRK dephosphorylation, a number of downstream protein effectors involved in triggering the stomatal closure remain deactivated, like S-type, R-type and CLCa channels and the NADPH oxidase involved in ROS production.

1.5.2.2.2. Stomatal closure

Water deficit, under drought and high salinity conditions, leads to the synthesis of the plant stress hormone ABA. This phytohormone is perceived by guard cells, although its origin is controversial. This hormone could travel from the roots to the aerial parts through the transpiration stream via the xylem (Sauter e*t al.*, 2001; Tardieu and Davies, 1993; Wilkinson and Davies, 2002; Wilkinson *et al.*, 2007; Zhang *et al.*, 1987) or ABA could be released from internal stores (Georgopoulou and Milborrow, 2012) or newly synthesized in leaves (Bauerle *et al.*, 2003, 2004; Bauer *et al.*, 2013a, b; Christmann e*t al.*, 2007; McAdam and Brodribb, 2015; McAdam *et al.*, 2016).

In guard cells, ABA triggers a fast response and a slow response. On the one side, the fast response lead to the stomatal closure within seconds or a few minutes through the activation of S-type and R-type anion channels (Roelfsema *et al*., 2004) and the repression of inward-rectifying K^+ channels, such as KAT1 and KAT2. On the other side, the slow ABA response takes place within minutes to hours and implicates the basic leucine zipper (bZIP) transcription factors that trigger the induction of genes involved in long-term drought tolerance (Kline *et al*., 2010).

1.5.2.2.2.1. Fast ABA signalling pathway

The increased ABA level in the leaves is perceived by members of the ABA receptor PYR/PYL/RCAR family (Fig. 1.23; Ma *et al*., 2009; Park *et al*., 2009). The interaction promotes a conformational change of the receptor that allows its following interaction with a protein phosphatase of the PP2C family (ABI1, ABI2, HAB1**;** Miyazono *et al*., 2009; Nishimura *et al*., 2009, 2010; Santiago *et al.,* 2009; Yin *et al*., 2009), inhibiting their enzymatic activity (Ma *et al*., 2009; Park *et al*., 2009). Accordingly to this inhibition, the PP2C phosphatases cannot suppress the SnRK and CPK kinases.

ABA also downregulates the H^+-ATPases located in the plasma membrane, inhibiting stomatal opening (Kinoshita *et al.*, 1995; Schroeder and Hagiwara, 1989).

Many second messengers regulate ABA signaling in guard cells, including reactive oxygen species (ROS), nitric oxide (NO), phosphatidic acid (PA), phosphatidyl-inositol-3-phosphate (PIP3) and inositol-3-phosphate (IP_3; Fan *et al*., 2004; Hirayama and Shinozaki, 2007; Israelsson *et al.*, 2006; Kim *et al*., 2010; Schroeder *et al.*, 2001a).

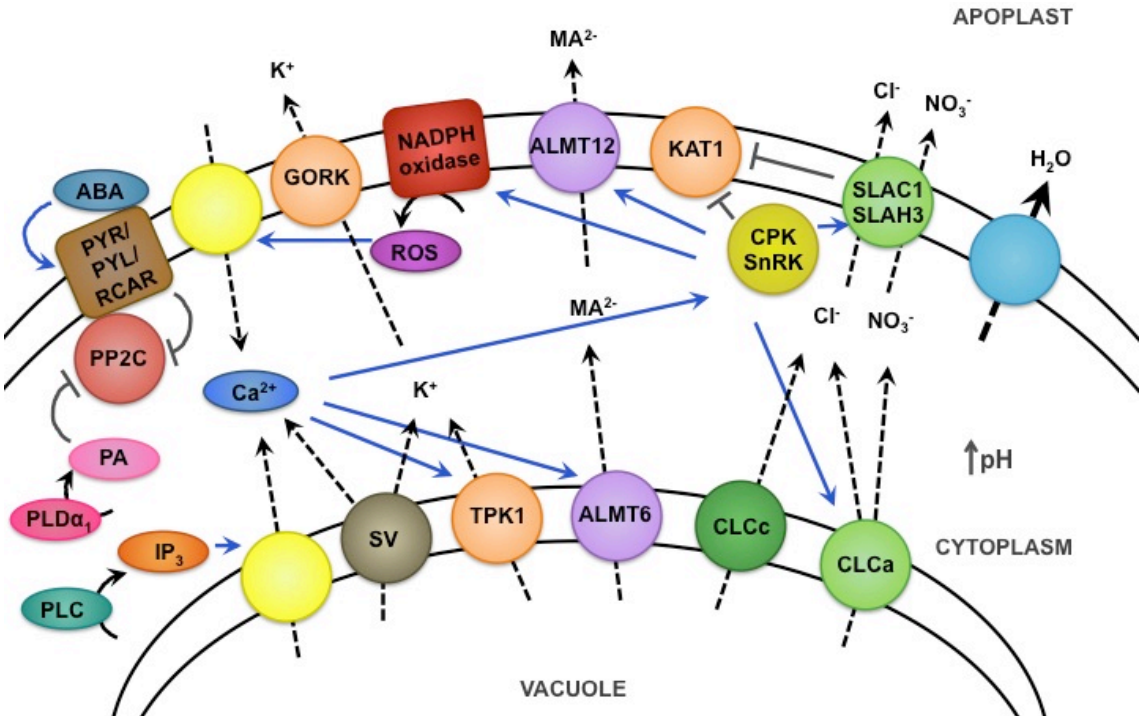

Figure 1.23. Stomatal closure by ABA induced signaling in guard cells. Blue arrows indicate activation or positive interactions between the factors. Grey arrows indicate inhibition. Dashed arrows indicate ion movements. ABA, abscisic acid; ALMT, aluminum-activated malate transporter; CLC, chloride channel; CPK, calcium-dependent protein kinase; GORK, guard cell outward rectifying K^+ channel; IP_3, inositol-3-phosphate; KAT1, K^+ channel in *Arabidopsis thaliana* 1; PA, phosphatidic acid; PLC, Phospholipase C; $PLD\alpha_1$, Phoshpholipase $D\alpha_1$; PP2C, protein phosphatase 2C; PYL, PYR1 like; PYR, pyrabactin resistance; RCAR, regulatory component of ABA receptor; SLAC1, slow anion channel associated 1; SLAH3, SLAC1-homolog 3; SnRK, Snf−1 related protein kinase; TPK1, two-pore K channel 1.

ABA also induces an increase in cytosolic Ca^{2+}, which is also an essential second messenger in plant signal transduction cascades. Increase of cytosolic Ca^{2+} is a consequence of both, Ca^{2+} uptake after activation of plasma membrane channels and Ca^{2+} release from internal stores (Hamilton *et al.*, 2000; MacRobbie, 2000; Nomura *et al.*, 2008; Staxen *et al.*, 1999). Following the activation of the Phospholipase C (PLC) that catalyses inositol 1,4,5-triphosphate (IP_3), this second messenger induces an increase in cytosolic Ca^{2+} by the activation of tonoplast Ca^{2+} channels (Fig. 1.23; Allen *et al.*, 1995; Takahashi *et al.*, 2001; Tang *et al.*, 2007).

Concurrently, ABA induces the production of the Phospholipase $D\alpha_1$ ($PLD\alpha_1$), which in turns synthetizes phosphatidic acid (PA). This PA binds to the PP2C ABI1, inhibiting its activity and promoting ABA signalling (Fig. 1.23; Mishra *et al.*, 2006; Zhang *et al.*, 2004; Zhao and Wang, 2004).

Cytosolic Ca^{2+} rise initiates the processes required for guard cell turgor loss through the modulation of ion channels and pumps in both the plasma and vacuolar membranes (Fig. 1.23).

Therefore, inhibition by PP2C phosphatases (ABI1, ABI2 and HAB1), together with the rise of Ca^{2+}, allow the activation of distinct SnRK and CPK protein kinases. Among them, OST1 together with CPK6 and CPK23 become active by autophosphorylation. However CPK3 and CPK21 additionally need Ca^{2+} to be functionally active. These kinases further interact with the plasma membrane channels SLAC1 and SLAH3 (Fig. 1.23), phosphorylating their cytosolic N-terminal moieties and likely these channels open by a conformational change involving their phenylalanine gate (section 1.5.1.2.3; Geiger *et al.*, 2009b, 2010, 2011). While SLAC1 can be

activated by all of these protein kinases, SLAH3 is stimulated only by all the CPKs but not by OST1 (Brandt *et al*., 2012; Geiger *et al*., 2010, 2011; Scherzer *et al*., 2012). Therefore these channels are activated in a Ca^{2+}-dependent (by CPK kinases) and -independent (by OST1 kinase) manner in guard cells (Geiger *et al*., 2010; Hetherington and Brownlee, 2004; Levchenko *et al*., 2005; Marten *et al*., 2007; Mori *et al*., 2006; Schroeder and Hagiwara, 1989).

OST1 also activates the R-type channel ALMT12 by phosphorilation, which mediates MA^{2-} efflux to the apoplast (Fig. 1.23; Imes *et al.*, 2013; Rasckle *et al.*, 2003; Roelfsema *et al.*, 2004).

In addition, OST1 induces ROS production by activating NADPH oxidases (Fig. 1.23), such as the plasma membrane *At*rbohF (respiratory burst oxidase homologue F; Kwak *et al.*, 2003; Murata *et al.*, 2001; Sirichandra *et al.*, 2009). This ROS signaling activates Ca^{2+} channels in the plasma membrane of guard cells, increasing intracellular Ca^{2+} (Fig. 1.23; Köhler *et al.*, 2003; Pei *et al.*, 2000), and stimulates NO and PIP3 signaling, which in turn modulates the concentration of cytosolic Ca^{2+} in the cell (Garcia-Mata and Lamattina, 2003; Neill *et al*., 2003, 2008; Park *et al.*, 2000, 2003). ROS, such as the hydrogen peroxide (H_2O_2), reduce the activity of ABI1 and ABI2 *in vitro* (Meinhard and Grill, 2001; Meinhard *et al.*, 2002).

Moreover, OST1 phosphorylates the N-terminal domain of *At*CLCa, enhancing its activity in releasing Cl^- and NO_3^- from the vacuole (Fig. 1.23; Wege *et al.*, 2014). Taken into account that ABA-induced stomatal closure of *clcc* knock-out mutants was impaired (Jossier *et al*., 2010), CLCc could also participate in the stomata closure pathway, transporting Cl^- out of the vacuole.

As mentioned above, the hyperpolarization-activated channel ALMT6 acts as a MA^{2-} influx or efflux channel, depending on the vacuolar pH and cytosolic MA^{2-} (Meyer *et al*., 2011). The cytosolic Ca^{2+} rise could activate this channel and thus MA^{2-} would be transported into the cytosol (Fig. 1.23).

The S-type anion channels SLAC1 and SLAH3 inhibit the inward rectifying K^+ channel KAT1, which is involved in stomata opening. This inhibition takes place by protein-protein interaction, preventing stomatal opening (Fig. 1.23; Wang *et al.*, 2016). Additionally, OST1 inhibits KAT1 activity by phosphorylation (Sato *et al*., 2009). As a consequence the passive influx of K^+ from the apoplast to the cytoplasm is interrupted.

Following the activation of anion channels (SLAC1, SLAH3 and ALMT12) in the plasma membrane, Cl^-, NO_3^- and MA^{2-} are released from guard cells, giving rise to depolarization of the plasma membrane. This in turn activates guard cell outward rectifying K^+ channels (GORK), leading to the release of K^+ from the cytoplasm to the apoplast (Fig. 1.23; Ache *et al*., 2000; Hosy *et al*., 2003; Kim *et al*., 2010).

The cytosolic Ca^{2+} activates the vacuolar K^+ (VK) channels TPK1 (two-pore K^+ channel 1), which drives the release of K^+ from the vacuole into the cytoplasm (Fig. 1.23; Gobert *et al.* 2007; Ward and Schroeder, 1994). This cation is subsequently transported out of the cell by the GORK channel.

The release of solutes from guard cells decreases the osmotic potential, causing a massive water movement out the cells. The loss of guard cell turgor finally leads to stomata closure, reducing transpirational loss of water from the leaf.

1.5.2.2.2.2. Slow ABA signaling pathway

As mentioned above, the inhibition of the phosphatase ABI1 enables the activation of distinct SnRK protein kinases. In *Arabidopsis* several kinases from the SrRK2 subfamily (SnRK2.2, SnRK2.3 and OST1) phosphorylate the bZIP transcription factors of ABF/AREB group in the nucleus (Furihata *et al*., 2006 Johnson *et al*., 2002; Lopez-Molina *et al*., 2001; Uno *et al*., 2000). The bZIP transcription factors in turn interact with the G-box ABA-response elements (ABRE) in the promoter of ABA-response genes, inducing their expression (Zhu, 2002).

Up-regulated genes encode proteins involved in abiotic stress tolerance, like transporters, PYR/PYL/RCAR receptors, transcription factors, protein kinases, protein phosphatases, hydrophilins, molecular chaperones, antioxidant enzymes, enzymes of phospholipid signaling, etc. (Cutler *et al*., 2010).

OBJECTIVES

2. OBJECTIVES

Net chloride (Cl^-) uptake is the result of the combination of active influx, governed by $Cl^-/2H^+$ symporters, and passive efflux through anion channels (Britto and Kronzucker, 2006; Roberts, 2006; White and Broadley 2001). Plasma membrane anion channels from root epidermal and cortical cells, which mediate the release of Cl^- to the apoplast or the soil, have been proposed to make a considerable contribution to the net Cl^- uptake at plasma membrane potentials more negative than −50 mV (Babourina *et al.,* 1998).

Chloride loading into the xylem is highly likely to be electrochemically passive, facilitated by anion efflux channels located at the plasma membrane of xylem-associated cells like pericycle and/or parenchyma cells (Henderson *et al*., 2014; Köhler and Raschke, 2000; Kollist *et al.,* 2011; Munns and Tester, 2008; Teakle and Tyerman, 2010; White and Broadley, 2001). In fact, root-to-shoot translocation of Cl^- has been described as the most important mechanism in the regulation of shoot Cl^- accumulation in plants (Brumós *et al*., 2010; Gong *et al.,* 2011; Tregeagle *et al.,* 2010).

Therefore, channels that mediate Cl^- efflux from the root either at the stele or epidermal levels are key points regulating Cl^- homeostasis at the whole-plant level, given that both activities modulate the degree of shoot Cl^- accumulation.

Chloride and nitrate (NO_3^-) play different functions in plant growth and development and both molecules are frequently transported through the same membrane transporters. Optimal growth of plants in the absence of stressful conditions requires the synchronic supply of both Cl^- and NO_3^- ions (Franco-Navarro *et al*., 2016; Raven, 2017; Wege *et al*., 2917). However, abiotic stress determines the ABA-specific inhibition of some type of ion channels like those regulating xylem translocation of potassium or Cl^- (Cram and Pitman, 1972; Pitman, 1977; Pitman and Wellfare, 1978; Pitman *et al*., 1974). A specific inhibition of shoot Cl^- translocation (not affecting NO_3^- translocation in the same extent) is expected to occur for instance under salt stress.

Nevertheless, neither the anion channels involved in net Cl^- uptake or in Cl^- loading into the xylem, nor the regulatory mechanism leading to an appropriate balance between NO_3^- and Cl^- in the plant according to environmental conditions have been characterized at the molecular level.

The general objective of this thesis was therefore to elucidate the molecular mechanisms regulating root Cl^- homeostasis and its possible interaction with NO_3^- transport.

Taking into account that:

1) X-SLAC, a slowly activating anion conductance, with slow activating/deactivating kinetics and permeable to NO_3^-, Cl^- and malate, was one of the anion conductances identified in protoplasts of root xylem parenchyma cells of barley and maize (Gilliham and Tester, 2005; Köhler and Raschke, 2000),

2) two members of SLAC/SLAH protein family recently characterised in *Arabidopsis* (SLAC1 and SLAH3) are permeable to NO_3^- and Cl^- (Geiger *et al*., 2009b, 2011),

3) the SLAH1 homologue can complement the phenotypes of *slac1-2* when expressed under the control of the SLAC1 guard-cell-promoter (Negi *et al*., 2008),

4) both *SLAH1* gene and its closest phylogenetic relative *SLAH4* are apparently expressed in the root (Negi *et al*., 2008; Zheng *et al*., 2015),

5) and these properties are compatible with involvement of *SLAH1* and *SLAH4* genes in the regulation of root Cl^- and/or NO_3^- homeostasis,

the specific objectives of this thesis were:

I. To identify the tissue- or cell-specific sites of expression of *AtSLAH1* and *AtSLAH4* genes.

II. To characterise developmental or environmental cues involved in the regulation of *AtSLAH1* and *AtSLAH4* gene expression.

III. To perform the functional expression of *SLAH1* gene in *Xenopus laevis* oocytes to address the kinetic properties, anion selectivity and relative permeability of the anion channel through electrophysiological techniques.

IV. To elucidate the biological function of the SLAH1 and SLAH4 anion channels through the identification and phenotyping of *slah1* and *slah4* knockout (KO) lines, lacking functional copies of the corresponding *SLAH* gene.

V. To propose a model describing the mode of action of the SLAH1 and SLAH4 channels.

MATERIALS AND METHODS

3. MATERIALS AND METHODS

3.1. BIOLOGICAL MATERIAL

3.1.1. Bacteria strains, culture media and growth conditions

3.1.1.1. *Escherichia coli*

Different *Escherichia coli* strains were used for different purposes (Table 3.1). The strains used for competent cells obtaining (section 3.5.1.1) were TOP10 and Mach1™-T1 (Invitrogen, Thermo Fisher Scientific Inc. Waltham, MA, USA) *E. coli*. In addition these *E. coli* strains were used for bacterial transformation (section 3.5.1.2).

The DB3.1 *E. coli* strain, which is resistant to CcdB effects, was used to propagate and maintain Gateway® vectors containing the *ccd*B gene. CcdB protein interferes with *E. coli* DNA gyrase, thus inhibiting its growth. CcdB effects are not supported by general *E. coli* cloning strains, including TOP10 and Mach1™-T1.

Table 3.1. *Escherichia coli* strains.

Strain	Genotype
TOP10	F^- *mcr*A Δ(*mrr-hsd*RMS-*mcr*BC) Φ80*lac*ZΔM15 Δ*lac*X74 *rec*A1 *ara*D139 Δ(*ara-leu*) 7697 *gal*U *gal*K *rps*L (Str^R) *end*A1 *nup*G
Mach1™-T1	F^- Φ80*lac*ZΔM15 Δ*lac*X74 *hsd*R(r_k^-, m_k^+) Δ*rec*A1398 *end*A1 *ton*A
DB3.1	F^- *gyr*A462 *end*A1 *gln*V44 Δ(*sr*1-*rec*A) *mcr*B *mrr hsd*S20(r_B^-, m_B^-) *ara*14 *gal*K2 *lac*Y1 *pro*A2 *rps*L20(Sm^R) *xyl*5 Δ*leu mtl*1

E. coli strains were cultivated in Luria-Bertani (LB) medium (Table 3.2). Solid LB medium was prepared with 15 g l^{-1} plant agar (Duchefa Biochemie, Haarlem, The Netherlands). This medium was supplemented with an antibiotic when the *E. coli* strains were transformed (the antibiotic to which the plasmid DNA provided resistance).

Table 3.2. LB medium.

Constituent	Concentration (g l^{-1})
Tryptone	10
Yeast extract	5
NaCl	10
pH was adjusted to 7.0 with NaOH 5 M	

Super optimal broth (SOB; Table 3.3) medium and Super optimal broth with catabolite repression (SOC) medium were used for growth and preparation of chemically competent cells (section 3.5.1.1). SOC medium had the same composition as the SOB medium, but it also contained 2 M glucose.

Table 3.3. SOB medium composition.

Constituent	Concentration
Tryptone	20 g l^{-1}
Yeast Extract	5 g l^{-1}
NaCl	0.58 g l^{-1}
KCl	0.18 g l^{-1}
$MgSO_4$	2 M

Escherichia coli strains were grown at 37ºC.

3.1.1.2. *Agrobacterium tumefaciens*

GV3101 *Agrobacterium tumefaciens* was the only strain used for obtaining chemically competent cells (section 3.5.2.1) in order to perform its transformation (section 3.5.2.2) with plasmid DNA.

The GV3101 *A. tumefaciens* strain contains the plasmid pTiC58 with resistance to rifampicin. Thus, *A. tumefaciens* was cultivated in LB medium (Table 3.2) supplemented with rifampicin (50 µg ml^{-1}). Solid LB medium was prepared as described above (section 3.1.1.1).

When the strain was transformed, the LB medium was supplemented with another antibiotic (that one to which the plasmid DNA provided resistance).

To prepare *A. tumefaciens* chemically competent cells (section 3.5.2.1) Yeast extract peptone (YEP) medium (Table 3.4) was used for growing.

Table 3.4. YEP medium composition.

Constituent	Concentration (g l^{-1})
Pectone	10
Yeast extract	10
NaCl	5

Agrobacterium tumefaciens was grown at 28ºC.

3.1.2. Plant material and growth conditions

3.1.2.1. Knockout (KO) mutant lines

Arabidopsis thaliana seeds from the *slah1-1* (SALK_039811), *slah3-1* (GK371G03) and *slah4-2* (SALK_091937) lines were obtained from the Nottingham Arabidopsis Stock Centre (NASC; Nottingham University, UK) and seeds from the *slah1-2* (INRA_FLAG_329G06) line from the Institut Jean-Pierre Bourgin (IJPB; Versailles, France). The mutant line *slah3-4* (SALK_111623) was provided by Dr. Sheng Luan (Zheng *et al*., 2015).

The *slah1-2* line was generated in the Wassilewskija (Ws) background, whereas the other lines were generated in the Columbia (Col) background.

3.1.2.2. Growth conditions

After 3-days vernalization at 4ºC in the dark, plants were grown according to the experimental requirements. Thus germination was synchronized.

All irrigation and experimental solutions were adjusted to pH 5.7.

3.1.2.2.1. *In vitro* growth conditions

Seeds were surface sterilized according to the liquid sterilization protocol from Clough and Bent (1998) and after vernalization they were placed on Petri dishes containing 0.5x Murashige and Skoog (MS) medium (Murashige and Skoog, 1962) supplemented with vitamins, MES buffer (Duchefa Biochemie) and 0.5% sucrose (Duchefa Biochemie) and solidified with 0.8% plant agar (Duchefa Biochemie).

Plants were grown in an *in-vitro* growth chamber at 24ºC, with a photoperiod of 16 h light, 30 μE m^{-2} s^{-1} of photosynthetically-active radiation (PAR) and without relative humidity (RH) regulation.

For GUS (β-Glucuronidase) and GFP (Green Fluorescent Protein) reporter gene expression analyses, P_{SLAH1}-GFP::GUS, P_{SLAH4}-GFP::GUS (section 3.4.2) and P_{SLAH3}-GUS (Negi *et al.*, 2008) transgenic plants were grown in Petri dishes containing the MS medium described above supplemented with 50 μg ml^{-1} kanamycin. Seedlings were directly analysed after growing in Petri dishes or resistant seedlings were grown for longer time after transferring them into hydroponics medium (section 3.1.2.2.3). In addition, resistant seedlings were transplanted to soil to produce seeds.

For obtaining independent *slah1/SLAH1* complemented lines, seeds obtained after *Arabidopsis* transformation (section 3.6) were also sown on MS supplemented with 20 μg ml^{-1} hygromycin. Resistant seedlings were transplanted to soil to obtain seeds.

3.1.2.2.2. Plant growth on soil

Peat was sieved and autoclaved before pots were filled. Prior to sowing, peat was washed with distilled water by irrigation from above to remove undesirable compounds, and afterwards with the corresponding solution.

Plants were watered by immersion of the base of the pots every 3 d approximately and were grown either under long photoperiod conditions in a growth chamber at 23ºC/18ºC, 16h/8h day/night photoperiod, 120 μE m^{-2} s^{-1} of PAR and 60±10% RH or under short photoperiod conditions in a phytotron chamber (Ing. Climas, Barcelona, Spain) at 23ºC/18ºC, 8h/16h day/night photoperiod, 120 μE m^{-2} s^{-1} of PAR and 60±10% RH.

For xylem sap collection assays, peat was washed with Basal Solution (BS), in which Cl^- salts were excluded. BS was based in 0.25x Arteca and Arteca (2000) nutritive solution, but removing all Cl^- ions. Macroelements composition of BS was 2 mM KNO_3, 0.625 mM KH_2PO_4, 0.5 mM $MgSO_4$ and 0.75 mM $Ca(NO_3)_2$. Modified microelements formulation was used, since $MnSO_4$ replaced the Cl^- salt in $MnCl_2$ and NaCl was removed (Somerville and Ogren, 1982). Therefore, BS had 3.5 mM NO_3^- as the sole nitrogen source and 70 μM Cl^- (coming from contaminant traces), enough to fulfil its requirement as a micronutrient (Franco-Navarro *et al.*, 2016a).

Potted plants of *slah1-2*, *slah3-1* and *slah3-4* T-DNA insertion mutant lines (section 3.7.1), the *slah1-slah3* double-KO mutant line (obtained by sexual crosses; section 3.7.2), and their corresponding azygous segregants or wild-type (WT) were grown under long photoperiod conditions and used for xylem sap collection assays.

For morphological measurements assays (section 3.8.1) to compare the development of *slah1-2* and *slah4-2* with their corresponding azygous segregating or WT lines, plants were grown in pots under short photoperiod conditions, but also hydroponically (section 3.1.2.2.3). Pots were watered by immersion of the base of the pots in a solution containing either low Cl^- (approximately 70 µM residual Cl^-) or 5 mM Cl^-. Both solutions consisted of a modified BS medium, containing double of $MgSO_4$ and $Ca(NO_3)_2$ salts, supplemented with the following salt mixtures ensuring the same cationic balance: 2.5 mM KCl, 0.625 mM $MgCl_2$, and 0.625 mM $CaCl_2$ for the 5 mM Cl^- treatment; and 1.25 mM KH_2PO_4, 0.625 mM K_2SO_4, 0.625 mM $MgSO_4$, and 0.625 mM $CaSO_4$ for the low-Cl^- treatment. The microelements composition was the same as the BS.

For *slah4-2* phenotypic assay with different Cl^- and NO_3^- concentrations, *slah4-2* and its WT line (Col-0) plants were grown 17 d with BS. By irrigation from above, peat was afterwards washed with the respective treatment solution, which consisted of a shared basal solution made with 0.625 mM KH_2PO_4 and 0.5 mM $MgSO_4$ as macroelements, together with the microelements composition as the BS. This solution was supplemented with different Cl^- and NO_3^- concentrations (Table 3.5) to obtain 5 treatment solutions and another treatment solution also contained ammonium as N source. Nitrate concentration was provided with KNO_3, $Mg(NO_3)_2$ and $Ca(NO_3)_2$ in relation (4:1:1), and Cl^- concentration was provided with the same cation composition, i.e. KCl, $MgCl_2$ and $CaCl_2$ (4:1:1). These plants were grown under long photoperiod condition.

Table 3.5. Nitrate (NO_3^-) and chloride (Cl^-) concentrations of the treatment solutions for the *slah4-2* phenotypic assay. A treatment also contained ammonium (NH_4^+)

Treatment solution	NO_3^- (mM)	Cl^- (mM)	NH_4^+ (mM)
1	5.00	-*	-
2	2.00	3.00	-
3	0.25	4.75	-
4	5.00	5.00	-
5	0.75	5.00	-
6	0.25	4.75	1.75

* 70 µM Cl^- coming from contaminant traces.

For *Arabidopsis* transformation (section 3.6) *A. thaliana* Col-0 plants were grown under short day conditions with an optimal solution.

3.1.2.2.3. Plant growth in hydroponic culture

For adequate normalization of ion translocation rates in xylem sap collection assays, *Arabidopsis* Col-0 plants were grown hydroponically in the BS described above under long photoperiod conditions. Plants were germinated in 1.5 ml bottomless Eppendorf tubes filled with rockwool previously imbibed in distilled water.

For morphological measurements assays (section 3.8.1) to compare the development of *slah1-2* and *slah4-2* with their corresponding WT lines, plants were also grown in hydroponics conditions under short and long photoperiod conditions, respectively. The solution described above containing either low Cl^- (70 µM residual Cl^-) or 5 mM Cl^- (section 3.1.2.2.2) was replaced every 3 d.

For reverse transcriptase PCR (RT-PCR) studies (section 3.2.4.2), *slah1-1*, *slah1-2* and *slah4-2* T-DNA insertion mutant lines (section 3.7.1), the *slah1/SLAH1* complemented lines (section 3.4.2) and their corresponding azygous segregating or WT lines were grown in liquid medium containing 0.25x MS solution supplemented with vitamins and MES buffer (Duchefa Biochemie) under short photoperiod conditions.

For GUS and GFP reporter gene expression analyses, P_{SLAH1}-GFP::GUS, P_{SLAH4}-GFP::GUS (section 3.4.2) and P_{SLAH3}-GUS (Negi *et al.*, 2008) transgenic seedlings were transferring into hydroponics medium containing 0.25x MS supplemented with vitamins and MES buffer after growing in Petri dishes to obtain older plants for further assays.

For quantitative real time PCR (qPCR) analyses (section 3.2.4.3), *Arabidopsis thaliana* Col-0 plants were grown under short photoperiod conditions in hydroponic medium with different solutions:

1. Plants grown for 6 weeks in the 0.25x MS solution described before were used for the salt treatment, the water deficit treatment and for the application of ABA. For the salt-stress treatment, plants were transferred to hydroponics jars containing 150 mM NaCl in 0.25x MS, meanwhile for the water-deficit treatment, plants were transferred to 0.25x MS with 287 g l^{-1} PEG-8000 (equivalent to −1 MPa of osmotic potential). And plants were transferred to 0.25x MS supplemented with 100 µM ABA for the exogenous ABA application. Plants used as control were transferred to 0.25x MS medium.

2. Plants grown for 2 weeks in 0.25x MS and 6 weeks more in BS solution supplemented with either 5 mM Cl^- or 70 µM Cl^- (using $KCl:MgCl_2:CaCl_2$ in a ratio 2:1:1) were subjected either to Cl^- supply and starvation assays or to indole-3-acetic acid (IAA) treatment. For chloride supply treatment, plants grown in optimal solution with 70 µM Cl^- were transferred to 5 mM Cl^- solution, while for chloride starvation treatment, plants grown in the solution with 5 mM Cl^- were transferred to the 70 µM Cl^- solution. And for the exogenous auxin application, plants were transferred to hydroponics jars containing 0.25x MS, with either 5 mM Cl^- or 70 µM Cl^-, supplemented with 100 µM IAA. Plants used as control were transferred to the same nutrient solution in which they were growing.

3. Plants grown for 5 weeks in 0.25x MS and 3 weeks more in a solution based in the BS, sharing the microelements composition with the BS but removing all NO_3^- ions from the macroelements. Thus the macroelements composition was 0.625 mM KH_2PO_4, 0.5 mM $MgSO_4$ and 0.5 mM $CaSO_4$, and was supplemented with either 5 mM NO_3^- ions (provided with $KNO_3:Mg(NO_3)_2:Ca(NO_3)_2$ in a ratio 4:1:1) or 2.5 mM ammonium succinate. Plants grown in these two solutions with different nitrogen source were subjected to either NO_3^- supply or starvation assays. For nitrate starvation treatment, plants grown in the solution containing NO_3^- as N source were transferred to the nitrate-free solution, and for nitrate supply treatment plants grown in nitrate-free solution were transferred to the solution containing NO_3^- as N source.

Plants used as control were transferred to the same nutrient solution in which they were growing

Three and 24 h after treatments application, roots and rosette leaves were harvested, quickly washed with distilled water and immediately frozen with liquid nitrogen and stored at −80°C.

3.2. DNA ANALYSES

3.2.1. DNA extraction

In order to genotype *Arabidopsis* plants (section 3.7.1), DNA extraction from leaves was performed with the REDExtract-N-Amp™ Plant PCR kit (Sigma-Aldrich Co., MO, USA). For each plant, a disk of leaf tissue of around 3 mm was incubated in 10 µl of the extraction solution at 95°C for 10 min. To neutralize inhibitory substances, an equal volume of dilution solution was added. For genotyping by polymerase chain reaction (PCR; section 3.7.1), 1 µl of the extracts was used.

In addition, to obtain template DNA for performing PCR (section 3.2.4.1), DNA was extracted from *Arabidopsis* fresh or frozen leaves through the *i*-genomic Plant DNA Extraction Mini Kit (Intron Biotechnology Inc., Kyeonggi-do, Korea) following the manufacturer's instructions.

Through the mini-preparations protocols, the plasmid DNA was isolated from bacteria.

The miniprep was performed the following day of growing single colonies in 2−3 ml of LB liquid medium (section 3.1.1) containing the appropriate antibiotic. The saturated culture was centrifuged at 12,100 × *g* for 2 min. The supernatant was discarded and the bacteria were resuspended with 125 µl of cold Solution I (Table 3.6). The samples were shaked with a Bio Vortex V1 (Biosan, Riga, Latvia). Subsequently 225 µl of freshly prepared Solution II (Table 3.6) was added and the samples were gently mixed and placed on ice for 3 min. Afterwards 118 µl of cold Solution III (Table 3.6) was added.

Table 3.6. Composition of solutions I, II and III.

Solution I		Solution II		Solution III	
Constituent	**Concentration (M)**	**Constituent**	**Concentration**	**Constituent**	**Concentration (M)**
Glucose	0.050	Sodium hidroxide	0.2 M	Potassium acetate	3
Tris-Cl 1M (pH 8.0)	0.025	SDS	1 %	Glacial acetic acid	5
EDTA 0.5 M (pH 8.0)	0.010				

The samples were gently mixed by inversion and placed on ice for at least 10 min to allow most of the protein, high molecular weight RNA and chromosomal DNA to precipitate. Then 20 µl of chloroform-isoamyl alcohol (24:1) was added to the samples and after a gently shaked, they were centrifuged 5 min at 12,100 × *g*. The supernatant was transferred into a second microcentrifuge tube and 560 µl of phenol-chloroform-isoamyl alcohol (24:24:1) was added. The samples were shaked and centrifuged 5 min at 12,100 × *g*. The supernatant was transferred into a new microcentrifuge tube and after adding 500 µl of cold chloroform-isoamyl alcohol the samples were shaked and centrifuged 3 min at 12,100 × *g*. The clear supernatant was transferred into a new microcentrifuge tube and two volume of ice-cold 100% ethanol was used to precipitate the plasmid DNA. The samples were maintained at least 10 min at −20ºC.

Afterwards samples were centrifuged 15 min, the supernatant was discarded and 1 ml of cold 70% ethanol was used for washing them. After a centrifugation of 5 min at 12,100 × *g*, the ethanol was discarded and pellets were dried at 40ºC. Finally, pellets were resuspended in 20–30 µl water containing RNase A (20 µg ml^{-1}). An aliquot of the plasmid DNA was subsequently digested with restriction enzymes (section 3.2.7) and analysed in agarose gels (section 3.2.5).

The Qiaprep spin Miniprep kit (Qiagen, Germany) and the Plasmid PLUS DNA Purification Mini Spin Column kit (Genaxxon Bioscience, Ulm, Germany) were used for plasmid DNA extraction from *E. coli* previously transformed (section 3.5.1.2) with USER cloning (section 3.4.1). The day before single bacterial colonies were picked into a vial of 5 ml of LB medium (section 3.1.1.1) supplemented with ampicillin (50 µg ml^{-1}) and shaked overnight at 37ºC. After centrifuging at 6,800 × *g* for 1–3 min at room temperature, the obtained pellet was used according to the manufacturer's protocols. Finally the concentration of the 50 µl extracted DNA samples was quantified (section 3.2.3) and its size was verified by electrophoresis in agarose gel (section 3.2.5). After obtaining the right sequence (section 3.2.8), the DNA samples were used for the IVT-PCR (section 3.2.4.5)

Together with mini-preparations, maxi-preparations are a way for long-term storage of plasmid vectors and the constructs contained therein at –20ºC.

For maxi-preparations, a colony of *E. coli* containing the plasmid of interest, was inoculated in 100 ml of LB medium (section 3.1.1.1) and grown overnight at 37°C with shaking. Culture was centrifuged 5 min at 4,300 × *g*. Supernatant was discarded and cell pellet was washed with 20 ml distilled milli-Q water, gently shaked and centrifuged 3 min at 4,300 × *g*. Water was discarded and the pellet was well resuspended with 5 ml of Solution I (Table 3.6) by shaking in the Bio Vortex V1 (Biosan). The sample was subsequently maintained 10 min on ice. Afterwards, 10 ml of freshly prepared Solution II (Table 3.6) was added and mixed by gentle inversion and then maintained 10 min on ice. Following the addition of 7.5 ml of cold Solution III (Table 3.6), the sample was mixed by gentle inversion and incubated 30–60 min on ice to allow the precipitation of proteins, high molecular weight RNA and chromosomal DNA. Then 800 µl of chloroform-isoamyl alcohol (24:1) was added to the sample and after a quickly shaked, it was centrifuged 15 min at 14,600 × *g* for at 4°C. The supernatant was transferred into a new tube and one volume of isopropanol was added. The sample was incubated 10 min at –20ºC to precipitate the nucleic acids. A centrifugation of 10 min at 6,700 × *g* was performed and afterwards the supernatant was discarded. The pellet was resuspended with 2.5 ml Tris-EDTA (TE; Table 3.7) buffer by shaking in the vortex, followed by the addition of 5 ml of 4 M LiCl.

Table 3.7. TE buffer composition.

Constituent	Concentration (M)
Tris-Cl 1M (pH 8.0)	0.010
EDTA 0.5 M (pH 8.0)	0.001

The sample was incubated 15 min on ice. The RNA was precipitated by centrifuging 10 min at 6,700 × *g*. The supernatant was transferred into a new microcentrifuge tube and after adding 1ml isopropanol and centrifuging 10 min at 6,700 × *g* the DNA was precipitated. The DNA was resuspended with 1.6 ml TE buffer, containing RNase A (20 µg ml^{-1}), by shaking in a vortex and the sample was incubated 15 min at 37ºC. Then 500 µl of phenol-chloroform-isoamyl

alcohol (24:24:1) was added. The sample was mixed and centrifuged 5 min at 6,700 × *g*. The supernatant was mixed with 500 µl and centrifuged 3 min. Afterwards, the DNA of the supernatant was precipitated with 0.1 volume of 3 M Sodium acetate together with a volume of isopropanol. The sample was gently mixed and following the incubation for 20 min on ice, it was centrifuged 10 min at 6,700 × *g*. The pellet was washed with cold 70% ethanol, which was then discarded and the pellet was dried at 42ºC. Finally the pellet, containing the DNA, was resuspended with 15 µl milli-Q water.

A microliter was used for quantifying DNA concentration (section 3.2.3)

3.2.2. Complementary DNA (cDNA) synthesis from RNA

One microgram of total RNA obtained from plant tissues (section 3.3.1) was used as template for the first strand cDNA synthesis in a 10-µl reaction using the iScript™ cDNA synthesis kit (Bio-Rad Laboratories, Hercules, CA, USA).

Each reaction mix (Table 3.8) had a final volume of 10 µl and was incubated 5 min at 25ºC followed by 30 min at 42ºC and 5 min at 85ºC.

Table 3.8. cDNA synthesis reaction.

Components	Volume (µl)
5x iScript reaction mix	2
iScript reverse transcriptase	0.5
RNA template	1
Nuclease-free water	6.5

cDNA samples were used either for determining the integrity of the *AtSLAH* mRNA in the T-DNA insertion mutant lines through RT-PCR (section 3.2.4.2) and to perform qPCR analyses (section 3.2.4.3) with the samples obtained from *Arabidopsis* Col-0 (WT) line.

3.2.3. DNA quantification

The determination of the DNA concentration of the samples was performed with 1 µl using either the NanoDrop® ND-1000 or the NanoDrop® 2000c spectrophotometer (Thermo Fisher Scientific).

3.2.4. DNA Amplification

3.2.4.1. Conventional and high fidelity Taq polymerase reactions

For genotyping by PCR, 1 µl of DNA extracted from leaves (section 3.2.1) of *Arabidopsis* T-DNA insertion mutant lines (section 3.1.2.1) and double mutants (section 3.7.2) was used.

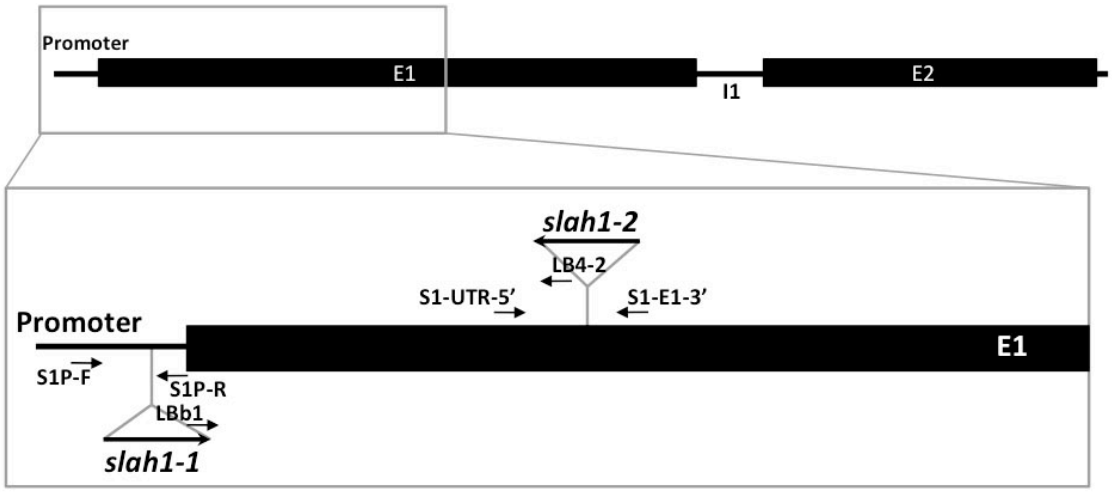

Figure 3.1. T-DNA insertion mutants in *AtSLAH1.*

Homozygous and azygous segregating *Arabidopsis* plants were screened by using primers suitable for the left border of the T-DNA for the corresponding gene and gene-specific primers flanking the position of the T-DNA inserts (Fig. 3.1, 3.2 and 3.3). The design of the primers was conducted using Primer3 (Rozen and Skaletsky, 2000) and OligoCalc software.

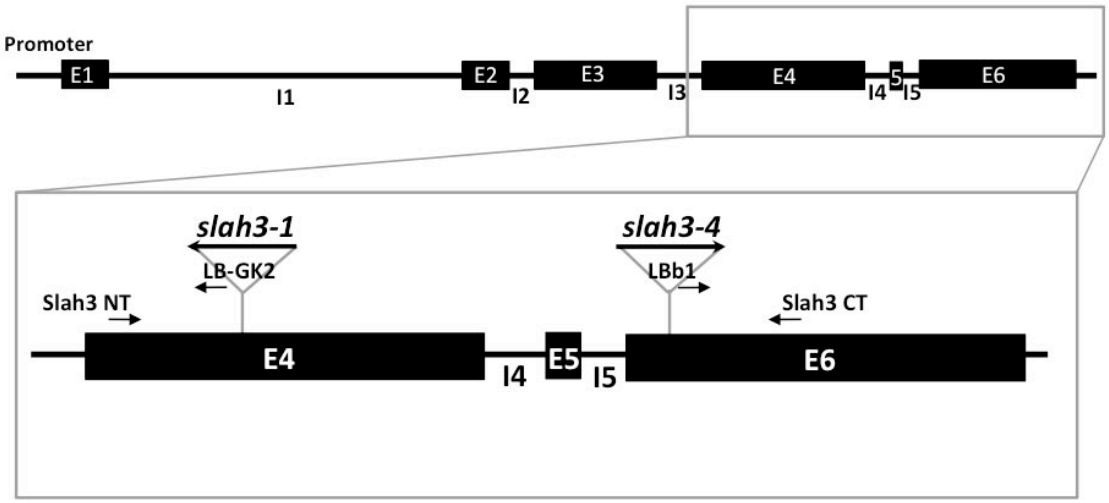

Figure 3.2. T-DNA insertion mutants in *AtSLAH3.*

The PCRs (Table 3.9) were performed with the Maxime™ Taq DNA polymerase (Intron Biotechnology Inc.) in a BIOER XP Cycler (Bioer Technology Co., Hangzhou, China).

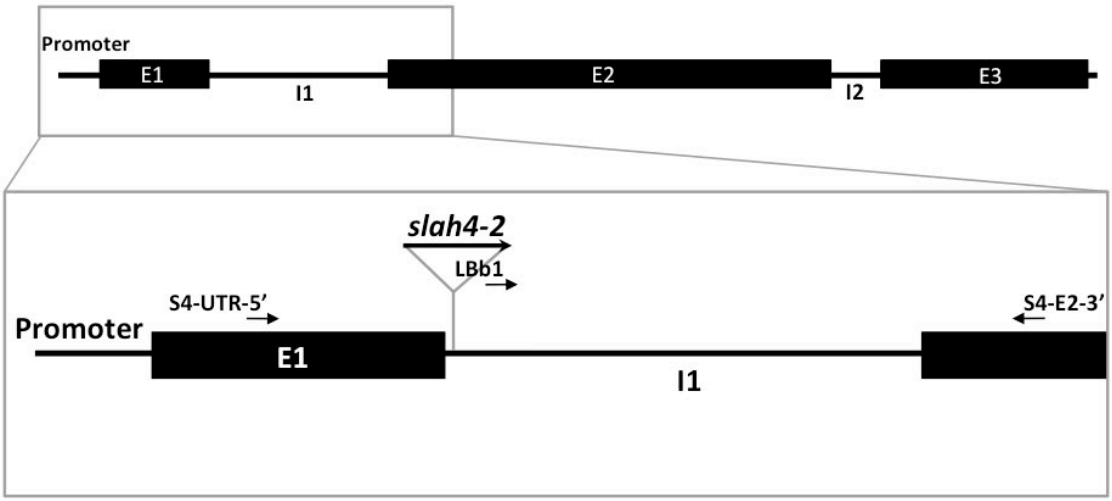

Figure 3.3. T-DNA insertion mutant in *AtSLAH4.*

For genotyping the T-DNA insertion mutants in *SLAH1* and *SLAH4* genes, 58ºC and 20 s in the annealing step were used, meanwhile 60ºC and 25 s were used for T-DNA insertion mutants in *SLAH3*.

Table 3.9. Cycling parameters for genotyping.

PCR cycle		Temperature (ºC)	Time (s)
Initial denaturation		94	120
35 cycles	Denaturation	94	20
	Annealing	58/62	20/25
	Extension	72	60
Final extension		72	300

Each reaction mix contained 1 µl of DNA, 0.5 µM of both forward and reverse primers (Table 3.10), 0.2 mM dNTPs, 2 µl of 10x PCR buffer and 0.4 µl of Maxime™ Taq DNA polymerase (5 U μl^{-1}) in a volume of 20 µl.

Table 3.10. Primers used for genotyping.

Name	Sequence (5' ➔ 3')
S1-UTR-5'	ACCATAGAGCCAAACAAGCCAAT
S1-E1-3'	CACGAGGTTTGCGATTACCGA
S1P-F	CACCGGGCAAAAGGTTTCAATGG
S1P-R	GGTTTATCGATGAAAAAGAGGTATTG
Slah3 NT	ACCCCATTTCCACCTTCGGTATG
Slah3 CT	GGATAATGGTGGTCACGAGCAG
S4-UTR-5'	ATTGAGAAGGGCTCATGGTCAAC
S4-E2-3'	TCCCGCATGGAGACTACTCAAAA
LBb1	GCGTGGACCGCTTGCTGCAACT
LB4-2	CCGTCGGCTATTGGTAATAGGAC
LB-GK2	CCCATTTGGACGTGAATGTAGACAC

PCR products were run in 1% agarose gel by electrophoresis (section 3.2.5) to verify DNA fragment sizes.

High fidelity Taq polymerases were used for genes amplification for the purpose of Gateway® technology cloning in the BIOER XP Cycler (Bioer Technology Co.). Genomic DNA from *Arabidopsis* ecotype Columbia was used as template for amplifications (section 3.2.1).

The primer design (Table 3.11) was performed according to the selected entry vector and the manufacturer's instructions. The pENTR/D-TOPO® vector (Invitrogen), which contains the *att*L sites, was used as entry vector for *SLAH1* promoter cloning. Hence four bases were added to the forward primer sequence designed for generating a 3' blunt-end DNA complementary to a region in the vector generated by restriction enzymes, achieving directionally cloning. Nevertheless, pDONR™201 was the entry vector chosen for *SLAH4* promoter and *AtSLAH1* gene cloning. Therefore 25 bp *att*B sites were incorporated in both primers.

Table 3.11. Primers used in Gateway® cloning.

Name	Sequence (5' ➔ 3')
S1P-F	CACCGGGCAAAAGGTTTCAATGG
S1P-R	GGTTTATCGATGAAAAAGAGGTATTG
S4PattB1-F	GGGGACAAGTTTGTACAAAAAAGCAGGCTCTTGTTTTATCACCTTTTCCTACGTG
S4PattB2-R	GGGGACCACTTTGTACAAGAAAGCTGGGTGCTTATTTTGCTCTATGTTGTGCT
S1gen-F	GGGGACAAGTTTGTACAAAAAAGCAGGCTGGGCAAAAGGTTTCAATGGTTAAG
S1gen-R	GGGGACCACTTTGTACAAGAAAGCTGGGTCTAGTTTTGGTTAGTCGCATTGAG

For constructing the *SLAH1* promoter-GFG::GUS reporter fusion, a genomic fragment including 1.25 kb upstream of the *AtSLAH1* gene start codon, containing the promoter and the 5'-UTR region of the *AtSLAH1* gene was amplified by PCR (Table 3.12) using the suitable primers (S1P-F and S1P-R; Table 3.11) and the *i*-Pfu DNA polymerase (Intron Biotechnology Inc.).

Each reaction mix contained 1 µl of template DNA, 0.5 µM of both forward and reverse primers, 0.2 mM dNTPs, 3 µl of 10x DNA polymerase buffer and 0.5 µl of *i*-Pfu DNA polymerase (2.5 U μl^{-1}) in a volume of 30 µl.

Table 3.12. Cycling conditions for *SLAH1* promoter amplification by *i*-Pfu DNA polymerase.

PCR cycle		Temperature (ºC)	Time (s)
Initial denaturation		94	120
35 cycles	Denaturation	94	20
	Annealing	58	15
	Extension	70	180
Final extension		72	300

For constructing the *SLAH4* promoter-GFG::GUS reporter fusion, a 2.91 kb DNA fragment (1.313 kb longer than the construction used by Zheng and colleagues [2015]), containing the promoter and the untranslated 5-UTR' region of the *AtSLAH4* gene, was amplified by PCR (Table 3.13) using the suitable primers (S4PattB1-F and S4PattB2-R; Table 3.11) and the Velocity DNA polymerase (Bioline, London, UK).

Each reaction mix contained 1 µl of DNA, 0.5 µM of both forward and reverse primers, 0.2 mM dNTPs, 6 µl of 5x DNA polymerase buffer and 0.6 µl of Velocity polymerase (2 U μl^{-1}) in a volume of 30 µl.

Taken into account that 29 bases were added to the specific sequence of the primers regarding the Gateway® technology, the PCR consisted of two parts (Table 3.13). At the first ten cycles of annealing, only the primer regions that complement the gen specific sequence hybridize to the strand. At the rest of the cycles, all the primer bases (included the *attB* sites) could be efficiently amplified.

Table 3.13. Cycling parameters for *SLAH4* promoter amplification by Velocity DNA polymerase.

PCR cycle		Temperature (ºC)	Time (s)
Initial denaturation		94	120
10 cycles	Denaturation	98	30
	Annealing	59	30
	Extension	72	90
25 cycles	Denaturation	98	30
	Annealing	72	30
	Extension	72	90
Final extension		72	600

Since only a *slah1* T-DNA insertion mutant line was obtained (section 3.1.2.1), the mutant line *slah1-2*, homozygous for the T-DNA insertion, was complemented with the *AtSLAH1* gene containing its own promoter region (denoted *slah1/SLAH1*). For complementation of *slah1-2*, a 2.59 kb genomic fragment containing the whole *AtSLAH1* gene was amplified from genomic DNA by PCR (Table 3.14), using the suitable primers (S1gen-F and S1gen-R; Table 3.11) and the *i*-Pfu DNA polymerase (Intron Biotechnology Inc.). As in the case of *SLAH4* promoter amplification, the PCR consisted of two parts.

Each reaction mix contained 1 µl of DNA, 0.5 µM of both forward and reverse primers, 0.2 mM dNTPs, 3 µl of 10x DNA polymerase buffer and 0.5 µl of *i*-Pfu DNA polymerase (2.5 U μl^{-1}) in a volume of 30 µl.

Table 3.14. Cycling conditions for *AtSLAH1* amplification by *i*-Pfu DNA polymerase.

PCR cycle		Temperature (ºC)	Time (s)
Initial denaturation		94	120
10 cycles	Denaturation	94	20
	Annealing	61	20
	Extension	70	240
25 cycles	Denaturation	94	20
	Annealing	70	20
	Extension	70	240
Final extension		72	300

The PCR products of *SLAH* promoters and *AtSLAH1* were purified from agarose gel (section 3.2.6). DNA concentration was quantified (section 3.2.3) and DNA samples were subsequently sequenced (section 3.2.8).

3.2.4.2. cDNA amplification by Reverse Transcriptase PCR (RT-PCR)

For determining the integrity of the *AtSLAH* mRNA (section 3.3.1) in the *slah1* and *slah4* T-DNA insertion mutant lines and the two independent *slah1*/*SLAH1* complemented lines (section 3.6) through RT-PCR, gene-specific primers flanking the position of the T-DNA inserts (Table 3.15) were used.

Table 3.15. Primers used in the RT-PCR.

Gene	Name	Sequence (5' ➔ 3')
AtSLAH1	S1-UTR-5'	ACCATAGAGCCAAACAAGCCAAT
	S1-E1-3'	CACGAGGTTTGCGATTACCGA
AtSLAH4	S4-UTR-5'	ATTGAGAAGGGCTCATGGTCAAC
	S4-E2-3'	TCCCGCATGGAGACTACTCAAAA
AteIF4A1	eIF4-RT-F	GGTATTGATGTCCAACAAGTCTCCC
	eIF4-RT-R	ATTGATCGCAACACCCTTTCTCCC

PCR amplification was performed with cDNA obtained from T-DNA insertion mutant lines and their respective *Arabidopsis* WT lines, using the Maxime™ Taq DNA polymerase (Intron Biotechnology Inc.) in a BIOER XP Cycler (Bioer Technology Co.) and amplification of cDNAs was arrested at the exponential phase of the PCR reaction.

The eukaryotic translation Initiation Factor 4A1 (*eIF4A1;* At3g13920) expression level was used as loading control.

Each reaction mix contained 2 µl of cDNA, 0.5 µM of the both forward and reverse primers (Table 3.15), 0.2 mM dNTPs, 5 µl of 10x PCR buffer and 0.75 µl of Maxime™ Taq DNA polymerase (5 U μl^{-1}) in a volume of 50 µl.

The RT-PCR was performed using the same cycling conditions described for genotyping the T-DNA insertion mutants in *SLAH1* (section 3.2.4.1).

3.2.4.3. Quantitative Real Time PCR analyses (qPCR)

To analyse *SLAH* gene expression regulation by qPCR, RNA was extracted (section 3.3.1) from *Arabidopsis* Col-0 WT plants grown hydroponically under different conditions (section 3.1.2.2.3). The cDNA, synthesised from RNA (section 3.3.2), was used to quantify gene transcript levels by qPCR.

For the qPCR analyses, the *i*-Taq™ Universal SYBR® Green Supermix (Bio-Rad Laboratories) was used in a Bio-Rad CFX Connect Real-Time Detection System (Bio-Rad Laboratories), following the manufacturer's instructions. PCR (Table 3.16) was carried out with gene-specific primers (Table 3.17), designed by Primer3 (Rozen and Skaletsky, 2000) and OligoCalc software, in 96-well plates. After amplification, a melting cycle analysis was performed to ensure a single amplification product. Data were analysed using the Bio-Rad CFX Manager software (Bio-Rad Laboratories).

Table 3.16. Cycling parameters for qPCR amplification.

PCR cycle		Temperature (ºC)	Time (s)
Initial denaturation		95	300
40 cycles	Denaturation	95	25
	Annealing	62	15
	Extension	72	20

The gene encoding for the dehydrin *AtLEA-M* was used as a positive control of stress treatment responses, since it is a stress-inducible gene.

Table 3.17. Primers used in the qPCR.

Gene	Name	Sequence (5' → 3')
AtSLAH1	S1-RT-F	ATCCGGTCGGTTCTGGCTTAATGC
	S1-RT-R	AGGATCGTGTCTGAGTAGTCTATTGC
AtSLAH3	S3-RT-F	TTATCCACGCCTTTGTCCTCC
	S3-RT-R	CCGGTGTTGGCTATTCTGTTTGG
AtSLAH4	S4-RT-F	GATTACTTAGACGTGATCATGTCCTCTGG
	S4-RT-R	GCTTTGGTTTACAAGTTTCGCCATACACG
AteIF4A1	eIF4-RT-F	GGTATTGATGTCCAACAAGTCTCCC
	eIF4-RT-R	ATTGATCGCAACACCCTTTCTCCC
AtLEA-M	LEA-RT-F	ACTCACTCGACCACTGGACAAGTCGG
	LEA-RT-R	CAGTTCCAGTGTTCCTTCCAATCGGG

To transform fluorescence intensity measurements into relative mRNA levels, 10-fold dilution series of the corresponding PCR products were used as standard curves and two reactions containing template concentrations within the linear response region of the standard curve were used in every run. All mRNA levels were calculated from threshold cycle values and normalized with respect to the transcript level of the housekeeping *AteIF4A1* gene. Three biological and two technical repeats were used per treatment in every run. The level of the gene expression of plants subjected to the corresponding treatment was compared to the level of the gene expression of plants without treatment application and results were given as fold-change since the transcript abundance of the gene under treatment was divided by the control value.

In addition, the transcript level of *AtSLAH4* gene in *slah4-2* plants was tested by qPCR to know whether the *AtSLAH4* coding region was disrupted, since the T-DNA was inserted upstream of the predicted ATG start codon in this line (Fig. 3.3). This analysis was performed as described above using the suitable primer to amplify *AtSLAH4* gene (Table 3.17)

3.2.4.4. Mutagenesis PCR

Through the mutagenesis PCR, a point mutation, a deletion or an insertion of a sequence can be performed in plasmid DNA, therefore an exchange of whole gene segments in the pNBlu vectors (section 3.4.1) can be achieved.

Channels with directed point mutations were obtained through a modified USER™ method (Nørholm, 2010; Nour-Eldin *et al.,* 2006), in which the mutation is inserted into the gene to be examined through designed primers that contain the desired mutation in the middle of their sequence (Dadacz-Narloch *et al*., 2011).

The USER-compatible mutagenesis primers used in this method do not adhere to the ends of the construct, as in the USER™ method (section 3.4.1), but rather to the site where the mutation is to be inserted, covering 8 to 12 bp of the mutagenesis site. The only requirement for USER-based mutagenesis is an adenosine (A) at the 5' and a thymidine (T) 8–12 bp downstream of the desired fusion product (Fig. 3.4). This T residue in the tail region of the desired USER primers has to be replaced by a uracil (U). Point mutation can be inserted by modifying individual bases in the overlapping sequence of the two primers.

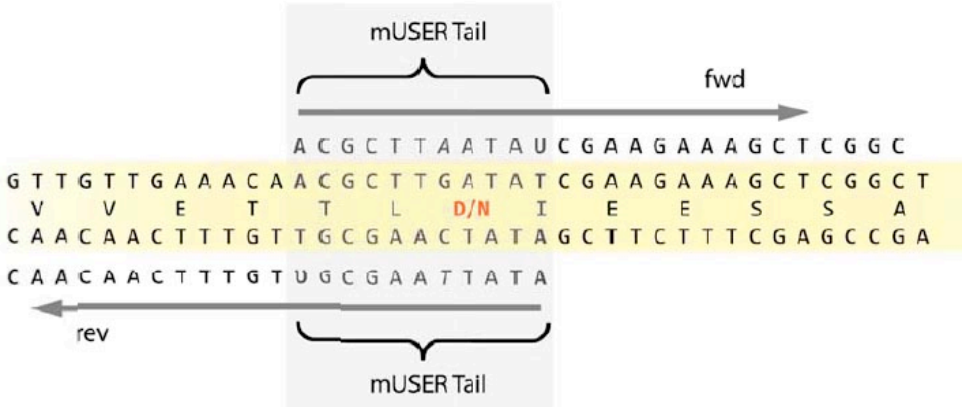

Figure 3.4. Design of USER-compatible mutagenesis primers. The primers cover 8–12 bp of the mutagenesis site. The primers have an adenosine (A) at the 5' and a thymidine (T) 8–12 bp downstream of the desired fusion product. This T residue in the tail region of the desired USER primers has to be replaced by a uracil (U). In this diagram GAT (encoding Asp [D; in red]) will be mutated into AAT (encoding Asn [N; in red]). Obtained from Dadacz-Narloch *et al.*, 2011.

A second primer pair that adheres in another part of the vector (in the ampicillin resistance in the case of the USER cassette of the pNBlu vectors, which is located in the opposite part of the gene of interest) is necessary to obtain the desired construct. The forward-directed mutagenesis primer is used together with the reverse primer located in the ampicillin resistance gene in a PCR reaction and the reverse-directed mutagenesis primer is used together with the forward-ampicillin primer in another PCR reaction (Table 3.18).

Table 3.18. Primers used for site-directed mutagenesis.

Name	Sequence (5' ➔ 3')
SLAH1 F307A user fwd	AGCACCACUCACTTTTCTTGCGTTAGA
SLAH1 F307A user rev	AGTGGTGCUGAGTAAGCCCACCACGC
SLAH1 F307L user fwd	ATTACCACUCACTTTTCTTGCGTTAGA
SLAH1 F307L user rev	AGTGGTAAUGAGTAAGCCCACCACGCG
SLAH1 S130V user fwd	ATTGTATGGCUTCTCATGCTTCAATCAGCTCC
SLAH1 S130V user rev	AGCCATACAAUAGATGGAGCGTAGAGATAGTTCACT
SLAH1 R47D user fwd	ATTTCGATAUAAGCCTCTCTCTTTGCAGCC
SLAH1 R47D user rev	ATATCGAAAUAGCCCGCGTGGAG
SLAH3 F517A user fwd	ACCGCTCCGAUGACCGGAGCTGC
SLAH3 F517A user rev	ATCGGAGCGGUGTACGCCCACCAGGAC
SLAH3 F517L user fwd	ACCTTACCGAUGACCGGAGCTGC
SLAH3 F517L user rev	ATCGGTAAGGUGTACGCCCACCAGG
SLAH3 G264D user fwd	ACCTTCGATAUGTGCCTAGGAGTGAGCAGC
SLAH3 G264D user rev	ATATCGAAGGUGGAAATGGGGTAA
Amp overlap user fwd	AGACCCACGCUCACCGGCTC
Amp overlap user rev	AGCGTGGGTCUCGCGGTATC

The DNA amplification was performed with the proof-reading Phusion C_x polymerase (Table 3.19; Thermo Fisher Scientific), which has been modified so that it does not regard uracil as a defect in a DNA molecule (Nørholm, 2010).

Table 3.19. Mutagenesis PCR reaction components.

Components	Volume (µl)
DNA template (vector with the gene of interes)	1
5x Phusion HF Reaction Buffer	10
dNTP Mix 10 mM	1
Forward primer 10 µM	1
Reverse primer 10 µM	1
Phusion Cx DNA polymerase 2 U μl^{-1}	1
Nuclease free water	35

The reactions were incubated (Table 3.20) in a Mastercycler Personal (Eppendorf, Wesseling-Berzdorf, Germany). The elongation time was determined by the size of the constructs, taking into account that the extension time of this enzyme is 40 seconds per kilobase.

Table 3.20. Cycling parameters.

PCR cycle		Temperature (ºC)	Time (s)
Initial denaturation		98	60
30 cycles	Denaturation	98	25
	Annealing	60	25
	Extension	72	100
Final extension		72	120

The resultant two halves of the vector were assembled by the USER™ cloning method (section 3.4.1), after removing the methylated template DNA by DpnI (section 3.2.7).

Through the modification of the bases in the overhangs of the mutagenesis primers, the desired mutation is inserted into the gene and is located directly at the same transfectable vector. By positioning the second primer pair in the antibiotic resistance of the vector, it is at the same time ensured that only one vector from the two different PCR products can be linked to form a functional vector and that no random ligation of one of the halves occurs alone.

In the case of performing an exchange of whole gene segments from one vector to another (Table 3.29; section 3.4.1), for example to obtain the examined gen from the *Xenopus* oocytes expression vector (pNBLu) into a vector that contains the half of the Yellow Fluorescent Protein (YFP), the PCR reaction (Table 3.19) contained the specific primers (Table 3.21) to amplify the whole gene. The vector containing the examined gene was used as template DNA and the reactions were incubated in the Mastercycler Personal (Eppendorf) with the conditions described above (Table 3.20).

Table 3.21. Primers used for gene cloning in pNBlu vectors.

Name	Sequence (5' ➔ 3')
SLAC1 user fwd	GGCTTAAUATGGAGAGGAAACAGTCAAATGCTC
SLAC1 user rev	GGTTTAAUTTAGTGATGCGACTCTTCCTCTGCTTC
SLAH1 user fwd	GGCTTAAUATGGAAATTCCGAGGCAAGAAATT
SLAH1 user rev	GGTTTAAUCTAGTTTTGGTTAGTCGCATTGAG
SLAH2 user fwd	GGCTTAAUATGAATAATCCAAGATCGGTTAGTCC
SLAH2 user rev	GGTTTAAUTTAATTTGAATTCTGAACCGTGGAAC
SLAH3 user fwd	GGCTTAAUATGGAGGAGAAACCAAACTATGTG
SLAH3 user rev	GGTTTAAUTTATGATGAATCACTCTCTTGAGTTTT
SLAH4 user fwd	GGCTTAAUATGGAAATACCTAGTCAAGAAATTCAC
SLAH4 user rev	GGTTTAAUTTATTTGTCTTTTGGACCAGTAGAAG
CIPK23 user fwd	GGCTTAAUATGGCTTCTCGAACAACGCCTTC
CIPK23 user rev	GGTTTAAUTTATGTCGACTGTTTTGCAATTG
CBL1 user fwd	GGCTTAAUATGGGCTGCTTCCACTCAAAG
CBL1 user rev	GGTTTAAUTCATGTGGCAATCTCATCG
CPK3 user fwd	GGCTTAAUATGGGCCACAGACACAGCAAG
CPK3 delta EF user rev	GGTTTAAUTTACTCCCCATCTTCTCTAATCCAC
CPK6 user fwd	GGCTTAAUATGGGCAATTCATGTCGTGGTTC
CPK6 user rev	GGTTTAAUCTACACATCTCTCATGCTGATGTTTAG
CPK21 user fwd	GGCTTAAUATGGGTTGCTTCAGCAGTAAACAC
CPK21 delta EF user rev	GGTTTAAUTTATTCTCCCCCTTTGATCCAAGG
CPK23 user fwd	GGCTTAAUATGGGTTGTTTCAGCAGTAAACAC
CPK23 user rev	GGTTTAAUTCAGTGGAATGGATACTGTTTCCC
SnRK2.2 user fwd	GGCTTAAUATGGATCCGGCGACTAATTCAC
SnRK2.2 user oS rev	GGTTTAAUCCGAGAGCATAAACTATCTCTCCACTAC
SnRK2.3 user fwd	GGCTTAAUATGGATCGAGCTCCGGTGAC
SnRK2.3 user oS rev	GGTTTAAUCCGAGAGCGTAAACTATCTCTCCGC
OST1 user fwd	GGCTTAAUATGGATCGACCAGCAGTGAGTGG
OST1 user oS rev	GGTTTAAUCCCATTGCGTACACAATCTCTCCGC
SnRK2.7 user fwd	GGCTTAAUATGGAGAGATACGACATCTTAAGAG
SnRK2.7 user oS rev	GGTTTAAUCCTAGAGCACATACGAAATCACCATTTC
SnRK2.8 user fwd	GGCTTAAUATGGAGAGGTACGAAATAGTGAAGG
SnRK2.8 user oS rev	GGTTTAAUCCCAAAGGGGAAAGGAGATCAGC

Following the remove of the methylated template DNA by DpnI (section 3.2.7), the DNA product (the gene of interest) was used, together with the destination vector, in a USER™ reaction (section 3.4.1) for obtaining the whole vector.

3.2.4.5. IVT-PCR

The *in vitro* PCR (IVT-PCR) was used to linearize the DNA plasmid extracted from bacteria (section 3.2.1) coming from the transformation of chemically competent *E. coli* cells (section 3.5.1.2) with the USER reaction (section 3.4.1).

The IVT-PCR is a conventional PCR with specific primers (IVT primers; Table 3.22) designed specially for the pNBlu vectors. All the used vectors contained the T7 promoter of the T7 RNA polymerase together with the *Xenopus* β-globin UTRs and the ampicilin resistance gene. Taking that into account for the design of the IVT primers, the resultant DNA from the PCR contained the insert of interest together with the T7 promoter (necessary for the *in vitro* transcription (IVT); section 3.3.3) and the 5' and 3' untranslated regions (UTRs) of the β-globulin

from *Xenopus.* From the pNBlu vectors numbers 18–21 (Table 3.29; section 3.4.1), the sequence of the reporter gene YFP (necessary for BiFC; section 3.11) was also amplified.

Table 3.22. IVT primers sequences.

Name	Sequence (5' ➔ 3')
IVT fwd	CAA GGC GAT TAA GTT GGG TAA C
IVT rev	GAT TAC GCC AAG CTA TTT AGG TG

The DNA amplification was performed with the proof-reading Phusion C_x polymerase (Thermo Fisher Scientific), as in the Mutagenesis PCR. The reaction mix composition and the cycling parameters were as described for the Mutagenesis PCR (section 3.2.4.4).

Afterwards, the linearized DNA samples were checked in an electrophoresis 1% agarose gel (section 3.2.5) and subsequently purified (section 3.2.6) for being used as template in the *in vitro* transcription (IVT; section 3.3.3.).

3.2.5. DNA electrophoresis

For DNA electrophoresis, agarose gel contained 0.7–2% agarose melted in 1x TAE buffer (Table 3.23) was used for the separation of differently sized nucleic acid fragments. In order to visualize the fragments within the gel, either Red Safe (50 µl l^{-1}; Intron Biotechnology Inc.) or GelGreen™ (0.05 µl l^{-1}; Biotium, Hayward, CA, USA) was added.

Different agarose concentrations were used for different fragment sizes. For DNA fragments larger than 700 bp, 1% agarose gel was used, meanwhile 1.5–2% agarose was utilised for DNA strands with smaller length.

The samples were mixed with 6x DNA buffer (Table 3.23) and loaded into the pockets of the agarose gel. The 6x DNA loading buffer contained glycerol to give the samples a higher density compared to the TAE run buffer, leaving them in the gel packs and not diffusing into the buffer.

Table 3.23. TAE buffer and DNA loading buffer composition.

1x TAE Buffer		6x Loading Buffer	
Constituent	**Amount**	**Constituent**	**Concentration (%)**
Tris base	0.04 M	Bromophenol blue	0.25
Glacial acetic acid	1.14 ml	Glycerol	30.0
EDTA (pH 8.0)	0.01 M		

As a reference for the length of the samples, either a DNA Ladder from different companies (Intron biotechnology Inc.; Favorgen Biotech Corp., Kaohsiung, Taiwan) or a λ-PstI marker obtained by the digestion of the DNA of the λ phage with the restriction enzyme PstI was used.

The agarose gel was run in a gel electrophoresis chamber with 1x TAE buffer at 70–120V.

The samples migrate through the gel along the applied electric field. As DNA molecules are negatively charged due to the phosphate backbone of the strands, they migrate in an electric field to the positive pole (anode) in the electrophoresis chamber.

After electrophoresis the gel was photographed with either the ChemiDoc™ XRS Gel documentation system (Bio-Rad Laboratories) or the transiluminator Intas UV Imager (Intas, Göttingen, Germany).

3.2.6. DNA purification

DNA purification from either agarose gel or PCR products was performed with either the FavorPrep™ gel/PCR purification kit (Favorgen Biotech corp.) or the MEGAquick-spin™ Total Fragment DNA Purification Kit (Intron Biotechnology Inc.), both according to manufacturers' protocols. The DNA was finally eluted with 40–50 µl of the corresponding elution buffer.

After the IVT-PCR (section 3.2.4.5), DNA products were purified with the QIAquick PCR purification kit (Qiagen) following the manufacturer's protocol. The DNA was eluted with 35 µl of elution buffer. The purified DNA samples were further sequenced (section 3.2.8) and used for cloning (section 3.4.1) or cRNA synthesis by the *in vitro* transcription (IVT; section 3.3.3).

3.2.7. DNA digestion with restriction enzymes

In order to verify the presence and the appropriate size of the insert in the bacterial transformed cells (sections 3.51.2 and 3.5.2.2) restriction enzyme analyses with the suitable enzymes (Thermo Fisher Scientific) were done after plasmid DNA extraction (section 3.2.1).

Each reaction mix contained 3 µl of plasmid DNA, 1.5 µl of the appropriate 10x buffer (Table 3.24) and 0.4–0.5 µl of restriction enzyme (10 U μl^{-1}) in a volume of 15 µl. The enzymatic reaction including the NotI enzyme also contained 1.5 µl of 10x BSA and 1.5 µl of 10x Triton. Restriction reactions with two enzymes were performed with a proper buffer for both of them.

Reactions were incubated overnight at the optimal temperature for the activity of the corresponding enzyme. Apart from SmaI, whose optimal activity temperature is 30ºC, all the enzymes were incubated at 37ºC.

Table 3.24. Restriction enzymes and their suitable buffer.

Restriction enzyme	Buffer
EcoRI	EcoRI
HindIII	R (red)
MluI	R (red)
PstI	O (orange)
SmaI	Tango™
XhoI	R (red)

Following the DNA digestion with restriction enzymes, DNA digestion products were separated by electrophoresis in agarose gels (section 3.2.5).

In the Gateway cloning (section 3.4.2), DNA digestion with restriction enzymes was performed after bacteria transformation (sections 3.51.2 and 3.5.2.2) to verify the presence of the insert. HindIII and MluI were the enzymes used for *SLAH1* promoter-pENTR/D-TOPO® restriction analyses, EcoRI and PstI for *SLAH4* promoter-pDONR™201 and PstI, together with a double reaction of XhoI and PstI, were used for *AtSLAH1* gene-pDONR™201 restriction analyses. In addition, SmaI and HindIII were used for *SLAH* promoter-pKGWFS7 restriction analyses and HindIII, PstI, and a double reacton PstI/XhoI were used for *AtSLAH1* gene-pK7WG restriction analyses.

DpnI restriction enzyme (Thermo Fisher Scientific) was used after the Mutagenesis-PCR (section 3.2.4.4) and before the USER reaction (section 3.4.1). DpnI eliminates the plasmid DNA used in the Mutagenesis-PCR as template because it digests methylated DNA. One microliter of this enzyme was added directly in the PCR products, without buffer. After incubating the reactions 1 h at 37ºC, the DpnI enzyme was inactivated by maintaining the sample 20 min at 80ºC.

3.2.8. DNA sequencing

Purified DNA fragments (section 3.2.6) that were produced by high fidelity Taq polymerase amplification (section 3.2.4.1) and the isolated plasmid DNA (section 3.2.1) obtained after transformation during the Gateway® cloning method were sequenced by Secugen S.L. (Madrid, Spain) and Stab Vida (Caparica, Portugal).

To verify the amplified and cloned genes obtained through the USER™ cloning, isolated plasmid DNA (section 3.2.1) and purified DNA samples (section 3.2.6) were sequenced by GATC-Biotech (Germany).

All DNA samples were diluted according to the company protocol. Only after a positive complete sequencing, DNA samples were used for further work steps.

3.2.9. Amino acid sequences alignments

Database searches looking for sequence similarities were performed using the Basic Local Alignment Search Tool (BLAST) program (Altschul *et al.,* 1997) from the National Center for Biotechnology Information (NCBI; https://blast.ncbi.nlm.nih.gov/Blast.cgi). Multiple sequence alignments were performed using the ClustalW2 program (Larkin *et al*., 2007).

3.3. RNA ANALYSES

3.3.1. RNA extraction

RNA was extracted from *Arabidopsis* Col-0 WT plants in order to perform qPCR analyses (section 3.2.4.3) and also from the T-DNA insertion mutant lines and the two independent *slah1*/*SLAH1* complemented lines (P1-12 and P1-31) to determine the integrity of the *AtSLAH* mRNA through RT-PCR (section 3.2.4.2).

Plant RNA extraction was performed either by the Isolate II RNA Plant kit (Bioline), following the manufacturers' protocol, or by TRIsure™ reagent procedure (Bioline).

Through TRIsure™ reagent procedure total RNA was extracted from frozen tissues. Following the homogenization of frozen samples with 1 ml TRIsure™ per 50–100 mg of tissue by shaking in a Bio Vortex V1 (Biosan), insoluble material was removed by centrifugation at 12,000 × *g* for 10 min at 4ºC and the clear supernatant was transferred to a new microcentrifuge tube. Afterwards, 200 µl of chloroform per millilitre of used TRIsure™ was added to the samples and they were shaked vigorously by hand for 15 s. After incubating the samples 3 min at room temperature, they were centrifuged at 12,000 × *g* for 15 min at 4ºC. The aqueous phase, which contained the RNA, was transferred into a new microcentrifuge tube. The RNA was subsequently precipitated by mixing the samples with 600 µl of cold isopropyl alcohol per millilitre of used TRIsure™. After 10 min of incubation at room temperature, the samples were centrifuged 10 min at 12,000 × *g* at 4ºC and the supernatant was discarded and the pellet was dried. Afterwards, the pellet was washed with 1ml of 70% cold-ice ethanol per millilitre of used TRIsure™. Following the shaked of the samples with the Vortex, they were centrifuged 5 min at 7,500 × *g* at 4ºC. The ethanol was then discarded and the pellet died. Finally, the pellet was resuspended in 20–30 µl milli-Q water treated with 0.1% DEPC.

The RNA concentration of the samples was quantified (section 3.3.4) and the quality of them was verified by electrophoresis in 1% agarose gel (section 3.3.2).

Previously to perform the RNA retrotranscription (section 3.2.4.2), contaminated DNA was eliminated by RNAse-free DNase I (Thermo Fisher Scientific) according to manufacturers' protocol and RNases were also inhibited using RiboLock RNase Inhibitor (Thermo Fisher Scientific). Each reaction mix (Table 3.25) had a final volume of 10 µl and was incubated 30 min at 37ºC followed by 10 min at 65ºC.

Table 3.25. DNase reaction mix.

Components	Volume (µl)
10x Reaction buffer with $MgCl_2$	1
DEPC-treated water	6.75
RNA	1
Dnase I, Rnase-free (1U μl^{-1})	1
Ribolock Rnase Inhibitor (40Uμl^{-1})	0.25
EDTA 0.5 M (pH 8.0)	1

3.3.2. RNA electrophoresis

Agarose gel was also used for RNA separation by electrophoresis to verify the purity and degree of denaturation of the RNA.

For RNA electrophoresis, agarose gel contained 1% agarose melted in 1x MAE buffer (Table 3.26) and 3.7% formaldehyde.

Table 3.26. 1x MAE buffer.

Constituent	Concentration (mM)
MOPS	20
Sodium acetate (pH 7.0)	5
EDTA (pH 8.0)	1

In order to visualize the fragments within the gel, ethidium bromide was added to the RNA loading buffer (Table 3.27). RNA samples were mixed with 1.25x RNA loading buffer, heated at 56ºC for 15 min to open its secondary structures and immediately placed on ice.

Table 3.27. 1.25x RNA loading buffer composition.

Constituent	Concentration
Formamide	55.0 %
Formaldehyde	7.37 %
10x MAE	1.25 %
Bromophenol blue	0.5 g l^{-1}
Glycerol	8.0 %
Ethidium bromide	40 g l^{-1}

The samples were charged into the gel and the electrophoresis was carried out at a voltage of 70–80 V. RNA molecules are negatively charged, like DNA molecules, and thus migrate to the anode in the electrophoresis chamber.

Finally the gel was photographed with either the ChemiDoc™ XRS Gel documentation system (Bio-Rad Laboratories) or the transiluminator Intas UV Imager (Intas).

3.3.3. Complementary RNA (cRNA) synthesis by *in vitro* transcription (IVT)

Since the optimal templates for *in vitro* transcription are linear double-stranded DNA (dsDNA) molecules with 5'-protuding ends, the linearized IVT-PCR products (section 3.2.4.5), which were purified (section 3.2.6), were used as templates for the complementary RNA (cRNA) synthesis.

Taking into account that all the vectors contained the T7 promoter of the T7 RNA polymerase from the T7 bacteriophage, T7 RNA polymerase was used to synthesise cRNAs from the different purified constructs using the AmpliCap-Max™ T7 High Yield Message Maker Kit (Cellscript, Madison, US).

Each IVT reaction mix (Table 3.28) had a final volume of 10 µl and was incubated 90 min at 37ºC.

Table 3.28. IVT reaction mix.

Component	Volume (µl)
10x AmpliCap-Max T7 Transcription Buffer	1
100 mM Dithiothreitol (DTT)	1
AmpliCap-Max Cap/NTP PreMix	4
ScriptGuard Rnase Inhibitor	0.25
AmpliCap-Max T7 Enzyme Solution	1
Linearized template DNA with T7 RNAP promoter	2.75

The transcription products were purified using ammonium acetate (NH_4Ac) precipitation that selectively precipitates RNA, while leaving most of the protein, DNA and unincorporated NTPs in the supernatant. A volume of 60 µl of 5 M NH_4Ac was added to each

reaction and they were stored at −20ºC for at least 1 h. The cRNAs were precipitated by centrifugation at 20,000 × *g* for 1 h at 4ºC. The supernatant was removed with a pipette and gently washed with 75% ice-cold ethanol. The cRNAs were dried and subsequently resuspended in 16 µl RNase-free water.

The concentration of the samples was quantified (section 3.3.4) and the quality of them was verified by electrophoresis in 1% agarose gel (section 3.3.2).

3.3.4. RNA quantification

The determination of the concentration of the cRNA samples obtained from the *in vitro* transcription (IVT; section 3.3.3) was performed with 1 µl in a NanoDrop® 2000c spectrophotometer (Thermo Fisher Scientific). The concentration of the samples was generally adjusted to 500 ng μl^{-1} in order to electrophysiologically examine the clones generated by the two-electrode voltage clamp (TEVC) technique (section 3.12),

The concentration of RNA samples obtained from plant tissues (section 3.3.1) was measured using the spectrophotometer NanoDrop® ND-1000 (Thermo Fisher Scientific). The samples whose RNA concentration was higher than 1.5 µg μl^{-1}, were adjusted to a final concentration of 1.5 µg μl^{-1} with milli-Q water treated with 0.1% DEPC.

3.4. CLONING METHODS AND PLASMID CONSTRUCTION

Through cloning, a DNA fragment is integrated into a vector. This construct can be transformed into different hosts, like *Escherichia coli.* Plasmid vectors are DNA molecules replicated and amplified in bacterial cells.

In conventional cloning techniques, restriction endonucleases are used to cut plasmid vectors at the cloning site so that single-stranded overhangs are formed at the interfaces. Thus, DNA fragments with complementary overhangs can be subsequently inserted at these sites. The disadvantage of this cloning technique is that two different restriction sites are required in both the DNA of interest and the vector for directional cloning. And through conventional restriction enzymes only short overhangs of 2–4 bases are formed, which require an additional ligation step during cloning.

3.4.1. USER™ cloning

The USER™ (uracil-specific excision reagent) cloning technique (Nour-Eldin *et al.*, 2006) allows fast and very efficient cloning of a PCR fragment without a ligation step. The cloning method is based on the fact that 8 nucleotides (nt) long complementary overhangs are generated at the 3' ends of a PCR amplified DNA fragment (insert with the point mutation) and a linearized destination vector to make a stable hybridization product without ligation (Fig. 3.5).

On the one side, a 38 bp-long PacI-USER cassette makes vectors compatible with the USER process (Nour-Eldin *et al.*, 2006). Treatment with the restriction enzyme PacI (Fig. 3.5; New England Biolabs Inc., UK) cut the vectors and together with the enzyme Nt.BbvCI (Fig. 3.5; New England Biolabs Inc.), which only cuts one strand of the double-stranded DNA, 3' overhangs

of 8 bp are produced, which are not complementary between each others. This fact prevents a rehybridization of the vector and also ensures a directed insertion.

On the other side, PCR products must have 5' overhangs complementary to the 3' overhangs of the vectors (Fig. 3.5). These overhangs are generated on PCR fragments by adding to the gene-specific sequence 8 bp sequences to both overhangs, whose eighth nucleotide is a uracil residue (U). For this purpose, a specific sequence is contained in the forward (5'-GGCTTAAU-3') and the reverse (5'-GGTTTAAU-3') primer at the 5' region. Following the DNA amplification by a DNA polymerase that does not regard uracil as a defect in a DNA molecule (section 3.2.4.4), the resulting PCR product is treated with an USER enzyme mix (New England Biolabs Inc.) consisting of a uracil DNA glycosylase and a DNA glycosylase-lyase Endo VIII (New England Biolabs Inc.). These enzymes remove the uracil residues and enable the dissociation of the single-stranded fragments lying upstream from the cleavage sites (Fig. 3.5). Thus vector-compatible single-stranded overhangs are formed.

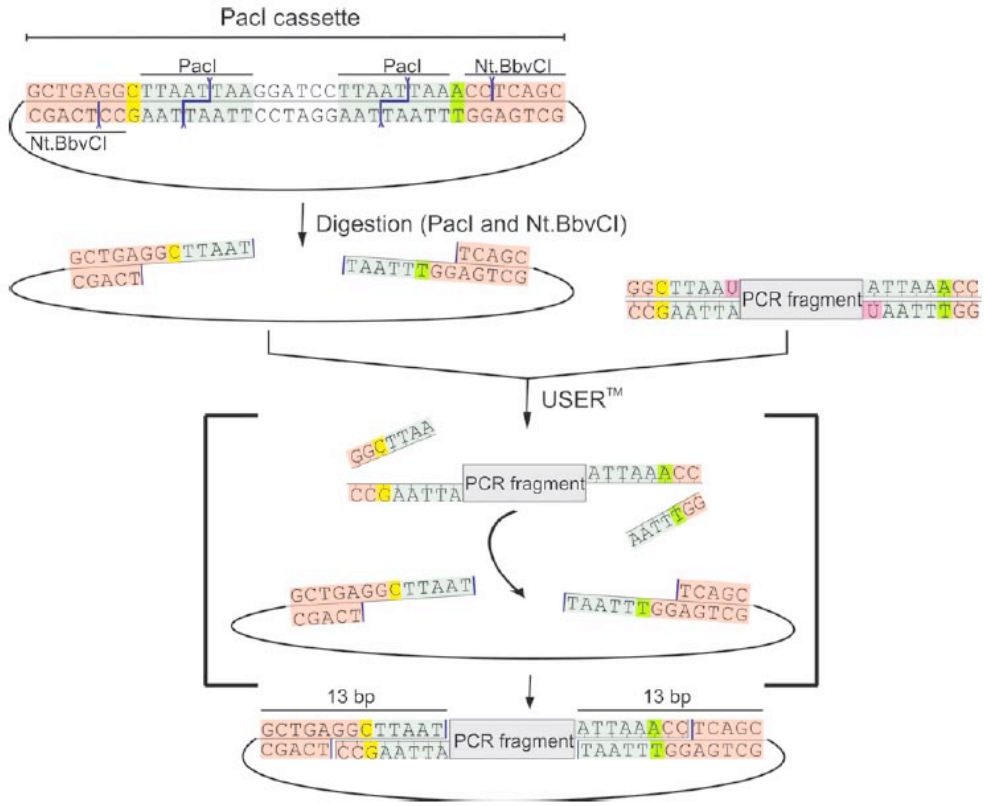

Figure 3.5. USER™ cloning technique. A 38 bp-long PacI cassette (upper left corner) contained in a USER vector is digested with the restriction enzymes PacI and Nt.BbvCI to produce 8 nt single-stranded 3' overhangs. An amplified PCR fragment containing uracil (pink) is added to the linearized vector and through the USER enzyme Mix, the uracils are removed and subsequently the vector and the fragment hybridize. Yellow and green mark single base differences between the generated 3' overhangs, which are responsible for the directional insertion of the PCR fragment. Obtained from Nour-Eldin *et al*., 2006.

The vectors (Table 3.29) used in this study for expression in the heterologous expression system *Xenopus laevis* oocytes were provided by Prof. Dr. Dietmar Geiger (Julius-von-Sachs Institute, Würzburg University, Germany). All the vectors contained the T7 promoter of the T7 RNA polymerase together with the *Xenopus* β-globin UTRs and the ampicillin resistance gene in the USER cassette (Nour-Eldin *et al.,* 2006). The vector pNBlu number 16 was used for constitutive gen expression in *Xenopus* oocytes and TEVC recordings (section 3.12) and the rest

of the vectors were also used for performing the protein interaction assays with the bimolecular fluorescence complementation (BiFC) analyses (section 3.11).

Table 3.29. USER™ vectors used for expression in *Xenopus laevis* oocytes. Nomenclature and description of the oocytes expression vectors. For the BiFC experiments, the Yellow Fluorescent Protein (YFP) was cleaved into the N-terminal (amino acids 1-155) and C-terminal (amino acids 156-239) halves.

Vector number	Name	Description
16	pNBlu	*Xenpus* oocytes expression vector made USER compatible
17	pNBlu N-term YC	C-terminal half of YFP placed upstream of the USER cassette
18	pNBlu C-term YC	C-terminal half of YFP placed downstream of the USER cassette
19	pNBlu N-term YN	N-terminal half of YFP placed upstream of the USER cassette
20	pNBlu C-term YN	N-terminal half of YFP placed downstream of the USER cassette
21	pNBlu N-term YFP	YFP placed upstream of the USER casette

Therefore, to perform the insertion of the gene of interest into the desired vector, the DNA sequence of this gene previously obtained (section 3.2.4.4) was cloned in the pNBlu vector through the USER enzyme mix described above. The USER reaction (Table 3.30) was incubated at 37ºC for 25 min followed by 25 min at 25ºC in a Mastercycler Personal (Eppendorf).

Table 3.30. Components of the USER cloning reaction.

Component	Volume (µl)
Vector	1.5
PCR product	4
TE Buffer	3.5
USER-Enzyme Mix (1 U μl^{-1})	1

As explained before, site-directed mutations (section 3.2.4.4) could be introduced in the gene of interest by a modified USER fusion method (Dadacz-Narloch *et al.*, 2011). In this case, the USER reaction contained (Table 3.31) the two PCR products that constitute the two halves of a pNBlu vector with the gene of interest. The samples were incubated at 37ºC for 25 min followed by 25 min at 25ºC.

Table 3.31. Components of the modified USER cloning reaction.

Component	Volume (µl)
PCR product 1	2
PCR product 2	2
TE Buffer	5
USER-Enzyme Mix (1 U μl^{-1})	1

The whole vector produced in the USER reaction was immediately transformed into chemically competent *E. coli* cells (section 3.5.1.2). After bacteria selection in LB supplemented

with ampicillin (section 3.11), single colonies were picked to perform the DNA plasmid extraction (section 3.2.1). After obtaining the right sequence, the DNA samples were used for the IVT-PCR (section 3.2.4.5) by which the resulting pNBlu plasmid with the insert of interest was linearized. The product reaction was purified (section 3.2.6) and the DNA concentration was determined (section 3.2.3). Afterwards, the dsDNA was *in vitro* transcribed (section 3.3.3) followed by a verification of the RNA purity (section 3.3.2).

3.4.2. Gateway® technology

The Gateway® cloning method (Invitrogen) is based on the site-specific recombination system of bacteriophage lambda (λ) (Landy, 1989), which facilitates the integration of lambda into the *E. coli* chromosome, and provides a quick and efficient way to transfer DNA sequences between different vectors for different objectives, like functional analysis or protein expression (Hartley *et al.*, 2000).

The recombination occurs between specific DNA recombination sequences (*att* sites) by a mixture of lambda and *E. coli*-encoded recombination proteins that catalyse the recombination reaction. The DNA segments flanking the recombination sites are switched, so the *att* sites are hybrid sequences comprised of sequences donated by each parental vector after recombination. The crossover occurs between homologous 15 bp core regions on the two sites, but the surrounding sequences are essential since they contain the binding sites for the recombination enzymes (Landy, 1989).

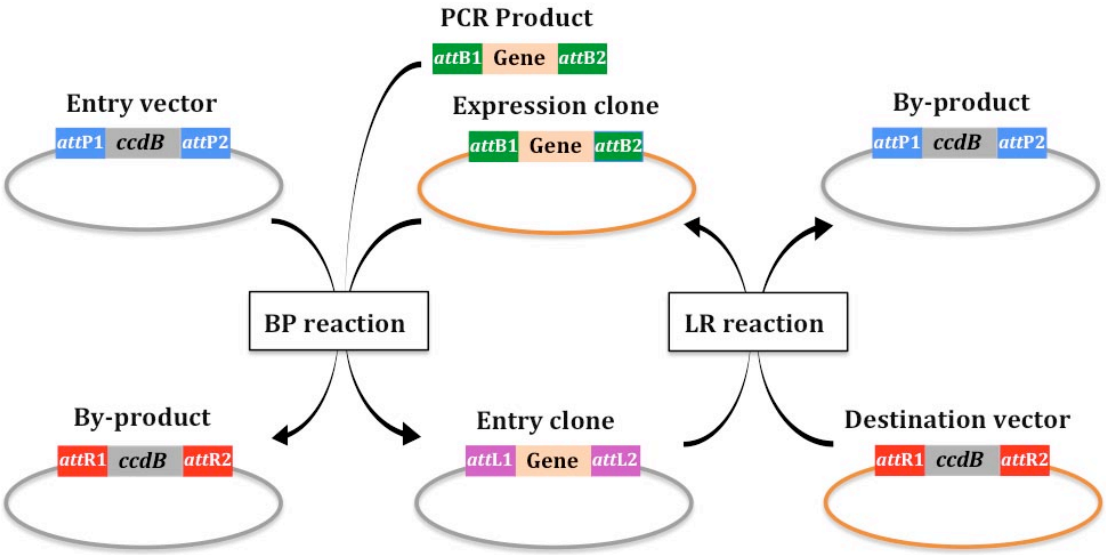

Figure 3.6. Gateway® cloning technology. The BP reaction generates the entry clone (with *att*L sites) after the recombination between the entry vector (containing *att*P sites) and the DNA of interest flanked by *att*B sites or an expression clone. In the LR reaction takes places the recombination of the entry clone with a destination vector (with the *att*R sites), leading to an expression clone containing *att*B sites. Genes can be transferred between different vectors once it is cloned in a Gateway vector. The by-product molecules containing the *ccd*B gene do not generate negative clones.

Two recombination reactions constitute the basis of this cloning method. In the BP reaction takes places the recombination of a PCR product flanked by *att*B sites (or a linearized *att*B expression clone) with an entry vector containing *att*P sites, leading to an *att*L-containing entry clone (Fig. 3.6). And the LR reaction leads to an *att*B-containing expression clone after the

recombination of an *att*L-containing entry clone with a destination vector containing the *att*R sites (Fig. 3.6). In the design of the primers, the *att*B sites have to be incorporated to generate a suitable PCR product.

The *att* sites flank a cassette that contains the chloramphenicol resistance gene (Cm^R) and also the *ccd*B gene, which allow negative selection in *E. coli* since the CcdB protein interferes with the DNA gyrase, supressing its growth when the recombination does not take place (Bernard and Couturier, 1992). After each recombination reaction this cassette is replaced by the gene of interest.

3.4.2.1. Producing entry clones

The *AtSLAH1* promoter (section 3.2.4.1) was cloned into the entry vector pENTR/D-TOPO® using the pENTR™/D-TOPO® Cloning kit (Invitrogen). The cloning reaction (Table 3.32) was performed following the manufacturer's instructions.

Table 3.32. TOPO® cloning reaction composition.

Components	Volume (µl)
PCR Product	4
pENTR/D-TOPO vector	1
Salt Solution	1

The *AtSLAH4* promoter (section 3.2.4.1) for constructing the *SLAH4* promoter-GFG::GUS reporter fusion and the *AtSLAH1* gene (section 3.2.4.1) for complementation of the *slah1-2* T-DNA insertion mutant were cloned into the pDONR™201 entry vector using the Gateway BP Clonase™ II Enzyme Mix kit (Table 3.33 ; Invitrogen).

Table 3.33. BP recombination reaction.

Components	Volume (µl)
PCR Product	5
pDONR201 vector	1.5
TE Buffer, pH 8.0	1.5
BP Clonase II enzyme mix	2
Proteinase K solution	1

The reaction products from *SLAH1* promoter-pENTR/D-TOPO®, *SLAH4* promoter-pDONR™201 and *AtSLAH1*-pDONR™201 were used for transforming TOP10 or Mach1™-T1 chemically competent *E. coli* cells (section 3.5.1.2). Following the bacteria selection in LB (section 3.1.1) supplemented with 50 µg ml^{-1} kanamycin, single colonies were picked to perform the DNA plasmid extraction (section 3.2.1). In order to verify the presence of the insert enzymatic restriction analyses were performed (section 3.2.7). The DNA plasmid was then sequenced (section 3.2.8). After obtaining the right sequences, the LR reaction (section 3.4.3.2) was performed with these DNA plasmids.

3.4.2.2. Producing expression clones

Constructs in pENTR/D-TOPO® and pDONR™201 vectors were subcloned into a binary destination vector using the Gateway LR Clonase™ II Enzyme Mix kit (Table 3.34; Invitrogen).

Table 3.34. LR recombination reaction.

Components	Volume (µl)
Entry clone	1
Destination vector	1
TE Buffer, pH 8.0	6
LR Clonase II enzyme mix	2
Proteinase K solution	1

On the one side, *SLAH* promoter constructs were subcloned into the binary destination vector pKGWFS7 (Plant Systems Biology Department, Ghent University, Belgium), resulting in a transcriptional fusion with the GFP::GUS cassette. And on the other side, *AtSLAH1* promoter was subcloned into the binary destination vector pH7WG7 (Plant Systems Biology Department).

The reaction products from *SLAH1* promoter-pKGWFS7, *SLAH4* promoter-pKGWFS7 and *AtSLAH1* gene-pH7WG were used for transforming chemically competent *E. coli* cells (section 3.5.1.2). The bacteria selection took place in LB (section 3.1.1) supplemented with 100 µg ml^{-1} streptomycin. Single colonies were picked to perform the DNA plasmid extraction (section 3.2.1).

The DNA was then sequenced (section 3.2.8). After obtaining the right sequences, *Agrobacterium tumefaciens* transformation (section 3.5.2.2) followed by enzymatic restriction analyses, was performed (section 3.2.7).

Constructs in pKGWFS7 and pH7WG vectors were transformed into *A. thaliana* Col-0 and *slah1-2* plants respectively via the *Agrobacterium thumefaciens*-mediated floral dip method (section 3.6).

3.5. BACTERIAL COMPETENT CELLS OBTAINING AND TRANSFORMATION

3.5.1. *Escherichia coli*

3.5.1.1. Competent cells obtaining

In order to prepare TOP10 and Mach1™-T1 (Invitrogen) *E. coli* high efficiency chemically competent cells, these strains were grown on a LB plate (section 3.1.1) at 37ºC overnight for obtaining single colonies, which were afterwards picked into a vial of 2 ml of LB medium and shaked overnight at 37ºC. This vial was used to inoculate 200 ml of SOB medium (section 3.1.1.1) and it was shaked at 28ºC overnight. The optical density (OD) at 600nm (OD_{600}) of the culture was obtained using the spectrophotometer BioMate™ 3 (Thermo Fisher Scientific). The growth was stopped when the optical density reached 0.25–0.3 maintaining the bacteria in ice for 20 min. It was centrifuged 10 min at 3000 × *g* at 4ºC. Following the discard of the supernatant, the cells were gently resuspended in 80 ml of cold CCMB80 buffer (Table 3.35) and incubated on ice 20 min. The centrifugation and discard of the supernatant steps were repeated and bacteria were resuspended in 10 ml of cold CCMB80 buffer. Finally the OD_{600} of a mixture of

400 µl SOC medium (section 3.1.1.1) and 100 µl of the resuspended cells was tested to verify that it was 1.0−1.5. Aliquots of 100 µl were done and the vials were store at −80ºC.

Table 3.35. CCMB80 buffer composition.

Constituent	Concentration
KOAc (pH 7.0)	10 mM
$CaCl_2$	80 mM
$MnCl_2$	20 mM
$MgCl_2$	10 mM
Glicerol	100 ml l^{-1}
pH was adjusted to 6.4 with HCl 0.1 N	

3.5.1.2. Competent cells transformation

The DNA products obtained in the Gateway® cloning (section 3.4.2) were used for transforming TOP10 or Mach1™-T1 chemically competent *E. coli* cells (section 3.5.1.1). For this purpose, a vial of competent *E. coli* cells stored at −80ºC was thawed for 5 min on ice and afterwards 2 µl of the DNA products were added and gently mixed. After 5 min on ice, a heat-shock of 30 s at 42ºC was performed to alter membrane fluidity, creating pores. And it was immediately transferred to ice again. Then 250 µl of SOC medium (section 3.1.1.1) was added and it was incubated 1 h at 37ºC with agitation. The bacteria were plated on LB plates supplemented with the selection antibiotic (the kanamycin resistance gene is in pENTR/D-TOPO® and pDONR™201 vectors, meanwhile the streptomycin resistance gene is in pKGWFS7 and pH7WG vectors). Plates were incubated overnight at 37ºC.

The complete DNA product obtained from the USER cloning reaction (10 µl; section 3.4.1) was used for bacteria transformation. A vial containing chemically competent *E. coli* cells stored at −80ºC was thawed for 5 min on ice. Subsequently, the USER reaction was added and a heat shock of 45 s at 42ºC was applied. The bacteria were then incubated 3 min on ice. Afterwards, the bacteria were plated on LB (section 3.1.1.1) agar plate supplemented with ampicillin (50 µg ml^{-1}) and incubated overnight at 37ºC.

The antibiotic-resistant cells containing the plasmid of interest were picked into vial of 2 ml with LB medium (section 3.1.1.1) and shaked overnight at 37ºC. DNA plasmid extraction (section 3.2.1) was performed the following day.

In the case of Gateway® cloning, enzymatic restriction analyses (section 3.2.7) were performed with DNA plasmid in order to verify the presence of the insert in the plasmid.

For the long-term storage at −80ºC of the positive transformed bacteria, which contained the correct sequencing vector, 500 µl of an overnight culture was gently mixed with 500 µl of 30% glycerol and immediately frozen with liquid nitrogen.

3.5.1.3. Transformation efficiency calculation

The transformation efficiency is defined as the number of colony forming units (CFU) that would be produced by transforming 1 µg of plasmid into a given volume of competent cells.

To obtain the transformation efficiency a 100 µl vial of competent cells was transformed with 1 µl of standard pUC10 plasmid (10 pg μl^{-1}; Invitrogen) following the transformation procedure described above.

The followed equation was used for calculating the transformation efficiency:

$$\frac{\text{CFU on plate}}{\text{10 pg pUC19 added}} \text{x} \frac{\text{1 x } 10^6 \text{ pg}}{\text{1 µg}} \text{x} \frac{\text{total volume}}{\text{volume plated}} = \text{CFU } \mu g^{-1}$$

3.5.1. *Agrobacterium tumefaciens*

3.5.2.1. Competent cells obtaining

To prepare *A. tumefaciens* GV3101 chemically competent cells, this strain was grown on a LB (section 3.1.1) plate with rifampicin (50 mg ml^{-1}) at 28ºC overnight. Single colonies were picked into a vial of 5 ml of YEP medium (section 3.1.1.2) and shaked overnight at 28ºC. Afterwards 80 ml of YEP medium was inoculated with the 5 ml vial and it was shaked 3–4 h at 28ºC. The growth was stopped at OD_{600} of 0.5–1.0 maintaining the bacteria in ice for 5 min. It was centrifuged at 3000 × *g* at 4ºC for 5 min. Following the discard of the supernatant, the cells were gently resuspended in 11 ml of cold 20 mM $CaCl_2$. Finally aliquots of 100 µl were done and the vials were store at −80ºC.

3.5.2.1. Competent cells transformation

In order to transform these competent cells, the required volume of plasmid DNA to obtain approximately 500 ng was added to a 100 µl-vial containing chemically competent *A. tumefaciens* cells on ice. After mixing gently, the vial was frozen in liquid nitrogen. Afterwards it was removed and incubated 5 min at 37ºC. A volume of 400 µl of LB (section 3.1.1.1) was added and it was shaked 2 h at 28ºC. The content was plated on LB supplemented with rifampicin (50 µg ml^{-1}) and streptomycin (100 µg ml^{-1}) using sterile glass beads. Plates were incubated overnight at 28ºC.

The bacterial transformation was followed by DNA extraction (section 3.2.1) and enzymatic restriction analyses in order to verify the presence of the insert (section 3.2.7).

3.5.2.1. Transformation efficiency calculation

The transformation efficiency of the *Agrobacterium* competent cells was calculated as described before (section 3.5.1.3)

3.6. *Arabidopsis thaliana* TRANSFORMATION

Arabidopsis Col-0 plants were grown under short day conditions. When the first bolts appeared, they were eliminated to allow proliferation of many secondary inflorescences from rosette auxiliary buds. One week later, the stems were partly cut to promote de development of auxiliary buds. Three days before the transformation, developed flowers were removed in order to reduce the non-transformed seeds.

Agrobacterium single colonies, containing the desired construct (section 3.4.2), were grown in 3 ml of LB medium (section 3.1.1.1) supplemented with rifampicin (50 mg ml^{-1}) and streptomycin (100 μg ml^{-1}) at 28ºC overnight with shaking. Afterwards, 250 ml of LB medium supplemented with antibiotics was inoculated with the 3 ml vial and it was shaked at 28ºC until the OD_{600} was approximately 0.5−1.0 in order that the cells were at the growth exponential phase. Then it was centrifuged 12 min at 5500 × *g* at 4ºC. After discarding the supernatant, the cells were gently resuspended in infiltration medium (IM; Table 3.36) to a final OD_{600} of 0.8.

Table 3.36. Infiltration medium (IM) composition.

Constituent	Concentration (%)
Sucrose	0.50
Silwet L-77	0.03

Arabidopsis plants were transformed by the floral dip method (Clough and Bent, 1998). Plants were submerged in the IM containing the *A. tumefaciens* inoculum and gently agitated for 15 s. After inoculation, plants were maintained 24 h under a plastic dome for humidity retaining and in darkness in the greenhouse. Plants continued growing until siliques were brown. Seeds were harvested and after desiccation they were kept at 4ºC.

Seeds were surface sterilized according to the liquid sterilization protocol from Clough and Bent (1998) and transgenic plants were selected on 0.5x MS (section 3.1.2.2.1) supplemented with either 50 μg ml^{-1} kanamycin (for pKGWFS7) or 20 μg ml^{-1} hygromycin (for pH7WG). Resistant seedlings were transplanted to soil to produce seeds. T_2 individuals homozygous for the t-DNA insertion were identified according to the percentage of antibiotic resistant plants in the segregating T_3 progeny.

Independent transgenic lines of P_{SLAH1}-GFP::GUS (five lines), P_{SLAH4}-GFP::GUS (eight lines) and the complementing lines (*slah1/SLAH1*; two lines) were used for further analyses.

In the one side, the two obtained *SLAH* promoter lines were used to localise the promoter expression through *in vivo* observation of Green Fluorescent Protein (GFP) and, together with P_{SLAH3}-GUS (Negi *et al.*, 2008), through histochemical analysis of GUS activity (section 3.9). GFP signal was examined on the FluoView 1000 Confocal Microscope (Olympus, Hamburg, Germany). Images were analysed and processed with the Olympus FluoView 10-ASW1.7 software (Olympus).

In the other side, xylem sap collection assays were made with the *slah1-2* complementing lines (denoted *slah1/SLAH1*; section 3.8.2).

3.7. SINGLE AND DOUBLE T-DNA KO MUTANT LINES OF *ARABISOPSIS THALIANA*

3.7.1. Genotyping

Plants with T-DNA insertion from the segregating populations obtained from knockout mutant lines (section 3.1.2.1) were genotyped to confirm the presence of the trans-genes and select homozygous lines. In order to get the control lines (WT), azygous lines for the T-DNA insertion were also searched.

In addition, the segregating populations obtained from double mutants lines (*slah1-2* x *slah3-1***;** section 3.7.2) were genotyped to find the double homozygous for the T-DNA insertion and its corresponding control line (i.e., line lacking the T-DNA insertion from the same segregating population).

The genotype was performed by conventional PCR with Maxime™ Taq DNA polymerase as described in section 3.2.4.1.

Homozygous T-DNA insertion mutant lines were further used for several purposes, like RNA extraction (section 3.3.1) to determine the mRNA integrity through RT-PCR (section 3.2.4.2) and afterwards for sexual crosses (section 3.7.2), and for phenotyping (section 3.8).

In addition, the *slah1-2* T-DNA insertion mutant line was complemented with the *AtSLAH1* gene (section 3.4.2)

3.7.2. Sexual crosses

To obtain the *slah1-slah3* double-KO mutant line, sexual crosses were conducted with the *slah1-2* plant serving as the male parent and *slah3-1* as the female parent.

Plants were grown in individual pots (section 3.1.2.2.2) and they were used with bolts 10−15 cm tall.

In the plant used as female parent, an individual close and immature flower per inflorescence was chosen and the other flowers were removed. Open flowers and siliques were also eliminated. Anthers were carefully removed (emasculation) from the immature flower using micro-dissecting forceps (Sigma-Aldrich Co.) under the stereomicroscope Olympus SZ-CTV (Olympus).

In the plant serving as the male parent, a flower in the same developmental stage as the chosen female flower was used for obtaining the stamens. The anther of a stamen was rubbed over the stigma papillae of the female parent.

After crosses were performed, any new flower buds were removed to ensure that all developed siliques were those from crosses.

The mature siliques were harvested and F1 plants were sown on soil (section). Afterwards, F1 plants were genotyped (section 3.2.4.1) to confirm the heterozygous line for the T-DNA insertion in both SLAH1 and SLAH3 genes.

The following generation (F2) was obtained by self-pollination of F1 plants. This F2 generation was also sown and genotyped to obtain the double homozygous T-DNA KO mutant line (thereafter named *slah1-slah3*) and at the same time the double azygous line for the T-DNA insertion (thereafter named Col-0 x WS) to use it as a control in further assays.

The double mutant *slah1-slah3* and its azygous segregating line were used for phenotyping (section 3.8).

3.8. KO MUTANT LINES PHENOTYPING

Knockout mutant lines, homozygous for the T-DNA insertion (section 3.7.1), unable to synthesise the mRNA of the interrupted gene (section 3.2.4.2) were further utilised for phenotyping.

The *slah1-slah3* double-KO mutant line and *slah1/SLAH1* complemented lines were also used. As control, plants from the same segregating populations lacking the T-DNA insertion or wild-type *Arabidopsis* lines were utilised.

3.8.1. Morphological measurements

To compare the development of *slah1-2* and *slah4-2* homozygous T-DNA insertion mutant lines in relation to their corresponding wilt-type lines (the azygous segregating SLAH1-2 and Col-0 lines, respectively), phenotypic analyses by collecting morphological data were performed (Boyes *et al.*, 2001).

Arabidopsis plants were grown in pots (section 3.1.2.2.2), but also hydroponically (section 3.1.2.2.3). The morphological measurements took every 3 d in the phenotypic analyses were: rosette diameter and number of rosette leaves and, after the reproductive stage started, floral stem length too. In addition root length was also measured in the case of plants grown in hydroponic culture. The resulting data reflect the rate of plant growth and development (Boyes *et al.*, 2001).

Moreover, fresh and dry weights from the harvested plants were obtained.

Since the expression of *AtSLAH1* was found in the flower (section. 4.1.2.1), the number of siliques during plant reproductive development was obtained in *slah1-2* plants. In addition, the harvest index (HI) for *slah1-2* plants grown in pots with Aracons™ seed collectors (Arasystem-Betatech, Gent, Belgium) under short photoperiod was calculated using the following equation:

$$HI = \text{Seeds dry weight} / \text{Shoot dry weight} \cdot 100$$

For this purpose, all seeds from individual plants were weighed separately from the shoot biomass. Furthermore, total number of seeds per plant was obtained by counting the seeds with a stereomicroscope Olympus SZ-CTV (Olympus) of aliquots and getting their weight. The average value of 5 aliquot replicates from each plant was used to estimate the total number of seeds of each plant, according to the total seeds dry weight. The dried weight per seed was also calculated through the aliquots used for counting.

In addition, for *slah1-2* and *slah4-2* plants, together with their respective WT plants, Cl^- contents in the shoot were determined (section 3.8.4.1), and root Cl^- content in *slah1-2* plants was also obtained.

3.8.2. Xylem sap collection assays

The *slah1-2*, *slah3-1* and *slah3-4* T-DNA insertion mutant lines (section 3.7.1) were used to collect xylem sap. As control for the mutant line *slah1-2*, *SLAH1-2* azygous segregating WT line together with two independent *slah1*/*SLAH1* complemented lines (P1-12 and P1-31) were used, while wild-type *Arabidopsis* Col-0 was the control for the *slah3* homozygous T-DNA insertion

mutant lines. In addition, the *slah1-slah3* double-KO mutant, obtained by sexual crosses (section 3.7.2), and its azygous segregating line (Col-0 x WS) were also used.

When the first bolt appeared, it was removed to promote further bolting. Plants were used with secondary bolts 5–15 cm tall. For collection of xylem sap all rosette leaves were removed with blunted scissors to prevent loss of xylem solution from the cut area. In addition, floral stems were cut with a scalpel, allowing secretion of xylem sap droplets from the base of the stem. The container was sealed to maintain saturating humidity. Drops of xylem sap at the cutting surface of the stem were then collected using a micropipette (Gaymard *et al.*, 1998; Shi *et al.*, 2002; Sunarpi *et al.*, 2005). Xylem sap was collected at different times (1 h, 2 h, 3 h and 5 h after starting the assay) and Cl^- and NO_3^- concentrations were quantified (section 3.8.4.2).

We observed that xylem sap was more efficiently and abundantly extracted from potted plants than from hydroponically grown plants. Ion translocation rate values are usually normalized with root biomass but it was difficult to obtain intact roots from plants grown in solid substrate. Under the premise that the volume of exuded xylem sap maintains a linear relationship with the root biomass, we used plants grown in hydroponics medium (section 3.1.2.2.3) to test this hypothesis. The linear correlation between the volume of xylem sap secreted per plant and the root biomass of hydroponically grown plants was confirmed (Fig. 3.7). Therefore we decided to normalize ion translocation rate with the total volume of xylem sap secreted per potted plant. For further xylem sap ion content quantifications, only results from assays where the sap volume of mutant and WT plants were comparable were used.

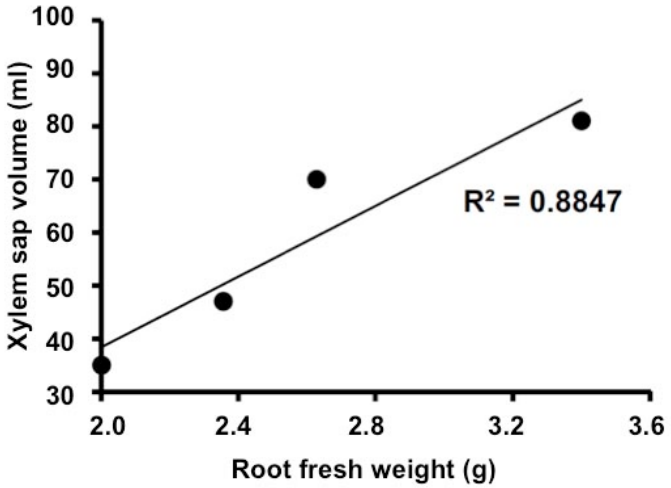

Figure 3.7. Xylem sap correlation with root biomass. Correlation of sap flux with root biomass. Wild-type (WT) plants were grown hydroponically with Basal Solution (BS). Xylem sap was collected one hour after shoot trimming. Sap secretion volume was linearly correlated with root biomass.

To quantify the Cl^- translocation into the xylem, six-week-old plants grown in pots with BS solution (containing 70 µM Cl^-; section 3.1.2.2.2) were transferred to a container and submerged in the same solution supplemented with 5 mM Cl^- almost up to substrate level.

Moreover, to perform different Cl^- salt stress treatments with *slah1*-2 plants, pots were transferred to BS solution supplemented with different Cl^- salt concentrations (15, 30, 60 and 120 mM Cl^-). To avoid interference caused by sodium toxicity, the following combination of Cl^- salts was used $KCl:MgCl_2:CaCl_2$ in a ratio 2:1:1. Xylem sap from these plants was collected 3 h after starting the salt exposure and its Cl^- concentration was afterwards quantified (section 3.8.4.2).

3.8.3. Growth at different Cl^- and NO_3^- concentrations

For *slah4-2* phenotypic assay with solutions containing different Cl^- and NO_3^- concentrations, *slah4-2* and its WT line (Col-0) plants were first grown with BS (section 3.1.2.2.2) to allow their proper beginning development and 17 days after sowing (das) Cl^- and NO_3^- treatments started (section 3.1.2.2.2; Table 3.5).

slah4-2 and WT plants were harvested according to their developmental stage at different times:

T1: Vegetative phase: plants with growing rosette without inflorescence.

T2: Reproductive onset: beginning of bolting stem elongation.

T3: Flowering stage: plants with abundant flowers and few siliques.

T4: Fruit maturation stage: plants with abundant siliques and few flowers.

Plants were dried in an oven Selecta (JP Selecta SA, Barcelona, Spain) at 70ºC until the determination of Cl^- content (section 3.8.4.1).

3.8.4. Chloride and nitrate contents quantification

3.8.4.1. Anion content in plants

slah1-2 KO mutants and WT plants harvested at the end of the phenotypic assay where different morphological measurements were took (section 3.8.1), were dried in an oven Selecta (JP Selecta SA) to determine its Cl^- content. Dried root and shoots were ground to a fine powder with mortar and pestle. The powder was incubated in an acidic solution (0.1 M HNO_3, 10% glacial acetic acid) with gentle shaking overnight at 28ºC in the dark. Afterwards, samples were centrifuged 5 min at 1,500 rpm in the centrifuge 5403 (Eppendorf) and 100 µl of the samples were used to determine the Cl^- concentration by silver ion-titration according to Gilliam (1971), using a chloride meter Corning 926 (Sherwood Scientific Ltd., Cambridge, UK).

Dried *slah4-2* KO mutant and WT (Col-0) plants from the phenotypic assay with different Cl^- and NO_3^- concentrations (section 3.8.3) were used for Cl^- content determination. Samples were ground to a fine powder with mortar and pestle and the dry powder was incubated in milli-Q water with gentle shaking. Samples were centrifuged 5 min at 1,500 rpm in the centrifuge 5403 (Eppendorf) and the content of Cl^- was determined by colorimetric assays, as it is described for xylem sap samples in the following section (section 3.8.4.2).

3.8.4.2. Anion content in xylem sap samples

Nitrate and Cl^- content in xylem sap samples (section 3.8.2) was determined by colorimetric assays with the spectrophotometer SPECTROstar® Omega, (BMG Labtech GmbH, Ortenberg, Germany). Nitrate concentration was determined according to Cataldo *et al*. (1975) and Cl^- concentration as described in Frankenberger *et al.* (1996).

For NO_3^- content determination, 5 µl of the sample was mixed with 20 µl of 10% sodium salicylate (dissolved in sulphuric acid), forming a complex of NO_3^- with salicylic acid under this highly acidic condition. Afterwards, 200 µl of 4.75 M NaOH were added and the samples were incubated at room temperature for 1 h in the dark. Nitrate content was obtained measuring the

samples at 410 nm by the spectrophotometer. To transform the absorbance measurements into NO_3^- content, 13-fold dilution series of 50 mM KNO_3 dilutions were used as standard curves. Absorbance of the chromophore is directly proportional to the amount of NO_3^- present in the sample.

For determination of Cl^- content, each reaction mix contained 40 µl of the sample, 20 µl of 0.4 % mercury thiocyanate (dissolved in methanol), 20 µl of 20.2% ferric nitrate and 170 µl of milli-Q water, in a volume of 250 µl. Based on known concentrations of mercury thiocyanate and ferric nitrate, 10-fold dilution series were prepared and used as standard curves. This colorimetric method is based on the displacement of the thiocynate (from the mercury thiocyanate) by Cl^- ions, leading to mercury chloride and ferric thiocyanate (colored product). The absorbance of the resulting colored compound is measured at 480 nm by the spectrophotometer.

The anion content in the xylem sap was used afterwards to obtain the translocation efficiency for Cl^- and NO_3^- and the NO_3^-/Cl^- selectivity in the different ecotypes assayed (WS, Col-0, and the WS x Col-0 hybrid). The translocation efficiency for Cl^- and NO_3^- was calculated as the ratio between the anion content in the xylem sap and the anion content in the nutrient solution. And the NO_3^-/Cl^- selectivity was obtained by dividing the translocation efficiency for NO_3^- by that for Cl^- in each ecotypes assayed.

3.9. HISTOLOGICAL TECHNIQUES

3.9.1. Histochemical analysis of β-Glucuronidase (GUS) activity

Independent transgenic lines of P_{SLAH1}-GFP::GUS (five lines), P_{SLAH3}-GUS (two lines; Negi *et al.*, 2008) and P_{SLAH4}-GFP::GUS (eight lines) were tested for GUS histochemical activity (Jefferson, 1987) to localise the promoter expression.

Samples at various developmental stages were incubated 20 min in 90% acetone, vacuum-infiltrated for 5 min in the β-Glucuronidase (GUS) staining solution (Table 3.37) and incubated at 37 °C in the dark for either 3 h (P_{SLAH1}-GFP::GUS and P_{SLAH3}-GUS) or 5 h (P_{SLAH4}-GFP::GUS).

Table 3.37. GUS reaction composition.

Components	Concentration
X-Gluc (5-bromo-4-chloro-3-indolyl β-D-glucuronide)	1 mM
$K_4Fe(CN)_6$	2 mM
$K_3Fe(CN)_6$	2 mM
Triton X-10	2 %
$NaPO_4$ (pH 7.2)	50 mM

During the activity of the β-Glucuronidase, an uncoloured product is produced, but its oxidative dimerization leads to an insoluble blue product.

To stop the staining and remove chlorophyll, samples were cleared with a series of ethanol washings, ending with 70% ethanol.

Samples were analysed under the stereomicroscope Olympus SZ-CTV (Olympus) and micrographs of GUS-stained tissues were obtained with a Zeiss Axioskop microscope (Carl Zeiss, Jena Gmbh, Jena Germany) and the AxioVision Release 4.8.2. Zeiss software (Carl Zeiss).

Independent transgenic lines of *SLAH* promoter-GUS showing consistent staining pattern were selected for further analyses.

3.9.1.1. GUS after hormonal assays

To elucidate the possible regulation of abscisic acid (ABA) and indole-3-acetic acid (IAA) in *SLAH* gene expression, *Arabidopsis* plants expressing the GUS reporter gene under the control of *SLAH1*, *SLAH3* or *SLAH4* promoter were used.

Thirteen-day-old seedlings of P_{SLAH1}-GFP::GUS, P_{SLAH3}-GUS and P_{SLAH4}-GFP::GUS lines grown in Petri dishes (section 3.1.2.2.1) were sprayed with either 100 µM ABA or the control (water) solution using an airbrush spray device (Pintuc Screw Compressors, Barcelona, Spain).

Additionally, given that *SLAH4* gene was expressed in organs associated with high primary auxin production, P_{SLAH4}-GFP::GUS line seedlings were also subjected to 100 µM IAA to further explore its promoter expression regulation.

After 15 h incubation, plants were subjected to GUS staining as described previously.

3.9.2. Cryostat sectioning of plants expressing GUS

Following GUS staining, cross sections of roots using a cryostat were performed. For sectioning, samples were rehydrated and then fixed with formaldehyde (Table 3.38) for 4 h at 4ºC. To stop the fixation, samples were washed with sodium phosphate buffer pH 7.2.

Table 3.38. Fixing solution.

Components	Concentration
Formaldehyde	4 %
$NaPO_4$ (pH 7.2)	100 mM

Samples were embedded in tissue freezing medium (Leica Biosystems, Nussloch, Germany) and frozen at −20ºC. Sections (15 µm) were prepared using a cryomicrotome (Cryostat Leica CM1950, Leica Biosystems). They were afterwards transferred to microscope slides and covered with cover-slip once embedded in glycerol:PBS (80:20).

Samples were analysed with a Zeiss Axioskop microscope (Carl Zeiss) and the AxioVision Release 4.8.2. Zeiss software.

3.10. *Xenopus laevis* AS HETEROLOGOUS EXPRESSION SYSTEM

The ease of obtaining large number of *Xenopus laevis* oocytes together with their size and robust nature have made them a suitable system to investigate transport processes on a cellular level. The oocytes of the South Africa clawed toad *Xenopus laevis* have been extensively used in biological and pharmacological research (Weber, 1999). The mature oocytes have a diameter of

1–1.3 mm (which facilitates its handling) and pigmentation with marked polarization into the dark animal hemisphere and the beige vegetative hemisphere.

During oogenesis, oocytes accumulate large quantities of proteins and organelles that form a reserve for early embryonic development. Among them the ribosomes, tRNAs and other components important for translation may be used to translate exogenous RNA (Theodoulou and Miller, 1995). They also carry out most post-translational modifications to foreign proteins as well as their correct incorporation into the cell membrane.

The heterologous expression system of the *Xenopus* oocytes allows the characterization of proteins isolated from their natural environment. This expression system has been widely employed to study the structure and function of ion channels and receptors (Guan *et al.*, 2013). The oocyte system allows performing a whole plethora of different techniques for the investigation of ion channels and transporters (Weber, 1999) like the two-electrode voltage clamp (TEVC) technique and the bimolecular fluorescence complementation (BiFC) analysis.

Although the *X. laevis* oocyte is endogenously equipped with a host of ion channels, transport systems and receptors, heterologously expressed ion channels can be clearly distinguished from the endogenous ones. Most of the time, currents produced by the endogenous ion channels are small compared with the currents produced by the expressed channels (Sigel, 1990; Weber, 1999)

Today this expression system is one of the recognized standard methods for the translation and expression of animal and plant ion channels, transporters and receptors and for their electrophysiological investigation.

3.10.1. Oocytes preparation

Xenopus laevis female frogs were kept in aquaria at a water temperature of 20–22ºC. A cover was used to prevent escape. The frogs were fed twice weekly and the tanks were cleaned every week. The oocytes were obtained from adult frogs.

The frog was hypodermically anesthetized with tricaine (0.75 g l^{-1}) and cooled down with ice. The abdominal skin and the underlying muscle tissue were surgically opened and the ovary lobes were removed with tweezers and collected in the ND96 solution (Table 3.39). After removing the oocytes, the abdomen of the frog was sewn.

Table 3.39. ND96 solution composition.

Constituent	Concentration (mM)
NaCl	96
KCl	2
$MgCl_2$	1
HEPES	10
pH was adjusted to 7.4 with NaOH	
Osmolarity was adjusted to 220 mosmol kg^{-1} with sorbitol	

The oocytes were subsequently divided into smaller portions as carefully as possible under the stereomicroscope Olympus SZ-40 (Olympus) with fine watchmaker tweezers to improve the accessibility of the oocytes to the collagenase in the following step. After several

washes of the oocytes in Ca^{2+}-free ND96 solution, they were subjected to a collagenase digestion (0.25–0.27 PZ U mg^{-1}, 12 mg ml^{-1}) to remove the remaining connective tissues, blood capillaries, and the follicular layer, thus isolating the oocytes (Guan *et al.*, 2013). The digestion in Ca^{2+}-free solution was necessary because the collagenase shows an uncontrollable activity in the presence of Ca^{2+}, which would prevent uniform oocyte digestion. The oocytes were incubated for 90 min at room temperature with gentle shaking. Afterwards, the oocytes were washed several times with the ND96 solution in order to remove the collagenase and the residues of the digestion.

Finally, the individual oocytes were placed in ND96 solution supplemented with 1 mM Ca^{2+} (1mM $CaCl_2$) and gentamycin (50 μg ml^{-1}) and were stored at 16ºC.

Since not all oocytes were suitable for further use due to different size or injuries, they were sorted according to optical characteristics and only the undisturbed oocytes were used. The oocytes were screened daily to remove either non-healthy looking or damaged oocytes and to change the culture medium when it was necessary.

3.10.2. cRNA injection in oocytes

After obtaining glass capillary by the Narishige PC-10 micropipette puller (Narishige Co., Tokio, Japan) with single stage pulling, their tip was obliquely cut off with the aid of a Hund Wetzlar microscope (Helmut Hund GmbH, Wetzlar, Germany) in order to not damage the membrane of the oocyte. The diameter of the truncated tip of the microinjection needles was 10–20 μm.

The microinjection needle was completely filled with mineral oil containing a small amount of Sudan (enough to impart a distinct red colour). The oil-soluble dye was incorporated to facilitate the visualization of the interface between the RNA and the mineral oil used in the needle (Smart and Krishek, 1995). It is essential to avoid the introduction of air bubbles in the microinjection needle.

The cRNA obtained from the *in vitro* transcription (IVT; section 3.3.3) was injected into the oocytes with the Nanoliter-2000 Injector (World Precision Instruments, Berlin, Germany) mounted on a micromanipulator (Drummond Scientific Co., Broomall, PA, US) under a stereomicroscope Olympus SZ-40 (Olympus). To draw cRNA into the glass needle, a drop of oil was previously forced out of the needle. The oocytes were located in a specially prepared chamber in individual wells to stabilize them. The chamber was filled with ND96 solution supplemented with 1 mM Ca^{2+} and gentamycin. For injection, the needle was inserted into the oocytes by means of the micromanipulator, and each oocyte was injected with 50 nl of cRNA. Water was injected as a negative control.

For oocyte BiFC and electrophysiological experiments, 10 ng each of SLAC1, SLAH1, SLAH2, SLAH3, SLAH4, SLAH mutants, CPKs, SnRKs and CBLs cRNA and 5 ng of CIPKs cRNA was injected. Electrical recordings were done with native proteins (without any fusions). To avoid differences in the kinase activity due to different Ca^{2+}-dependencies and calcium levels in *Xenopus* oocyte batches, truncated kinases were used, i.e. Ca^{2+} independent mutants of CPK3 and 21 (CPK3ΔEF, CPK21ΔEF, [Geiger *et al.*, 2010, 2011; Maierhofer *et al.*, 2014a; Scherzer *et al.*, 2012]).

The injected oocytes were subsequently stored in Petri dishes containing the same solution at 16ºC and after 2–3 d they were used either in the TEVC technique (section 3.12) or in the BiFC analyses (section 3.11).

3.11. PROTEIN INTERACTION STUDIES THROUGH THE BIMOLECULAR FLUORESCENCE COMPLEMENTATION (BiFC) TECHNIQUE

This method is based on two non-fluorescent fragments of the yellow fluorescent protein (YFP) that can reconstitute the fluorophore when fused to proteins that interact with each other (Hu *et al*., 2002; Kerppola, 2006; 2008). The association of the two halves of the YFP (the C-terminal and the N-terminal half), because of the nearness of the examined proteins, cause the formation of a bimolecular fluorescent complex (Fig. 3.8). BiFC analysis allows direct visualization of protein interactions in living cells environment.

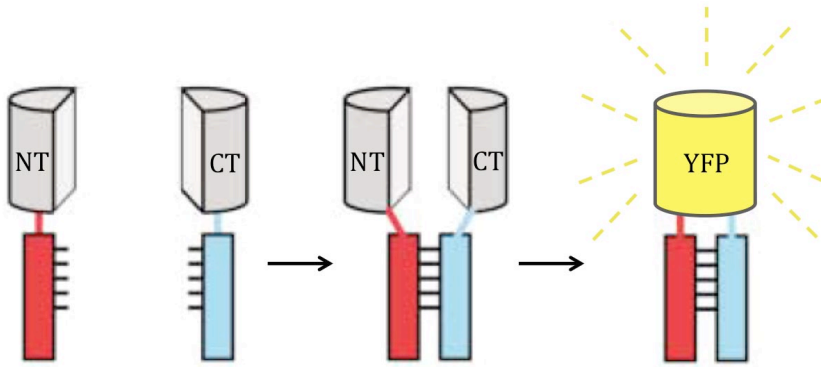

Figure 3.8. Diagram representing the principle of the BiFC assay. Two fragments, the N-terminal (NT) and the C-terminal (CT) halves, of the yellow fluorescent protein (YFP) are fused to two putative interaction partners. In the absence of an interaction between the proteins, the fluorophore halves remain non-functional. But the interaction between the proteins facilitates the association between the two YPF fragments and a functional fluorophore is constituted, exhibiting emission of fluorescence upon excitation with an appropriate wavelength. Modified from Hu *et al.*, 2002.

The BiFC method has the limitation that fluorescent protein fragments can associate with each other when they are nearby, independently of an interaction between the proteins fused to the fragments, obtaining false positives (Kerppola, 2006). Generally, this disadvantage can be alleviated by expressing the fusion proteins at concentrations approximating their endogenous counterparts or testing alternative fusions.

The expression of the examined protein in the pNBlu vector numbers 17 and 18 (Table 3.29; section 3.4.1) enabled the fusion of the protein to the C-terminal end of the YFP, as well as the expression in the vector numbers 19 and 20 enabled the fusion of the protein to the N-terminal end of the YFP.

The DNA of the examined proteins (SLAH/SLAC channels and kinases) was previously cloned into a *Xenopus* oocyte expression vector by the USER™ cloning (section 3.4.1). Forty-eight hours after cRNA injection, oocytes images were taken. The oocytes expressing the YFP where focused on the equatorial plane and pictures were taken with a Leica SP5 confocal laser scanning microscope (Leica Microsystems CMS GmbH, Mannheim, Germany) equipped with a Leica HCX IRAPO L25x/0.95W objective.

3.12. TWO-ELECTRODE VOLTAGE CLAMP (TEVC) RECORDINGS

To investigate the properties of ion channels in *Xenopus laevis* oocytes, the electrophysiological technique of two-electrode voltage clamp (TEVC) was used.

In this technique two microelectrodes are inserted into the oocytes to set the membrane potential at desired values and record the membrane current to analyse ion channel activities (Fig. 3.9; Guan *et al*., 2013).

The difference in electric potential between the cytosolic side of the oocyte and the surrounding liquid medium is the membrane potential (V_m). The voltage electrode senses the membrane potential in relation to the potential of the reference electrode in the bath (conventionally set to zero) and the current electrode injects the current to set the membrane potential at the desired value.

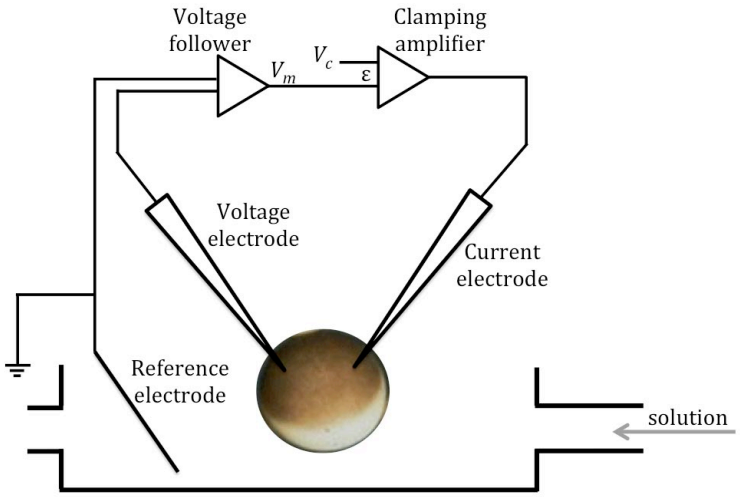

Figure 3.9. Schematic representation of the two-electrode voltage clamp (TEVC) technique on an oocyte. The membrane potential (V_m) is monitored by connecting the voltage electrode to the input of a voltage follower. The clamping amplifier compares the V_m with the voltage command signal (V_c). The resulting current flows through the current electrode into the oocyte.

The clamping amplifier (Fig. 3.9) compares the membrane potential (V_m) with the voltage of command signal (V_c) applied to the input terminal and the difference between them results in a output current which is injected in the cell by the current electrode (Guan *et al*., 2013). The applied current for maintaining the membrane potential in the oocyte is therefore directly proportional to the current flowing through a transporter protein at the plasma membrane of the oocyte.

In order to characterize a channel, rapid voltage changes are applied to the oocyte membrane and the resulting currents are recorded. These currents are composed of the instantaneous capacitive current and the current flowing through the transport proteins.

The capacitive current results from very fast charge transitions in the membrane and can only be recorded in a short period of time (1–2 ms) after the voltage change. By means of an offset reading of the measured voltages, these rearrangement effects can be avoided and therefore does not interfere with the characterization of the channel.

3.12.1. Measurement setup

Both the voltage and current microelectrodes were placed on micromanipulators (Marzhauser MM33, Drummond Scientific Co.) located on opposite sides of the oocyte. The reference electrode was connected to the ground of the preamplifier of the voltage electrode and placed in the measuring chamber in the close to the oocyte. The measuring computer was connected to the clamping amplifier (Turbo TEC 10CD, NPI Electronics GmbH, Tamm, Germany). Different voltage pulse protocols and data acquisition were established with the PatchMaster software (HEKA Elektronik, Lambrecht, Germany). The recorded data were evaluated with both the software Excel (Microsoft) and IGOR (WaveMetrics).

The oocyte was registered in a measuring chamber that was uniformly perfused with different bath solutions (section 3.12.3).

Borosilicate glass capillaries (Kwik-Fill™, World Precision Instruments) were obtained by the Narishige PC-10 micropipette puller (Narishige Co.) with two stage pulling and they were filled with 3 M KCl solution. The reference electrode was placed in a polyvinyl tube, which also contained 3 M KCl solution. An agar plug in the tube opening, consisting of 3 M KCl and 2% agar, prevented the highly concentrated electrolyte solution from flowing into the low-molar bath solution without showing too much electrical resistance.

3.12.2. Voltage protocols, data collection and data analysis

Before starting the measurement, the electrodes were immersed in the bath solution. Since the measuring solutions always had a lower chloride concentration than the electrode solution, a potential gradient occurred, which was adjusted to zero.

The impalement of the electrodes into the oocyte was controlled both microscopically and by an acoustic signal.

In the whole-cell configuration, the membrane potential of the oocytes was measured. Following a holding potential (V_H) of 0 mV, the instantaneous currents (I_{inst}) at single voltage pulses of 50-ms in 10 mV decrements from +70 to −150 mV were extracted.

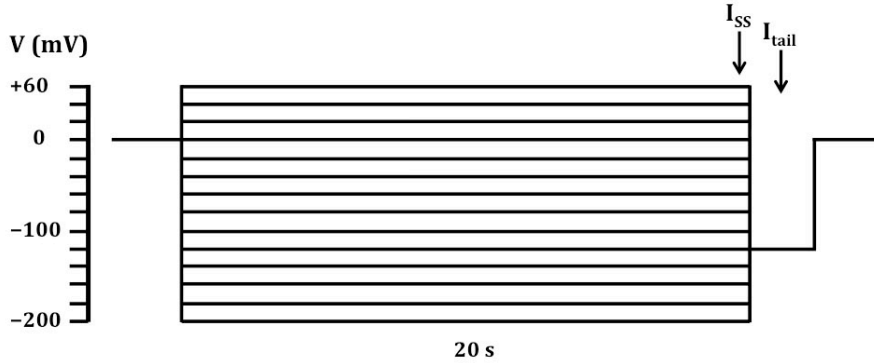

Figure 3.10. Current traces of the voltage protocol used for measurement of current-voltage (I-V) relations. At the beginning the cell is clamped to a holding potential of 0 mV. Afterwards, single voltage pulses of 20 s were applied in 20 mV decrements from +60 to −200 mV. The equilibrium currents (I_{SS}) are obtained after 19 s. In a subsequent pulse at −120 mV, the tail streams (I_{tail}) were obtained.

For recording representative current traces, steady state currents (I_{SS}) and for calculating the voltage dependent relative open probability (rel. P_O), standard voltage protocol

(Fig. 3.10) was as follows: Starting from a V_H of 0 mV, single voltage pulses were applied in 20 mV decrements from +60 to −200 mV. The steady state currents (I_{SS}) were extracted at the end of this test pulses lasting 20 s. In a subsequent pulse at −120 mV, the tail streams (I_{tail}) were obtained, which was used for determining the relative open probability (rel. P_O).

For an ion channel in which only one state is conductive, the whole cell current amplitude (*I*) measured at a membrane voltage (V) across the oocyte membrane can be expressed by the following equation:

$$I\,(\mathrm{V}) = \mathrm{P_O}\,(\mathrm{V}) \cdot \mathrm{N} \cdot i\,(\mathrm{V})$$

where, N is the total number of activated channels, *i* is the single channel current (i.e., amplitude of the current flowing through the single channel), and P_O is the open probability of the channel.

Since both the number of channels (N) and the single-channel current (*i*) remain unchanged during the constant voltage at the representative current traces recordings (Fig. 3.9), the open probability (P_O) can be directly attributed from the tail streams (I_{tail}) obtained at −120 mV:

$$I\,(\mathrm{V}) = \mathrm{P_O}\,(\mathrm{V})$$

The experimental data points were fitted with a single Boltzmann equation (Hoth *et al.*, 1997). The currents were normalized to the saturation value of the calculated Boltzmann distribution. The half-maximal activation potential ($V_{½}$) was obtained from the curve obtained after applying the Boltzmann equation.

The reversal potentials (V_{rev}) used for the calculation of the relative permeability were recorded in the current-clamp mode, in which the current across the membrane is clamped to zero**,** to avoid loading of oocytes with NO_3^- and to keep the cytosolic anion composition constant for correct reversal potential determination in response to either nitrate concentration changes in the external medium or during anion selectivity measurements. For determination of V_{rev} for the respective anion, oocytes were preincubated in 50 mM NO_3^- to gain full activity of SLAH3. The permeability relative to nitrate for gluconate and chloride of the expressed channels were based on measurements of current reversal potential in the presence of different solutions, each containing only one anion species. The Goldman-Hodgkin-Katz equation (Goldman, 1943; Hodgkin and Katz 1949) describes the dependence of the membrane potential on all the different permeable ions:

$$\mathrm{V}_m = \frac{RT}{F} \ln \frac{P_x[\mathrm{x}^+]_\mathrm{o} + P_y[\mathrm{y}^-]_\mathrm{i} + P_z[\mathrm{z}^-]_\mathrm{i}}{P_x[\mathrm{x}^+]_\mathrm{i} + P_y[\mathrm{y}^-]_\mathrm{o} + P_z[\mathrm{z}^-]_\mathrm{o}}$$

where V_m is the membrane potential, *P* is the permeability coefficient of the individual ion, $[x^+]$,$[y^-]$ and $[z^-]$ are the concentrations of the individual ions outside (o) or inside (i) the cell, *F* is the Faraday's constant, *R* is the gas constant, and *T* is the absolute temperature.

Considering that channels were examined in the presence of a single permeating anion so the oocyte membrane was permeable only for this species, the equation above can be simplified with the Nerst equation for monovalent anions as:

$$\mathrm{V}_{rev} = \frac{RT}{\mathrm{z}_j F} \ln \frac{P_j[\mathrm{j}^-]_\mathrm{i}}{P_j[\mathrm{j}^-]_\mathrm{o}}$$

where V_{rev} is the reversal potential and Z_j is the charge of the anion (*j*).

Taking into account that a monovalent anion has a charge of 1 and that the absolute temperature in our recordings was 298.15 K:

$$V_{rev} = 59.1 \log \frac{P_j[j^-]_i}{P_j[j^-]_o}$$

Since the intracellular ion concentrations are not exactly known in oocytes, the permeability was determined in relation with a control medium with 50 mM $NaNO_3^-$. Thus, the permeability for an anion (*j*) relative to nitrate (P_j/P_{NO3^-}) was calculated as:

$$\frac{P_j}{P_{NO_3^-}} = 10^{\left(\frac{V_j - V_{NO_3^-}}{59.1}\right)} \cdot \frac{[NO_3^-]_o}{[j^-]_o}$$

where $V_j - V_{NO3}$ is the difference between the reversal potentials measured in nitrate and another anion (*j*) solution.

Permeability for nitrate was set to 1. Standard bath solution contained 50 mM of the respective anion (used as a sodium salt) and the pH was adjusted to 5.6

For ion channels, conductance is a natural measure of their ability to allow ions to move. The plasma membrane can be considered as a parallel electrical circuit, so the current (I) through a channel between the two sides of the membrane is directly proportional to the voltage, like the Ohm's law states:

$$I_j = \frac{V_m - V_{rev}}{R_j}$$

where V_m is the membrane potential and V_{rev} is the reversal potential of the anion (*j*) and R is the electrical resistance.

The conductance (*g*) is the inverse of the resistance:

$$g_j = \frac{1}{R_j}$$

Thus, the current (*I*) through a given ion channel across the oocyte plasma membrane is determined by the voltage difference between the electrodes and the electrical conductance of the solution between them:

$$I_j = (V_m - V_{rev}) \cdot g_j$$

where g_j is the conductance of the anion (*j*).

To calculate the chord conductance from oocytes expressing SLAH3 with either SLAH1 or CPK21ΔEF, the V_{rev} was determined by fitting the instantaneous currents surrounding reversal potentials in either chloride- or nitrate-containing standard buffers with a linear fit. Thus, the chord conductance at −120 mV was calculated as:

$$g_j = \frac{I_j}{V_m - V_{rev}}$$

3.12.3. Standard solutions

For the electrophysiological characterization of *At*SLAH1 and the SLAH1/SLAH3 complex, different ionic solutions at different concentrations were used. To balance the ionic strength, changes in the anion concentration were compensated with calcium gluconate, since gluconate is not able of permeating the S-type channel. Osmolality was adjusted to 200 mosmol kg^{-1} (Vapor Pressure Osmometer 5520, Wescor Inc., Utah, USA) with D-sorbitol.

The solutions (Table 3.40) for obtaining the instantaneous currents at single voltage pulses of 50 ms in 10 mV decrements from +70 to −150 mV were composed of Cl^-, NO_3^- or gluconate at a final concentration of 100 mM.

Table 3.40. Standard solutions.

Constituent	Concentration (mM)
Sodium salt of the examined anion	50 or 100
$Ca(gluconate)_2$	1
$Mg(gluconate)_2$	1
MES	10
pH was adjusted to 5.6 with Tris 1 M	

For the assays with the standard voltage protocol, the standard solutions (Table 3.40) had a final concentration of the examined anion of 30 mM and to avoid the activation of endogenous oocyte channels 1 mM $LaCl_3$ was added to the measurement solutions. To obtain the relative open probability of the channels, different concentrations of the chloride and nitrate solutions were used (3, 10, 30 mM Cl^- and 30 mM NO_3^-). To balance the ionic strength, the NO_3^- and Cl^- variations were compensated with gluconate.

For selectivity measurements the different anion solutions (Table 3.40) were composed of 50 mM Cl^-, NO_3^-, or $gluconate^-$ sodium salts.

3.13. STATISTICAL ANALYSES

The statistical analyses were performed using the program IBM SPSS Statistics 20.

The normality of the data obtained from KO mutants and their WT plants were verified using the Shapiro-Wilk test and the homogeneity of variances was tested by the Levene test. Differences between KO mutants and WT plants in the phenotypic parameters measured (section 3.8) were checked with either one-way ANOVA, when there was homocedasticity, or Student's t test, when no homogeneity was observed.

To analyse the repeated morphological measurements obtained from KO mutants and their WT plants over time, linear mixed models were performed to test developmental differences either between each mutant and its WT or between different treatments in the same plant line, using the time of observation as covariate.

RESULTS

4. RESULTS

4.1. SLAH1 CHARACTERIZATION

4.1.1. *At*SLAH1 function within the root

4.1.1.1. *AtSLAH1* and *AtSLAH3* are co-expressed in the xylem-pole pericycle

Although *AtSLAC1* is not expressed in the root, the expression of its homolog genes has been partially established (Negi *et al*., 2008; Zheng *et al*., 2015). According to Zheng and colleagues (2015), *AtSLAH1* expression is apparently located to the vascular cylinder, while *AtSLAH3* is apparently expressed in the outside part of the root. To verify these findings and to precisely localize the tissue- and cell-specific expression pattern of these genes, different transgenic lines of *Arabidopsis thaliana* plants that expressed the β-Glucuronidase (GUS) or the green fluorescent protein (GFP) genes under the control of the *AtSLAH1* and the *AtSLAH3* gene promoters were obtained.

Using Gateway® technology (section 3.4.2), a genomic fragment including 1.25 kb upstream of the *AtSLAH1* start codon was subcloned upstream of the gene encoding the chimeric GFP::GUS protein, giving rise to a transcriptional fusion between the *AtSLAH1* promoter and the chimeric reporter gene. Through histochemical analysis of GUS activity (section 3.9.1), using five P_{SLAH1}-GFP::GUS independent transgenic lines, *AtSLAH1* expression was localized at the vascular cylinder of the root (Fig. 4.1 a-c), confirming the previously published results.

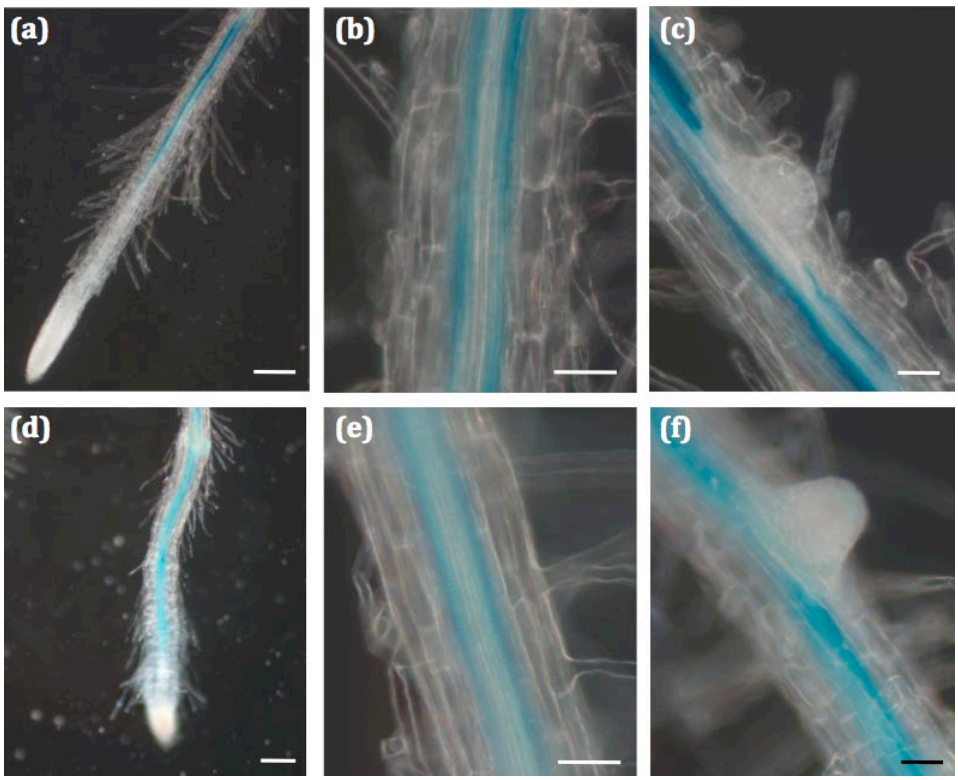

Figure 4.1. Expression of *AtSLAH1* and *AtSLAH3* in the root vascular cylinder. Histochemical localization of GUS activity in transgenic *Arabidopsis* plants, harbouring the constructions P_{SLAH3}-GFP::GUS and P_{SLAH3}-GUS, expressing the GUS reporter gene under the regulation of the *AtSLAH1* (a-c) and the

AtSLAH3 (d-f) native promoter regions. **(a)** *AtSLAH1* is expressed in the root, but no expression could be detected at the apical meristems. **(b)** The expression of *AtSLAH1* within the root is located at the vascular cylinder. **(c)** *AtSLAH1* is not expressed in emerging secondary roots. **(d)** Similarly to *AtSLAH1*, *AtSLAH3* is expressed in the root, but not in the apical meristem. **(e)** *AtSLAH3* is also expressed in the root vasculature. **(f)** *AtSLAH3* is not expressed in emerging secondary roots. Scale bars, 200 µm (a, d), 50 µm (b, c, e, f).

For localization of *AtSLAH3* expression, two independent transgenic lines of *A. thaliana* expressing the GUS gene under the regulation of the *AtSLAH3* promoter were obtained from Dr. Negi's laboratory. Contrary to the previously published results, *AtSLAH3* expression was located in the root vasculature (Fig. 4.1 d-f), exhibiting an expression pattern very similar to that of *AtSLAH1* (Fig. 4.1 a-c). Gene expression of both *AtSLAH1* and *AtSLAH3* genes was absent from apical meristems (Fig. 4.1 a, d) and emerging lateral root primordia (Fig. 4.1 c, f).

Confocal images of GFP fluorescence showed that *AtSLAH1* expression was associated to cells adjacent to xylem vessels (Fig. 4.2 a-c), an expression pattern similar to that exhibited by the *AtSLAH3* gene according to histochemical GUS activity obtained in longitudinal root sections (Fig. 4.2 e). A closer inspection using cross sections of GUS-expressing roots (section 3.9.2) identified the xylem-pole pericycle as the specific cell type where *AtSLAH1* and *AtSLAH3* were co-expressed in the root (Fig. 4.2 d, f).

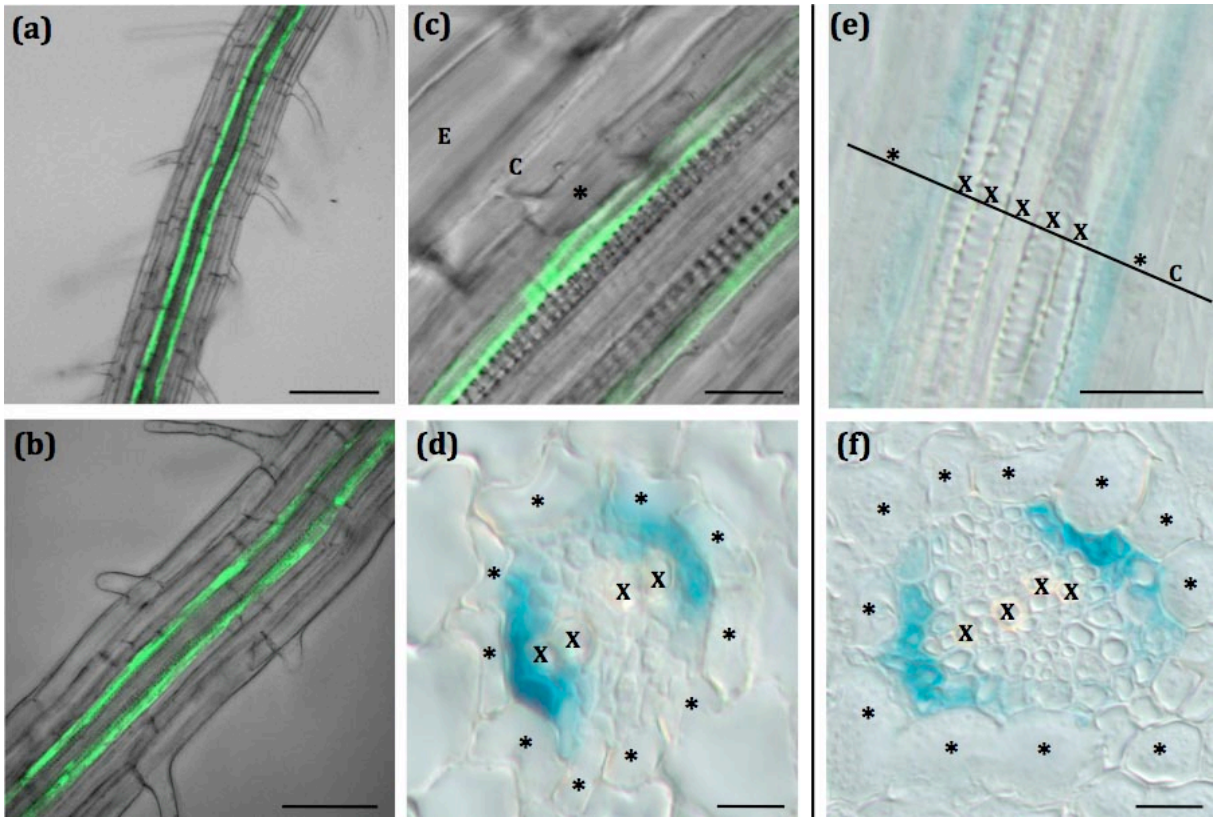

Figure 4.2. *AtSLAH1* and *AtSLAH3* are co-expressed in the xylem pole pericycle. (a-c) Localization in xylem-associated cells of green fluorescent protein (GFP) activity in roots of transgenic lines harbouring the construction P_{SLAH1}-GFP::GUS. **(d)** Localization in xylem-pole pericycle cells of GUS activity in cross sections of the root of transgenic lines harbouring the construction of P_{SLAH1}-GFP::GUS. **(e)** Localization in xylem-associated cells of GUS activity in longitudinal sections of the root of transgenic lines harbouring the construction P_{SLAH3}-GUS. **(f)** Localization in xylem-pole pericycle cells of GUS activity in cross sections of the root of transgenic lines harbouring the construction P_{SLAH3}-GUS. E: epidermis; C: cortex; asterisk: endodermis; red spot: protoxylem; blue spot: metaxylem. Scale bars, 100 µm (a), 50 µm (b), 20 µm(c, e), 10 µm (d, f).

Co-expression of *AtSLAH1* and *AtSLAH3* genes in xylem-pole pericycle cells suggests that both S-type anion channels might be involved in the regulation of NO_3^- and/or Cl^- secretion into root xylem vessels.

4.1.1.2. Identification of *AtSLAH1* T-DNA knockout and *slah1*-complemented lines

Arabidopsis thaliana seeds from the *slah1-1* (SALK_039811) and *slah1-2* (INRA_FLAG_329G06) lines were obtained from the Nottingham Arabidopsis Stock Centre and the Institut Jean-Pierre Bourgin, respectively (section 3.1.2.1). The *slah1-1* and *slah1-2* T-DNA insertions were generated in the Columbia (Col) and the Wassilewskija (Ws) backgrounds, respectively. Following the extraction of DNA from leaves of segregating plants (section 3.2.1), *Arabidopsis* lines, homozygous and azygous for the T-DNA insertions, were screened by PCR (section 3.2.4.1) using primers suitable for the left border of the T-DNA and *SLAH1*-specific primers flanking the position of the T-DNA inserts (Fig. 4.3).

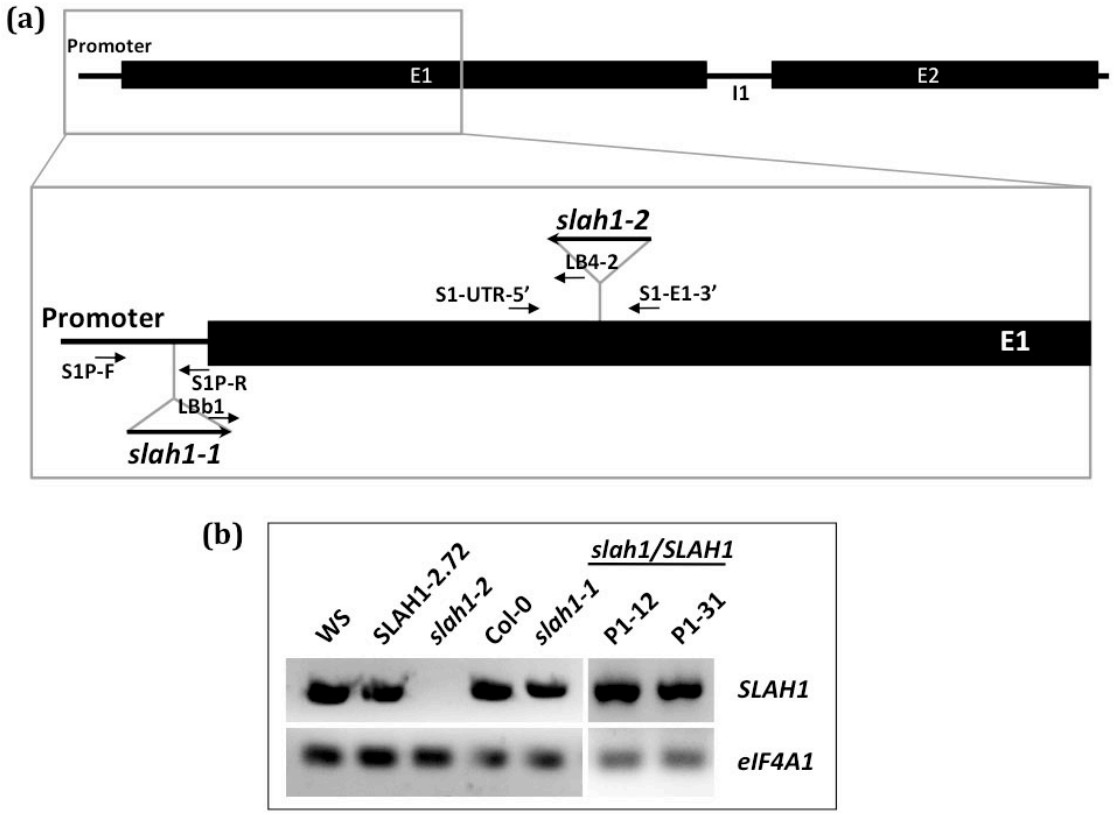

Figure 4.3. Identification and complementation of the *slah1* knockout line. (a) Gene structure of *AtSLAH1* and localization of the T-DNA insertions in the *slah1-1* (SALK_039811) and *slah1-2* (INRA_FLAG_329G06) transgenic lines. Closed boxes represent exons (E) and solid lines represent introns (I). PCR amplification primers used for genotyping and retro-transcription of total RNA are indicated with arrows. **(b)** *AtSLAH1* transcript integrity determined by RT-PCR analysis of total RNA isolated from roots of: wild-type plants (WS, Col-0), homozygous KO mutant lines (*slah1-1* and *slah1-2*), an azygous line obtained from segregation of a plant heterozygous for the T-DNA insertion of the *slah1-2* line (SLAH1-2.72), and *slah1-2* complemented plants (P1-12, P1-31). The housekeeping translation initiation factor *eIF4A1* expression level was used as RNA- or cDNA- loading control.

To complement the *slah1-2* KO mutant line, plants homozygous for the T-DNA insertion were transformed (section 3.6) with a construct containing the whole *AtSLAH1* gene, including its own promoter region. The segregating progeny was screened by PCR as explained above.

The mRNA integrity of genotyped plant lines, homozygous for the T-DNA insertion, *slah1-1* (SALK_039811), *slah1-2* (INRA_FLAG_329G06), together with two independent *slah1*/*SLAH1* complemented lines, was determined through its retrotranscription to cDNA (section 3.2.2) and amplification by Reverse Transcriptase PCR (RT-PCR) (section 3.2.4.2). In addition to the homozygous plants, an azygous line (SLAH1-2.72) and wild-type lines (WS, Col-0) were also screened.

The T-DNA insertion in the *slah1-1* line mapped into the promoter region of the *AtSLAH1* gene (Fig. 4.3 a), meanwhile in the *slah1-2* line the T-DNA insertion mapped into the Exon-1 (E1; Fig. 4.3 a). RT-PCR analysis of total RNA isolated from roots showed that the *slah1-1* line maintained the ability to synthesize the native *AtSLAH1* transcript (Fig. 4.3 b), whereas the *AtSLAH1* transcript was disrupted in the *slah1-2* line (Fig. 4.3 b).

Since no additional knockout lines were obtained, the *slah1-2* line was complemented with the *AtSLAH1* gene as previously explained (section 3.4.2). RT-PCR analysis of he *slah1*/*SLAH1* complemented lines P1-12 and P1-31 revealed that both complemented lines synthesized the *AtSLAH1* transcript (Fig. 4.3 b).

For further studies of the *slah1-2* mutant lines phenotype, the segregating azygous line SLAH1-2.72 lacking the T-DNA insertion, thereafter named WT, was used as a control.

4.1.1.3. Loss of *AtSLAH1* function impairs shoot growth

Given the localization of *AtSLAH1* gene expression in cells facing xylem vessels, one could predict that the S-Type anion channel feeds the xylem sap ascending from root to shoot with NO_3^- and/or Cl^- anions. To test this assumption, the *AtSLAH1* gene KO mutant line, *slah1-2*, was inspected under two chloride feeding regimes (70 µM and 5 mM Cl^-) in plants growing under hydroponic conditions (section 3.1.2.2.3) and in pots (section 3.1.2.2.2) under short photoperiod conditions.

The development of the *slah1-2* KO line was compared with its WT line by taking morphological measurements every 3 d approximately (section 3.8.1).

No differences in the root length of *slah1*-2 mutant and WT lines grown in the low chloride nutrient solution (70 µM Cl^-) were observed (Fig. 4.4 a). However, in the high chloride solution (5 mM Cl^-) the root of *slah1-2* KO plants was significantly shorter than the root of WT plants since 44 days after sowing (Fig. 4.4 b). When the root length of both genotypes was represented according to the Cl^- nutrition regime, no differences were observed between low chloride (70 µM Cl^-) and high chloride (5 mM Cl^-) treatments in the WT line (Fig. 4.4 d), and only small differences could be appreciated in the *slah1-2* mutant line (Fig. 4.4 c).

At the end of the phenotypic characterization, plant organs were harvested. No differences between *slah1-2* and WT lines were observed in either root biomass (data not shown) or root Cl^- content (Fig. 4.4 e, f).

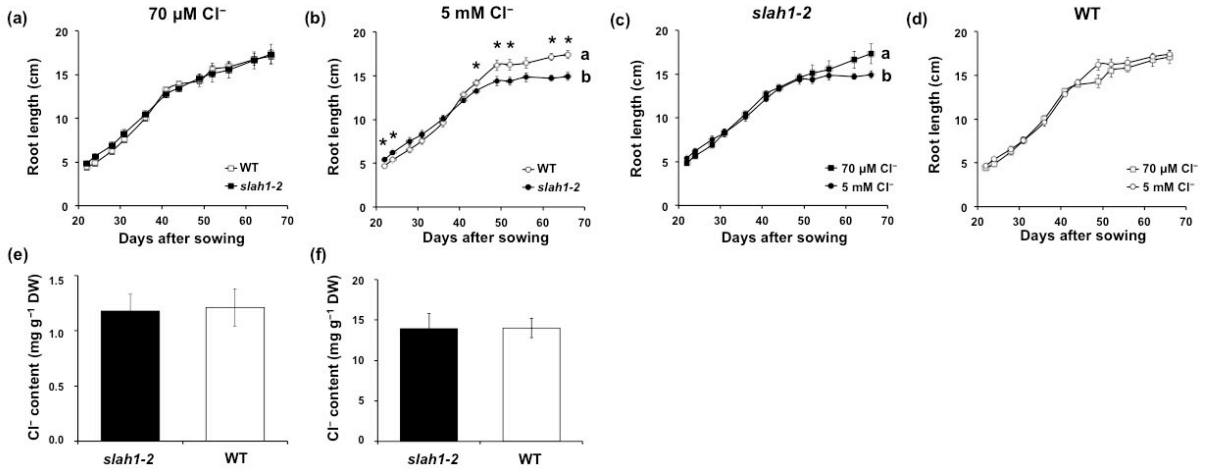

Figure 4.4. Phenotypic differences in the root of *slah1-2* mutant and its wild-type (WT) azygous line grown hydroponically under two different chloride treatments. Plants were grown hydroponically in nutrient solutions containing either low (70 µM) or high (5 mM) chloride (Cl^-). In the low chloride solution, Cl^- salts were replaced with sulphate and phosphate salts, maintaining the same balance of cations in comparison to the 5 mM chloride solution. **(a)** Root length of *slah1-2 versus* WT plants grown in a nutrient solution containing low chloride (70 µM Cl^-). **(b)** Root length of *slah1-2 vs.* WT plants grown in a nutrient solution containing high chloride (5 mM Cl^-). **(c)** Root length of *slah1-2* plants alternatively grown under low (70 µM Cl^-) or high (5 mM Cl^-) chloride. **(d)** Root length of WT plants alternatively grown under low (70 µM) or high (5 mM) chloride. **(e)** Root Cl^- content in *slah1-2* and WT plants grown in a nutrient solution containing low chloride (70 µM Cl^-). **(f)** Root Cl^- content in *slah1-2* and WT plants grown in a nutrient solution with containing high chloride (5 mM Cl^-). Asterisks indicate statistically significant differences (one-way ANOVA, $*P < 0.05$, n≥ 5). Different letters indicate a statistically significant difference in *slah1-2* and WT plants development over time (linear mixed models, $P < 0.05$).

No significant differences were observed in the rosette diameter of *slah1-2* and WT plants grown hydroponically in either low chloride (70 µM Cl^-; Fig. 4.5 a) or high chloride (5 mM Cl^-; Fig. 4.5 b) nutrient solutions. However, the growth of the rosettes in both genotypes was higher with high chloride (5 mM Cl^-; Fig. 4.5 c) compared to the low chloride treatment (70 µM Cl^-; Fig. 4.5 d), indicating that macronutrient content of Cl^- stimulates leaf growth.

The *slah1-2* mutant exhibited significantly fewer number of rosette leaves than the WT under the low Cl^- treatment (Fig. 4.5 e). However this difference was abolished when the mutant line was grown in 5 mM Cl^- (Fig. 4.5 f), indicating that the *slah1-2* mutant line was specifically more sensitive to low Cl^- nutrition than the WT line. This finding was more clearly observed when the number of leaves in high- and low-Cl^- solutions was compared separately in each genotype. Whereas the number of leaves is distinctly reduced by the low chloride treatment (70 µM Cl^-) in the *slah1-2* mutant line (Fig. 4.5 g), no differences between the two different chloridefeeding regimes in the WT line were observed (Fig. 4.5 h).

Similarly, significant differences in rosette biomass linked to Cl^- nutrition were specifically observed in the *slah1-2* mutant line (Fig. 4.5 k), but not observed in the WT line (Fig. 4.5 l), suggesting again higher sensitivity to Cl^- nutrition in the *slah1-2* mutant line, possibly as a consequence of the reduced Cl^- content close to the nutrient deficiency threshold (0.2 mg g^{-1} DW; Xu *et al.*, 2000).

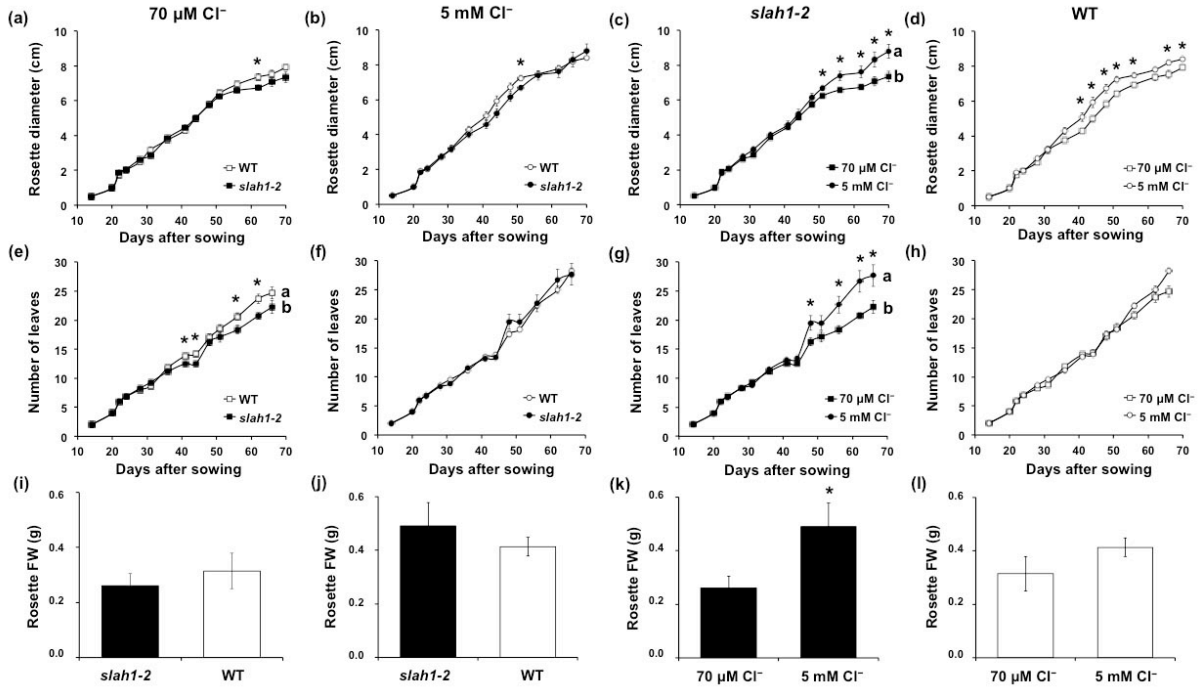

Figure 4.5. Vegetative growth phenotype of the *slah1-2* mutant and its wild-type (WT) azygous line grown hydroponically under two different chloride treatments. Plants grown hydroponically in a solution containing either 70 µM or 5 mM chloride (Cl^-). In the low chloride solution, Cl^- salts were replaced with sulphate and phosphate salts, maintaining the same balance of cations in comparison to the 5 mM chloride solution. **(a)** Rosette diameter of *slah1-2 versus* WT plants watered with a nutrient solution containing low chloride (70 µM Cl^-). **(b)** Rosette diameter of *slah1-2 vs.* WT plants watered with a nutrient solution with high chloride (5 mM Cl^-). **(c)** Rosette diameter of *slah1-2* plants alternatively watered with low (70 µM Cl^-) or high (5 mM Cl^-) chloride. **(d)** Rosette diameter of WT plants alternatively watered with low (70 µM) or high (5 mM) chloride. **(e)** Number of rosette leaves of *slah1-2 versus* WT plants watered with a nutrient solution containing low chloride (70 µM Cl^-). **(f)** Number of rosette leaves of *slah1-2 vs.* WT plants watered with a nutrient solution containing high chloride (5 mM Cl^-). **(g)** Number of rosette leaves of *slah1-2* plants alternatively watered with low (70 µM Cl^-) or high (5 mM Cl^-) chloride. **(h)** Number of rosette leaves of WT plants alternatively watered with low (70 µM) or high (5 mM) chloride. **(i)** Rosette fresh weight (FW) of *slah1-2 versus* WT plants grown in a nutrient solution containing low chloride (70 µM Cl^-). **(j)** Rosette fresh weight of *slah1-2 vs.* WT plants grown in a nutrient solution containing high chloride (5 mM Cl^-). **(k)** Rosette fresh weight of *slah1-2* plants alternatively grown under low (70 µM Cl^-) or high (5 mM Cl^-) chloride. **(l)** Rosette fresh weight of WT plants alternatively grown under low (70 µM) or high (5 mM) chloride. Asterisks indicate statistically significant differences (one-way ANOVA, $*P < 0.05$, n≥ 5). Different letters indicate a statistically significant difference in *slah1-2* and WT plants development over time (linear mixed models, $P < 0.05$).

No differences in the length of the inflorescence were observed when *slah1-2* mutant plants were compared with WT plants grown hydroponically in either low (70 µM Cl^-; Fig. 4.6 a) or high (5 mM Cl^-; Fig. 4.6 b) chloride treatments. In addition, the concentration of chloride in the nutrient solution did not affect the length of the inflorescence in either *slah1-2* (Fig. 4.6 c) or WT (Fig. 4.6 d) lines. However, the number of siliques was stimulated by high Cl^- addition in the WT line, but not in the *slah1-2* mutant line (Fig. 4.6 e-f). This finding was clearly visible when the number of siliques in high- and low-Cl^- solutions is compared separately in each genotype (Fig. 4.6 g-h), suggesting that SLAH1 could be involved in flower fertilization of seed developmental processes. Moreover, the significantly higher biomass of inflorescences from plants treated with high chloride (5 mM Cl^-) compared to low chloride (70 µM Cl^-) in both genotypes (Fig. 4.6 k-l) point to a role of Cl^- nutrition in plant reproductive development and fertilization (as it is proposed in section 4.1.2.1).

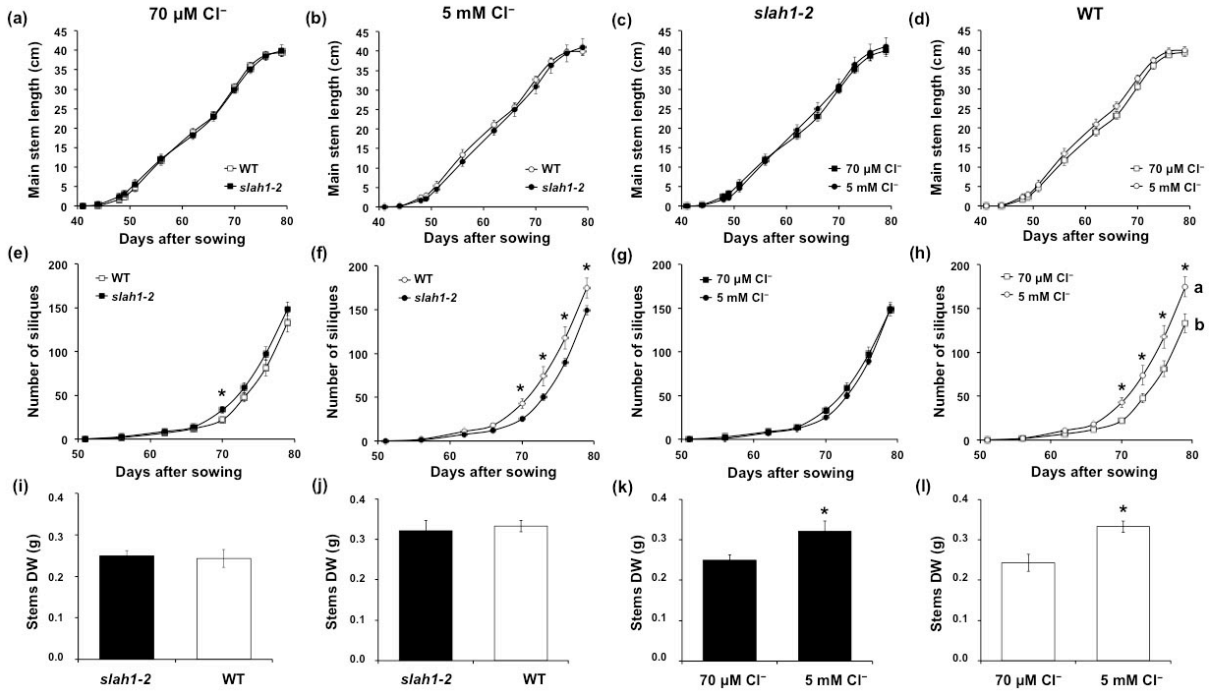

Figure 4.6. Differential shoot and inflorescence stem growth of mutant (*slah1-2*) and wild-type (WT) plants grown hydroponically under two different chloride feeding regimens. Plants were grown hydroponically with nutrient solutions containing 70 µM or 5 mM chloride (Cl^-). In the 70 µM Cl^- solution, Cl^- salts were replaced with sulphate and phosphate salts maintaining the same balance of cations of the 5 mM Cl^- solution. **(a)** Main inflorescence stem length of *slah1-2 versus* WT plants grown in a nutrient solution containing low chloride (70 µM Cl^-). **(b)** Main inflorescence stem length of *slah1-2 vs.* WT plants grown in a nutrient solution containing high chloride (5 mM Cl^-). **(c)** Main inflorescence stem length of *slah1-2* plants alternatively grown under low (70 µM Cl^-) or high (5 mM Cl^-) chloride. **(d)** Main inflorescence stem length of WT plants alternatively grown under low (70 µM) or high (5 mM) chloride. **(e)** Number of siliques produced by *slah1-2 versus* WT plants grown in a nutrient solution containing low chloride (70 µM Cl^-). **(f)** Number of siliques produced by *slah1-2 vs.* WT plants grown in a nutrient solution containing high chloride (5 mM Cl^-). **(g)** Number of siliques produced by *slah1-2* plants alternatively grown under low (70 µM Cl^-) or high (5 mM Cl^-) chloride. **(h)** Number of siliques produced by WT plants alternatively grown under low (70 µM) or high (5 mM) chloride. **(i)** Inflorescence stems dry weight (DW) of *slah1-2 versus* WT plants grown in a nutrient solution containing low chloride (70 µM Cl^-). **(j)** Inflorescence stems dry weight of *slah1-2 vs.* WT plants grown in a nutrient solution containing high chloride (5 mM Cl^-). **(k)** Inflorescence stems dry weight of *slah1-2* plants alternatively grown under low (70 µM Cl^-) or high (5 mM Cl^-) chloride. **(l)** Inflorescence stems dry weight of WT plants alternatively grown under low (70 µM) or high (5 mM) chloride. Asterisks indicate statistically significant differences (one-way ANOVA, $*P < 0.05$, $n \geq 5$). Different letters indicate a statistically significant difference in *slah1-2* and WT plants development over time (linear mixed models, $P < 0.05$).

Altogether the results show a clear interaction between SLAH1 function and chloride nutrition that impacts the development of shoot organs, indicating that this anion channel is involved in chloride nutrition in plants.

When monitoring the phenotype of the *Arabidopsis* mutant and the WT lines growing with 5 mM Cl^- in pots, the *slah1-2* mutant exhibited significantly smaller rosettes (Fig. 4.7 a) and significantly lower number of leaves than the WT (Fig. 4.7 b). However, the rosette development of mutant plants reached the WT rosette development (Fig. 4.7 a), indicating that the mutant line phenotype consisted on a delayed rather than a reduced growth compared to the WT, which began the senescence stage earlier. Thus it is not surprising that *slah1-2* KO mutant plants had

significantly higher rosette fresh and dry weight (Fig. 4.7 c-d) relative to WT plants when plants were harvested at the end of the development cycle.

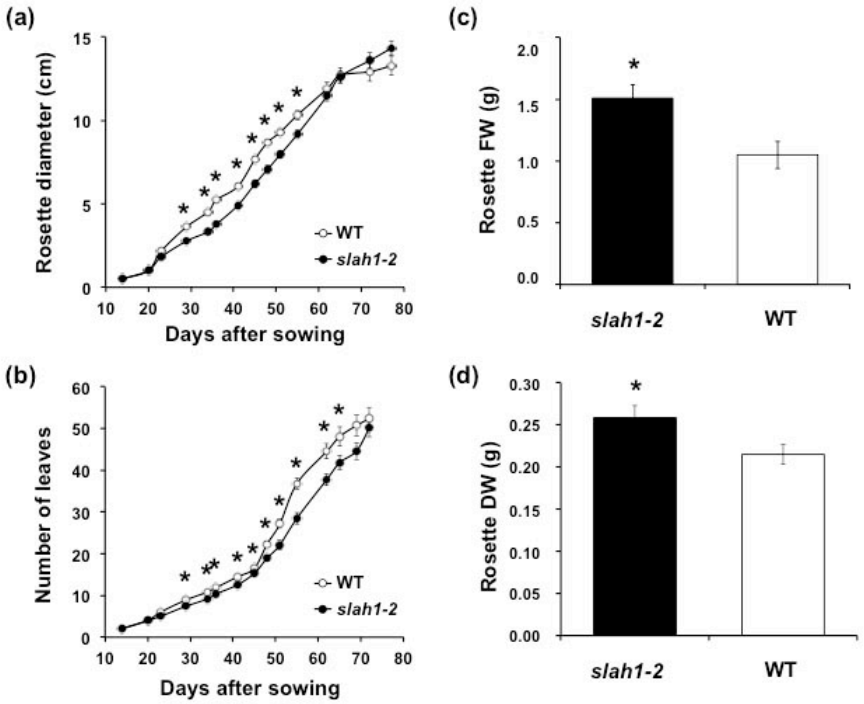

Figure 4.7. Differential rosette growth of *slah1-2* KO line and its wild-type (WT) azygous line grown in solid substrate treated with 5 mM chloride. (a) Rosette diameter of *slah1-2 versus* WT plants. **(b)** Number of rosette leaves of *slah1-2 vs.* WT plants. **(c)** Rosette fresh weight (FW) of *slah1-2 versus* WT plants. **(d)** Rosette dry weight (DW) of *slah1-2 versus* WT plants. Asterisks indicate statistically significant differences (one-way ANOVA, **P* < 0.05, n≥ 10).

Inflorescence development of the *slah1-2* mutant line grown in pots with 5 mM Cl^- was lower at the beginning of the reproductive phase in relation with the development of WT plants (Fig. 4.8 a), although it reached the WT stem development (75 days after sowing) and became even significantly higher, similarly to the rosette development observed (Fig. 4.7 a). However, no differences in the production of siliques between both lines were observed (Fig. 4.8 b).

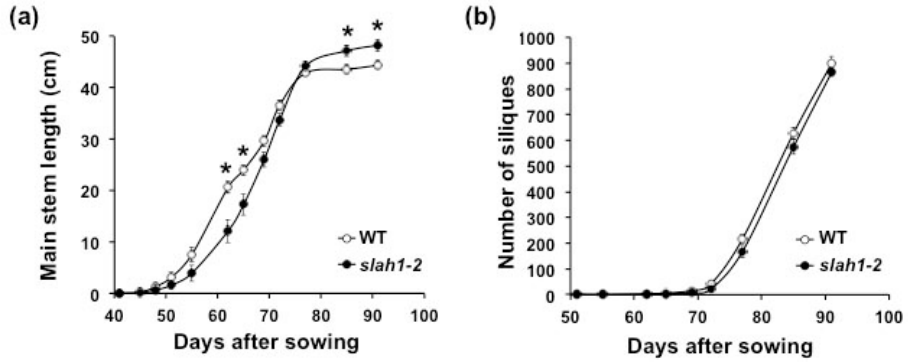

Figure 4.8. Differential main inflorescence stem development and siliques production of *slah1-2* mutant and wild-type (WT) plants grown in solid substrate treated with 5 mM chloride. (a) Main inflorescence stem length of *slah1-2 versus* WT plants. **(b)** Number of siliques produced by *slah1-2 vs.* WT plants. Asterisks indicate statistically significant differences (one-way ANOVA, **P* < 0.05, n≥ 10).

After plant harvesting (93 days after sowing), chloride content in the shoot was determined (section 3.8.4.1). The chloride contents of *slah1-2* plants were significantly lower than that of WT plants grown in pots treated with 5 mM Cl^- (Fig. 4.9).

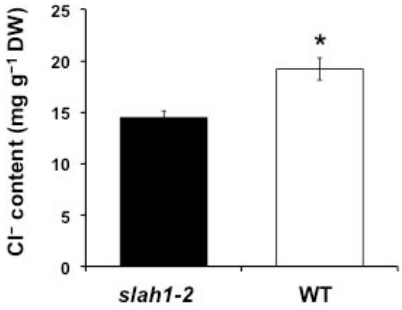

Figure 4.9. Shoot chloride content was significantly lower in *slah1-2* plants. Plants grown in pots and watered with a nutrient solution containing 5 mM chloride (Cl^-) were harvested at late-senescence stage. *slah1-2* KO plants had significantly lower chloride content in shoots than WT plants. Asterisks indicate statistically significant differences (one-way ANOVA, $*P < 0.05$, n≥ 10).

To find out whether and how the loss of function of the *AtSLAH1* gene affects the Cl^- content of *Arabidopsis* plants, *slah1-2* mutant and WT lines were grown in pots under the two feeding regimes, 70 µM and 5 mM Cl^-.

Plants were harvested at late-senescence stage (130 days after sowing) and shoot chloride content was determined (section 3.8.4.1). It could be observed that *slah1-2* KO mutant plants accumulated significantly less Cl^- in the shoot than the WT plants, independent from the chloride treatment (Fig. 4.10 a-b).

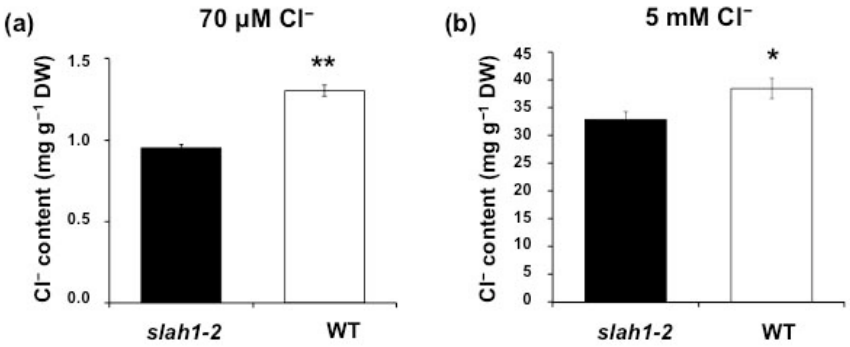

Figure 4.10. Chloride content in shoots of *slah1-2* T-DNA knockout and wild-type (WT) plants grown in solid substrate treated with two different chloride feeding regimens. Plants were watered with nutrient solutions containing 70 µM or 5 mM chloride (Cl^-). In the 70 µM Cl^- solution, Cl^- salts were replaced with sulphate and phosphate salts maintaining the same balance of cations of the 5 mM Cl^- solution. **(a)** Chloride content of *slah1-2* and WT plants watered with a nutrient solution containing 70 µM Cl^-. **(b)** Chloride content of *slah1-2* and WT plants watered with a nutrient solution containing 5 mM Cl^-. Asterisks indicate statistically significant differences (one-way ANOVA, $*P < 0.05$, $**P < 0.01$, n≥ 6).

Altogether the results indicate that *AtSLAH1* regulates Cl^- homeostasis at the whole-plant level, probably through the regulation of root-to-shoot Cl^- transport.

4.1.1.4. SLAH1, together with SLAH3, contributes to chloride feeding of root xylem

The lower shoot Cl^- content of the *AtSLAH1*-mutant line suggested that SLAH1 was engaged in Cl^- homeostasis. To reach the shoot, nutrients that enter the root have to be loaded into the root xylem vessels. Since *AtSLAH1* and *AtSLAH3* expression was localized in the pericycle cells facing the xylem vessels in the root (Fig. 4.2), the pericycle cells should contribute to the anion composition of the ascending xylem sap.

To inspect whether *AtSLAH1* and its co-expressed homolog *AtSLAH3* are involved in anion transport from xylem parenchyma cells into xylem vessels, genotyped KO plant lines (section 3.2.4.1), homozygous for the T-DNA insertion, together with the respective wild-type lines were grown in pots under long photoperiod conditions and watered with Basal Solution (BS; section 3.1.2.2.2) and used for xylem sap collection assays (section 3.8.2). Afterwards, Cl^- and NO_3^- contents in the xylem sap were colorimetrically quantified (section 3.8.4.2).

For quantification of root-to-shoot anion translocation rates, Cl^- and NO_3^- concentration was measured in the root sap exudates of WT and *slah1-2* mutant line (Fig. 4.11). To collect sap ascending from the root xylem, the shoot had to be removed. After trimming the shoot, sap droplets were collected at different times (1 h, 2 h, 3 h and 5 h after starting the assay). The Cl^- and NO_3^- concentration obtained from this samples was plotted at each collection point. It could be observed that Cl^- concentration in the xylem sap of both lines decreased gradually after trimming the shoot, meanwhile NO_3^- concentration increased within the first 2–3 h, and then decreased (Fig. 4.11). The gradually drop of Cl^- concentration in the xylem sap observed in *slah1-2* plants (Fig. 4.11) could be due to the negative regulation of the *AtSLAH1* gene expression by stress. It could be also observed that xylem sap Cl^- concentration of *slah1-2* plants was significantly lower that that of WT plants (Fig. 4.11).

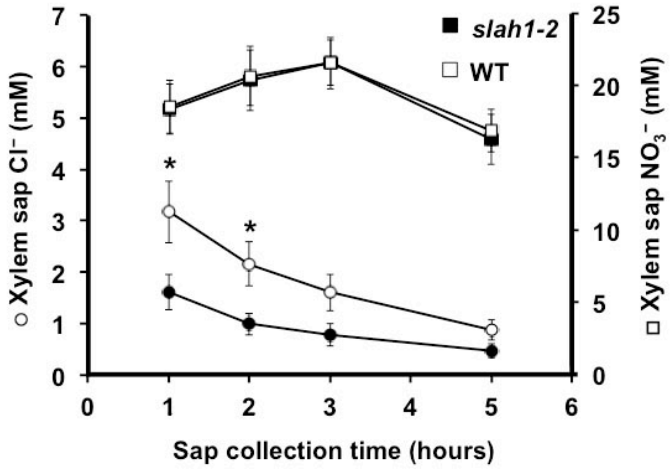

Figure 4.11. Anion concentration in xylem sap of *slah1-2* plants relative to wild-type (WT) plants at different collecting times. Plants were grown hydroponically with Basal Solution (BS). Evolution of chloride (Cl^-) and nitrate (NO_3^-) content in xylem sap after shoot trimming represented as percentage of the WT in the first collection point. Asterisks indicate statistically significant differences (Student's t test, $^*P < 0.05$, n = 12 experiments; mean ± SE).

Therefore, for minimizing artifactual responses inherent to the experimental technique (e.g. the response to mechanical damage caused by cutting the rosette), only the xylem sap anion content of the first collecting time was represented in subsequent assays.

For quantification of root-to-shoot anion translocation rates, Cl^- and NO_3^- concentration was measured in the root sap exudates of s*lah1*-2 and *slah3-1* mutant lines and their respective WT lines (section 3.8.4.2). Only assays where the sap exudation rate of mutant and WT plants were comparable, indicating similar root biomass, were used (Fig. 4.12 a, f).

Xylem sap Cl^- concentration was significantly lower in both *slah1-2* and *slah3-1* mutant lines in relation to their respective WT lines (Fig. 4.12 b, g), meanwhile NO_3^- concentration of the mutant lines remained similar to WT values (Fig. 4.12 d, i).

Root-to-shoot translocation rates were obtained through multiplying their concentrations in the exudates (Fig. 4.12 b, d, g, i) by the sap exudation rates of each plant (Fig. 4.12 a, f) and then compared with their respective WT lines. Reduction of Cl^- content in the xylem sap of plants lacking functional copies of *AtSLAH1* or *AtSLAH3* genes was a consequence of a lower root-to-shoot translocation rate of Cl^- (Fig. 4.12 c, h), meanwhile the NO_3^- translocation rate did not significantly change (Fig. 4.12 e, j).

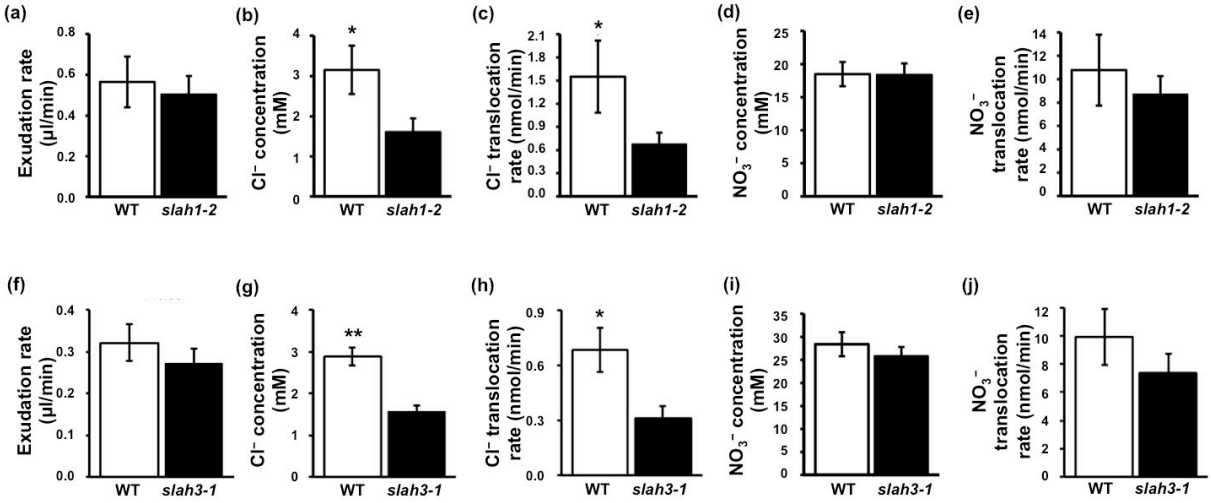

Figure 4.12. SLAH1 and SLAH3 are involved in chloride translocation into the xylem. (a) Exudation rate of wild-type (WT) and s*lah1-2* plants used to quantify anion translocation into the xylem. **(b)** Chloride (Cl^-) concentration in the xylem sap of WT and s*lah1-2* plants. **(c)** Root-to-shoot translocation rate of Cl^- in WT and s*lah1-2* plants. **(d)** Xylem sap nitrate (NO_3^-) concentration of WT and s*lah1-2* plants. **(e)** NO_3^- root-to-shoot translocation rate of WT and s*lah1-2* plants. **(f)** Exudation rate of WT and s*lah3-1* plants used for Cl^- and NO_3^- quantification in the xylem sap. **(g)** Xylem sap Cl^- concentration of WT and s*lah3-1* plants. **(h)** Cl^- root-to-shoot translocation rate of WT and *slah3-1* plants. **(i)** NO_3^- concentration in the xylem sap of WT and s*lah3-1* plants. **(j)** Root-to-shoot translocation rate of NO_3^- in WT and s*lah3-1* plants. The translocation rates were obtained by multiplying their concentrations in the exudates by the sap exudation rates. Asterisks indicate significant differences between WT and either the *slah1-2* mutant line (Student's t test, **P* < 0.05, n≥ 12, n = 12 experiments; mean ± SE) or the *slah3-1* mutant line (one-way ANOVA, **P* < 0.05, ***P* < 0.01, n≥ 6, n = 2 experiments; mean ± SE).

Given the absence of a second independent mutant line, to confirm that the reduction of Cl^- content in the xylem sap of *slah1-2* plants was specifically due to the lack of *AtSLAH1* gene function, xylem sap of the complemented lines, P1-12 and P1-31, expressing the wild-type *AtSLAH1* gene under the control of its native promoter (section 3.4.2), was inspected. With the same purpose, another independent *AtSLAH3*-mutant line, *slah3-4*, was used to confirm that the reduction of Cl^- content in the xylem sap was specifically due to the lack of *AtSLAH3* gene function in the *SLAH3*-mutant background.

In line with the assumed role of SLAH1 in Cl^- feeding (Fig. 4.12), the s*lah1-2* line contained approximately 50% less Cl^- concentration in the xylem sap while the complemented lines, P1-12 and P1-31, reached Cl^- levels similar to the WT (Fig. 4.13 a). In addition, the NO_3^- translocation in the complemented lines was not affected in relation to the WT line (Fig. 4.13 b).

Interestingly the two independent *slah3* KO lines also exhibited similar reductions in the xylem sap Cl^- concentration than the *slah1-2* line (Fig. 4.13 c) as a consequence of the reduction of the Cl^- translocation rate (Fig. 4.12 h), while NO_3^- levels remained unchanged (Fig. 4.13 d).

Moreover, the *slah1-2* KO mutant was crossed with the *slah3-1* KO mutant (section 3.7.2) and the resulting double-KO mutant, homozygoys for the respective T-DNA insertions, was named *slah1-slah3*. Ion content from the xylem sap of the double–KO mutant and its azygous segregating line (thereafter named Col-0 x WS) was quantified. Interestingly, the analysis of the xylem sap of *slah1-slah3* showed a significant reduction of the Cl^- content in the xylem sap similar to that of the respective single mutant lines (Fig. 4.13 c), while the NO_3^- concentration remained WT-like (Fig. 4.13 d).

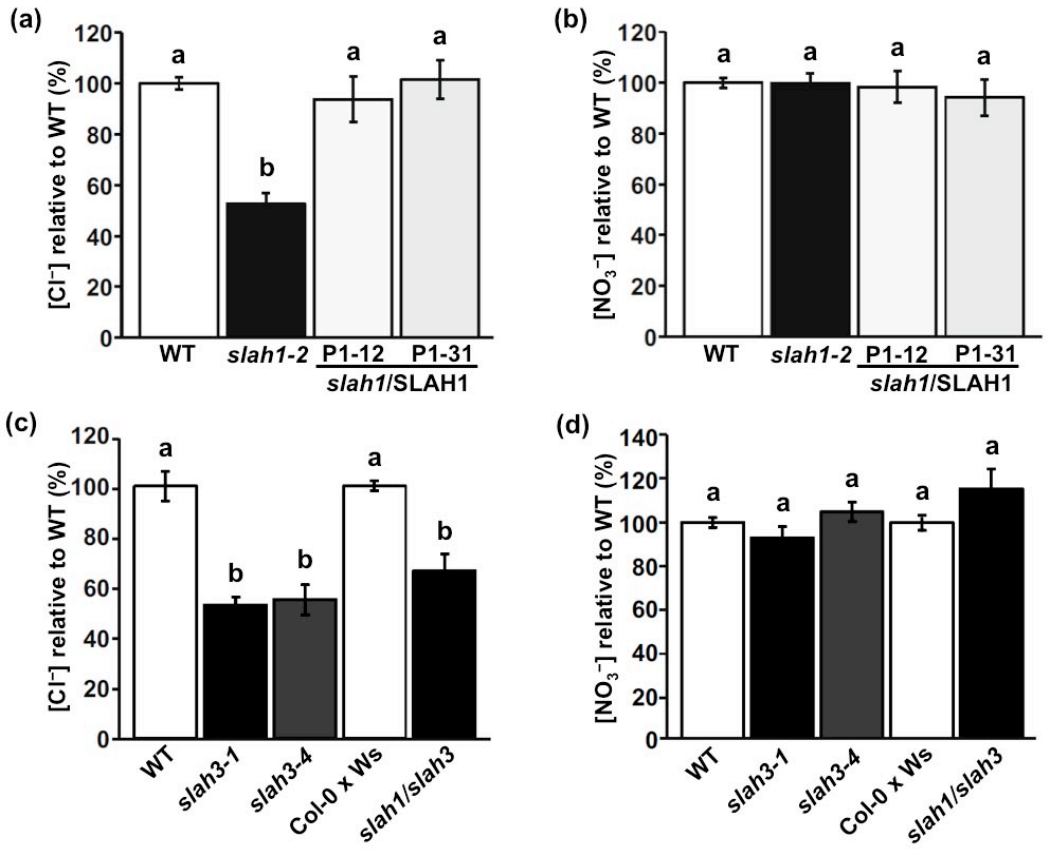

Figure 4.13. SLAH1 and SLAH3 regulate root-to-shoot translocation of chloride. (a) Percentage of chloride (Cl^-) concentration in the xylem sap in the *slah1-2* mutant and in two *slah1/SLAH1* complemented lines (P1-12 and P1-31) relative to the wild-type (WT; 100%) at the first collecting time. **(b)** Percentage of nitrate (NO_3^-) xylem sap concentration in the *slah1-2* mutant and in the two *slah1/SLAH1* complemented lines relative to the WT (100%). **(c)** Percentage of Cl^- xylem sap concentration in two *slah3* KO lines (s*lah3-1* and *slah3-4*) and in the *slah1-slah3* double-KO mutant line relative to their WT lines (100%) at the first collecting time. **(d)** Percentage of NO_3^- concentration in the xylem sap in two *slah3* KO lines and in the *slah1-slah3* double-KO mutant line relative to their WT lines (100%). Different letters indicate statistically significant differences (Student's t test, $P < 0.05$, n≥ 3, n = 1−12 experiments; mean ± SE).

The anion content in the xylem sap *vs.* the anion content in the nutrient solution ratio was calculated for Cl^- and NO_3^- in the different ecotypes assayed (WS, Col-0, and the WS x Col-0 hybrid) and this ratio was called translocation efficiency. In the different ecotypes much higher translocation efficiencies for NO_3^- than for Cl^- were observed (Table 4.1). The translocation efficiency for NO_3^- divided by the translocation efficiency for Cl^- was also calculated and this ratio was called NO_3^-/Cl^- selectivity. The NO_3^-/Cl^- selectivity varied between the WS and Col-0 wild-type ecotypes, but the NO_3^-/Cl^- selectivity of all the mutant lines was approximately twice the value of the respective WT (Table 4.1).

Table 4.1. Root-to-shoot anion translocation efficiency and nitrate (NO_3^-)/chloride (Cl^-) selectivity obtained under low salinity conditions.

Ecotype	Line	NO_3^-		Cl^-		NO_3^-/Cl^- selectivity[c]
		Xylem sap concentration (mM)[a]	Translocation efficiency[b]	Xylem sap concentration (mM)[a]	Translocation efficiency[b]	
Wassilevskija	**wild-type**	18.50 ± 1.83	5.29 ± 0.52	3.17 ± 0.60	0.63 ± 0.12	8.40
	slah1-2	18.37 ± 1.74	5.25 ± 0.50	1.62 ± 0.34	0.32 ± 0.07	16.41
Col-0	**wild-type**	28.40 ± 2.60	8.12 ± 0.74	2.92 ± 0.33	0.58 ± 0.07	14.00
	slah3-1	25.83 ± 1.98	7.38 ± 0.57	1.23 ± 0.20	0.25 ±0.04	29.52
Col-0 x Wassilevskija	**wild-type**	24.94 ± 2.69	7.13 ± 0.77	2.45 ± 0.24	0.49 ± 0.05	14.54
	slah1-slah3	26.83 ± 1.39	7.67 ± 0.40	1.63 ± 0.22	0.33 ±0.04	23.55

[a]Xylem sap NO_3^- and Cl^- concentration measured in the first sap extraction simple.
[b]Calculated as the anion content in the xylem sap divided by the anion content in the nutrient solution.
[c]Regarding the root-to-shoot translocation process and calculated as the translocation efficiency of NO_3^- divided by the translocation efficiency of Cl^-.

The fact that the phenotypes of the single and the double mutants were similar indicates that Cl^- release into xylem vessels requires the concerted participation of both channels, SLAH1 and SLAH3, in the same transport mechanism.

Since SLAH1 facilitates root-to-shoot transfer of Cl^-, this channel might serve as a pathway for shoot Cl^- accumulation under salt stress conditions. To test this assumption, *slah1-2* KO and WT plants were subjected to increasing concentrations of Cl^- salt (15, 30, 60 and 120 mM Cl^-; section 3.8.2). After quantifying Cl^- concentration in the xylem sap, it could be observed that *slah1-2* KO plants accumulated less chloride that WT plants in the xylem sap collected 3 h after salt exposure (Fig. 4.14) and this difference became significant in roots exposed to higher salt concentrations (60 and 120 mM; Fig. 4.14).

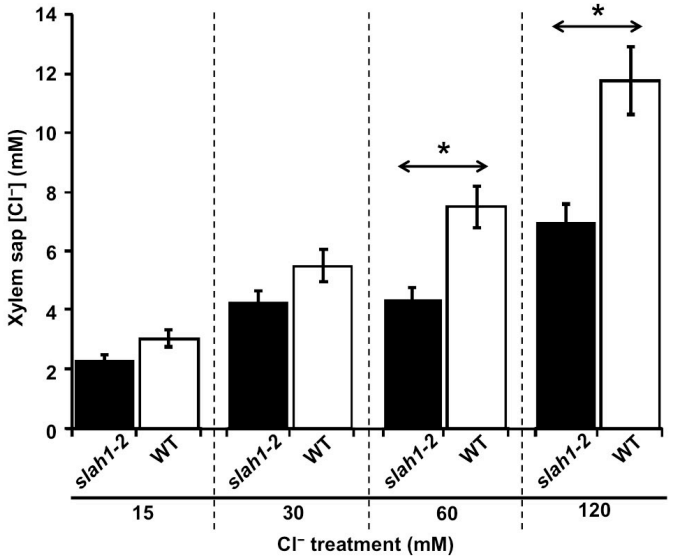

Figure 4.14. SLAH1 is involved in chloride (Cl^-) transfer to the shoot. Chloride concentration in the xylem sap of the *slah1-2* and the WT line 3 h after high salt load treatments (15, 30, 60, and 120 mM Cl^-). Asterisks indicate statistically significant differences (Student's t test, $*P < 0.05$, n= 3).

4.1.1.5. *AtSLAH1* and *AtSLAH3* gene expression regulation

To analyse the regulatory properties of *AtSLAH1* and its co-expressed homolog *AtSLAH3*, their transcript expression levels in *Arabidopsis* plants grown hydroponically under different conditions (section 3.1.2.2.3) were quantified by quantitative real time PCR (qPCR; section 3.2.4.3).

4.1.1.5.1. Stress and ABA strongly down-regulate *AtSLAH1* expression

Although water deficit and abscisic acid (ABA) have limited effect on ion uptake within the root from the external medium, they have been shown to increase solute accumulation in roots through the inhibition of ions release into the xylem (Cram and Pitman, 1972; Pitman, 1977; Pitman and Wellfare, 1978; Pitman *et al*., 1974). In addition, water deficit and ABA also down-regulates genes that encode transporters involved in anion translocation into the xylem, like the *AtSKOR* gene, which mediates K^+ release into the xylem sap (Gaymard *et al*., 1998).

Therefore, since *AtSLAH1* and *AtSLAH3* co-localize in the xylem-pole pericycle cells, negative regulation of both genes expression might take place during acclimatization of plants to water deficit or salinity. To determine whether *AtSLAH1* and *AtSLAH3* gene expression is regulated by abiotic stress and ABA, *A. thaliana* Col-0 plants, grown hydroponically (section 3.1.2.2.3), were subjected to a salt stress treatment with 150 mM NaCl, a water deficit treatment applied with 287 g l^{-1} PEG-8000 and a treatment consisting on exogenous application of 100 µM ABA. Roots were harvested 3 and 24 h after treatments application and the RNA extracted (section 3.3.1) from the root was used for cDNA synthesis (section 3.3.2) and qPCR analyses (section 3.2.4.3). All mRNA levels were calculated from threshold cycle values and normalized with respect to the transcript level of the housekeeping *AteIF4A1* gene.

AtSLAH1 and *AtSLAH3* gene expression level of plants subjected to these treatments was compared to that of control plants (transferred to untreated hydroponics solutions). Results are given as Fold-change of treated *vs.* untreated transcript abundance.

Upon an increase in the salt content of the soil, the water potential drops. Soil salinity and water deficit leads to an increase of the stress hormone ABA level, which in turn induces the expression of drought tolerance genes (Vahisalu *et al.*, 2008). The gene encoding for the dehydrin *AtLEA-M*, a member of the Late-Embryogenesis Abundant (LEA) family, was used as positive control of stress-responsive gene (Fig. 4.15), since the members of the LEA family are strongly induced in vegetative tissues in response to osmotic stress and ABA application (Colmenero-Flores *et al.*, 1997).

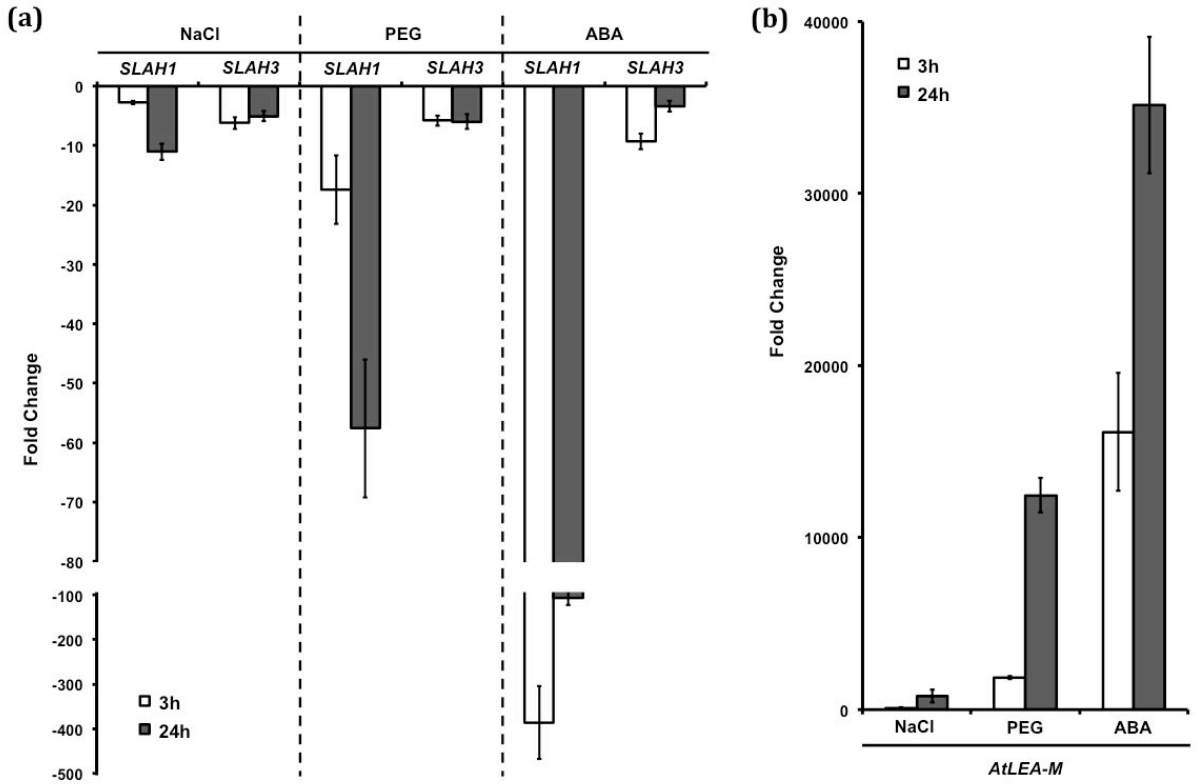

Figure 4.15. Relative expression of *AtSLAH1* and *AtSLAH3* under abiotic stress treatments. (a) Fold-change relative to control conditions of *AtSLAH1* and *AtSLAH3* transcript levels quantified 3 h and 24 h after treatment application. Abiotic stress treatments consisted of salinity induced with 150 mM NaCl (NaCl), water deficit caused with 287 g l^{-1} PEG-8000 (PEG) and exogenous application of 100 µM ABA (ABA). **(b)** Expression of the stress-responsive gene *AtLEA-M* was used as a control of the same treatments described in (a). Transcript abundance was quantified with standard curves calculated for the individual PCR products and normalized with the housekeeping translation initiation factor *AteIF4A1* gene ($n \geq 3$; mean ± SE).

Under salt stress, Cl^- uptake by the root is facilitated while that of NO_3^- is hampered. To prevent non-physiological chloride levels reaching the shoot on one side, and nitrate depletion on the other, the entry of Cl^- relative to NO_3^- has to be well controlled.

Twenty-four hours after the 150 mM NaCl treatment, root transcript levels of the stress marker *AtLEA-M* strongly increased (Fig. 4.15), while those of *AtSLAH1* and *AtSLAH3* dropped 13 times and approximately 5 times, respectively (Fig. 4.15).

To distinguish between a response induced by salt stress and osmotic stress caused by water deficit, roots were exposed to the non-permeable PEG-8000 (Van der Weele *et al.*, 2000). When water deficit was applied with 287 g l^{-1} PEG-8000, maintaining the same osmolarity of the salt stress treatment, *AtLEA-M* transcripts also increased (Fig. 4.15) whereas *AtSLAH1* and *AtSLAH3* decreased about 70 and 6 times respectively (Fig. 4.15).

Therefore, both genes were down-regulated by osmotic stress treatment, although *AtSLAH3* showed a stress response weaker than *AtSLAH1*.

The phyto-hormone ABA mediates the osmotic stress response in plants through the induction of drought-tolerance genes (Colmenero-Flores *et al.*, 1997). Thus plants were also treated with exogenous ABA application. *AtLEA-M* transcript levels strongly increased, however both *AtSLAH1* and *AtSLAH3* genes were down-regulated by this hormone (Fig. qPCR), although the response was much stronger for *AtSLAH1*, which reduced transcript accumulation by 400 times, compared to *AtSLAH3*, that decreased it around 9 times.

This response is in accordance with the disappearance of *AtSLAH1* promoter activity in the vascular cylinder of GUS-expressing plants 15 h after pre-incubation with ABA (Fig. 4.16).

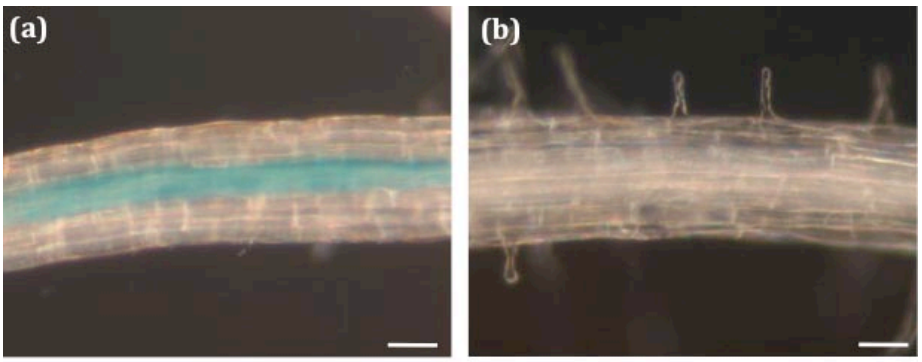

Figure 4.16. *AtSLAH1* gene expression is down-regulated by abscisic acid (ABA). Histochemical localization of *AtSLAH1* expression in transgenic plants expressing the GUS reporter gene under the control of the promoter. **(a)** P_{SLAH1}-GFP::GUS transgenic root without ABA (control). **(b)** P_{SLAH1}-GFP::GUS transgenic root treated with 100 µM ABA. Scale bars, 50 µm.

Therefore, *AtSLAH1* and *AtSLAH3* genes expression was down-regulated by osmotic stress treatments in an ABA-dependent manner, although this response was much stronger for *AtSLAH1* in comparison to *AtSLAH3*.

4.1.1.5.2. Nutritional treatments (NO_3^- and Cl^- starvation and supply) regulate *AtSLAH1* and *AtSLAH3* gene expression

Gene expression of membrane transporters is frequently regulated by nutrient availability. To determine whether *AtSLAH1* and *AtSLAH3* gene expression changes in response to modifications in the availability of NO_3^- and Cl^-, nutrient starvation and nutrient supply (after starvation) treatments were applied.

With this aim, Col-0 plants were grown hydroponically (section 3.1.2.2.3). On the one side, plants alternatively grown with nitrate (5 mM NO_3^-) or without nitrate (2.5 mM ammonium), were subjected to either NO_3^- application (transfer of ammonium-treated plants to 5 mM NO_3^- medium) or NO_3^- starvation (transfer of NO_3^- plants to a nutrient solution containing no NO_3^-) treatments respectively. On the other side, plants alternatively grown with low chloride (70 µM Cl^-) or high chloride (5 mM Cl^-) were subjected to either Cl^- application (transfer of low-Cl^- plants to 5 mM Cl^- medium) or Cl^- starvation (transfer of high-Cl^- plants to 70 µM Cl^- medium) treatments respectively. Plants used as control were transferred to the same nutrient solution.

On the one side, the nitrate starvation treatment reduced *AtSLAH1* and *AtSLAH3* transcript levels 24 h after plant transfer to NO_3^-–free medium (Fig. 4.17). However, the repression response was about 9 times stronger for *AtSLAH1* (46 times reduction) than for *AtSLAH3* (6 times reduction). These data indicate that nutritional stress also down-regulates gene expression of these anion channels. In addition, nitrate supply after starvation induced transcript accumulation of both genes 24 h after plant transfer to NO_3^-–medium (Fig. 4.17): 22 times induction for *AtSLAH1* and 8 times induction for *AtSLAH3*.

On the other side, gene expression responses to changes in the availability of Cl^- were also analysed. *AtSLAH1* and *AtSLAH3* root transcript levels slightly and transiently decreased approximately 6 and 3 times, respectively, after plant transfer to Cl^-–free medium (Fig. 4.17), while no changes were observed in response to chloride supply after starvation.

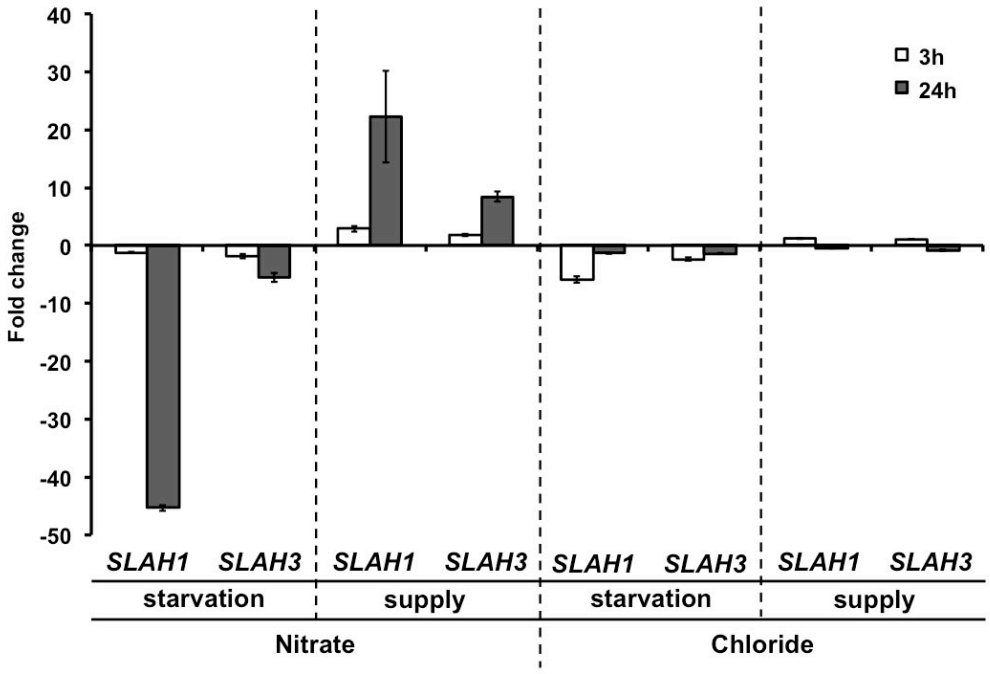

Figure 4.17. Relative expression of *AtSLAH1* and *AtSLAH3* in response to changes in the nutritional status of nitrate (NO_3^-) and chloride (Cl^-). Fold-change relative to control conditions of *AtSLAH1* and *AtSLAH3* transcript levels quantified 3 h and 24 h after different nutritional treatments. Nitrate supply: plants growing hydroponically in a nutrient solution with 2.5 mM ammonium acetate as the sole nitrogen source were transferred to a nutrient solution containing 5 mM NO_3^- as the sole nitrogen source. Nitrate starvation: plants growing hydroponically in a nutrient solution with 5 mM NO_3^- as the sole nitrogen source were transferred to a nutrient solution with 2.5 mM ammonium acetate as the sole nitrogen source. Chloride supply: plants growing hydroponically in a nutrient solution containing low chloride (70 µM Cl^-) were transferred to a nutrient solution with high chloride (5 mM Cl^-). Chloride starvation: plants growing hydroponically in a nutrient solution with high chloride (5 mM Cl^-) were transferred to a nutrient solution containing low chloride (70 µM Cl^-). Transcript abundance was quantified with standard curves calculated for the individual PCR products and normalized with the housekeeping translation initiation factor *AteIF4A1* gene ($n \geq 3$; mean ± SE).

Altogether the results show that S-type channels, particularly *AtSLAH1*, have strong transcriptional regulation to ABA-mediated responses (e.g. osmotic stress), moderate responses to NO_3^- availability treatments and slight responses to Cl^- availability treatments.

4.1.1.6. SLAH1 is a silent anion channel

Kinetic and regulatory properties of the SLAH1 and SLAH3 anion channels were studied through functional expression of the corresponding genes in the heterologous expression system of *Xenopus* oocytes (section 3.10) in combination with the two-electrode voltage clamp (TEVC) technique (section 3.12).

In previous studies the S-type anion channel function of SLAC1, SLAH2, and SLAH3 was studied in *Xenopus* oocytes after expressing them alone or with activating kinases from different (Ca^{2+}-dependent and independent) families (Brandt *et al*., 2012; Geiger *et al*., 2009b, 2010; Lee *et al*., 2009; Maierhofer *et al*., 2014a,b; Scherzer *et al.*, 2012).

To find interacting kinases of SLAH1 and to study its regulatory properties, the anion channel was fused to the C-terminal half of the yellow fluorescent protein (YFP) and candidate kinases to the N-Terminal half of YFP. Besides the kinases that are known to activate channels of the SLAC/SLAH family (CPK3, CPK6, CPK21, CPK23, CIPK23, SnRK2.6 (OST1); Brandt *et al*., 2012; Geiger *et al*., 2009b, 2010; Lee *et al*., 2009; Maierhofer *et al*., 2014a,b; Scherzer *et al.*, 2012) or that interact with them (SnRK2.3, SnRK2.8; Geiger *et al.*, 2009), several members of the same kinase families, whose expression is predicted in the root pericycle (www.genevestigator.org), were tested. Following the expression in *Xenopus* oocytes, bimolecular fluorescence complementation (BiFC; section 3.11) analyses revealed pronounced YFP signals with the Ca^{2+}-dependent kinases CPK6 and CPK21 (Fig. 4.18), but only weak fluorescence with CPK23 and CIPK23/CBL1, as well as with the Ca^{2+}-independent SnRK2 kinases SnRK2.2, SnRK2.3, SnRK2.6 (OST1), SnRK2.7 and SnRK2.8 (Fig. 4.18). In addition, no YFP signal was obtained with CPK3 (Fig. 4.18). The fluorescence obtained suggested a physical interaction between SLAH1 and different potential regulatory kinases.

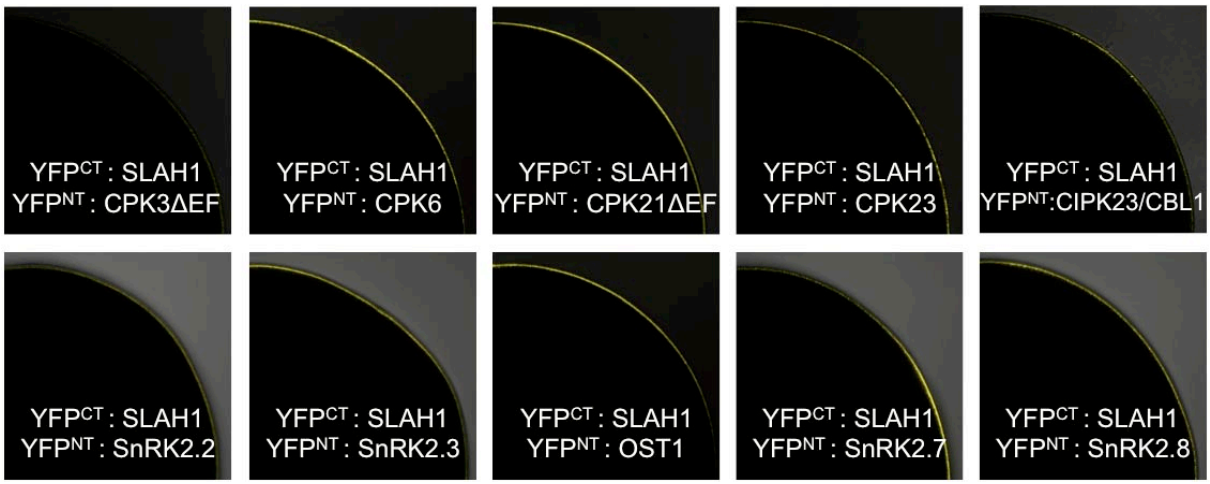

Figure 4.18. Physical interaction of SLAH1 with members of different kinase families revealed by BiFC experiments. The SLAH1 anion channel was fused with the C-terminal half of the yellow fluorescent protein (YFP^{CT}) and candidate kinases to the N-Terminal half of YFP (YFP^{NT}) previously to co-expression in *Xenopus* oocytes. Representative images of one-quarter of *Xenopus* oocytes are shown. When the co-expressed components interact between them, the YFP can be reconstituted, emitting fluorescence given its excitation with an appropriate wavelength. Ca^{2+}-independent truncated kinases of CPK3 (CPK3ΔEF) and CPK21 (CPK21ΔEF) were used.

To test whether these kinases, that activate other SLAC/SLAH S-type anion channels, could also activate SLAH1 in *Xenopus* oocytes, the channel was co-expressed with SnRK2.2,

SnRK2.3, SnRK2.6, SnRK2.7, SnRK2.8, CIPK23/CBL1 or with one of the Ca^{2+}-dependent protein kinases CPK3, CPK6, CPK21 or CPK23. To avoid differences in the kinase activity due to different Ca^{2+}-dependencies and calcium levels in *Xenopus* oocyte batches, truncated Ca^{2+}-independent mutants of CPK3 and CPK21 were used (CPK3ΔEF, CPK21ΔEF, Geiger *et al*., 2010, 2011; Maierhofer *et al*., 2014a,b; Scherzer *et al*., 2012). However, neither SLAH1 expression alone or in combination with the kinases that were effective with SLAC1, SLAH2 or SLAH3 resulted in macroscopic anion currents in *Xenopus* oocytes (data not shown).

SLAH3, which co-expresses with SLAH1 in root pericycle cells facing xylem vessels, requires a Ca^{2+}-dependent kinases such as CPK21 to conduct NO_3^- and Cl^- anions, but only when gated open by NO_3^- at the extracellular entrance of the channel pore (Geiger *et al*., 2011; Maierhofer *et al*., 2014b). Nevertheless, oocytes expressing SLAH1 in the absence or presence of CPK21ΔEF did not respond to extracellular Cl^- nor NO_3^- (Fig. 4.19 a-b), meanwhile it could be observed that the kinase activation and the NO_3^- in the external medium were enough to get SLAH3 channel open (Fig. 4.19 c-d).

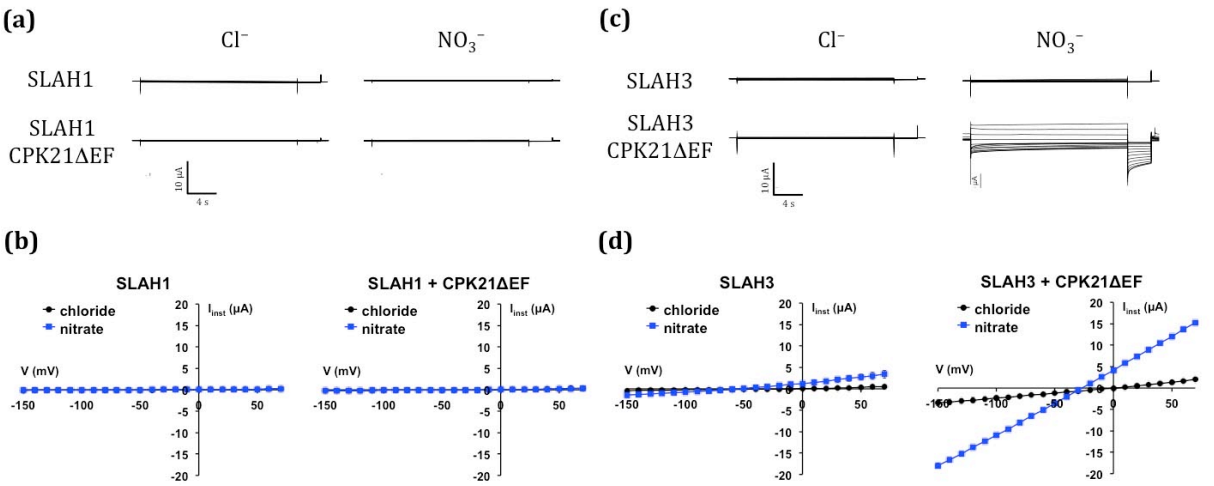

Figure 4.19. SLAH1 remains electrically silent after co-expression with CPK21 in chloride and nitrate buffers. (a) Whole-oocyte currents of *Xenopus* oocytes expressing SLAH1 alone or together with CPK21ΔEF in the presence of 30 mM chloride (Cl^-) or nitrate (NO_3^-) (representative cells are shown). **(b)** Instantaneous currents (I_{inst}) of oocytes co-expressing SLAH1 in the absence or presence of CPK21ΔEF in standard buffers containing either 100 mM Cl^- or NO_3^-. **(c)** Whole-oocyte currents of oocytes expressing SLAH3 alone or with CPK21ΔEF in the presence of 30 mM Cl^- or NO_3^- (representative cells are shown). **(d)** I_{inst} of *Xenopus* oocytes co-expressing SLAH3 in the absence or presence of CPK21ΔEF in standard buffers containing either 100 mM Cl^- or NO_3^-. Ca^{2+}-independent truncated kinase of CPK21 (CPK21ΔEF) was used ($n \geq 3$; mean ± SE).

Chen and colleagues (2010) crystallized the bacterial homologue of SLAC1 from *Haemophilus influenza* (HiTehA) and found a central conserved phenylalanine (Phe) residue (F450) in the pore region of SLAC1 linked to the anion gate. Replacement of this pore residue by alanine (Ala) turned *At*SLAC1 into a constitutively open anion channel, even in the absence of an activating kinase. This residue is conserved in the entire SLAC/SLAH protein family (Chen *et al*., 2010; Dreyer *et al*., 2012) and the mutation of this Phe in the *Arabidopsis* SLAC1-homolog SLAH2 by replacing this residue by alanine (F402A) also led to an anion conducting state (Maierhofer *et al*., 2014b). Furthermore it has been recently shown that this open-gate mutation shifts kinase-insensitive *Arabidopsis* SLAC1-homologues from alga and liverwort (Lind *et al*., 2015) into active channels.

Based on multiple alignments of amino acid sequences (section 3.2.9) and homology models of *At*SLAH1 and *At*SLAH3 to the crystal structure of HiTehA (Chen *et al.*, 2010), the corresponding Phe residues were identified at the transmembrane (TM) domain 9 (Fig. 4.20).

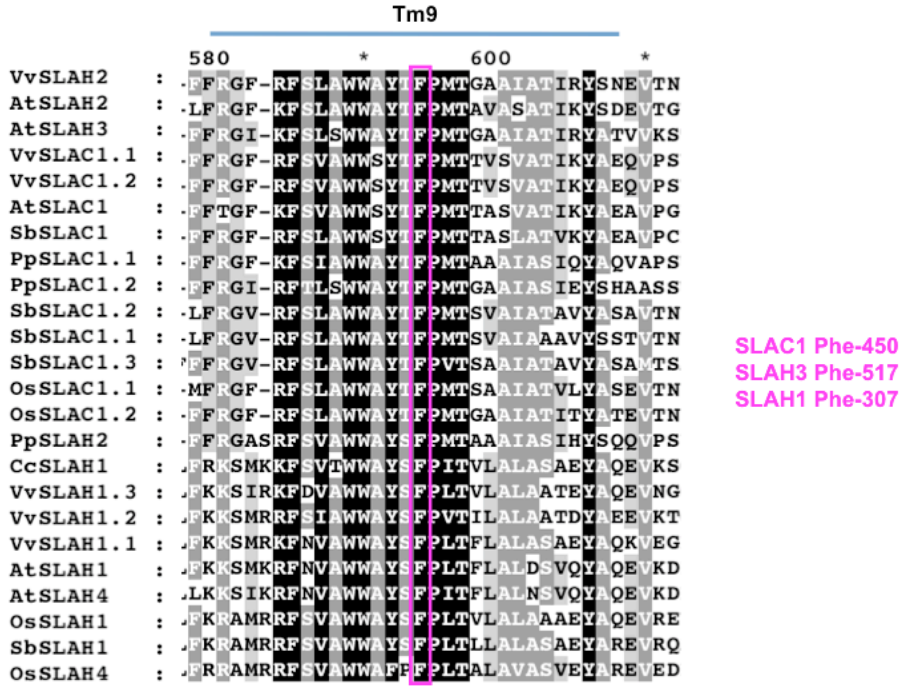

Figure 4.20. Sequence alignment of SLAC/SLAH proteins from different species. Shading levels indicate degree of conservation (black, denotes very high conservation; dark grey, medium-high conservation, light grey, moderate conservation; and white, no conservation). Tm9, Transmembrane domain 9. Phe, Phenyalanine. At, *Arabidopsis thaliana*; Cc, *Citrus clementina*; Os, *Oryza sativa*; Pp, *Physcomitrella patens*; Sb, *Solanum bicolor*; Vv: *Vitis vinivera*.

The Phe residues were mutated to Ala in SLAH1 (F307A) and SLAH3 (F517A) to obtain deregulated open channels. After their expression in *Xenopus* oocytes it could be observed through TEVC recordings that while SLAH3 F517A mutant led to an open conducting state, the SLAH1 F307A anion channel remained electrically silent (Fig. 4.21).

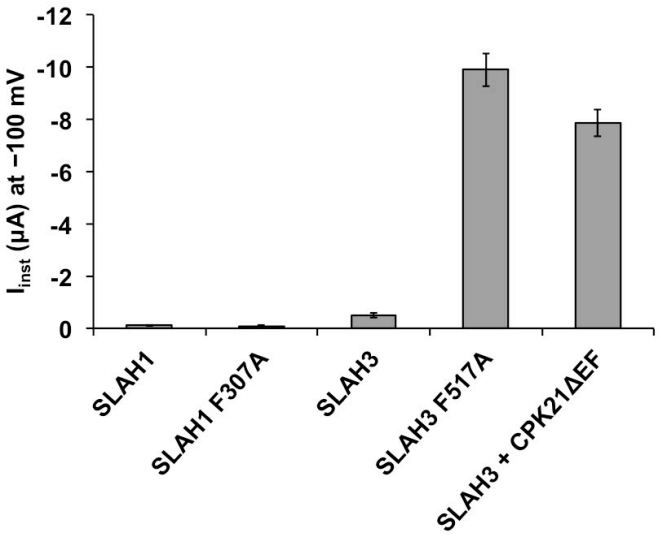

Figure 4.21. SLAH1 F307A mutant remains as a silent channel. Instantaneous currents (I_{inst}) recorded at −100 mV of *Xenopus* oocytes expressing the "gating mutants" SLAH1 F307A or SLAH3 F517A in comparison to WT SLAH1 and WT SLAH3 ± CPK21ΔEF in 100 mM nitrate buffer (n ≥ 4 experiments; mean ± SE).

4.1.1.7. SLAH1 and SLAH3 form heteromeric anion channels

Given that the three-dimensional (3D) homology model of HiTehA revealed a trimeric structure with three subunits, each forming an individual pore (section 1.5.1.2.3; Chen *et al.*, 2010), the physical interaction within SLAH1 homomeric channel complexes, as well as in SLAH3, was verified through BiFC technique after co-expressing the anion channel subunit fused to the C-terminal half of the YFP (YFP^{CT}) or to the N-Terminal half of YFP (YFP^{NT}) in *Xenopus* oocytes. A strong interaction between individual SLAH1 subunits, as well as between individual SLAH3 subunits, was observed (Fig. 4.22).

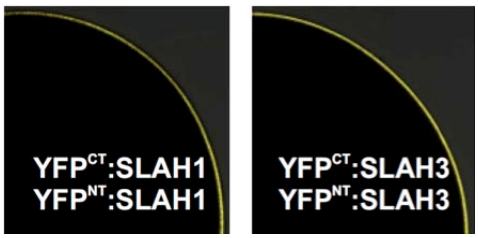

Figure 4.22. Physical interaction between S-type monomers revealed by BiFC experiments. SLAC/SLAH subunits are able to assemble, leading to homomeric channel complexes. The C-terminal (YFP^{CT}) or N-terminal (YFP^{NT}) half of YFP was fused to the N-terminus of SLAH1 or SLAH3. Representative images of one-quarter of *Xenopus* oocytes are shown.

Similar to the situation with the Shaker K^+ channel subunits AKT1 and ATKC1, which are expressed in the same root cells in *A. thaliana* and form heteromeric complexes (Geiger *et al.*, 2009a; Jeanguenin *et al.*, 2011), the S-Type anion channel subunits SLAH3 and SLAH1 co-express in the same cell type. To test whether SLAC/SLAH subunits also assemble to heteromeric anion channels and whether SLAH1 might function as a channel modulator rather than an autonomous S-type anion channel, SLAH1 was co-expressed together with its *Arabidopsis* homologues in *Xenopus* oocytes.

Using BiFC constructs with one half of YFP fused to the N-terminus of SLAH1 and the other half fused to the N-terminus to each of the other SLAC/SLAH family members, YFP fluorescence signals pointed to an interaction between all tested S-type anion channel subunits (Fig. 4.23), indicating that SLAC/SLAH subunits are able to assemble heteromeric channel complexes.

Figure 4.23. Physical interaction of SLAH1 with SLAC/SLAH Family members. BiFC experiments revealed that SLAC/SLAH subunits are able to assemble, leading to heteromeric channel complexes. The C-terminal (YFP^{CT}) or N-terminal (YFP^{NT}) half of YFP was fused to the N-terminus of SLAC1, SLAH1, SLAH2, SLAH3 or SLAH4. Representative images of one-quarter of *Xenopus* oocytes are shown.

4.1.1.7.1. SLAH1 substitutes for kinase- and nitrate- dependent activation of SLAH3

Given that BIFC images showed that SLAC/SLAH subunits could constitute heteromeric channels with SLAH1, each member of the *Arabidopsis* SLAC/SLAH anion channel family was co-expressed with SLAH1 in *Xenopus* oocytes to further explore their putative functional interaction. TEVC recordings revealed that only the interaction between SLAH1 and SLAH3 dramatically changed the electrical current characteristics (Fig. 4.24 a), since macroscopic currents could be measured in the absence of an activating kinase with similar amplitudes as those recorded with kinase-activated SLAH3 (e.g. with CPK21ΔEF, Fig. 4.24 b) and without the need of NO_3^- in the bath solution (Fig. 4.24 b-c). In contrast, co-expression of SLAH1 with SLAC1, SLAH2 or SLAH4 did not result in macroscopic anion currents (Fig. 4.24 a) compared with the activation of the channels SLAC1, and SLAH2, by CPK21ΔEF (Fig. 4.24 b).

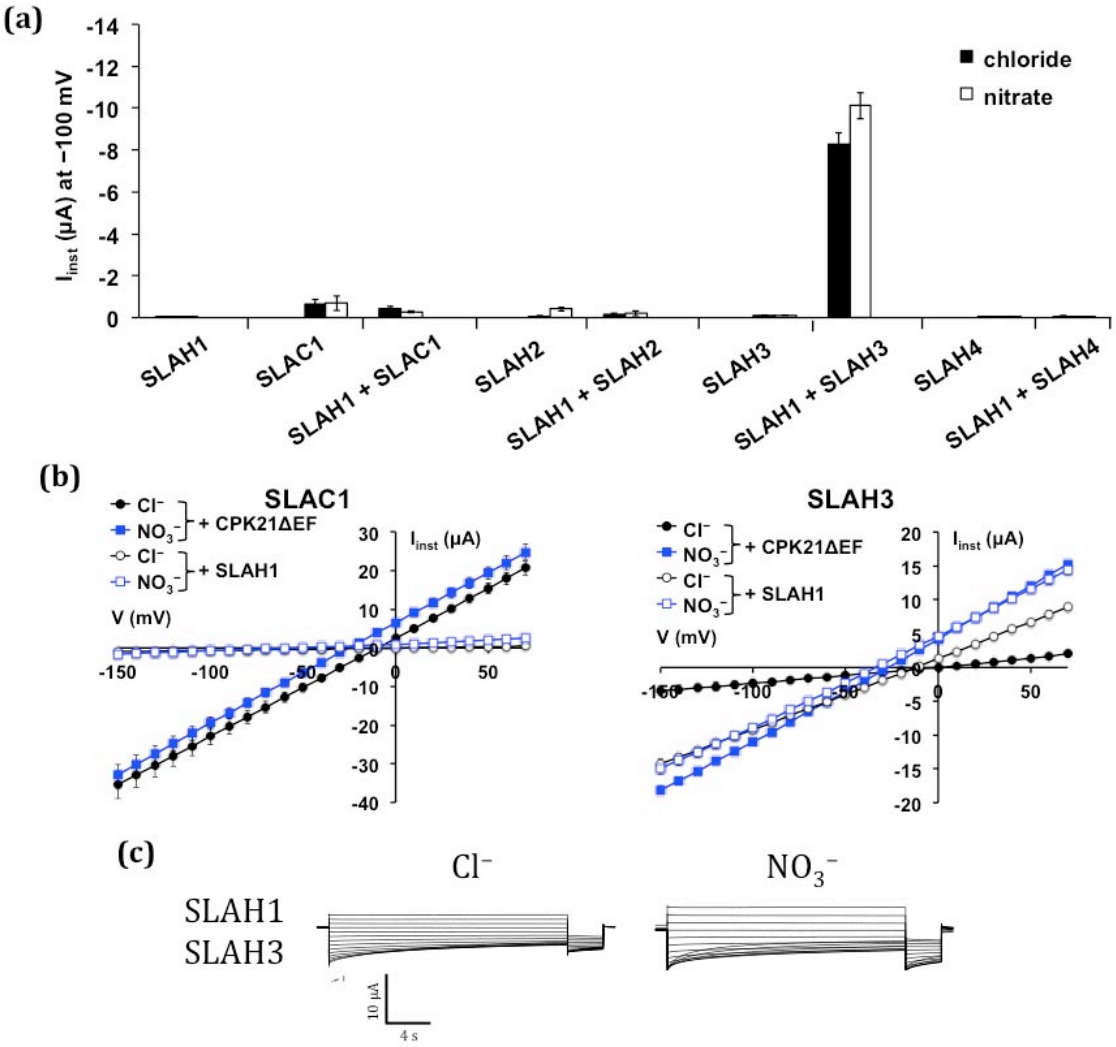

Figure 4.24. Influence of SLAH1 on the activity of S-type anion channels. (a) Instantaneous currents (I_{inst}) of *Xenopus* oocytes co-expressing SLAH1 with other SLAC/SLAH channels recorded at −100 mV in the presence of either 100 mM chloride or 100 mM nitrate (n ≥ 3; mean ± SE). **(b)** Instantaneous currents (I_{inst}) of oocytes expressing SLAC1 or SLAH3 in the presence of SLAH1 or CPK21ΔEF in standard buffers containing 100 mM chloride (Cl^-) or 100 mM nitrate (NO_3^-). Currents are plotted against the applied voltage (n ≥ 3; mean ± SE). **(c)** Whole-oocyte currents of *Xenopus* oocytes expressing SLAH1 with SLAH3 in the presence of 30 mM chloride or nitrate (representative cells are shown).

Oocytes expressing SLAH1/SLAH3 with different Ca^{2+}-independent SnRK2 kinases (SnRK2.2 and SnRK2.3) were recorded by TEVC technique but, in the same way as NO_3^- did not change the current amplitude associated with constitutively active SLAH1/SLAH3 heteromeric complexes (Fig. 4.24 b-c), co-expression of SLAH1/SLAH3 with these kinases did not further increase the amplitude (Fig. 4.25), suggesting that the channels complex was already fully active.

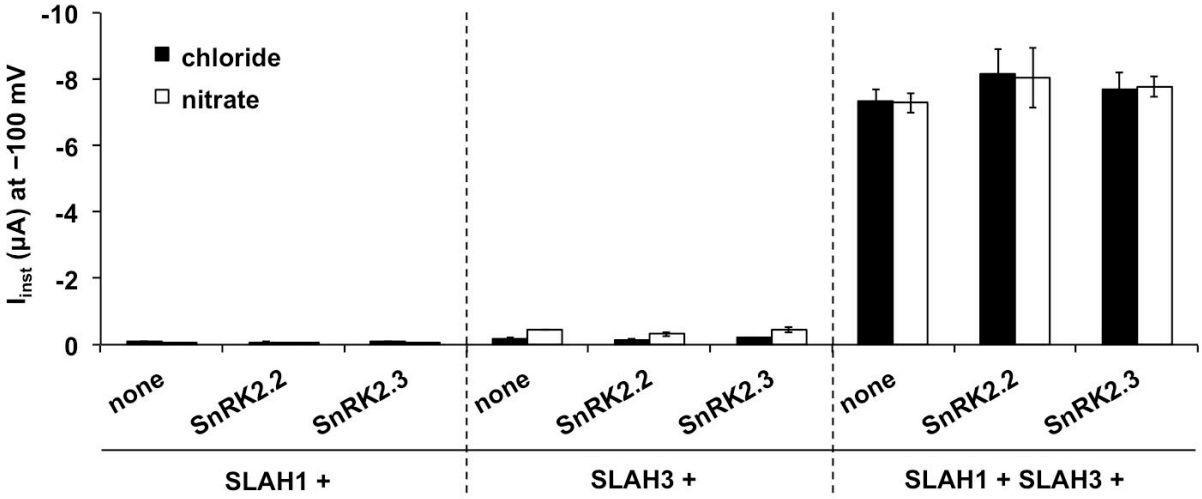

Figure 4.25. SLAH1 substitutes for kinase- and nitrate- dependent activation of SLAH3. Instantaneous currents (I_{inst}) of *Xenopus* oocytes expressing SLAH1/SLAH3 with SnRK2.2 and Snrk2.3 kinases recorded at −100 mV in the presence of either 100 mM chloride or 100 mM nitrate show SLAH1/SLAH3 heteromer is kinase-independent (n ≥ 3; mean ± SE).

The fact that the co-expression of SLAH1 with SLAC1, SLAH2 or SLAH4 did not result in macroscopic anion currents in the absence of an activating kinase indicates that SLAH1-SLAH3 interaction and activation is S-type channel subunit specific.

4.1.1.7.2. SLAH1 is a modulatory subunit

The observed kinase-independent activity of the heteromeric channel complex SLAH1/SLAH3, as well as the NO_3^--independent activation, could be the consequence of the addition of a SLAH1-intrinsic-chloride conductance superimposing on the NO_3^-/Cl^- conductance of SLAH3 or alternatively SLAH1 might represent a silent subunit that modulates the properties of SLAH3. To test the contribution of each interaction partner to the observed anion currents, inactive channel mutants of SLAH3 and SLAH1 were originated.

The 3D homology model of SLAC1 predicted that the substitution of the central conserved Phe residue (F450) in the pore region by leucine (F450L), as well as the exchange of the glycine (Gly) residue G194 present in the transmembrane domain 1 (Fig. 4.26) to a negatively charged aspartate (Asp), would block the pore. Indeed, it has been shown in *At*SLAC1 that the point mutations F450L and G194D lead to a non-functional channel (Chen *et al*., 2010; Negi *et al*. 2008).

Based on multiple alignments of amino acid sequences (section 3.2.9) and on homology models of SLAH1 and SLAH3, the respective mutants in *At*SLAH1 (F307L and R47D; Fig. 4.26) and *At*SLAH3 (F517L and G264D; Fig. 4.26) were generated.

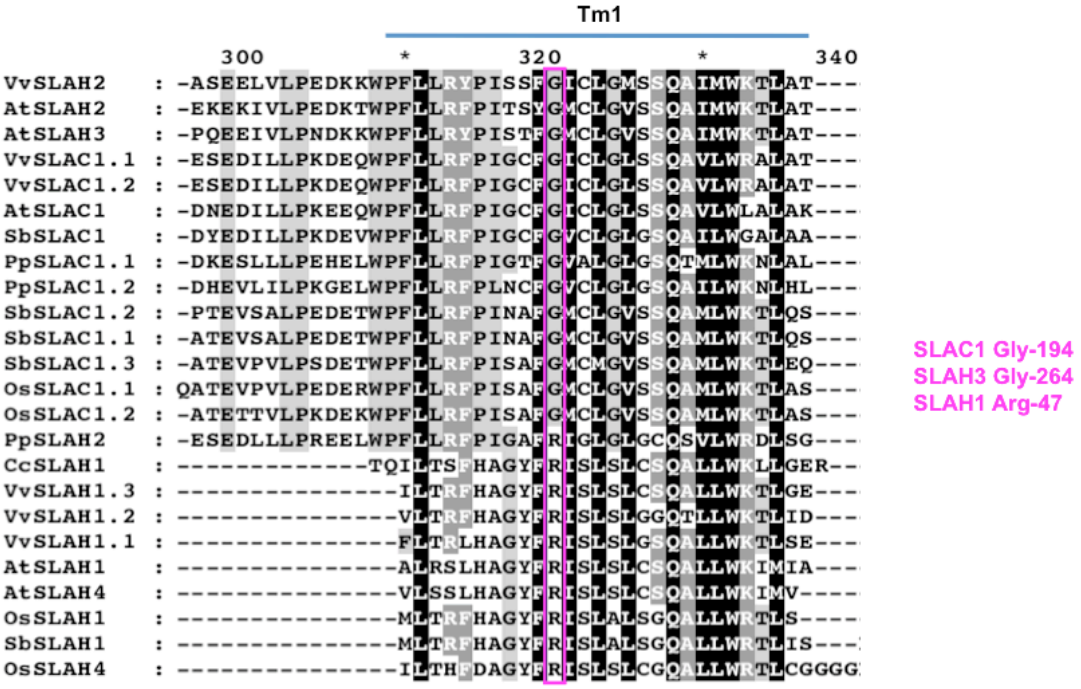

Figure 4.26. Sequence alignment of SLAC/SLAH proteins from different species. Shading levels indicate degree of conservation (black, denotes very high conservation; dark grey, medium-high conservation, light grey, moderate conservation; and white, no conservation). Tm1, Transmembrane domain 1. Arg, Arginine; Gly, Glycine. At, *Arabidopsis thaliana*; Cc, *Citrus clementina*; Os, *Oryza sativa*; Pp, *Physcomitrella patens*; Sb, *Solanum bicolor*; Vv: *Vitis vinivera*.

Using the pore-blocking mutants, TEVC recordings were performed after their expression in *Xenopus* oocytes. Neither the co-expression with CPK21ΔEF nor co-expression with SLAH1 could elicit macroscopic currents in SLAH3 F517L and G264D (Fig. 4.27). In contrast, the mutations at the equivalent positions in SLAH1 (SLAH1 F307L and R47D) did no significantly affect the anion currents mediated by the SLAH1/SLAH3 channel complex when they were co-expressed with SLAH3 (Fig. 4.27).

The background currents of the SLAH3 F517L mutant, when co-expressed with CPK21ΔEF, SLAH1 WT, or SLAH1 mutants (Fig. 4.27), result from the residual activity of the SLAH3 mutant rather than from a conductivity of SLAH1.

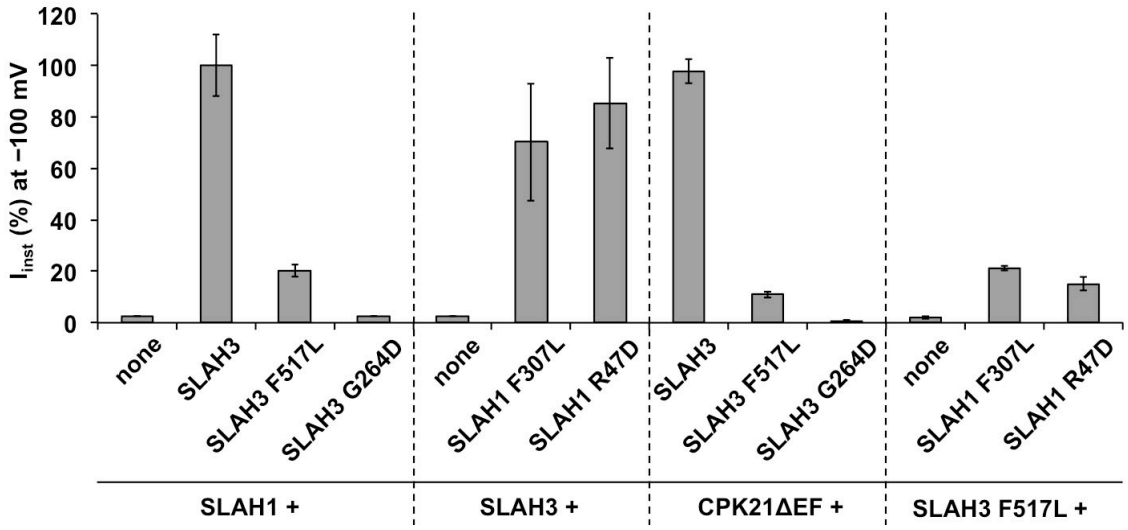

Figure 4.27. SLAH1 modifies the activation properties of SLAH3. Instantaneous currents (I_{inst}) recorded at −100 mV in *Xenopus* oocytes expressing different combinations of SLAH1 WT or mutants and SLAH3 WT or mutants as indicated in the figure in 100 mM nitrate buffer solution (n ≥ 3; mean ± SE).

To exclude the possibility that the loss in anion conductance with the SLAH3 G264D or F517L mutants was due to a reduction in the channel abundance, YFP was fused to the N-terminus of either SLAH3 WT or mutants and they were expressed in oocytes. BiFC analysis revealed that the fluorescence signals associated with the *Xenopus* oocyte expression of these constructs had similar intensity and plasma membrane localization (Fig. 4.28).

Figure 4.28. SLAH3 G264D or F517L mutants did not exhibited a decrease in channel abundance. BiFC experiments showed that the fluorescence signal associated with oocytes expressing SLAH3 G264D or F517L mutants was similar to that associated to SLAH3 WT.

The finding that non-functional channel mutants of SLAH3 did not elicit macroscopic currents when co-expressed with either CPK21ΔEF or SLAH1, while the equivalent mutants in SLAH1 did no significantly modify the anion currents mediated by the SLAH1/SLAH3 channel complex, in combination with the fact that the replacement of the conserved Phe residue by Ala in SLAH1 (F307A) to obtain a constitutively open anion channel did not elicited macroscopic currents, indicate that rather than adding a separate anion conductance to the conductance of SLAH3, SLAH1 modifies the electrical properties of SLAH3, making it independent of kinase and NO_3^- activation.

4.1.1.7.3. The SLAH1/SLAH3 heteromeric complex exhibits higher Cl^- conductance than the SLAH3 homomer

Since the chloride currents of the SLAH1/SLAH3 heteromeric complex were markedly increased compared to the currents of SLAH3 activated by CPK21 (Fig. 4.24 b), the relative permeability to nitrate (P_j/P_{NO3^-}) of this complex was calculated for Cl^- after the co-expression of both channels in oocytes. Nevertheless, it could be observed that the permeability for Cl^- relative to NO_3^- (P_{Cl^-}/P_{NO3^-}) of the SLAH1/SLAH3 heteromer was unaltered with respect to the SLAH3 homomer (Fig. 4.29).

Based on the homology model of SLAH2 and SLAC1, the exchange of the polar serine (Ser) at position 228 in SLAH2 to a nonpolar valine (Val), the amino acid in SLAC1 at the respective position, turned the nitrate-selective SLAH2 into a chloride/nitrate-permeable anion channel (Maierhofer *et al*., 2014b). Taken this finding into account to further explore the selectivity of the SLAH1/SLAH3 heteromer, the corresponding Ser residue in SLAH1 was substituted to the nonpolar Val (S130V) according to multiple alignments of amino acid sequences (Fig. 4.29; section 3.2.9) and on homology models.

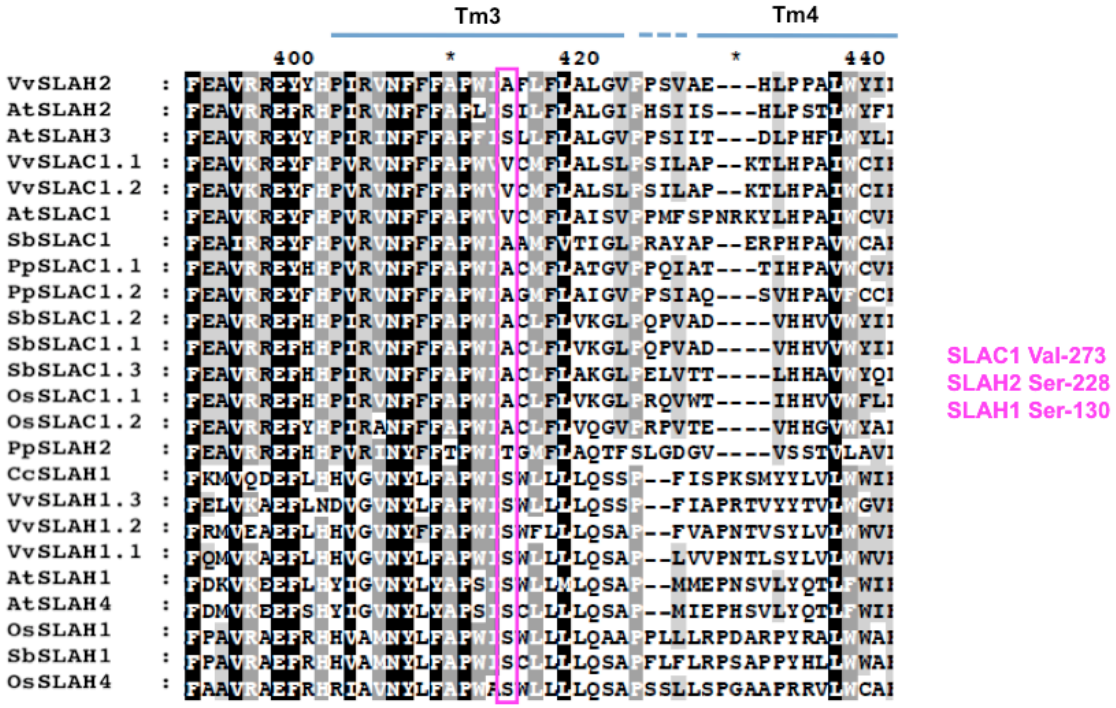

Figure 4.29. Sequence alignment of SLAC/SLAH proteins from different species. Shading levels indicate degree of conservation (black, denotes very high conservation; dark grey, medium-high conservation, light grey, moderate conservation; and white, no conservation). Tm3, Transmembrane domain 3. Ser, Serine; Val, Valine. At, *Arabidopsis thaliana*; Cc, *Citrus clementina*; Os, *Oryza sativa*; Pp, *Physcomitrella patens*; Sb, *Solanum bicolor*; Vv: *Vitis vinivera*.

The relative permeability of SLAH3 co-expressed with this SLAH1 mutant was then checked in oocytes. However the substitution of the Ser 130 residue in SLAH1 to Val (S130V) did not modify the anion selectivity of the SLAH1/SLAH3 channel complex (Fig. 4.30).

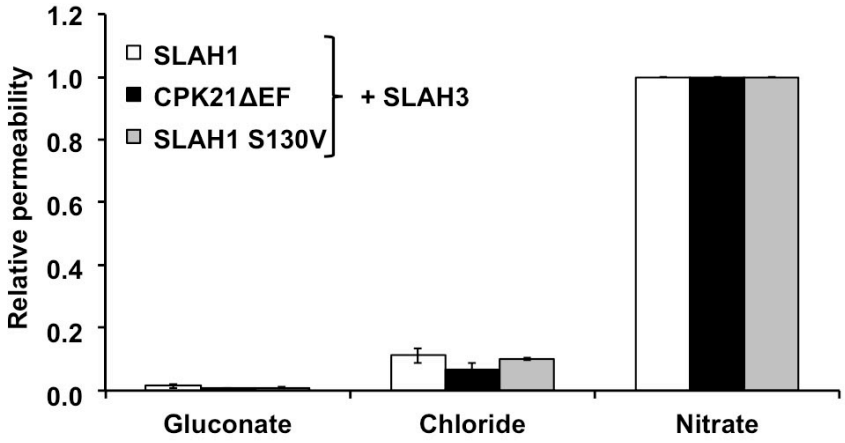

Figure 4.30. SLAH1/SLAH3 and SLAH3 channels share the same relative permeability for chloride. Relative permeability of SLAH3 co-expressed with SLAH1, CPK21ΔEF or SLAH1 S130V mutant in *Xenopus* oocytes (permeability for nitrate was set to 1). Standard bath solution contained 50 mM of the respective anion (n ≥ 4; mean ± SE).

The finding that the relative permeability for Cl^- obtained in SLAH3 (co-expressed with CPK21) remained unchanged compared with its co-expression with SLAH1 indicates that the elevated Cl^- currents mediated by the SLAH1/SLAH3 heteromeric complex result from the NO_3^--independent activation of SLAH3 rather than from an increased Cl^- permeability. To elucidate

this assumption the chord conductance for Cl^- in SLAH3 homomer and SLAH1/SLAH3 heteromer was obtained. It could be observed that while the NO_3^- conductance did not change between oocytes expressing SLAH1/SLAH3 and SLAH3 with CPK21, the conductance for Cl^- was seven times higher in oocytes expressing SLAH1/SLAH3 compared with the kinase-activated SLAH3 channels (Fig. 4.31).

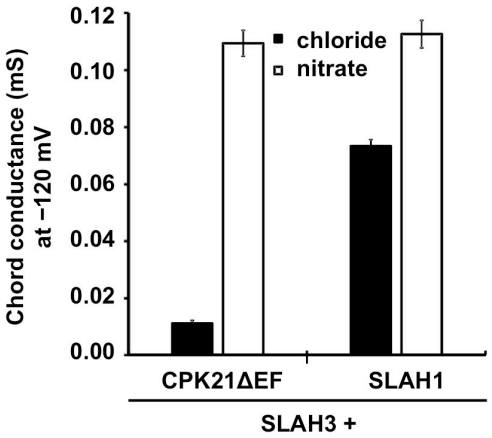

Figure 4.31. SLAH1/SLAH3 channels have a higher chloride conductance than the kinase-dependent SLAH3 channels. Chord conductance of *Xenopus* oocytes co-expressing SLAH3 together with either CPK21ΔEF or SLAH1. Standard bath solution contained 100 mM chloride or nitrate (n ≥ 4 experiments; mean ± SE).

To investigate the molecular mechanism underlying the enhanced Cl^- current amplitudes of the SLAH1/SLAH3 heteromeric complex, the NO_3^--dependent gating properties of the kinase-activated SLAH3 homomeric channel compared to the SLAH1/SLAH3 heteromer were analysed. On the one side, the relative open probability (rel. P_O) of oocytes co-expressing SLAH3 and CPK21ΔEF exposed to varying Cl^- concentrations shifted to more negative membrane potentials with increasing Cl^- concentrations. However, even with 30 mM Cl^- in the external buffer, the half-maximal ($V_{½}$) open probability did not reach the physiological membrane potential range (Fig. 4.32; between –80 and –200 mV [Fromm and Lautner, 2007]). In contrast, with 30 mM of external NO_3^- the rel. P_O of SLAH3 markedly shifted to hyperpolarized (physiological) membrane potentials (Fig. 4.32). On the other side, the rel. Po of SLAH1/SLAH3 channel complexes appeared independent from the external anion composition (Fig. 4.32), indicating that interaction of SLAH1 with SLAH3 already gated SLAH3 open without the need of NO_3^-.

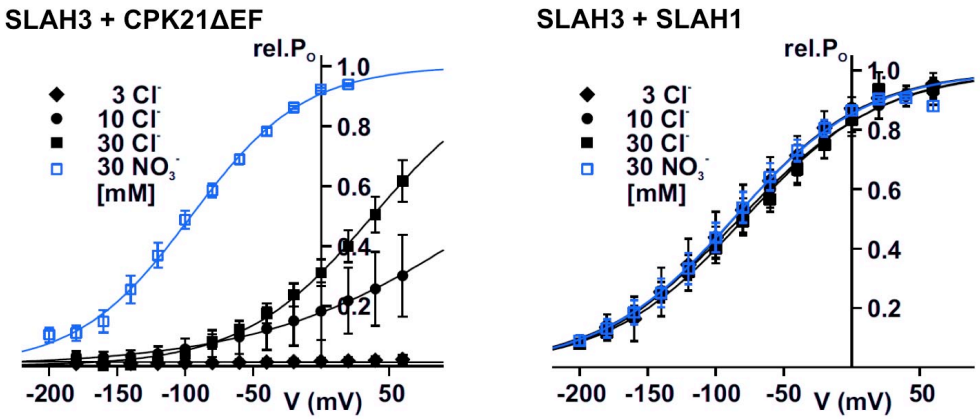

Figure 4.32. SLAH1 gates SLAH3 open without the need of nitrate. Relative voltage-dependent open probabilities (rel. Po) derived from oocytes co-expressing SLAH3 with either CPK21ΔEF or SLAH1 in the

presence of 3, 10, 30 mM chloride (Cl^-; black) or 30 mM nitrate (NO_3^-; blue). Data points were fitted by a Boltzmann equation (continuous line) (n ≥ 4 experiments; mean ± SE).

Therefore, CPK21-activated SLAH3 required extracellular NO_3^- to gate open at physiological membrane potentials (Fig. 4.32), whereas the SLAH1/SLAH3 heteromeric complex appeared to be open in the absence of NO_3^- (Fig. 4.32). Thus, it became obvious that the elevated Cl^- currents of the SLAH1/SLAH3 channel (Fig. 4.24 b-c) result from the NO_3^--independent activation of SLAH3 and thus from a massive increase of its Cl^- conductance (Fig. 4.31), rather than from an increased Cl^- permeability (Fig. 4.30).

Functional expression of *AtSLAH1* in *Xenopus* oocytes and electrophysiological recordings strongly suggested that, rather than mediating Cl^- transport itself, SLAH1 protein modifies the kinetic and regulatory properties of SLAH3 through formation of heteromeric SLAH1/SLAH3 channels.

4.1.2. *At*SLAH1 function in the shoot

4.1.2.1. *AtSLAH1* and *AtSLAH3* are co-expressed within flower organs

Histochemical analysis of GUS activity (section 3.9.1) in P_{SLAH1}-GFP::GUS transgenic plants showed that the *AtSLAH1* promoter was expressed in flower organs like the anther filament and at the stigmatic papillae cells (Fig. 4.33), indicating a putative role of SLAH1 in flower and reproductive development.

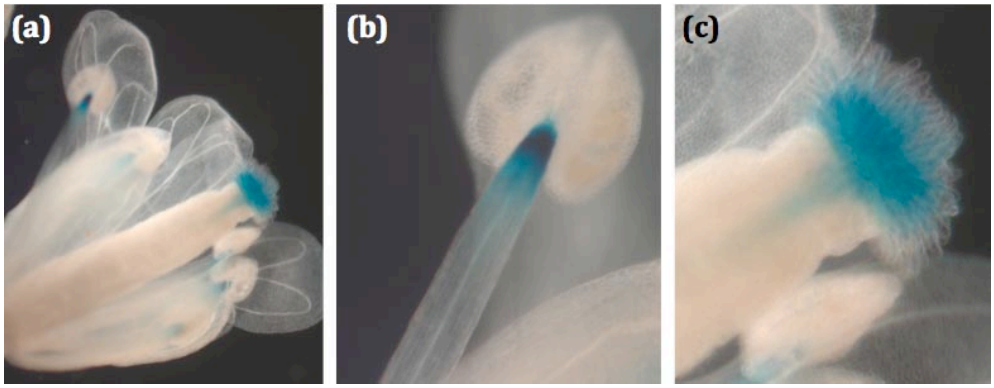

Figure 4.33. *AtSLAH1* is expressed at the flower. **(a)** Histochemical localization of GUS activity in P_{SLAH1}-GFP::GUS transgenic plants at the flower. **(b)** *AtSLAH1* gene expression at the filament insertion. **(c)** *AtSLAH1* gene was expressed at the stigmatic papillae cells in the flower.

GUS activity in transgenic plants expressing P_{SLAH3}:GUS was localized at guard cells in leaves (Fig. 4.34 a), supporting previously published studies (Geiger *et al*., 2011; Zheng *et al*., 2015). In addition, the expression of *AtSLAH3* promoter was also located in other aerial organs such as leaf trichomes (Fig. 4.34 b). *AtSLAH3* expression was also observed in the stigma (Fig. 4.34 c), similarly to *AtSLAH1*, and in the in the valves margins in the carpel (Fig. 4.34 d). Moreover, P_{SLAH3}:GUS transgenic plants showed GUS staining in the stamens, as it has been reported (Fig. 1.15; Gutermuth *et al.*, 2013).

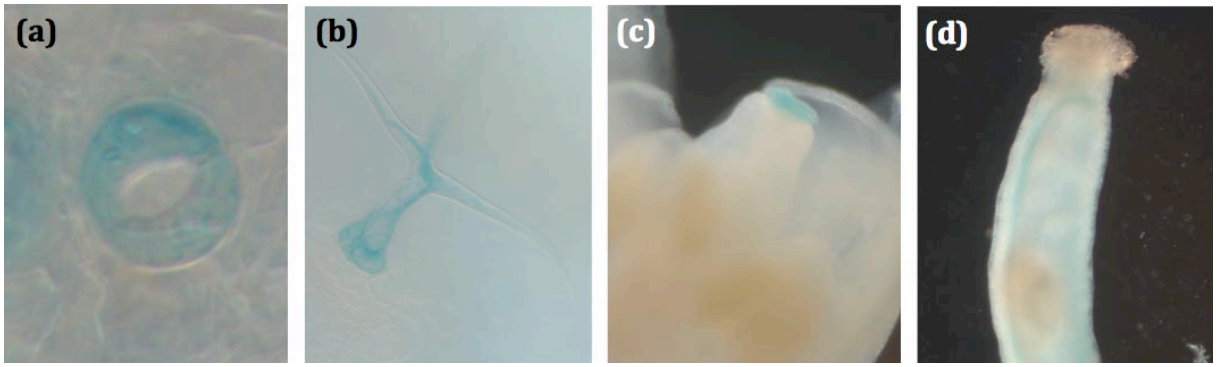

Figure 4.34. *AtSLAH3* expression within the shoot. **(a)** Histochemical localization of GUS activity at guard cells in leaves in P_{SLAH3}:GUS transgenic plants. **(b)** Trichome localization of GUS activity. **(c)** *AtSLAH3* promoter expression at the stigmatic papillae cells in the flower. **(d)** *AtSLAH3* was expressed in the valves margins in the carpel.

4.1.2.2. Loss of *AtSLAH1* leads to lower seeds production

Given the participation of SLAH1 in regulating Cl^- transport through increasing plasma membrane Cl^- conductance, promoter activity of *AtSLAH1* and *AtSLAH3* genes might indicate a role of SLAH1 and SLAH3 channels in providing anions to sexual organs. Rapid mobilization of electrolytes, mediated by ion transporters, and water, is a physiological mechanism that is expected to occur in fast-growing sexual organs during flower dehiscence, a mechanism that precedes fertility competence. To test the possible participation of SLAH1 in flower fertility, seed production was quantified in the *AtSLAH1* gene mutant line, *slah1-2*, and its wild-type (WT) line.

Plants were grown with 5 mM Cl^- in pots under short photoperiod conditions (section 3.1.2.2.2) and seed production, calculated as the seed harvest index (HI; section 3.8.1) of plants was obtained after collecting mature seeds. The harvest index defines the biomass ratio of the dried seeds to the total dry biomass of the aerial organs of the plant, and serves as indicator of resource allocation toward harvestable organs (Kronberg *et al.*, 2007).

It could be observed that the harvest index of *slah1-2* KO mutant line was significantly reduced in relation to the WT line (Fig. 4.35 a), while the shoot biomass was similar between *slah1-2* and WT lines (Fig. 4.35 b). Therefore, *slah1-2* mutant plants produced significantly fewer total seeds than WT plants (Fig. 4.35c).

There was no difference in the dry weight per seed between both lines (Fig. 4.35 d), although the total number of seeds produced per plant was significantly lower in the *slah1-2* line in relation to the WT line (Fig. 4.35 e).

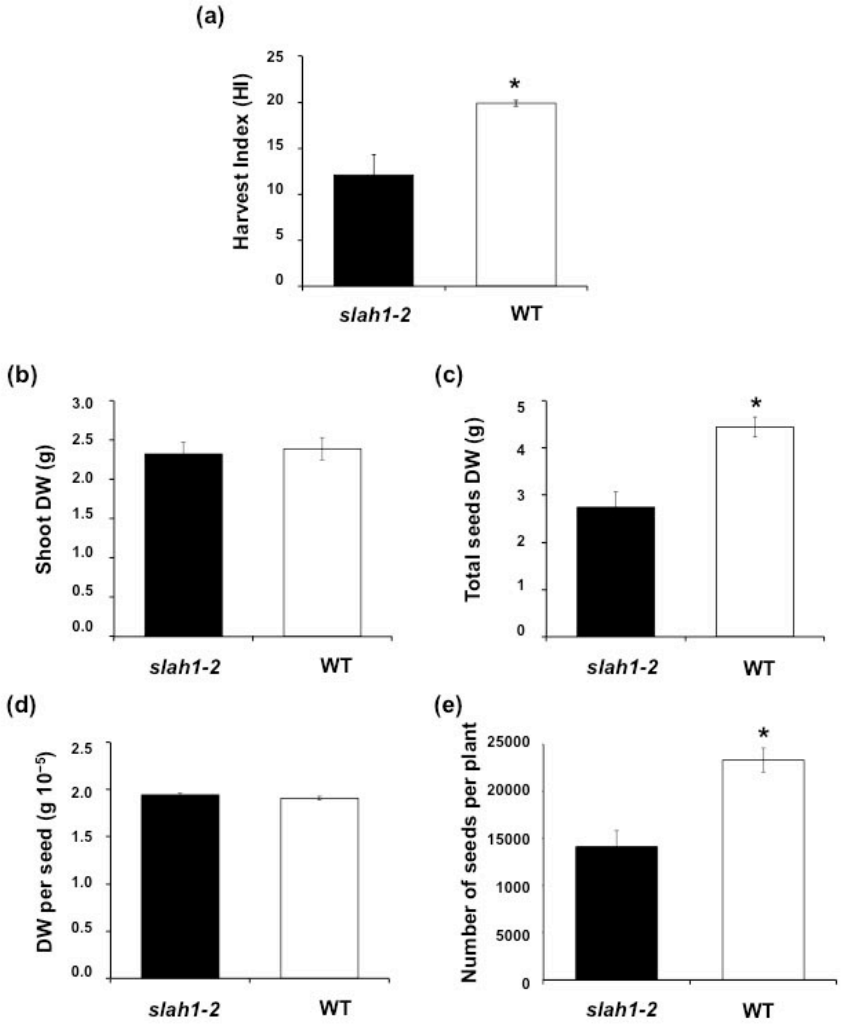

Figure 4.35. Seeds production was significantly lower in *slah1-2* line relative to the wild-type (WT) line. Plants were grown in pots and watered with a nutrient solution containing 5 mM chloride (Cl^-) and they were harvested at late-senescence stage. **(a)** Harvest index (HI) of *slah1-2* mutant and WT plants. **(b)** Shoot dry weight (DW) of *slah1-2* mutant and WT plants. **(c)** Dry weight (DW) of total seeds produced by *slah1-2* mutant and WT plants. **(d)** Dry weight (DW) per seed of *slah1-2* mutant and WT plants. **(e)** Number of seeds produced per plant in *slah1-2* mutant and WT lines. Asterisks indicate statistically significant differences (one-way ANOVA, $*P < 0.05$, $n \geq 3$).

4.2. SLAH4 CHARACTERIZATION

In *Arabidopsis thaliana*, *AtSLAH4* is the closet homologue of *AtSLAH1* in the SLAC/SLAH gene family (Fig. 1.14). In this family of S-type anion channels, SLAH4 remains uncharacterized. *AtSLAH4* gene promoter have been suggested to be expressed in the root, although its precisely localization has not been determined so far. In addition, the subcellular localization of the SLAH4 protein has not been confirmed yet and the physiological role of SLAH4 *in planta* remains unknown.

4.2.1. *At*SLAH4 expression pattern in *Arabidopsis thaliana*

Since the localization of the expression of a protein provides insights about its function, the *AtSLAH4* gene tissue- and cell-specific expression pattern has been characterized.

4.2.1.1. *AtSLAH4* is expressed in root epidermal and cortical cells

The expression of *AtSLAH4* has recently been identified within the root of *Arabidopsis thaliana*, apparently located in the vasculature (Zheng *et al.*, 2015). To verify the tissue- and cell-specific expression pattern of *AtSLAH4*, different transgenic lines of *A. thaliana* expressing the chimeric GFP::GUS gene fusion under the control of the *AtSLAH4* promoter were obtained (section 3.6). These P_{SLAH4}-GFP::GUS lines include a 2.91 kb DNA fragment, containing the promoter and the untranslated 5-UTR' region of the *AtSLAH4* gene (1.31 kb longer than the construction used by Zheng and colleagues [2015]).

Histochemical analysis of GUS activity (section 3.9.1) in eight independent P_{SLAH4}-GFP::GUS independent transgenic lines showed that *AtSLAH4* expression was apparently located throughout all root tissues (Fig. 4.36 a-c), excluding the root tips.

Taking advantage of the promoter-regulated GFP activity, confocal microscopy analysis detected *AtSLAH4* gene expression in the cortex and epidermal cells of the root (Fig. 4.36 d-e). In addition the *AtSLAH4* expression in these peripheral cell layers of the root was verified afterwards by cryostat sectioning of transgenic plants expressing GUS (Fig. 4.36 f; section 3.9.2).

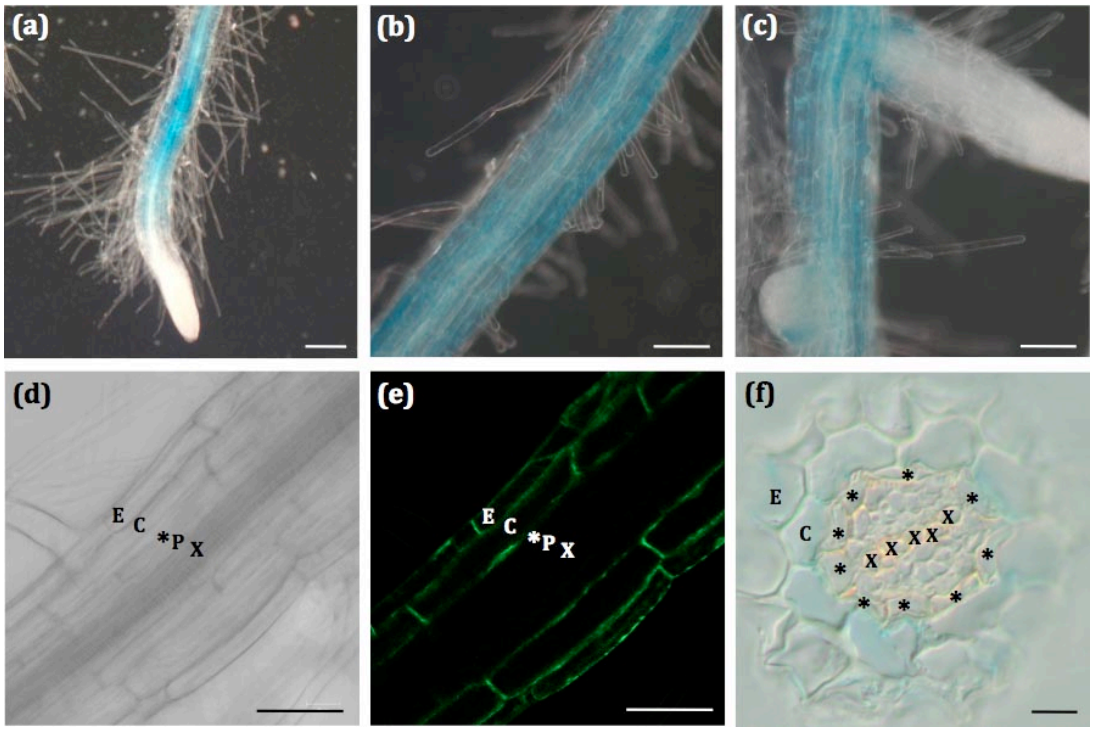

Figure 4.36. *AtSLAH4* is expressed in root cortecal and epidermal cells. Localization of GUS and GFP activity in the root of *Arabidopsis* transgenic lines expressing the P_{SLAH4}-GFP::GUS construction. **(a-c)** Histochemical localization of GUS activity. **(d)** Bright field **(e)** and GFP fluorescence images of root tissue. GFP fluorescence was localized in cortical and epidermal cells. **(f)** GUS staining in a transversal root section showing *AtSLAH4* expression in cortical and epidermal cell types. E: epidermis; C: cortex; asterisk: endodermis; red spot: protoxylem; blue spot: metaxylem. Scale bars, 200 µm (a), 100 µm (b, c), 50 µm (d, e), 10 µm (f).

AtSLAH4 expression in root cortical and epidermal cells suggests that this channel could play a role in the release of anions (e.g. NO_3^- and/or Cl^-) from peripheral cell layers to the apoplast or to the external soil medium, given that anion channels are passive transporters that normally mediate anion efflux.

4.2.1.2. *AtSLAH4* expression within the shoot

Histochemical analysis of GUS activity in shoots (section 3.9.1) using the same P_{SLAH4}-GFP::GUS transgenic lines showed that *AtSLAH4* expression was restricted to leaf hydathodes (Fig. 4.37 a-b) and leaf meristems(Fig. 4.37 c), which are organs associated with high primary auxin production.

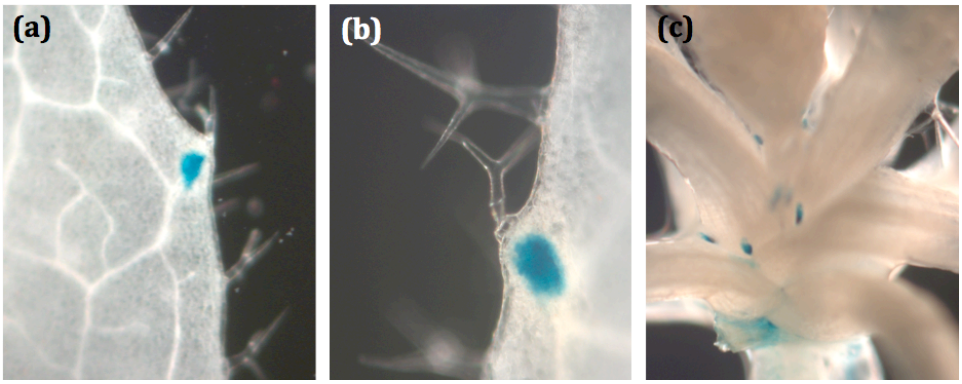

Figure 4.37. *AtSLAH4* is expressed in leaves. Localization of GUS activity in the shoot of *Arabidopsis* transgenic lines expressing the P_{SLAH4}-GFP::GUS construction. **(a,b)** Histochemical localization of GUS activity in leaf hydathodes. **(c)** Histochemical localization of GUS activity in leaf meristems of the rosette.

4.2.1.3. *AtSLAH4* root expression is delayed during seedling establishment in comparison to *AtSLAH1*

The *AtSLAH4* root expression kinetics during seedling development after germination was analysed using the P_{SLAH4}-GFP::GUS lines. With this aim, plants from the T_3 generation, that were homozygous for the t-DNA insertion, were grown in Petri dishes (section 3.1.2.2.1) and seedlings, harvested at different days after germination during two weeks, were tested for GUS histochemical activity (section 3.9.1). Simultaneously, root expression of the *AtSLAH1* gene from P_{SLAH1}-GFP::GUS plants were used as a control.

It could be observed that *AtSLAH1* expression was constitutively present in the root since very early stages of seedling development (3-day-old plants; Fig. 4.38). In contrast, *AtSLAH4* did not exhibit visible root expression activity during the first days of seedling establishment (Fig. 4.38 a). This developmental repression of *AtSLAH4* expression in the root during early developmental stages was specific, since *SLAH4* promoter activity was clearly visible in cotyledon hydathodes of 3-day-old plants (Fig. 4.38 a).

AtSLAH4 promoter activity progressively increased during plant development. It was hardly detected in the root of 5-day-old plants (Fig. 4.38 b), increased in 7-day-old plants (Fig. 4.38 c) and reached maximal expression in 12-day-old plants (Fig. 4.38 e).

Repression of SLAH4 activity during early stages of seedling development suggests the importance of adequate Cl^- homeostasis during early vegetative plant growth.

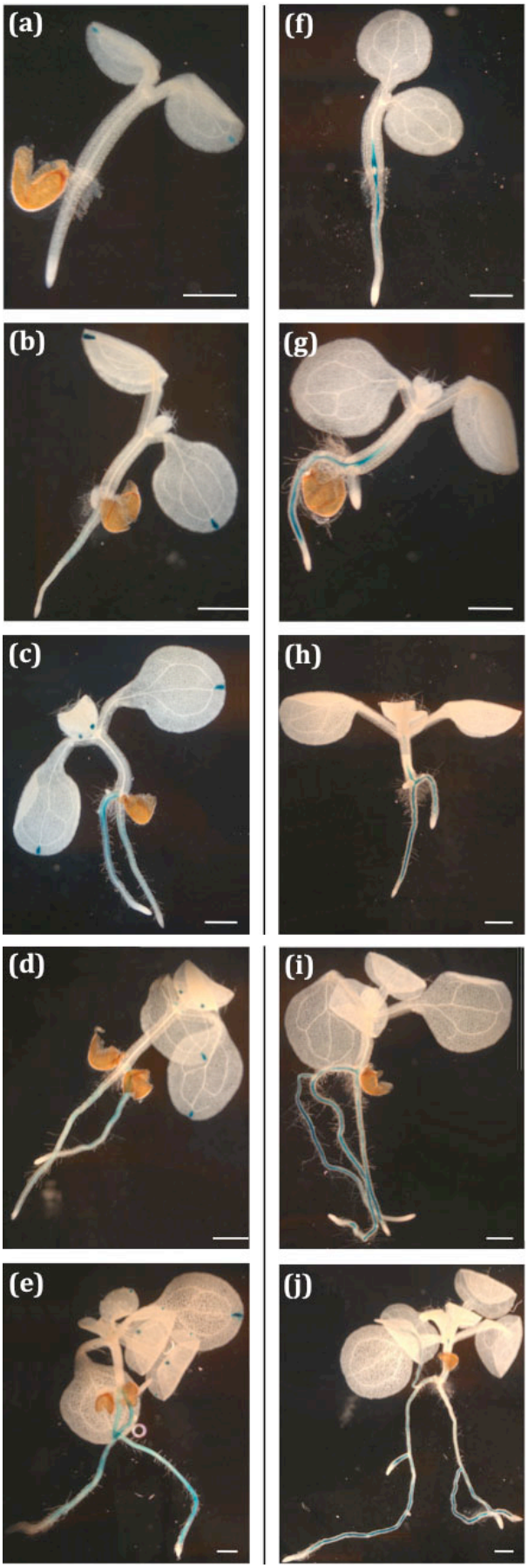

Figure 4.38. Expression of *AtSLAH4* and *AtSLAH1* in the root during seedling development. Histochemical localization of GUS activity in transgenic *Arabidopsis* plants expressing the GUS reporter gene under the regulation of *AtSLAH4* (a-e) and *SLAH1* (f-j) native promoter regions during seedling development (3 to 12 days after sowing, das). **(a)** *AtSLAH4* expression was not observed in 3-day-old seedlings. **(b)** *AtSLAH4* gene expression was weakly visible in 5-day-old seedlings. **(c)** GUS activity in P_{SLAH4}-GFP::GUS transgenic lines became stronger 7 das. **(d)** *AtSLAH4* expression pattern remained in the roots of 10-day-old seedlings. **(e)** GUS activity in P_{SLAH4}-GFP::GUS transgenic lines has maximal activity in 12-day-old seedlings. Permanent promoter activity on cotyledon and leaf hydathodes in P_{SLAH4}-GFP::GUS transgenic lines served as a control of adequate histochemical reactions along the experiment. **(f)** *AtSLAH1* expression was observed in the vascular cylinder of the root, but not in the apical meristems, and in the vascular cylinder at the bottom of the hypocotyl in 3-day-old seedlings. **(g)** *SLAH1*gene expression was also visible in the vascular cylinder of the root and the hypocotyl in 5-day-old seedlings. **(h)** GUS activity in P_{SLAH1}-GFP::GUS transgenic lines was detected in the vascular cylinder of the hypocotyl at the level of leaves emersion in 7-day-old seedlings. **(i)** *AtSLAH1* expression pattern remained unchanged in the roots 10 das. **(j)** GUS staining inP_{SLAH1}-GFP::GUS transgenic lines was also observed in the vascular cylinder of the roots in 12-day-old seedlings. Scale bars, 500 µm.

4.2.2. Identification of *AtSLAH4* T-DNA knockout line

Arabidopsis thaliana seeds from the *slah4-2* line (SALK_091937) were obtained from the Nottingham Arabidopsis Stock Centre (section 3.1.2.1) and the homozygous line was obtained through PCR genotyping (section 3.2.4.1) of the T_2 segregating population. Segregating plants were screened using primers suitable for the left border of the T-DNA and primers specific for the *AtSLAH4* gene flanking the position of the T-DNA insert (Fig. 4.39 a).

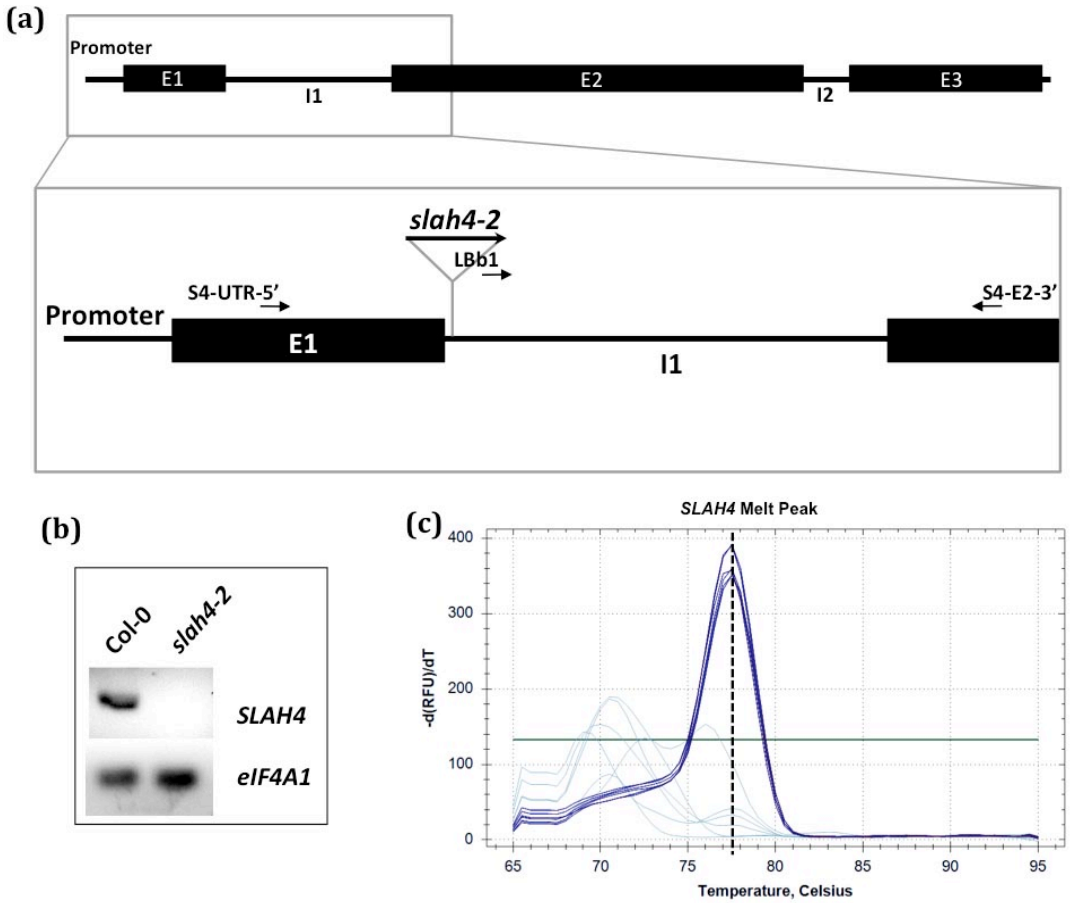

Figure 4.39. *slah4-2* line is a knockout line. (a) Gene structure of *AtSLAH4* and localization of the T-DNA insertion in the *slah4-2* line (SALK_091937). Closed boxes represent exons (E) and solid lines represent introns (I). PCR amplification primers used for genotyping and retro-transcription of total RNA are indicated with arrows. *slah4-2* T-DNA insertion mutant line mapped into the Intron-1 (I1). **(b)** *AtSLAH4* transcript determined by RT-PCR analysis of total RNA isolated from roots of wild-type (Col-0) and *slah4-2* plants. The housekeeping *eIF4A1* expression level was used as control of RNA loading. **(c)** Melting curve of the PCR product resulting from qPCR amplification of a coding fragment in Exon-3 of the *AtSLAH4* gene indicated the presence of the *AtSLAH4* transcript in WT plants (blue lines) and its absence in *slah4-2* plants (grey lines).

To verify whether the *slah4-2* line, homozygous for the T-DNA insertion, was a KO line, the integrity of its mRNA was determined. For this purpose, RNA was extracted (section 3.3.1) from roots of *slah4-2* and WT plants, retro-transcribed to cDNA (section 3.3.2) and amplified by RT-PCR (section 3.2.4.2).

In the *slah4-2* line, the T-DNA insertion mapped into the Intron-1 (I1) of the *AtSLAH4* 5' untranslated region (5'-UTR; Fig. 4.39 a). RT-PCR analysis of total RNA isolated from roots revealed that the T-DNA disrupted the 5'-UTR of the gene, since it could not be amplified through retro-transcription of total RNA (Fig. 4.39 b).

Since the T-DNA in the *slah4-2* line was inserted upstream of the predicted ATG start codon (Fig. 4.39 a), the *AtSLAH4* coding region was not disrupted. Therefore, the transcript level of *AtSLAH4* gene in both *slah4-2* and WT lines was tested by qPCR (section 3.2.4.3) using a pair of primers that amplified a fragment of the coding Exon-3 (E3; Table 3.17). As the melt peak of the *AtSLAH4* amplification fragment indicate (Fig. 4.39 c), no *AtSLAH4* transcript from the gene-coding region could be detected in the *slah4-2* line.

To determine the putative role of the *AtSLAH4* channel, the *slah4-2* KO mutant line was used for further studies.

4.2.3. Disruption of the *AtSLAH4* gene leads to higher chloride content and growth of shoot organs

To compare the development of the *slah4-2* KO line and the wild-type (Col-0) line, plants of both genotypes were grown in hydroponic culture (section 3.1.2.2.3) and in pots (section 3.1.2.2.2) under long and short photoperiod conditions, respectively, with a solution containing either low Cl^- (70 µM Cl^-, which fulfils micronutrient requirements) or high Cl^- (5 mM Cl^-). To identify phenotypic differences, morphological measurements were taken every 3 d approximately (section 3.8.1).

Under hydroponic conditions, root elongation of *slah4-2* KO plants was significantly higher relative to Col-0 in plants grown with high and low Cl^- treatments (Figs. 4.40 a-b and 4.41 a-b). High Cl^- nutrition (5 mM Cl^-) determined higher root development during late developmental stages in both lines, suggesting a link between Cl^- nutrition and root development (Figs. 4.40 c-d and 4.41 c-d).

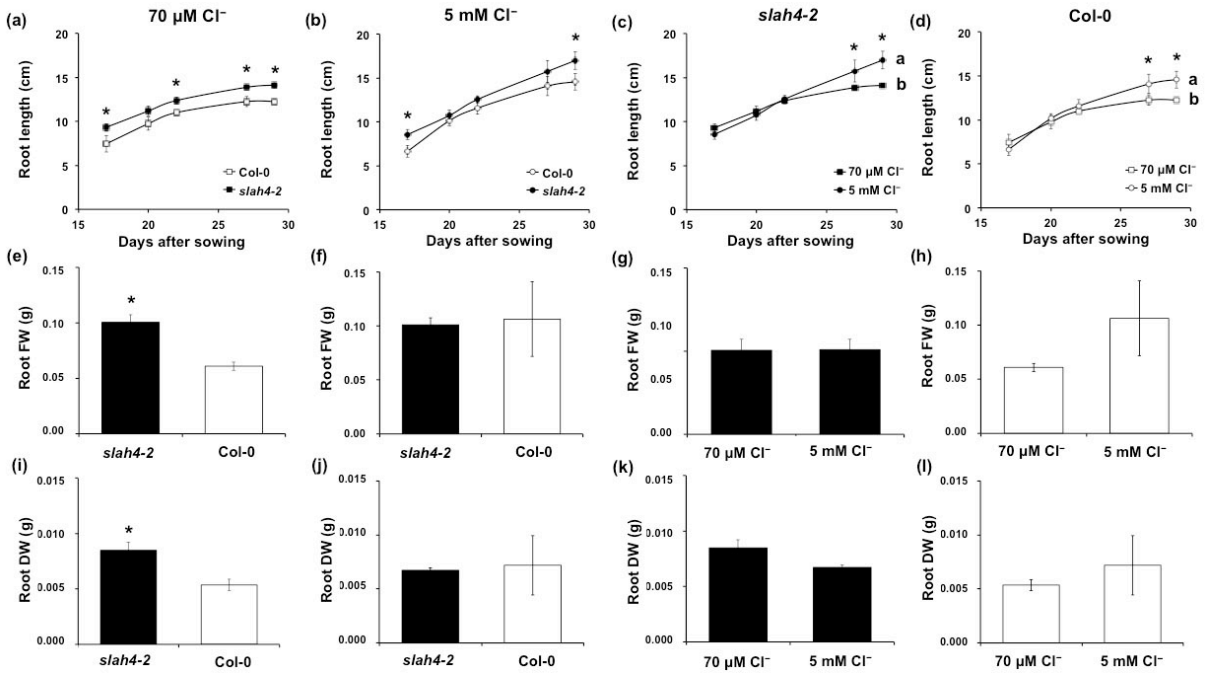

Figure 4.40. Differential root growth of *slah4-2* KO mutant and wild-type (Col-0) plants grown hydroponically under two different chloride treatments. Plants were grown hydroponically in nutrient solutions containing either low (70 µM) or high (5 mM) chloride (Cl^-). In the low chloride solution, Cl^- salts were replaced with sulphate and phosphate salts, maintaining the same balance of cations in comparison to the 5 mM chloride solution. **(a)** Root length of *slah4-2 versus* Col-0 plants grown in a nutrient solution containing low chloride (70 µM Cl^-). **(b)** Root length of *slah4-2 vs.* Col-0 plants grown

in a nutrient solution containing high chloride (5 mM Cl^-). **(c)** Root length of *slah4-2* plants alternatively grown under low (70 µM Cl^-) or high (5 mM Cl^-) chloride. **(d)** Root length of Col-0 plants alternatively grown under low (70 µM) or high (5 mM) chloride. **(e)** Root fresh weight (FW) of *slah4-2 versus* Col-0 plants grown in a nutrient solution containing low chloride (70 µM Cl^-). **(f)** Root fresh weight of *slah4-2 vs.* Col-0 plants grown in a nutrient solution containing high chloride (5 mM Cl^-). **(g)** Root fresh weight of *slah4-2* plants alternatively grown under low (70 µM Cl^-) or high (5 mM Cl^-) chloride. **(h)** Root fresh weight of Col-0 plants alternatively grown under low (70 µM) or high (5 mM) chloride. **(i)** Root dry weight (DW) of *slah4-2 versus* Col-0 plants grown in a nutrient solution containing low chloride (70 µM Cl^-). **(j)** Root dry weight of *slah4-2 vs.* Col-0 plants grown in a nutrient solution containing high chloride (5 mM Cl^-). **(k)** Root dry weight of *slah4-2* plants alternatively grown under low (70 µM Cl^-) or high (5 mM Cl^-) chloride. **(l)** Root dry weight of Col-0 plants alternatively grown under low (70 µM) or high (5 mM) chloride. Asterisks indicate statistically significant differences (one-way ANOVA, $*P < 0.05$, $n \geq 3$). Different letters indicate a statistically significant difference in *slah4-2* and WT plants development over time (linear mixed models, $P < 0.05$).

Root biomass (fresh weight [FW] and dry weight [DW]) of *slah4-2* plants treated with low Cl^- (70 µM Cl^-) was significantly higher than the root biomass of Col-0 plants (Fig. 4.40 e, i). However no difference could be observed between the mutant KO and the WT line when they were treated with high Cl^- nutrition (5 mM Cl^-; Fig. 4.40 f, j). Moreover, no difference in fresh and dry weight of the roots between plants of the same line grown with either 70 µM or 5 mM Cl^- could be observed (Fig. 4.40 g, h, k, l).

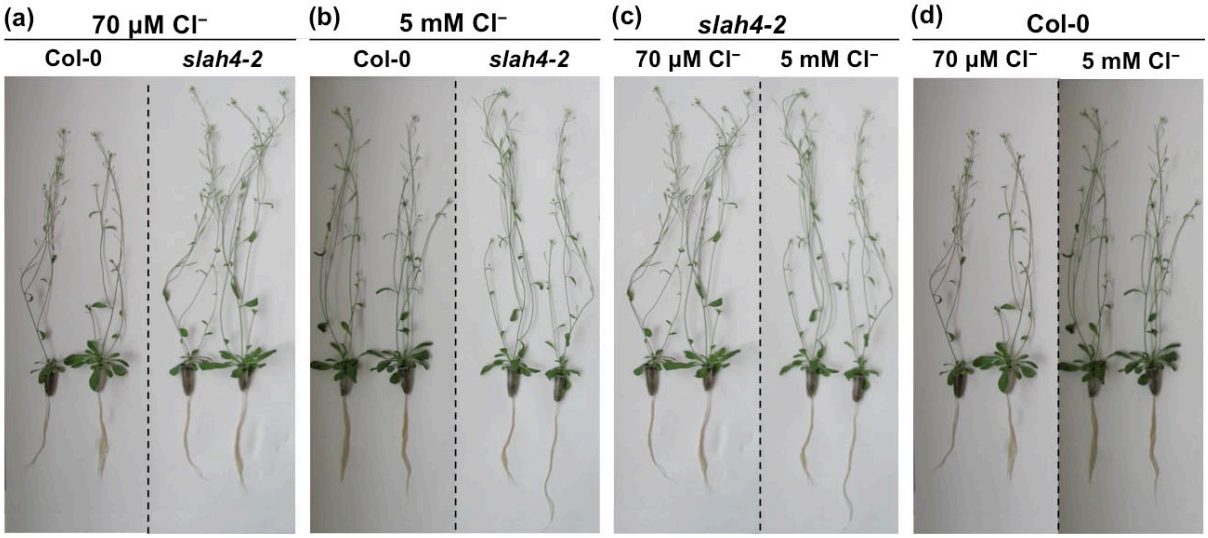

Figure 4.41. Differential growth of *slah4-2* KO mutant and wild-type (Col-0) plants grown hydroponically under two different chloride treatments. Plants were grown hydroponically in nutrient solutions containing either low (70 µM) or high (5 mM) chloride (Cl^-). In the low chloride solution, Cl^- salts were replaced with sulphate and phosphate salts, maintaining the same balance of cations in comparison to the 5 mM chloride solution. **(a)** Plants of *slah4-2* mutant and Col-0 lines grown with low chloride (70 µM Cl^-) treatment. **(b)** *slah4-2* mutant and Col-0 plants grown with high chloride (5 mM Cl^-) treatment solution. **(c)** *slah4-2* plants alternatively grown under low (70 µM Cl^-) or high (5 mM Cl^-) chloride. **(d)** Col-0 plants alternatively grown under low (70 µM Cl^-) or high (5 mM Cl^-) chloride.

slah4-2 KO mutant plants showed a higher development of inflorescence stems compared to wild-type plants, with significant differences only quantified in plants treated with 5 mM Cl^- (Figs. 4.42 a-b and 4.41 a-b). No differences were observed in *slah4-2* plants whatever the Cl^- treatment used (Figs. 4.42 c and 4.41 c), whereas lower chloride content in the medium (70 µM Cl^-) led to longer inflorescence stems in Col-0 plants during early development (Fig. 4.42 d).

Fresh and dry weight of shoots in *slah4-2* plants grown under 70 µM Cl^- was significantly higher than that of Col-0 line (Fig. 4.42 e, i), however these differences could not be observed with the 5 mM Cl^- treatment (Fig. 4.42 f, j). In addition, no phenotype linked to shoot weight between plants of the same line grown with either 70 µM or 5 mM Cl^- were observed (Fig. 4.42 g, h, k, l).

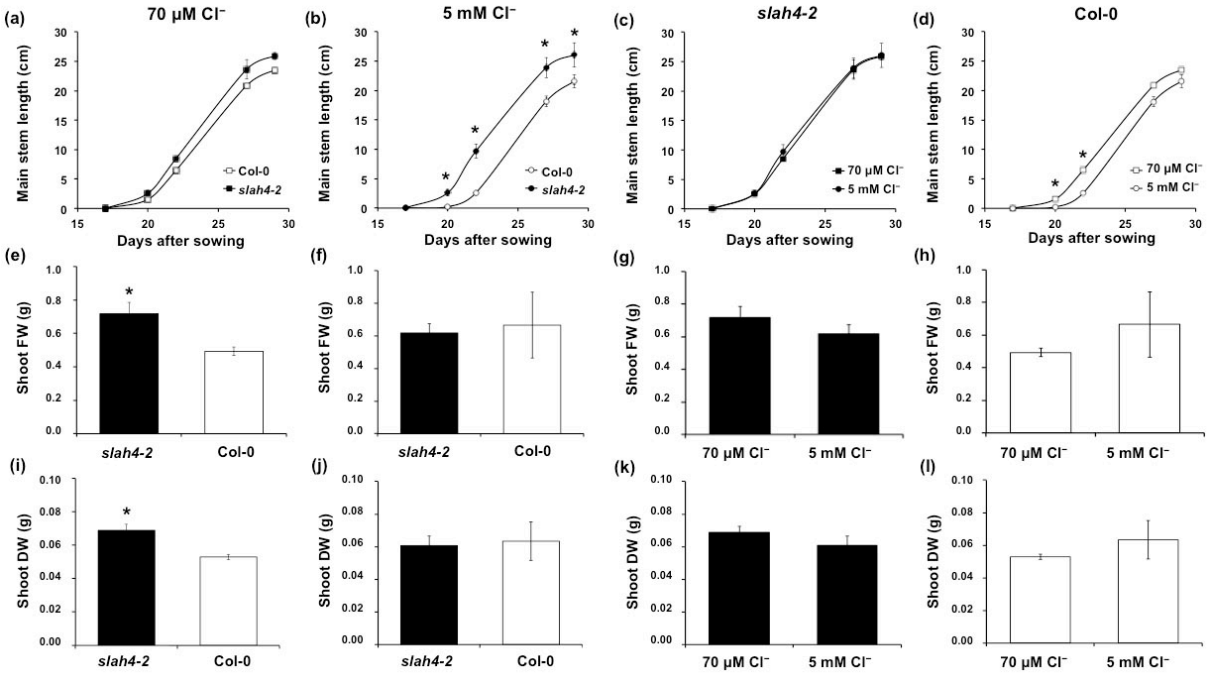

Figure 4.42. Differential shoot and inflorescence stem growth of mutant (*slah4-2*) and wild-type (Col-0) plants grown hydroponically under two different chloride treatments. Plants were grown hydroponically in nutrient solutions containing either low (70 µM Cl^-) or high (5 mM Cl^-) chloride. In the low chloride solution, Cl^- salts were replaced with sulphate and phosphate salts, maintaining the same balance of cations in comparison to the 5 mM chloride solution. **(a)** Main inflorescence stem length of *slah4-2 versus* Col-0 plants grown in a nutrient solution containing low chloride (70 µM Cl^-). **(b)** Main inflorescence stem length of *slah4-2 vs.* Col-0 plants grown in a nutrient solution containing high chloride (5 mM Cl^-). **(c)** Main inflorescence stem length of *slah4-2* plants alternatively grown under low (70 µM Cl^-) or high (5 mM Cl^-) chloride. **(d)** Main inflorescence stem length of Col-0 plants alternatively grown under low (70 µM) or high (5 mM) chloride. **(e)** Shoot fresh weight (FW) of *slah4-2 versus* Col-0 plants grown in a nutrient solution containing low chloride (70 µM Cl^-). **(f)** Shoot fresh weight of *slah4-2 vs.* Col-0 plants grown in a nutrient solution containing high chloride (5 mM Cl^-). **(g)** Shoot fresh weight of *slah4-2* plants alternatively grown under low (70 µM Cl^-) or high (5 mM Cl^-) chloride. **(h)** Shoot fresh weight of Col-0 plants alternatively grown under low (70 µM) or high (5 mM) chloride. **(i)** Shoot dry weight (DW) of *slah4-2 versus* Col-0 plants grown in a nutrient solution containing low chloride (70 µM Cl^-). **(j)** Shoot dry weight of *slah4-2 vs.* Col-0 plants grown in a nutrient solution containing high chloride (5 mM Cl^-). **(k)** Shoot dry weight of *slah4-2* plants alternatively grown under low (70 µM Cl^-) or high (5 mM Cl^-) chloride. **(l)** Shoot dry weight of Col-0 plants alternatively grown under low (70 µM) or high (5 mM) chloride. Asterisks indicate statistically significant differences (one-way ANOVA, **P* < 0.05, n≥ 3). Different letters indicate a statistically significant difference in *slah4-2* and WT plants development over time (linear mixed models, *P* < 0.05).

During the vegetative phase, *slah4-2* mutant plants grown in pots developed significantly bigger rosettes than Col-0 plants under both low (70 µM Cl^-) and high (5 mM Cl^-) chloride treatments (Figs. 4.43 a-b and 4.44), although during late development the diameter of the rosettes tended to converge (Fig. 4.43 a-b). Slight differences in the rosette size were observed when plants treated with low chloride were compared to plants treated with high chloride (Figs. 4.43 c-d and 4.44).

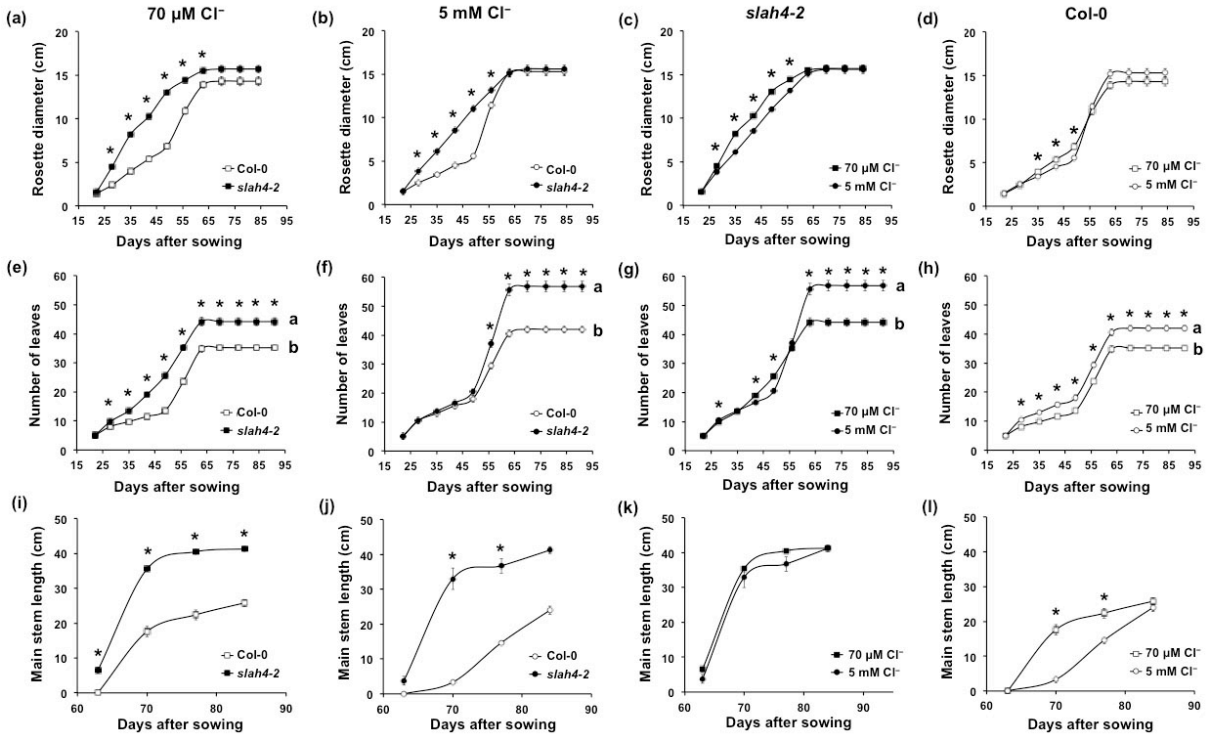

Figure 4.43. Differential shoot and inflorescence stem growth of *slah4-2* KO mutant and wild-type (Col-0) plants grown in solid substrate under two different chloride treatments. Potted plants were watered with nutrient solutions containing either low (70 µM) or high (5 mM) chloride (Cl^-). In the low chloride solution, Cl^- salts were replaced with sulphate and phosphate salts, maintaining the same balance of cations in comparison to the 5 mM chloride solution. **(a)** Rosette diameter of *slah4-2 versus* Col-0 plants watered with a nutrient solution containing low chloride (70 µM Cl^-). **(b)** Rosette diameter of *slah4-2 vs.* Col-0 plants watered with a nutrient solution containing high chloride (5 mM Cl^-). **(c)** Rosette diameter of *slah4-2* plants alternatively watered with low (70 µM Cl^-) or high (5 mM Cl^-) chloride. **(d)** Rosette diameter of Col-0 plants alternatively watered with low (70 µM) or high (5 mM) chloride. **(e)** Number of rosette leaves of *slah4-2 versus* Col-0 plants watered with a nutrient solution containing low chloride (70 µM Cl^-). **(f)** Number of rosette leaves of *slah4-2 vs.* Col-0 plants watered with a nutrient solution containing high chloride (5 mM Cl^-). **(g)** Number of rosette leaves of *slah4-2* plants alternatively watered with low (70 µM Cl^-) or high (5 mM Cl^-) chloride. **(h)** Number of rosette leaves of Col-0 plants alternatively watered with low (70 µM) or high (5 mM) chloride. **(i)** Main inflorescence stem length of *slah4-2 versus* Col-0 plants watered with a nutrient solution containing low chloride (70 µM Cl^-). **(j)** Main inflorescence stem length of *slah4-2 vs.* Col-0 plants watered with a nutrient solution containing high chloride (5 mM Cl^-). **(k)** Main inflorescence stem length of *slah4-2* plants alternatively watered with low (70 µM Cl^-) or high (5 mM Cl^-) chloride. **(l)** Main inflorescence stem length of Col-0 plants alternatively watered with low (70 µM) or high (5 mM) chloride. Asterisks indicate statistically significant differences (one-way ANOVA, $*P < 0.05$, n≥ 3). Different letters indicate a statistically significant difference in *slah4-2* and WT plants development over time (linear mixed models, $P < 0.05$).

However the number of rosette leaves was strongly impacted by both the genotype and the Cl^- treatment. The number of rosette leaves of *slah4-2* mutant plants was significantly greater than the number of leaves of Col-0 plants under both 70 µM and 5 mM Cl^- treatments (Figs. 4.43 e-f and 4.44). In addition, the 5 mM Cl^- treatment induced higher rosette size in both mutant and WT plants (Figs. 4.43 g-h and 4.44). In consequence, *slah4-2* mutant plants showed the highest number of leaves (Figs. 4.43 f –g and 4.44).

Moreover, *slah4-2* plants showed significantly longer inflorescences than WT plants grown under both chloride treatments (Fig. 4.43 i-j). This phenotype in *slah4-2* plants was independent on the Cl^--feeding regimen (Fig. 4.43 k), whereas lower chloride content in the medium led to significantly longer inflorescence stems in Col-0 line (Fig. 4.43 l), although this

difference in the growth with 70 µM and 5 mM Cl^- treatments disappeared at the end of the reproductive phase.

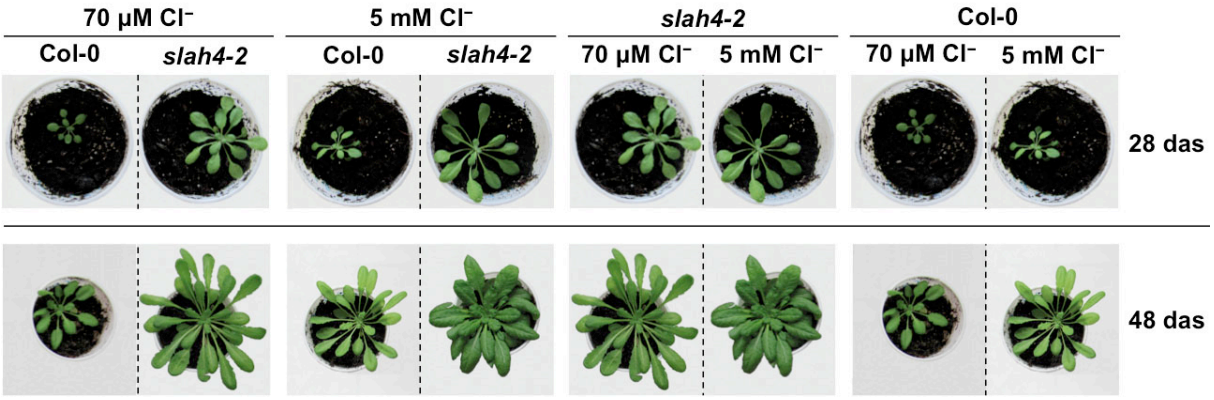

Figure 4.44. Differential rosette development of *slah4-2* KO mutant and Col-0 plants grown in solid substrate under two different chloride treatments. Potted plants were watered with nutrient solutions containing either low (70 µM) or high (5 mM) chloride (Cl^-). In the low chloride solution, Cl^- salts were replaced with sulphate and phosphate salts, maintaining the same balance of cations in comparison to the 5 mM chloride solution.

Therefore, the lack of function of the *AtSLAH4* gene resulted in higher root elongation and shoot organs growth (bigger rosettes, higher number of rosette leaves and longer inflorescences).

Chloride content was determined (section 3.8.4.1) in the shoot of *slah4-2* and Col-0 plants used in these and other experiments under different growing and treatment conditions: potted plants, hydroponics conditions; high and low Cl^- treatments, etc. Under the assumption that the SLAH4 channel is involved in the regulation of chloride efflux from the root, we expected a higher Cl^- concentration in the shoot of *slah4-2* plants. However this phenotype was not clearly observed in the different assays performed (results not shown). A new experiment was carefully designed in a systematic way, controlling different parameters that, according to previous results, could regulate the activity of the channel or the conditions that make it possible to observe a phenotype associated to the lack of function of the SLAH4 channel (section 4.2.4).

4.2.4. *slah4-2* KO plants accumulated more chloride in the shoot

Given the interaction between NO_3^- and Cl^- homeostasis (section 1.2), and to further explore the putative role of SLAH4 channel in the regulation of net chloride uptake from the root (e.g. mediating Cl^- efflux from the root epidermal and cortical cells), the contend of Cl^- in the shoot was quantified (section 3.8.4.1) in the KO mutant *slah4-2* and the wild-type Col-0 lines grown with different concentrations of NO_3^- and Cl^- in the nutrient solution. With this aim, seventeen-day-old *slah4-2* and Col-0 plants grown with low chloride (70 µM Cl^-) were treated with nutrient solutions containing different NO_3^-/Cl^- ratios (Table 3.5; section 3.8.3). Given also the differential regulation of *AtSLAH4* during plant development, plants were harvested according to their developmental stage: (1) during the vegetative phase, before the emergence of inflorescence stems; (2) at the onset of the reproductive stage (bolting); (3) during the flowering stage; and (4) during the fruit maturation stage, at the beginning of plant senescence.

The most significant phenotype associated to the lack of function of the *AtSLAH4* gene was a higher accumulation of Cl^- in the shoot of *slah4-2* plants treated with low nitrate

(0.25–0.75 mM NO_3^-) and high chloride (4.75–5 mM Cl^-), only observed during late developmental stages (Fig. 4.45 c, e).

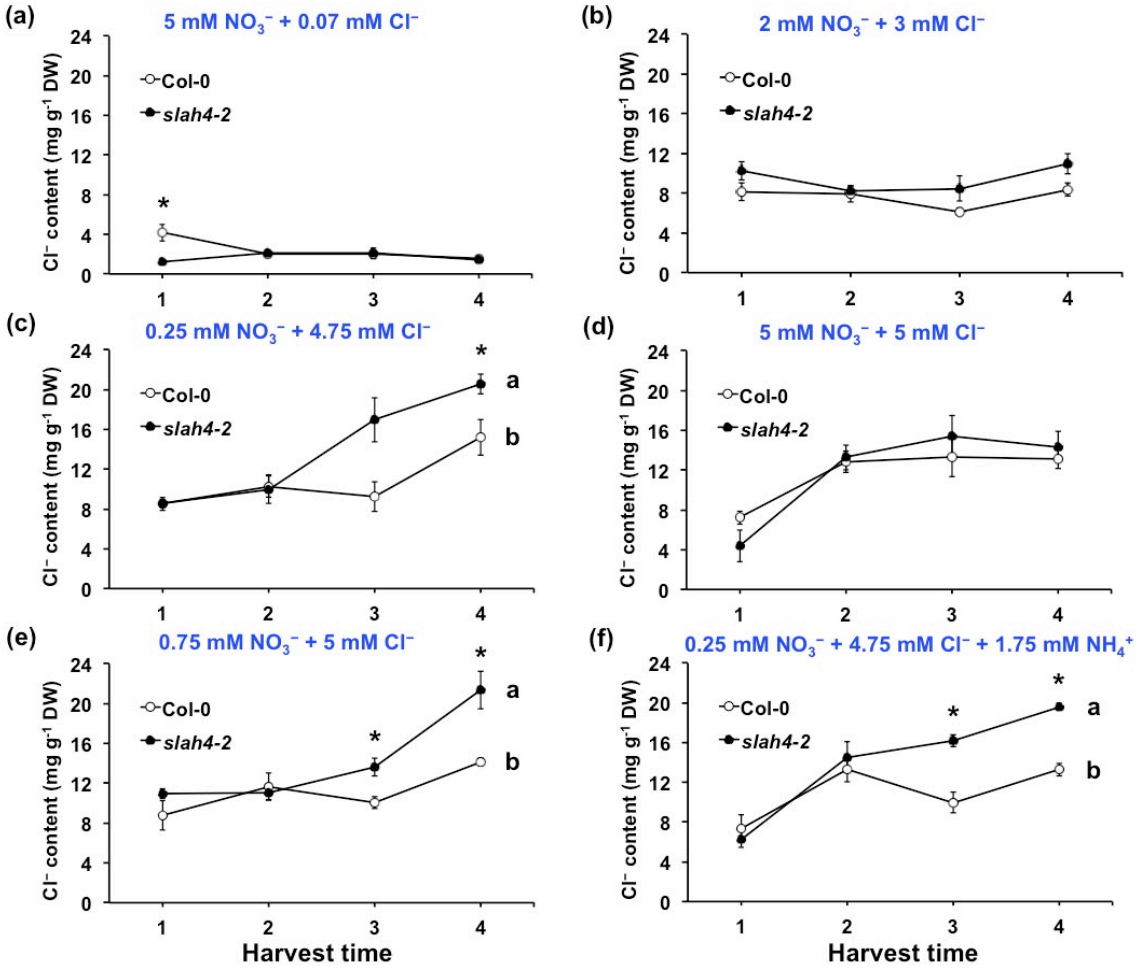

Figure 4.45. Chloride content in shoots of *slah4-2* T-DNA knockout and Col-0 wild-type plants growing with different nitrate (NO_3^-) and chloride (Cl^-) concentration treatments. Potted plants were watered with nutrient solutions containing different nitrate (NO_3^-)/ chloride (Cl^-) ratios. Plants were harvested according to their developmental stage: 1, vegetative phase; 2, onset of the reproductive stage (bolting); 3, flowering stage; 4, fruit maturation stage. **(a)** Cl^- content of *slah4-2 versus* Col-0 plants watered with a nutrient solution containing high nitrate (5 mM NO_3^-) and low chloride (70 µM Cl^-). **(b)** Cl^- content of *slah4-2 vs.* Col-0 plants watered with a nutrient solution containing 2 mM NO_3^- and 3 mM Cl^-. **(c)** Cl^- content of *slah4-2 vs.* Col-0 plants watered with a nutrient solution containing low nitrate (0.25 mM NO_3^-) and high chloride (4.75 mM Cl^-). **(d)** Cl^- content of *slah4-2 vs.* Col-0 plants watered with a nutrient solution containing high nitrate (5 mM NO_3^-) and high chloride (5 mM Cl^-). **(e)** Cl^- content of *slah4-2 vs.* Col-0 plants watered with a nutrient solution containing low nitrate (0.75 mM NO_3^-) and high chloride (5 mM Cl^-). **(f)** Cl^- content of *slah4-2 vs.* Col-0 plants watered with a nutrient solution containing low nitrate (0.25 mM NO_3^-), high chloride (4.75 mM Cl^-) and 1.75 mM ammonium (NH_4^+). Asterisks indicate statistically significant differences (one-way ANOVA, $*P < 0.05$, n≥ 4). Different letters indicate a statistically significant difference in *slah4-2* and WT plants development over time (linear mixed models, $P < 0.05$).

The high nitrate (5 mM NO_3^-) and low chloride (70 µM Cl^-) treatment led to reduced Cl^- content in the shoot of both *slah4-2* and WT plants, with Col-0 plants showing a slightly, but statistically significant, higher Cl^- content during the vegetative growth (Fig. 4.45 a). When nitrate was reduced to 2 mM NO_3^- and chloride increased to 3 mM Cl^- in the treatment solution (Fig. 4.45 b), Cl^- accumulation was slightly higher in the *slah4-2* KO mutant line than in the WT line, although the differences were not statically significant.

When nitrate was further reduced to 0.25 mM NO_3^- and chloride increased to 4.75 mM Cl^- in the treatment solution, shoot Cl^- accumulation become significantly higher in the *slah4-2* line than in the Col-0 line (Fig. 4.45 c). Interestingly, the differential higher accumulation of Cl^- in *slah4-2* plants occurred during late developmental stages corresponding to flowering and fruit maturation (Fig. 4.45 c).

When high levels of both anions were maintained in the nutrient solution (5 mM NO_3^-, 5 mM Cl^-), no differences in shoot Cl^- accumulation between *slah4-2* and Col-0 plants were observed (Fig. 4.45 d).

Other combinations of NO_3^- and Cl^- concentrations in the nutrient solution where the NO_3^-/Cl^- ratio had been strongly reduced also resulted in the specific higher accumulation of shoot Cl^- in the *slah4-2* line relative to the WT (Fig. 4.45 e-f). The presence of ammonium (1.75 mM NH_4^+) in the nutrient solution did not alter the phenotype (Fig. 4.45 f).

Hence, lack of function of the *AtSLAH4* gene resulted in higher accumulation of Cl^- in the shoot, essentially at late developmental stages when the NO_3^-/Cl^- ratio was strongly reduced**,** supporting the idea that the SLAH4 channel participates in the efflux of chloride from the root to either the apoplast or the rhizosphere and this activity is influenced by the plant NO_3^- content and/or availability.

4.2.5. Regulation of *AtSLAH4* gene expression

To study which environmental factors regulate the expression of the *AtSLAH4* gene, its transcript level was quantified through qPCR (section 3.2.4.3) in *A. thaliana* Col-0 plants.

4.2.5.1. Stress and ABA slightly down-regulate *AtSLAH4* expression

To analyse how the expression of the *AtSLAH4* gene is regulated by abiotic stress and ABA, *Arabidopsis* plants were grown hydroponically (section 3.1.2.2.3) and subjected to salt stress (150 mM NaCl), water deficit (287 g l^{-1} PEG-8000) and exogenous application of abscisic acid (100 µM ABA).

Salt stress (150 mM NaCl) reduced root transcript levels of *AtSLAH4* around 6–7 times (Fig. 4.46), similarly to the repression produced by NaCl in *AtSLAH1* expression (around 3–11 times). In addition, water deficit caused by 287 g l^{-1} PEG-8000 produced a slight repression of *AtSLAH4* expression (approximately 3–4 times), meanwhile the same treatment repressed *AtSLAH1* transcript accumulation up to 58 times.

As ABA signalling is downstream of salt and water stress, plants were treated with this stress hormone in a subsequent experiment. Exogenous application of 100 µM ABA in the nutrient solution produced a moderate repression of *AtSLAH4* expression (about 13–18 times; Fig. 4.46), whereas the same treatment repressed *AtSLAH1* transcript accumulation by 400 times.

As a control, the same treatments strongly increased transcript accumulation of the stress-responsive *LEA* gene *AtLEA-M* (Fig. 4.15 b).

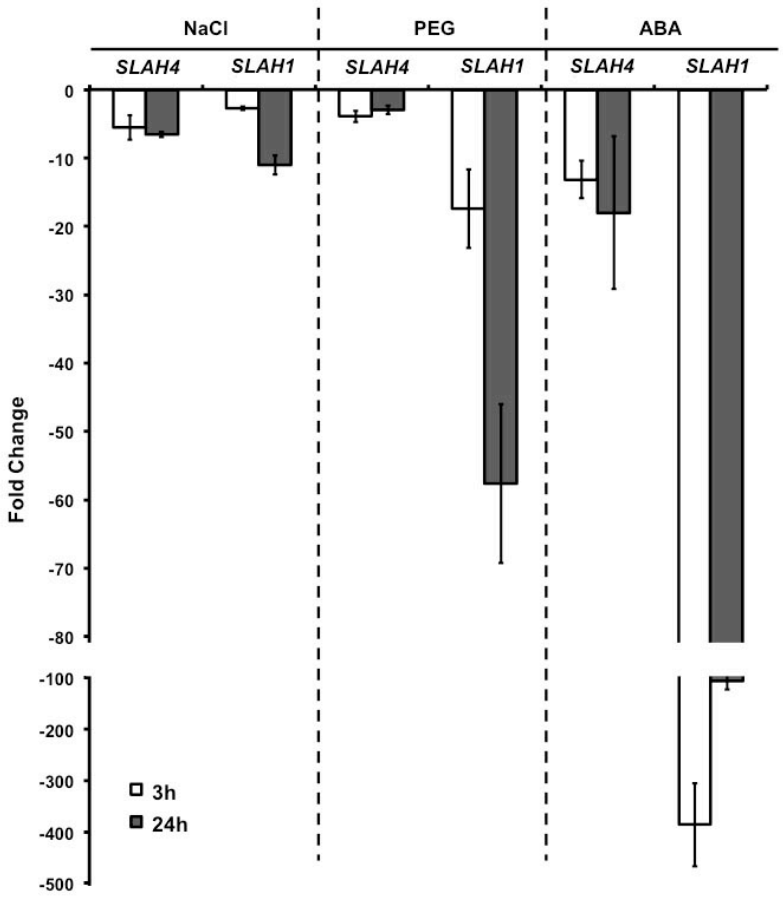

Figure 4.46. Relative expression of *AtSLAH4* under abiotic stress treatments. Fold-change relative to control conditions of *AtSLAH4* transcript levels quantified 3 h and 24 h after treatment application. Abiotic stress treatments consisted of salinity induced with 150 mM NaCl (NaCl), water deficit caused with 287 g l^{-1} PEG-8000 (PEG) and exogenous application of 100 µM ABA (ABA). Transcript abundance was quantified with standard curves calculated for the individual PCR products and normalized with the housekeeping translation initiation factor *AteIF4A1* gene (n ≥ 3; mean ± SE).

The down-regulation of *AtSLAH4* gene expression by ABA was further confirmed in P_{SLAH4}-GFP::GUS transgenic lines (Fig. 4.47) after incubation for 15h with 100 µM ABA (section 3.9.1.1).

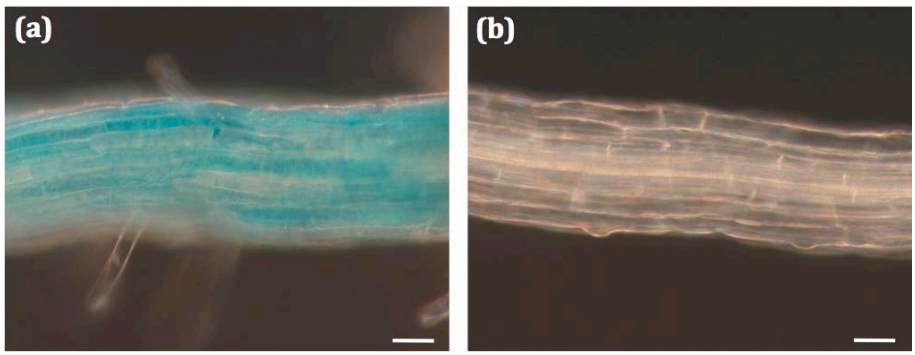

Figure 4.47. *AtSLAH4* expression is down-regulated by abscisic acid (ABA). Histochemical localization of *AtSLAH4* expression in transgenic *Arabidopsis* plants expressing the GUS reporter gene under the control of the *AtSLAH4* promoter (P_{SLAH4}-GFP::GUS). **(a)** Root without ABA (control). **(b)** Root treated with 100 µM ABA. Scale bars, 50 µm.

Together, these results indicate that *AtSLAH4* expression is down-regulated by abiotic stress and exogenous application of ABA, although the degree of repression by water deficit and ABA was clearly lower than that shown by the *AtSLAH1* gene.

4.2.5.2. *AtSLAH4* expression is not affected by changes in the nutritional status of Cl^- and NO_3^-

Since the availability of nutrients can influence in the expression of genes encoding membrane transporters, and given that SLAC/SLAH channels are permeable to chloride and nitrate, *AtSLAH4* transcript abundance was quantified by qPCR in response to changes in the nutritional status of these nutrients (NO_3^- and Cl^- starvation and supply treatments).

With this aim, Col-0 plants were grown hydroponically (section 3.1.2.2.3). On the one side, plants alternatively grown with nitrate (5 mM NO_3^-) or without nitrate (2.5 mM ammonium), were subjected to either NO_3^- application (transfer of ammonium-treated plants to 5 mM NO_3^- medium) or NO_3^- starvation (transfer of NO_3^- plants to a nutrient solution containing no NO_3^-) treatments respectively. On the other side, plants alternatively grown with low chloride (70 µM Cl^-) or high chloride (5 mM Cl^-) were subjected to either Cl^- application (transfer of low-Cl^- plants to 5 mM Cl^- medium) or Cl^- starvation (transfer of high-Cl^- plants to 70 µM Cl^- medium) treatments respectively. Plants used as control were transferred to the same nutrient solution.

AtSLAH4 did not respond to changes in the nutritional status of NO_3^- (Fig. 4.48). In contrast, *AtSLAH1* was negatively regulated by NO_3^- starvation and induced by NO_3^- supply after starvation (Fig. 4.48). Regarding Cl^- treatments, only *AtSLAH1* expression was slightly repressed by Cl^- starvation, and neither *AtSLAH1* nor *AtSLAH4* genes responded to the Cl^- application treatment (Fig. 4.48).

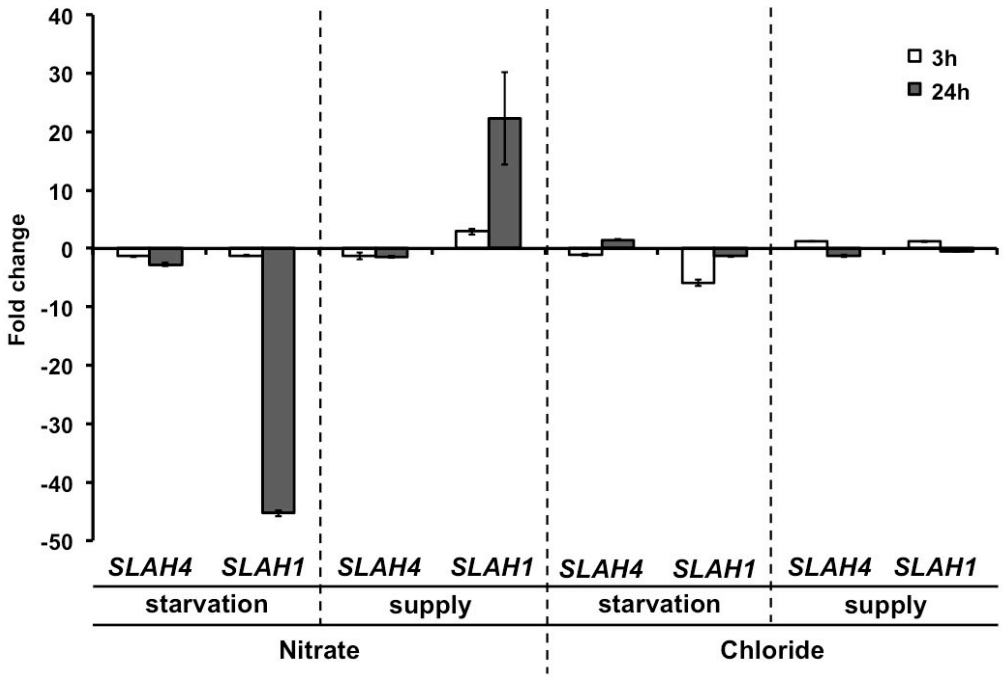

Figure 4.48. Relative expression of *AtSLAH4* in response to changes in the nutritional status of nitrate (NO_3^-) and chloride (Cl^-). Fold-change relative to control conditions of *AtSLAH4* transcript levels quantified 3 h and 24 h after different nutritional treatments. Nitrate supply: plants growing

hydroponically in a nutrient solution with 2.5 mM ammonium acetate as the sole nitrogen source were transferred to a nutrient solution containing 5 mM NO_3^- as the sole nitrogen source. Nitrate starvation: plants growing hydroponically in a nutrient solution with 5 mM NO_3^- as the sole nitrogen source were transferred to a nutrient solution with 2.5 mM ammonium acetate as the sole nitrogen source. Chloride supply: plants growing hydroponically in a nutrient solution containing low chloride (70 µM Cl^-) were transferred to a nutrient solution with high chloride (5 mM Cl^-). Chloride starvation: plants growing hydroponically in a nutrient solution with high chloride (5 mM Cl^-) were transferred to a nutrient solution containing low chloride (70 µM Cl^-). Transcript abundance was quantified with standard curves calculated for the individual PCR products and normalized with the housekeeping translation initiation factor *AteIF4A1* gene (n ≥ 3; mean ± SE).

4.2.5.3. IAA slightly regulates *AtSLAH4* gene expression

Spatial distribution of GUS activity in P_{SLAH4}-GFP::GUS plants showed a specific expression of *AtSLAH4* in leaf meristems and hydathodes (Fig. 4.37 a-b). Given that these organs are involved in primary auxin production (Aloni *et al*., 2003), we wonder whether *AtSLAH4* could be regulated by this phytohormone. Hence, *AtSLAH4* gene expression was analysed in response to exogenous application of indole-3-acetic acid (IAA).

Plants were grown hydroponically (section 3.1.2.2.3) for 2 weeks in 0.25x MS and 6 weeks more in BS solution supplemented with either 70 µM Cl^- or 5 mM Cl^-. Three and 24 h after the application of 100 µM IAA, transcript level of the *AtSLAH4* gene were quantified in roots and rosette leaves.

In the root, the auxin treatment resulted in a reduction of the *AtSLAH4* transcript level ranging from about 1.5 to 6.5 times, and did not appear to be affected by the level of chloride present in the medium (Fig. 4.49). In rosette leaves, the auxin treatment had no clear effect on the regulation of *AtSLAH4* expression (Fig. 4.49).

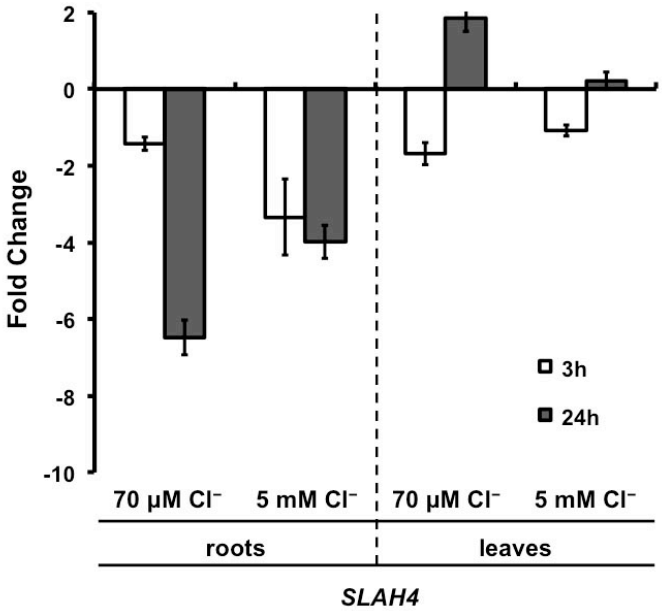

Figure 4.49. Effect of exogenous auxin application on the relative expression level of *AtSLAH4* in roots and leaves of wild-type plants. Fold-change relative to control conditions of *AtSLAH4* transcript levels quantified 3 h and 24 h after 100 µM indole-3-acetic acid (IAA) application in roots and leaves of plants grown in BS solution supplemented with either 70 µM or 5 mM chloride (Cl^-). Transcript abundance was quantified with standard curves calculated for the individual PCR products and normalized with the housekeeping translation initiation factor *AteIF4A1* gene (n ≥ 3; mean ± SE).

The down-regulation of *AtSLAH4* gene expression in the root by IAA was further confirmed in P_{SLAH4}-GFP::GUS transgenic lines after incubation for 15 h with 100 µM IAA (Fig. 4.50).

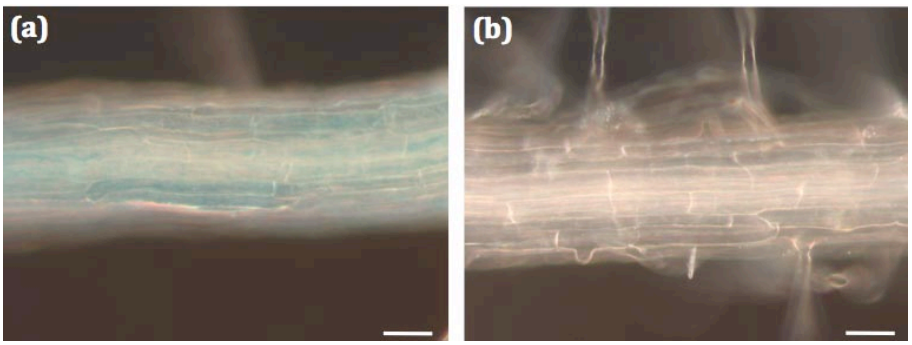

Figure 4.50. *AtSLAH4* expression is down-regulated by indole-3-acetic acid (IAA) in roots. Histochemical localization of *AtSLAH4* expression in transgenic *Arabidopsis* plants expressing the GUS reporter gene under the control of the *AtSLAH4* promoter (P_{SLAH4}-GFP::GUS). **(a)** Transgenic root without IAA (control). **(b)** Root treated with 100 µM IAA. Scale bars, 50 µm.

DISCUSSION

5. DISCUSSION

The relevance of chloride (Cl^-) in higher plants has traditionally been limited to two extreme situations. On the one hand, its importance as an essential micronutrient, which requires trace levels of Cl^- in the external medium to allow the proper development of plants. On the other hand, its detrimental effect when this anion is present in the soil at high, or even moderate, concentrations.

Our research group does not agree with this traditional view of the role of chloride in higher plants, mainly as a result of two recent discoveries. Firstly, we have shown that, when available, plants accumulate Cl^- to levels that are typical of the content of a macronutrient, specifically stimulating leaf tissue osmolarity, cell expansion and plant growth, improving also a number of important plant physiological traits like the leaf water balance, the water relations at the whole plant level (Franco-Navarro *et al.*, 2016a; Raven, 2017), the nitrate-use efficiency, the mesophyll diffusion conductance to CO_2, and the resistance to water deficit (Franco-Navarro *et al.*, 2012, 2016b, 2016c). Secondly, we have identified the early vegetative growth of plants as a developmental stage in which Cl^- is specifically required as a bona fide macronutrient (Franco-Navarro *et al.*, manuscript in preparation).

An important aspect that has classically been associated with the deleterious effects of Cl^- in the agriculture is its antagonism effect in NO_3^- uptake and accumulation. Both anions can be transported through the same membrane transporters, determining possible reciprocal competition in their flows and storage capacity in the plant (Xu *et al.*, 2000). However, we know nowadays that both nutrients fulfil complementary functions and optimal rates of NO_3^- *versus* Cl^- transport are regulated by the plant depending on different factors: the developmental stage (e.g. vegetative *vs.* reproductive stage), the environmental conditions (e.g. salt stress or water deficit *vs.* favourable conditions), or the nutritional status (e.g. the NO_3^-/Cl^- ratio).

Two essential root-dependent factors that determine the degree of Cl^- uptake and accumulation in plants are the net uptake and the xylem translocation rate. In this work, *AtSLAH1* and *AtSLAH4*, two root-expressing genes of the SLAC/SLAH family that encode slow-type anion channels, have been functionally characterized. These genes, together with other member of the same family, *AtSLAH3*, perform important functions in higher plants in the regulation of Cl^- homeostasis at the whole-plant level and in the regulation of Cl^- *vs.* NO_3^- interaction.

The results shown in this work indicate that: (1) SLAH4 controls the net Cl^- uptake in the root periphery through the regulation of Cl^- release at the root/soil interface; (2) SLAH1 controls the root-to-shoot Cl^- translocation rate in the xylem pole pericycle through the regulation of the SLAH3 Cl^- conductance at the root/xylem interface.

5.1. SLAH1 CHARACTERIZATION

5.1.1. Relevance of *At*SLAH1 in the regulation of Cl^- xylem translocation in the root

Uptake of nutrients is followed by their retention in the root or their load into the xylem for root-to-shoot transport. Under optimal growth conditions both Cl^- and NO_3^- anions are mostly mobilized to the shoot for different reasons: NO_3^- assimilation to ammonium and amino acids requires reducing power generated in photosynthetic organs (Marschner, 1995); and Cl^-, which is not assimilated, must be efficiently stored in the vacuoles of leaf and stem cells to regulate osmolarity, turgor and water homeostasis (Franco-Navarro *et al.*, 2016a). For root-to-shoot transport, the first step is the translocation of Cl^- and NO_3^- into the xylem vessels.

5.1.1.1. *AtSLAH1* and *AtSLAH3* transcripts accumulate in root vascular cells involved in the translocation of nutrients into xylem vessels

Several types of anion conductances identified in protoplast of xylem-associated cells of barley (*Hordeum vulgare*; Köhler and Raschke, 2000) and maize (*Zea mays*; Gilliham and Tester, 2005) by patch clamp studies, have been potentially involved in the release of NO_3^- and Cl^- anions into the xylem (Roberts, 2006). Among these anion conductances were the slowly activating (S-type) NO_3^- and Cl^- conductances.

We have shown that the expression of the *Arabidopsis thaliana* genes *AtSLAH1* and *AtSLAH3* is confined to xylem-pole pericycle cells in the root (Fig. 4.2), which predicts the co-localization of both S-type channels in the plasma membrane of this root cell type (Negi *et al.*, 2008; Zheng *et al.*, 2015).

According to previously published studies, the xylem pole pericycle cells are involved in the xylem loading of nutrients like: potassium (K^+), mediated by the *At*SKOR channel (Gaymard *et al.*, 1998); nitrate, mediated by the low and high affinity H^+/NO_3^- cotransporter *At*NRT1.5 (recently named as *At*NPF7.3), *At*NPF2.3 and *Le*NRT2.3, respectively (Chen et al., 2012; Fu *et al.* 2015; Lin *et al.*, 2008; Taochy *et al.*, 2015; Wang *et al.*, 2012); sulphate, mediated by the Sultr2;1 transporter (Kawashima *et al.*, 2009; Takahashi *et al.*, 2000); iron, mediated by the citrate transporter *Os*FRDL1 (Yokosho *et al.*, 2009) and phosphate, mediated by the phosphate channel *At*PHO1 (Hamburger *et al.*, 2002).

Xylem loading of nutrients has typically been associated to another cell type: the xylem parenchyma cells of roots. This cell type is located in more internal layers of the vascular cylinder with respect to the pericycle. The low affinity NO_3^- transporter gene *At*NRT1.8 (also named *At*NPF7.2; Léran *et al.*, 2014) is dominantly expressed in xylem-parenchyma cells and it has a role in removing NO_3^- from the xylem (Li *et al.*, 2010). Therefore, it is unclear whether xylem parenchyma cells could be preferentially involved in carrying nutrients into the xylem, in retrieving them from the xylem or in both processes.

5.1.1.2. Both SLAH1 and SLAH3 channels participate in xylem translocation and shoot accumulation of Cl^-

The negative plasma membrane potential of plant cells (up to −250 mV) and the outward-directed NO_3^- and Cl^- concentration gradients suggest that both anions enter the xylem vessels through anion efflux channels at plasma membrane potentials more negative than −50 mV (Babourina *et al.,* 1998b; Glass and Siddiqi, 1995; Roberts, 2006; White and Broadley, 2001). The translocation of NO_3^- and Cl^- into the root xylem is probably electrochemically passive, following the electrochemical potential gradient for these anions (Henderson *et al*., 2014; Kollist *et al.,* 2011; Munns and Tester, 2008; Roberts, 2006; Teakle and Tyerman, 2010; White and Broadley, 2001). Thus, it is expected that anion channels, rather than H^+-dependent active transporters (e.g. from the NPF family), are responsible for most of the flow of anions released from the xylem-pole pericycle cells to the xylem vessels.

Root sap exudates from the single mutants *slah1-2*, *slah3-1* and *slah3-4* and from the *slah1*-slah3 double mutant showed similar reductions of Cl^- concentration, up to 50% (Fig. 4.13 a, c and Table 4.1), indicating that Cl^- release into xylem vessels requires the concerted participation of both SLAH1 and SLAH3 channels in the same transport mechanism. As a consequence, the *slah1-2* mutant also presented a lower accumulation of Cl^- in the shoot (Figs. 4.9 and 4.10).

According to previous results, SLAH3 mediates the release of NO_3^- and Cl^- from guard cells (section 1.5.2.2.2; Geiger *et al*., 2011; Negi *et al*., 2008) and its permeability for NO_3^- is 20 times higher than the permeability for Cl^- from (Geiger *et al*., 2011). However, neither the NO_3^- content of the xylem sap nor the shoot NO_3^- accumulation were reduced in either the *AtSLAH1* and *AtSLAH3* single or double KO mutants (Fig. 4.13 b, d). Given that NO_3^- is the main source of nitrogen for higher plants, the translocation of this anion into root xylem vessels is very likely redundant, i.e., mediated by different proteins. Therefore, other ion channels and transporters have been reported to contribute to the release of NO_3^- into the xylem vessels, such as *At*NRT1.5/*At*NPF7.3 (Lin *et al.*, 2008), *At*NPF2.3 (Taochy *et al.*, 2015) and *AtSLAH2*, other stelar-localized anion channel from the SLAC/SLAH family that mediates NO_3^--selective currents (Maierhofer *et al.*, 2014b). This high functional redundancy associated with the transport of NO_3^- in plants probably makes the identification of phenotypes with altered levels of NO_3^- based on the use of single gene mutants difficult.

5.1.1.3. SLAH1 is a silent anion channel

The activity of the previously characterized S-type SLAC1, SLAH2 and SLAH3 channels requires the activation by protein kinases that belong to Ca^{2+}-dependent and Ca^{2+}-independent families (section 1.5.1.2.3). Different phosphorylation sites in SLAC/SLAH channels have been identified and their participation in the channels activation has been demonstrated (Fig. 1.17; Brandt *et al.*, 2012; Geiger *et al.*, 2009b, 2010, 2011; Lee *et al.*, 2009; Maierhofer *et al*., 2014ab; Scherzer *et al*., 2012). However, most of these phosphorylation sites have not been identified in either SLAH1 or SLAH4 channels. The N-terminal domain, containing most of the identified phosphorylation sites, encodes in Exon-1 (E1) of *AtSLAC1* and *AtSLAH2* genes and Exon-2 (E2) of *AtSLAH3* gene, but it is not present in SLAH1 and SLAH4 channels (Fig. 1.17). A screen for potential conserved targets for kinases identified a highly significant serine residue conserved in

the root-expressing SLAH1 (S179), SLAH3 (S391) and SLAH4 (S171) channels, in the cytosolic loop between the transmembrane domains TM4 and TM5 (Dreyer *et al.*, 2012).

We tested whether the SLAH1 channel could be activated by these or other related protein kinases that, according to Genevestigator database (www.genevestigator.org), are predicted to be expressed in the root pericycle (root stele). Thus, we firstly studied SLAH1-kinase interactions through heterologous gene expression in *Xenopus* oocytes and BiFC and positive interactions between SLAH1 and the Ca^{2+}-dependent kinases CPK6, CPK21, CPK23 and CIPK23/CBL1 as well as with the Ca^{2+}-independent kinases SnRK2.2, SnRK2.3, SnRK2.6 (OST1), SnRK2.7 and SnRK2.8 were observed (Fig. 4.18).

However, no electric activity was recorded by TEVC technique in *Xenopus* oocytes expressing the *AtSLAH1* alone or with the previously described interacting kinase genes (section 4.1.1.6). Besides the activating kinase, SLAH2 and SLAH3 also need NO_3^- to gate the channel open (Demir *et al.*, 2013; Geiger *et al.*, 2009b, 2010, 2011; Gutermuth *et al.*, 2013; Lee *et al.*, 2009; Maierhofer *et al.*, 2014ab). But SLAH1 did not respond to either extracellular Cl^- or NO_3^- (Fig. 4.24 a-b). In addition, the SLAH1 F307A mutant channel, harbouring a modified anion gate that leads to an open-conducting state channel in other members of the SLAC/SLAH family, did not result in macroscopic anion currents when expressed in *Xenopus* oocytes (Fig. 4.21).

5.1.1.4. Regulation of Cl^- conductance at the xylem-pole pericycle requires SLAH1/SLAH3 interaction

The co-localization of SLAH1 and SLAH3 transcripts in the same cell type, the identical phenotype of the single and the double mutants, as well as the inability of SLAH1 to transport NO_3^- or Cl^- anions by itself, pointed to a mechanism based on the interaction and concerted participation of both molecules in the xylem Cl^- translocation mechanism. Subunit heteromerization has been shown for plant ammonium transporters (Loqué *et al.*, 2007) and for potassium channels from the Shaker family (Geiger *et al.*, 2009b; Jeanguenin *et al.*, 2011). For example, *At*KC1 is an electrically silent channel that regulates the voltage dependence of the *Arabidopsis* K^+ transporter 1 (AKT1) root channel when forming heteromeric channels (Geiger *et al.*, 2009a; Jeanguenin *et al.*, 2011; Reintanz *et al.*, 2002; Wang *et al.*, 2010). Therefore, SLAH1-SLAH3 interaction was revealed as a possible mechanism required for adequate regulation of Cl^- xylem translocation.

Functional expression in *Xenopus* oocytes and BiFC assays showed positive interaction between all tested S-type anion channels (Fig. 4.23). This indicates that SLAC/SLAH subunits are able to assemble as heteromeric channels, probably arranged as trimeric complexes where each subunit harbours it own pore, as suggested by the three-dimensional (3D) homology model (Fig. 1.18; Chen *et al.*, 2010). Interestingly, only the interaction between SLAH1 and SLAH3 changed the electrical current characteristics of SLAH3 (Fig. 4.24 a). Thus, macroscopic currents could be measured in the absence of an activating kinase (and without extracellular NO_3^-) with higher amplitudes as those recorded with kinase-activated SLAH3 (e.g. with CPK21ΔEF; Fig. 4.24 b-c).

The specifically regulation of SLAH3 by SLAH1 has been recently shown to be a function conserved across species borders, considering that after co-expressing SLAH1 with SLAH3-type anion channels from *Medicago trunculata* (*Mt*), *Dionaea muscipula* (*Dm*), and *Populus tremula* x *P. tremuloides* (*Ptt*), *At*SLAH1 was capable of activating *Dm*SLAH3, *Ptt*SLAH3 and *Mt*SLAH3, even

in the absence of extracellular NO_3^- and without co-expressing an activating kinase (Cubero-Font *et al.*, 2016).

Our regulatory model based on SLAH1/SLAH3 heteromerization requires the demonstration of a functional SLAH1-SLAH3 interaction *in planta*, and this evidence has been recently obtained (Cubero-Font *et al.*, 2016). In guard cells the SLAH3 channel requires kinase-mediated activation and exhibits a higher preference for NO_3^- (Geiger *et al*., 2011). In contrast the guard cell-specific SLAC1, besides NO_3^-, has a pronounced permeability for Cl^- (Geiger *et al*., 2009b). Although *AtSLAH1* is not expressed in guard cells, when the *slac1-2* line was complemented with *SLAH1* under the control of the SLAC1 promoter, the mutant phenotype was rescued as much as with SLAC1 (Cubero-Font *et al.*, 2016; Negi *et al*., 2008). These findings in guard cells are well in line with the *SLAH1* loss-of-gene function phenotype of reduced xylem sap Cl^- levels (Figs. 4.12 a and 4.13 a) and activation of SLAH3 by SLAH1 in the *Xenopus laevis* oocyte system (Fig. 4.24). The guard cell data together with those shown in this work indicate that *SLAH1*, via formation of SLAH1/SLAH3 complex, facilitates Cl^- efflux by rendering SLAH3 nitrate- and phosphorylation- independent.

5.1.1.5. SLAH1 does not conduct anions but regulates the conductance of SLAH3 for Cl^-

One of the most remarkable findings of this work has been to understand how SLAH1 functions as a molecular switch that modulates the Cl^- conductance of SLAH3. Rather than mediating Cl^- transport by itself, SLAH1 modifies the kinetic and regulatory properties of SLAH3 by the formation of heteromeric SLAH1/SLAH3 channels.

Two independent point mutations in SLAC1 with the ability to block the pore without significantly altering the general structure of the channel were reported: the substitution of the conserved hydrophobic phenylalanine residue F450 in the pore region (Fig. 4.20) by leucine (F450L) and the exchange of the small neutral glycine residue G194 present in the TM1 domain (Fig. 4.26) to a negatively charged aspartate (G194D; Chen *et al*., 2010; Negi *et al*. 2008).

The equivalent point mutations in *At*SLAH1 (F307L and R47D; Figs. 4.20 and 4.26) and in *At*SLAH3 (F517L and G264D; Figs. 4.20 and 4.26) were used to functionally express in *Xenopus* oocytes heteromers containing alternatively a wild-type subunit together with a mutant interacting partner unable to conduct anions. The assays shown in Figure 4.27 clearly establish that the WT SLAH3 channel was critical to elicit electric currents, whereas the non-functional mutants of SLAH1 (F307L and R47D) remained as competent as the WT to gate SLAH3 open in the absence of kinases and NO_3^- in the external buffer. This finding, in combination with the fact that the replacement of the conserved phenylalanine residue by alanine in SLAH1 (F307A) to obtain a constitutively open channel did not elicit macroscopic currents (Fig. 4.21), indicates that SLAH1 modifies the electrical properties of SLAH3, rather than adding a separate anion conductance to SLAH3.

An important difference that distinguishes the activity of the SLAH1/SLAH3 heteromer from the SLAH3 homomer is the magnitude of the Cl^- currents. Although the permeability for Cl^- relative to NO_3^- (P_{Cl^-}/P_{NO3^-}) was unchanged between the homomer and the heteromer (Fig. 4.30), the Cl^- currents of the SLAH1/SLAH3 complex were markedly higher compared to the currents of CPK21-activated SLAH3 homomeric channels (Fig. 4.24 b). Specifically, the Cl^-

conductance of the SLAH1/SLAH3 heteromeric channel was seven times higher than the kinase-activated SLAH3 homomeric anion channel, whereas the conductance for NO_3^- remained unaltered (Fig. 4.31).

The molecular mechanism underlying the enhanced Cl^- current amplitudes of the SLAH1/SLAH3 heteromer is probably the gating properties of the kinase-activated SLAH3 that depend on the presence of NO_3^- in the external buffer compared to the NO_3^--independent gating properties of the SLAH1/SLAH3 heteromer. The kinase-activated SLAH3 channel gating is modified by NO_3^- (Fig. 4.32), meanwhile it remains unaffected by Cl^-, i.e. the half-maximal ($V_{½}$) open probability do not reach the physiological membrane potential range (between –80 and –200 mV; Fromm and Lautner, 2007), supporting the previously published results (Geiger *et al.*, 2011). However SLAH1/SLAH3 channel complex has a relative open probability (rel. Po) that remains unaffected by the external anion composition (Fig. 4.32), being an evidence that the interaction of SLAH1 with SLAH3 gated SLAH3 open without the need of NO_3^-.

Thus, at physiological membrane potentials, CPK21-activated SLAH3 channels require extracellular NO_3^- to gate open, whereas the SLAH1/SLAH3 heteromer is already open in the absence of NO_3^- (Fig. 4.32). Therefore, the elevated Cl^- currents of the SLAH1/SLAH3 heteromeric channels (Fig. 4.24 b-c) result from the NO_3^--independent activation of SLAH3 (Fig. 4.32) and from an increase of its Cl^- conductance (Fig. 4.31), rather than from an increment in its Cl^- permeability (Fig. 4.30).

According to Chen and colleagues (2010) each subunit of the SLAC/SLAH anion channel complex harbours its own pore, in contrast to other channels that form a joint pore between the different subunits, like the Shaker K^+ channels (Doyle *et al.*, 1998; Uozumi *et al.*, 1998; Zhou *et al.*, 2001). The novel mechanism described in this work, by which the SLAH1 joining to SLAH3 modifies its channel characteristics, increases the diversity in channels functional properties. However, further 3D-structure guided research involving chimeric channels might elucidate the molecular mechanism underlying SLAH1-SLAH3 assembly.

5.1.1.6. The SLAH1-SLAH3 interaction determines the plant NO_3^- *versus* Cl^- selectivity

Taking into account the NO_3^- and Cl^- ion concentrations applied in the nutrient solution (3.5 mM NO_3^- and 5 mM Cl^-) *versus* their concentrations in the xylem sap, the different translocation efficiency exhibited by both anions in WT plants is remarkable: around 5–8 for NO_3^- and 0.5–0.6 for Cl^- (Table 4.1). This result is consistent with the differential translocation rates for NO_3^- and Cl^- quantified in WT plants (Fig. 4.12 c, e, h, j) and points to NO_3^-/Cl^- selectivity values of 8.4 and 14.0 in Wassilevskija and Col-0 ecotypes respectively in the root-to-shoot translocation process. This ratio is similar to the relative NO_3^-/Cl^- permeability of the SLAH1/SLAH3 heteromer (9.95 ± 1.60) measured in *Xenopus* oocytes (Fig. 4.30), indicating that the differential permeability for NO_3^- and Cl^- of the SLAH1/SLAH3 channel is a major mechanism determining the differential translocation efficiency of NO_3^- *vs.* Cl^- in plants.

In the *slah1* and *slah3* KO mutant lines, as well as in the *slah1-slah3* double mutant, the Cl^- translocation efficiency was reduced by half (Fig. 4.13 a, c and Table 4.1), while the NO_3^- translocation remained unchanged (Fig. 4.13 b, d and Table 4.1), increasing twice the NO_3^-/Cl^- selectivity (Table 4.1).

Qiu and colleagues (2016) have recently reported that *35S:AtSLAH3* overexpression lines accumulated significantly less Cl^- in the shoot, while the NO_3^- content remained similar to that of the control line. This could be related to the functional redundancy of the NO_3^- xylem translocation process previously discussed (section 5.1.1.2). Additionally, this could be also a consequence of a higher formation of SLAH3 homomers in the xylem pole pericycle leading to the detriment of the SLAH1/SLAH3 heteromers, being expected the reduction of the Cl^- conductance at the root symplast-xylem boundary. Furthermore, this could be an artifactual result of the constitutive higher expression of *AtSLAH3* in many different cell types.

On the assumption that NO_3^- is assimilated while Cl^- is accumulated in photosynthetic tissues, the regulatory mechanism based on SLAH1/SLAH3 heteromerization keeps a suitable balance between NO_3^- and Cl^- in the root-to-shoot translocation process. Taking into account the translocation efficiency values, *Arabidopsis* behave as NO_3^- includer and Cl^- excluder at the anion concentrations used in this work (Table 4.1). However, it must be clarified that the analyses of Cl^- content in xylem sap and in aerial organs have been performed with mature *A. thaliana* plants in an advanced developmental stage. As it will be afterwards discussed, we have observed in our laboratory that young plants (seedlings) from different plant species are much more active in transporting Cl^- and they clearly behave as Cl^- includer (Franco-Navarro *et al.*, manuscript in preparation). For example, in *Arabidopsis thaliana* plants treated with low chloride (75 μM Cl^-), shoot tissue Cl^- contents of around 0.5 mg g^{-1} DW were measured, while the contents obtained from young seedlings were 10 times higher, around 5 mg g^{-1} DW (Franco-Navarro *et al.*, manuscript in preparation).

It should be also keep in mind that the Cl^- inclusion capacity or the degree of NO_3^-/Cl^- selectivity probably change among plant species and varieties, since adult plants of tobacco grown with a nutrient solution containing 5 mM Cl^- accumulated a concentration of Cl^- of approximately 40–50 mg g^{-1} DW (Franco-Navarro *et al.*, 2016a), whereas the same treatment led to 19–38 mg Cl^- g^{-1} DW accumulation in in adult *Arabidopsis thaliana* plants (WS ecotype; Figs. 4.9 and 4.10 b). The NO_3^- translocation efficiency in the xylem sap of *A. thaliana* and tobacco adult plants barely differs, being 5.29 in *A. thaliana* ecotype WS (Table 4.1), 8.12 in *A. thaliana* ecotype Col-0 (Table 4.1) and 7.14 in *Nicotiana tabacum cv* Petit Havana (Colmenero-Flores JM, personal communication). However, the resulting NO_3^-/Cl^- selectivity values significantly vary, being 8.40 in *A. thaliana* ecotype WS (Table 4.1), 14.00 in *A. thaliana* ecotype Col-0 (Table 4.1) and 1.66 in *N. tabacum cv* Petit Havana (Colmenero-Flores JM, personal communication). Therefore, it could be assumed that tobacco plants have a Cl^- translocation efficiency 5–7 times higher and a NO_3^-/Cl^- selectivity 5–8 times lower than the *A. thaliana* ecotypes WS and Col-0.

5.1.1.7. SLAH1 regulation according to environmental cues: biological significance

A negative regulation of *AtSLAH1* and *AtSLAH3* genes by abiotic stress and ABA application was observed (Fig. 4.15 a). The down-regulation of the gene expression was stronger for *AtSLAH1* in comparison with *AtSLAH3*: *AtSLAH1* gene underwent a repression approximately of the double with salt stress (24 h after the 150 mM NaCl treatment), of 10 times by water deficit (24 h after 287 g l^{-1} PEG-8000 treatment), and of 40 times with the exogenous ABA application (3 h and 24 h after 100 μM ABA treatment) in relation to *AtSLAH3* transcripts.

While *AtSLAH1* was repressed about 70 times by water deficit (PEG-8000), *AtSLAH3* transcript level was reduced 6 times. In addition, *AtSLAH3* transcripts showed little modification to exogenous ABA application, maintaining the same basal response of the osmotic stress and the salt stress treatments (Fig. 4.15 a). This observation suggests that, contrary to *AtSLAH1*, *AtSLAH3* gene activity is insensitive to ABA in the root. Thus, these results indicate that *AtSLAH1*, in preference to *AtSLAH3*, is specifically down-regulated by abiotic stresses through a signalling pathway mediated by ABA.

It has recently been published that, 24 h after 150 mM NaCl treatment, *AtSLAH1* endured transcript level reductions of 7.5 times, meanwhile no repression was observed for *AtSLAH3* (Qiu *et al*., 2016). In addition, they also reported that 4 h after 20 μM ABA treatment, *AtSLAH1* transcript were decreased about 50%, whereas *AtSLAH3* underwent no down-regulation. These results support the idea that *AtSLAH1* is repressed by abiotic stress and ABA to a higher extent than *AtSLAH3*. The reduced response to ABA application of Qiu and colleagues (2016) compared to our results could be due to the phytohormone concentration, which was 5 times higher in our experiments.

The electrical properties of anion conductances found in xylem parenchyma protoplast of barley (*Hordeum vulgare*; Köhler and Raschke, 2000) and maize (*Zea mays*; Gilliham and Tester, 2005; Roberts, 2006) conform closely to the characteristics of SLAH3 anion channels expressed in *Xenopus* oocytes. In addition, taking into account that xylem parenchyma anion channels are differentially regulated by water stress and ABA (Gilliham and Tester, 2005), the transcriptional down-regulation of *AtSLAH1* by water deficit and ABA (Figs. 4.15 a and 4.16) provides strong evidence for involvement of the SLAH1/SLAH3 complex in anion xylem loading.

We have evidence that other stresses might have a similar effect on the regulation of root S-type channels, like nutritional stress or mechanical damage. The NO_3^- starvation treatment reduces the transcript levels of *AtSLAH1* approximately 46 times and those of AtSLAH3 around 6 times, whereas the NO_3^- application treatment after starvation has the opposite effect (Fig. 4.17). Furthermore, other interesting information suggests a possible effect of mechanical damage on SLAH1 activity. After trimming the plant shoot during the quantification of xylem sap assays, the Cl^- content gradually declines, while the NO_3^- content is maintained or even increased as time goes on (Fig. 4.11). This behaviour might respond to the specific repression of *AtSLAH1*, and not *AtSLAH3*, by ABA, which is also known to mediate mechanical damage responses (Peña-Cortés *et al.*, 1995).

The effects of abiotic stresses and ABA on *AtSLAH1* and *AtSLAH3* regulation have only been studied at the transcriptional level in this work, but there is evidence from other plant ion channel studies that protein abundance directly follows the respective transcript level with delay times of tens of minutes to a few hours (Bemm *et al.*, 2016; Philippar *et al.*, 1999; Sano *et al.*, 2007).

We propose a model that describes the regulation of SLAH3 activity by SLAH1 according to the environmental conditions. In plants growing under favourable conditions, high transcript levels of both *AtSLAH1* and *AtSLAH3* genes are expected to determine a higher contents of the SLAH1/SLAH3 heteromer in the xylem-pole pericycle cells, channeling both Cl^- and NO_3^- from the root to the shoot for the adequate plant growth (Fig. 5.1).

In response to adverse conditions *AtSLAH1* transcript abundance is reduced, increasing the SLAH3:SLAH1 transcript ratio about threefold 2 times by salt stress, 10 times by water

deficit and more than 40 times by ABA application in the root (Fig. 4.15 a). Thereby the SLAH1/SLAH3 complex in the plasma membrane is expected to decrease dramatically in favour of a higher content of phosphorylation-dependent SLAH3 homomeric channels, which exhibits a considerably lower conductance for Cl^-. In this way, the NO_3^- nutrition will be satisfied in the shoot, meanwhile the root-to-shoot Cl^- translocation will be significantly reduced (Fig. 5.1).

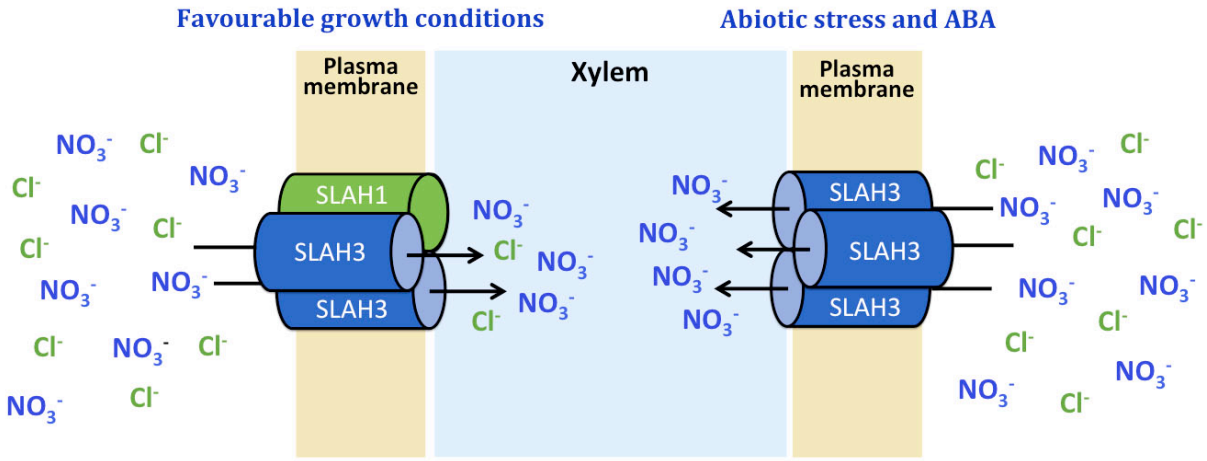

Figure 5.1. *At*SLAH1 modulates *At*SLAH3 anion conductance. Under favourable growth conditions (left) SLAH1/SLAH3 complex mediates chloride (Cl^-) and nitrate (NO_3^-) translocation into the xylem. However under different environmental stress situations (right), gene expression of *AtSLAH1* is strongly reduced by an abscisic acid-dependent regulatory pathway, favouring the formation of the SLAH3/SLAH3 homomers that significantly reduces the Cl^- conductance, decreasing its accumulation in the shoot.

Finally, it should be noted that the inhibition of ion channels activity by ABA in root vascular cells is opposite to the effects of this hormone in guard cells (Geiger *et al.*, 2009b, 2011; Maierhofer *et al.*, 2014a; Roelfsema *et al.*, 2012; Schroeder *et al.*, 2001a).

5.1.1.8. SLAH1 regulation during plant acclimatization to water deficit

The inorganic ions K^+, Cl^- and NO_3^- play essential roles in plant cell osmotic regulation. A well-known physiological mechanism of plant acclimatization to water deficit is an increased ability of the roots to reduce their solute potential in order to promote cell expansion, maintaining root growth capacity under stress conditions (Hsiao and Xu, 2000; Saab *et al.*, 1990; Sharp and Davies, 1979).

This response mediated by ABA triggers changes in expression of different sets of genes and post-translational modifications (Chandler and Robertson, 1994; Hoth *et al.*, 2002; Leung and Giraudat, 1998). Water deficit and ABA increase solute accumulation within the root by significantly inhibiting the release of ions into the xylem, but having little effect on ion influx into the root (Cram and Pitman, 1972; Pitman, 1977; Pitman and Wellfare, 1978; Pitman *et al.*, 1974).

In maize root stele, water stress and ABA down-regulate the activity of ion channels involved in xylem loading of inorganic ions, such as the stelar K^+ outwardly-rectifying channel SKOR (Roberts, 1998; Roberts and Snowman, 2000) and the xylem-parenchyma quickly activating anion conductance (X-QUAC; Gilliham and Tester, 2005) involved in xylem loading of NO_3^- and Cl^-. In addition, the *Arabidopsis thaliana AtSKOR* gene is down-regulated by ABA (Gaymard *et al.*, 1998), similarly to the transcriptional repression of *AtSLAH1* (Fig. 4.15 a). The

fact that stress represses more strictly *AtSLAH1* expression compared to *AtSLAH3* (Fig. 4.15 a), indicates that plants use preferentially Cl^- over NO_3^- for root osmotic regulation. This observation is consistent with recent data reporting a specific and central role of Cl^- in plant osmotic and water regulation (Franco-Navarro *et al*., 2016a). In addition, other important mechanism of stress tolerance is expected to require continuous supply of nitrogen (NO_3^-) to the shoot: the synthesis of N-compounds needed as cell-protectant molecules, such as compatible osmolytes (amino acids and derivatives, methylammonium and methylsulfonium solutes) as well as polypeptides like dehydrins and heat-shock proteins, whose biosynthesis is required for survival (Garay-Arroyo *et al.,* 2000; Kotak *et al*., 2007; Yancey 2005).

Following the same line of reasoning as the previously described model (Fig. 5.1), favourable growth conditions leads to a high amount of SLAH1/SLAH3 heteromers in the xylem-pole pericycle, mediating the translocation of both Cl^- and NO_3^- to the xylem This ensures an adequate flow of nitrogen and high quality osmolytes, favouring cell division and expansion in actively growing shoot tissues.

Under water deficit, our results indicate that the stress hormone ABA mediates a strong reduction of the SLAH1/SLAH3 heteromer and, consequently, of root-to-shoot Cl^- translocation. The biological process underlying this differential regulation could be the specific retention of Cl^-, not NO_3^-, in the root during plant acclimatization to water deficit, stimulating root osmoregulation and growth. Thus, the plant will be able to explore a wider volume of soil and therefore the roots will find more sources of water or nutrients to avoid the stress situation**.**

The effect of NO_3^- starvation (Fig. 4.17) on the reduction of *AtSLAH1* and *AtSLAH3* gene expression was similar to the osmotic stress response (Fig. 4.15 a). This finding indicates that this nutritional stress also stimulates the retention of Cl^- in the root, encouraging root growth to promote a wider root exploration capacity in search of new sources of nitrogen in the soil.

5.1.1.9. SLAH1 regulation during plant acclimatization to salinity

To date sodium (Na^+) is the salt component that has been most commonly associated with ion toxicity and crop yield decrement in soils affected by salt stress. However, in wood perennial species, like citrus (*Citrus* spp.; Brumós *et al*., 2009, 2010; Moya *et al*., 2003; Storey and Walker, 1999), grapevine (*Vitis* spp.; Fort *et al*., 2013; Gong *et al*., 2011; Tregeagle *et al*., 2010) and avocado (*Persea americana*; Bar *et al*., 1997; Mickelbart and Arpaia, 2002), and in legumes, as soybean (*Glycine max*; Luo *et al*., 2005), the accumulation of Cl^-, not Na^+, in leaves correlates better with reduced transpiration, photosynthesis, crop yield and quality, and with plant death (Li *et al*., 2017). These relationships are due to the fact that these species are able to release a higher proportion of Na^+ into the root and/or woody stems, rather than because Cl^- is metabolically more toxic than Na^+ to these plants.

Root-to-shoot translocation is the most important mechanism regulating shoot Cl^- accumulation in plants (Brumós *et al*., 2010; Gong *et al.,* 2011; Tregeagle *et al.,* 2010) and, as it has been previously discussed, it is expected that xylem loading of NO_3^- and Cl^- has to be tightly regulated for maintaining an appropriate balance between both anions.

We have shown that salt stress negatively regulates the *AtSLAH1* transcript accumulation (Fig. 4.15 a), with values very similar to those reported by Qiu and colleagues (2016). Unlike PEG-8000, which is not permeable to the root, NaCl ions enter the root and subsequently move

towards the shoot, without generating a water deficit so pronounced as PEG-8000. This fact probably explains why the saline treatment induced a lower gene expression (Fig. 4.15 a).

According to the regulatory model described before (Fig.5.1) the down-regulation of *AtSLAH1* transcript reduces the net transfer of Cl^- into the root xylem, limiting the accumulation of Cl^- in the leaves. Taking into account that Cl^- exclusion is an important agronomic trait, especially for Cl^- sensitive crops of great economic importance like citrus and grapevine, and since SLAH1 determines a significant contribution to the degree of Cl^- exclusion without affecting the inclusion of NO_3^-, the *AtSLAH1* gene arises as a novel biotechnological tool with great potential for engineering salinity-tolerant plants. For example, varieties of citrus rootstocks mutated in the corresponding ortholog gene of *AtSLAH1* could be created and, once grafted these varieties with the variety of interest, plants with a greater capacity to exclude Cl^- and, therefore, more tolerant to salinity would be obtained.

5.1.2. Putative function of SLAH1/SLAH3 in plant fertility

The *AtSLAH1* gene is expressed in the flower, specifically at the filament insertion in the anther and at the stigmatic papillae cells in the pistil (Fig. 4.33). The expression pattern of P_{SLAH1}-GFP::GUS construct within the flower, and also in the root stele, matches the tissue distribution data obtained from microarrays expression profiling experiments datasets (available at www.genevestigator.org). *AtSLAH3* expression is also located in stigmatic papillae cells as *AtSLAH1* (Fig. 4.34 c). The expression of other Cl^- transporters have also been located in the flower like the *At*CLCa and *At*CLCc (Lv *et al.*, 2009) or the Cation-Chloride Cotransporter *At*CCC, which is expressed in the staments and in pollen grains (Colmenero-Flores *et al.*, 2007).

Chloride and K^+ are required to maintain the turgor pressure necessary for cell growth (Babourina *et al.*, 1998b; Franco-Navarro *et al.*, 2016a; Long and Iino, 2001; Yamagami *et al.*, 2004), as well as for fast turgor regulation, e.g. in *Arabidopsis* epidermal root cells (Shabala and Lew, 2002). In addition Cl^- is involved in osmorregulation in the stigma of grasses. Chloride ions, together with K^+, account for 60% of the osmolality of stigma sap in the angiosperm *Pennisetum* (Heslop-Harrison, 1990; Heslop-Harrison and Reger, 1986) and these ions are crucial in maintaining the turgidity of the stigmatic cells, as well as in the anther filament (Heslop-Harrison, *et al.*, 1987). The transport of both ions into the stigma primordium from the surrounding tissue followed by a sudden flux of water probably provide the turgor required for fast cell elongation of the stigma within minutes, extending the stigma at the onset of the anthesis.

In addition, *AtSLAH3* expression was detected in pollen grains and pollen tubes within the pistil of *Arabidopsis* (Fig. 1.15; Gutermuth *et al.*, 2013), where the SLAH3 channel is implicated in the regulation of pollen tube growth. Similarly to *AtSLAH3*, the chloride channel *At*CLCc is expressed in guard cells and in the root, but also in pollen and shows enhanced expression in mature pollen grains (Bock *et al.*, 2006; Jossier *et al.*, 2010). Chloride also plays a role in pollen tube development since Cl^- fluxes are required for growth and cell volume regulation (Zonia *et al.*, 2002).

The significantly reduction observed in seed yield in *slah1-2* mutant line (Fig. 4.35 e) determined a significantly lower harvest index (HI; Fig. 4.35 a). The fact that there was no difference in the number of siliques produced by *slah1-2* and WT plants in one of the assays (Fig.

4.8 b) supports that the observed significant difference in the harvest index is exclusively due to the seed production.

Therefore, the function of SLAH1 and SLAH3 channels in mobilization of anions, the specific tissue expression pattern of both *AtSLAH1* (Fig. 4.33) and *AtSLAH3* (Fig. 4.34 c) in flower organs, and the reduced seed production and impaired harvest index phenotype of the *slah1-2* mutant line (Fig. 4.35 a), strongly suggest that the SLAH1/SLAH3 complex play an important role in flower anthesis and fertility.

5.2. SLAH4 CHARACTERIZATION

5.2.1. Postulated role of SLAH4 in the release of Cl^- from the root

According to phylogenetic analyses of the SLAC/SLAH family, *AtSLAH4* is the closest homologue of *AtSLAH1*, belonging to the same similarity group (the SLAH1/4 group; Brumós *et al.*, 2010; Dreyer *et al.*, 2012; Negi *et al.*, 2008; Zheng *et al.*, 2015). *Arabidopsis thaliana* SLAH1 and SLAH4 are highly homologous proteins that share 84% protein sequence identity. Within the SLAH1/4 group, channel identities are highly conserved in angiosperm (around 58%). In contrast, inter-group identities of the SLAH1/4 group with other groups are lower: 35% with the SLAH2/3 group and 36% with the SLAC1 group (Dreyer *et al.*, 2012).

5.2.1.1. *AtSLAH4* transcript accumulates in root epidermal and cortical cells

The *AtSLAH4* gene is specifically expressed in cortical and epidermal cells (Fig. 4.36 e-f). But, according to Zheng and colleagues (2015), *AtSLAH4* expression localizes to the vascular cylinder. Our P_{SLAH4}-GFP::GUS *Arabidopsis* transgenic lines contain a 2917 bp DNA fragment of the *AtSLAH4* promoter and the UTR 5' region (which contains the Intron-1, located upstream of the predicted the ATG start codon) of the *AtSLAH4* gene, being 1313 bp longer than the construction used in the work reported by Zheng and colleagues (2015). The GUS staining pattern that they reported in intact roots (Fig. 1.15) showed peripheral cell layers apparently unstained. This fact might be caused by the reflection of the white light at the surface of the root, similarly to our P_{SLAH4}-GFP::GUS stained roots shown in Figure 4.36 a. However Zheng and colleagues (2015) did not provide images from root sections or confocal microscopy to localize more accurately the *AtSLAH4* expression, as we did.

This localization indicates that SLAH4 mediates anion transport between the external medium and the plant symplast. The SLAC/SLAH channel family allows the fluxes of molecules across cell membranes along their electrochemical gradient. SLAC/SLAH channels are depolarization-activated anion channels, implying that they display the lowest degree of activity at negative membrane potentials (Vm < −150 mV) and are activated when the plasma membrane becomes more positive (depolarizes). Anion influx through anion channels only takes place when the membrane potential becomes more positive than the equilibrium potential for the anion, i.e., when the external concentration of the anion is higher than the internal concentration (e.g. under salt stress) or if the membrane potential in the cell depolarizes. In the absence of environmental stresses and under most physiological circumstances, the internal concentration of NO_3^- and Cl^- anions is higher than the external concentration and thus the membrane potential is more negative than the equilibrium potential for these anions, being

favoured the release of them from the cell through channels, which indicates that SLAC/SLAH channels mediate anion efflux from plant cells.

Under non-saline conditions net anion uptake in root epidermal and cortical cells results from the homeostatic equilibrium between the active uptake through anion/H^+ cotransporters and the passive release through anion channels (Britto and Kronzucker, 2006). Chloride-mediated anion efflux has been proposed to make a considerable contribution to the resultant net Cl^- uptake at plasma membrane potentials more negative than –50 mV (Babourina *et al.,* 1998b). Therefore, we propose that SLAH4 mediates anion (Cl^- and/or NO_3^-) efflux and participates in the regulation of net anion uptake in plants.

This hypothetical function assumes that SLAH4, as demonstrated for the other channels of the SLAC/SLAH family (Fig. 1.16; Negi *et al*., 2008), localizes to the plasma membrane. However SLAH4 localization has not been determined yet, although we have made transgenic *Arabidopsis* plants overexpressing the chimeric *SLAH4::GFP* construction to determine its subcellular localization.

5.2.1.2. Disruption of the *AtSLAH4* gene leads to a higher Cl^- content in the shoot

Since S-type anion channels are permeable to NO_3^- and Cl^- (Geiger *et al.*, 2009b, 2011; Schmidt and Schroeder, 1994), *slah4-2* KO mutant plants were grown with different chloride concentration treatments to identify possible phenotypic differences in relation to its wild-type (Col-0) line.

The most significant phenotype associated to the lack of the function of the *AtSLAH4* gene was a higher accumulation of Cl^- in the shoot of *slah4-2* plants treated with low nitrate (0.25–0.75NO_3^-) and high chloride (4.75–5 mM Cl^-), only observed during late developmental stages (Fig. 4.45 c, e, f). In the treatment with high nitrate (5 mM NO_3^-) and low chloride (0.075 mM Cl^-), the opposite phenotype was observed in the youngest developmental stage (vegetative phase stage [1] in Fig. 4.45 a), showing the Col-0 plants more Cl^- accumulated than the *slah4-2* mutant plants. This result might be in relation with the fact that the *AtSLAH4* gene is not expressed in the early vegetative stages during seedling establishment (Fig. 4.38).

In the presence of high Cl^- in the nutritional medium (around 5 mM Cl^-), Col-0 WT plants were able to maintain a homeostatic shoot Cl^- content of approximately 7–15 mg g^{-1} DW during their development (Fig. 4.45 c ,e, f). In contrast, *slah4-2* mutant plants showed a continuous increase in the Cl^- content (between 10–21 mg g^{-1} DW) from the onset of the reproductive stage (Fig. 4.45 c ,e, f). This might indicate that *AtSLAH4* is positively regulated at the transcriptional or post-transcriptional level during late developmental stages. Another possibility could be that SLAH4 activity remains constant and the continuous increase in the Cl^- content of *slah4-2* plants is as a consequence of the reduction of vegetative growth during late plant development, when plants allocate their energy to the production of flowers and siliques. Anyway, the progressive Cl^- accumulation in the shoot of *slah4-2* plants supports the idea that the SLAH4 channel is involved in Cl^- efflux from the root and regulates net Cl^- uptake during plant development.

Besides SLAH4, other ion channels and transporters expressed in cortical and/or epidermal cells have been suggested to contribute to the efflux of anions from the root. The NPF2.5 transporter has been proposed to modulate Cl^- efflux from roots of *A. thaliana* plants (Li

et al., 2017), and the *At*NPF2.7 (also called NAXT1) mediates NO_3^- excretion to alleviate cytoplasmic acidification (Segonzac *et al.*, 2007). Similarly to the higher Cl^- content in *slah4-2* mutant line, the *npf2.5* KO line also accumulated significantly higher Cl^- in the shoot relative to the WT line (Li *et al.*, 2016). The anion content of the nutritive solution, especially the Cl^- concentration, and the age of the harvested plants lead to differences in shoot Cl^- content, as it can be observed in Figure 4.45. Taking into account that *npf2.5* KO plants were grown with 75 mM NaCl applied to the basal nutrient solution (BNS; Conn *et al.*, 2013), which contained approximately 3.6 mM Cl^- and 9 mM NO_3^-, it had a Cl^-/NO_3^- ratio of 5.00/0.57, which is similar to the Cl^-/NO_3^- ratio applied in the nutrient solution in the *slah4-2* assay.

5.2.1.3. *AtSLAH4* gene disruption results in a higher growth of shoot organs

Chloride is specifically demanded as a beneficial and osmotically active solute that provides cell turgor and is necessary for optimal cell elongation (Franco-Navarro *et al.*, 2016a). There are physiological and genetic evidences that indicate that Cl^- participates in cell volume regulation and elongation processes in root and shoot organs in different cell types like: the coleoptile of grass seedlings (Babourina *et al.*, 1998a), the flower organs of grasses at the onset of flower anthesis (Heslop-Harrison and Reger, 1986) and of *Arabidopsis* plants (Fig. 4.33), the pulvini of *Mimosa pudica* (Fromm and Eschrich, 1988), and *Phaseolus vulgaris* (Iino *et al.*, 2001) during seismonastic leaf movements, epidermal cells from elongation internodes of *Pisum sativum* (Yamagami *et al.*, 2004) and from tobacco leaves (Franco-Navarro *et al.*, 2016a), and guard cells (Broadley *et al.*, 2012b). In addition, lack-of-function mutant lines of the cation-Cl^- cotransporter genes *AtCCC* from *A. thaliana* (Colmenero-Flores *et al.*, 2007) and *OsCCC* from *O. sativa* (Chen *et al.*, 2016) exhibit phenotypes of impaired growth or cell elongation in shoot and root organs, respectively.

Potted plants from the *slah4-2* mutant line grown in solid substrate with a nutrient solution containing either 70 µM Cl^- or 5 mM Cl^- had significantly bigger shoot organs than Col-0 plants (Figs. 4.43 and 4.44), given that *slah4-2* plants showed: rosettes with longer diameter (Figs. 4.43 a-b and 4.44) and higher number of leaves during the vegetative stage (Figs. 4.43 e, f and and 4.44), and longer floral stems at the reproductive phase (Fig. 4.43 i-j). Moreover, similar results were obtained in hydroponic plants (Figs. 4.41 and 4.42). This results obtained from phenotypic assays of the *slah4-2* line and those discussed above (section 5.2.1.2) are in accordance with the fact that Cl^- accumulation specifically determines a plant biomass increase (Franco-Navarro *et al.*, 2016a).

5.2.1.4. Expression of *AtSLAH4* in the root is switched off during seedling establishment

It is expected that Cl^- plays an important role as osmolyte, stimulating turgor and cell expansion during the fast vegetative growth stage of plants. The absence of *AtSLAH4* transcript accumulation is developmentally regulated during the seedling establishment in *A. thaliana* (from 0–7 days after germination; Fig. 4.38). This suggests that no activity of the SLAH4 channel is required for maximizing net Cl^- uptake in the root during early vegetative development. This point will be discussed to a greater extent in section 5.3.1.

5.2.1.5. Expression of the *AtSLAH4* gene in the root is negatively regulated by abiotic stresses

According to the proposition that SLAH4 regulates net Cl^- uptake in the plant root, the negative regulation of the *AtSLAH4* gene expression by osmotic stress and ABA application (Fig. 4.46), implies that the increase of root Cl^- content is an acclimatization mechanism to withstand osmotic stress (e.g. water deficit), probably for rapidly regulating the cell osmolarity in root tissues. This point will be further discussed in section 5.3.4.

Since the down-regulation of *AtSLAH4* assumes a greater uptake of Cl^- anions, is difficult to reconcile the negative regulation of the *AtSLAH4* gene by salt stress (Fig. 4.46) with our proposal that SLAH4 mediates Cl^- release to the rhizosphere. It is possible that the observed response to salinity is due to the rapid ABA-mediated regulation to the osmotic shock produced by the high concentration of NaCl. It could be expected no repression or even induction of the *AtSLAH4* gene at longer NaCl exposition times, when the toxic component of salt stress is harmful to the plant.

5.2.1.6. *AtSLAH4* expression is associated to auxin activity

AtSLAH4 was expressed within the hydathode pores of seedlings in cotyledons 3 days after sowing (das), in primary leaves 7 das and in the second pair of leaves 12 das (Fig. 4.38). In the shoot of thirteen-day old plants, *AtSLAH4* gene expression was localized in leaf hydathodes and meristems (Fig. 4.37). Leaf meristems are the first major sites of free-auxin production at very early stage of leaf development and contain high IAA concentrations (Aloni *et al.*, 2003). In addition, hydathodes are organs identified as primary sites of high free-auxin production (Aloni, 2001; Aloni *et al.*, 2003; Baylis *et al.*, 2013) and auxin accumulation (Teale *et al.*, 2006). The *Arabidopsis* Cation-Chloride Cotransporter *AtCCC* is also expressed in these leaf organs (Colmenero-Flores *et al.*, 2007).

In plants, IAA is the predominant auxin and an indispensable phytohormone involved in the regulation of many aspects of plant development (Teale *et al.*, 2006), mainly through its differential distribution within plant tissues. In particular, the auxin is involved in cell elongation and chloride is an import osmotic effector in plant cells to support the turgor pressure, necessary for plant growth (Babourina et al., 1998b; Long and Iino, 2001; Yamagami et al., 2004). Thus, it is expected that anion movements through plasma membranes, when coordinated together with cation fluxes, have a crucial role in the regulation of cell turgor, which is a key point in the control of cell elongation.

AtSLAH4 transcript levels in roots of plants grown in a solution containing either 70 µM or 5 mM Cl^- were down-regulated by IAA (Fig. 4.49). This suggests that IAA promotes higher net Cl^- uptake, which encourages plant cell osmoregulatory responses, including auxin-mediated stimulation of cell elongation.

5.2.1.7. Model of SLAH4 biological function

Considering that *AtSLAH4* is expressed in peripheral cell layers of the root (epidermis and cortex; Fig. 4.36), and probably SLAH4 channels are located in the plasma membrane of these cell types (section 5.2.12), together with the higher accumulation of Cl^- in the shoot of

slah4-2 line plants (Fig. 4.45), we propose that the biological function of the S-type anion channel SLAH4 in the root consists of mediating Cl^- release from the cytoplasm to the apoplast or to the rhizosphere.

Under control conditions, *At*SLAH4 participates in Cl^- efflux from the cytoplasm of epidermal and cortical cells of the root to either the apoplast or the rhizosphere when the Cl^- concentration inside the cell is higher than outside (Fig. 5.2).

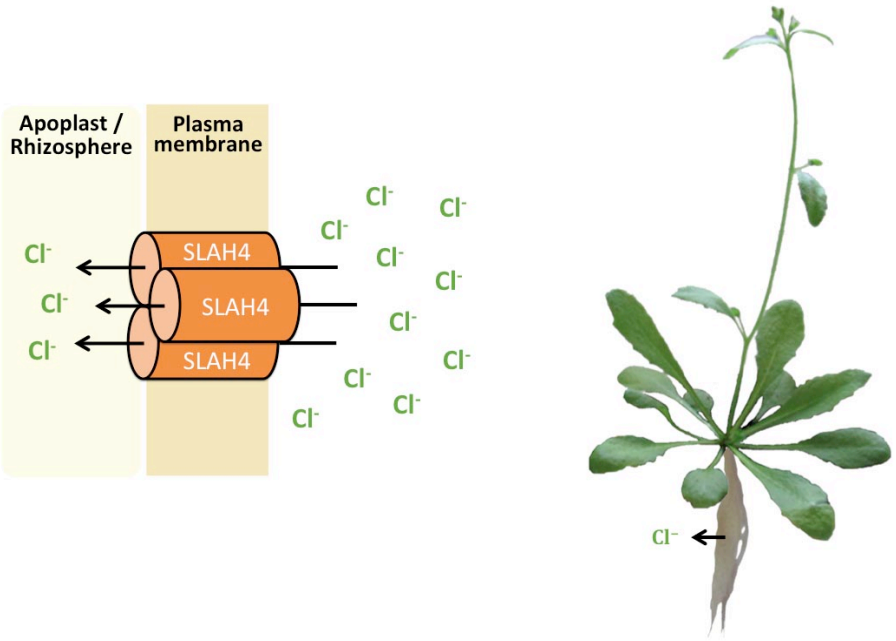

Figure 5.2. Model describing the hypothetical function of *At*SLAH4 in plant roots. SLAH4 channel mediates chloride (Cl^-) release from the plant root to the apoplast or the rhizosphere under favourable conditions.

In contrast, under stress conditions, *AtSLAH4* expression is down-regulated and the channel protein abundance will be reduced. Under this situation, Cl^- efflux from the root will be limited and net Cl^- uptake increased.

*At*SLAH4 protein localization at the plasma membrane has to be confirmed and SLAH4 remains to be functionally characterized in the heterologous *Xenopus* oocyte expression system to address its kinetic properties, anion permeability, the factors that control its gating and the molecular mechanisms that regulate the channel activity.

5.3. THE INTEGRATED FUNCTION OF THE ROOT SLAH1, SLAH3 AND SLAH4 CHANNELS IN THE REGULATION OF PLANT Cl^- HOMEOSTASIS

According to the results shown in this work, net Cl^- uptake (controlled by *AtSLAH4* gene expression in the root peripheral cell layers) and Cl^- root-to-shoot translocation (regulated by SLAH1/SLAH3 in the xylem-pole pericycle) are critical pathways for controlling Cl^- homeostasis at the whole plant level.

*At*SLAH2 is the fourth member of the SLAC/SLAH family expressed in the root, particularly in the root stele (Fig. 1.15; Maierhofer *et al.*, 2014b; Negi *et al.*, 2008; Zheng *et al.*, 2015). Although SLAH2 is a NO_3^--selective anion channel (Maierhofer *et al.*, 2014b), it could be

indirectly involved in the regulation of Cl^- fluxes through the control of NO_3^- transport, a well-known antagonistic anion to Cl^- transport and accumulation in plants (Xu *et al.*, 2000).

We propose the following model on the regulation of plant Cl^- homeostasis based on the activity of SLAH4, SLAH3 and SLAH1 root anion channels, which are in turn regulated by developmental and environmental factors.

5.3.1. Cl^- homeostasis during seedling establishment

Our group has shown that, besides being an essential micronutrient, Cl^- is a beneficial macronutrient (Franco-Navarro *et al.*, 2016). Chloride is specifically demanded as an osmotically active solute that provides cell turgor and is required for optimal cell elongation (Chen *et al.*, 2016; Franco-Navarro *et al.*, 2016). We have compiled evidence that demonstrates that Cl^- incorporation to macronutrient levels is essential for the proper development of different plant species during early vegetative growth (Franco-Navarro *et al.*, manuscript in preparation). After germination under favourable conditions, seedling establishment is a period of rapid vegetative growth that requires abundant acquisition of nutrients for an efficient development. An important part of these nutrients comes from the seed storage reserves, but the Cl^- content is expected to be low in the seeds, which are predominantly fed through the phloem (White and Broadley, 2001; Xu *et al.*, 2000). In tobacco plants grown with 5 mM Cl^-, the content of Cl^- in the seed is about 15 times lower than the leaf Cl^- content (Franco-Navarro *et al.*, manuscript in preparation).

Given the low Cl^- content in the seed and the high demand needed to satisfy an active growth of the seedling, it is expected that high Cl^- uptake is required during this developmental stage. Chloride enters the root symplast through high- and low- affinity active $Cl^-/2H^+$ symporters (Fig. 5.3; Beilby and Walker, 1981; Britto and Kronzucker, 2006; Felle, 1994; Sanders, 1980; White and Broadley, 2001), but net Cl^- uptake results from the homeostatic equilibrium between its active uptake and its passive release through anion channels.

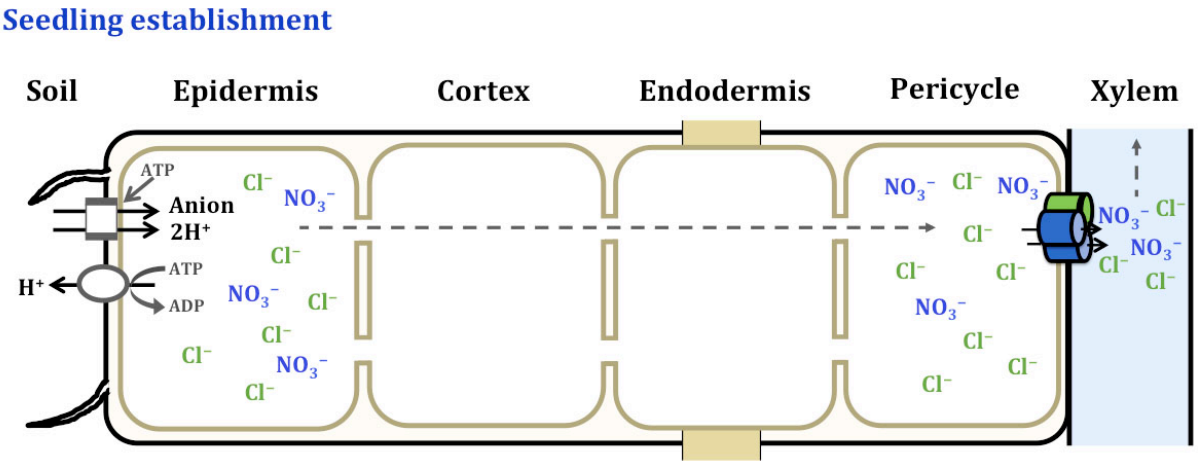

Figure 5.3. Model of SLAC/SLAH family channels activity within the root during early seedling development. During the first days of seedling establishment, the acquired chloride (Cl^-) and nitrate (NO_3^-) by H^+/Cl^- symporters at the root are allocated to the shoot through SLAH1/SLAH3 heteromers (green and blue). Further on the seedling development, SLAH4 channels (orange) have a role in net Cl^- uptake by releasing this anion from the root to the apoplast or the rhizosphere.

AtSLAH4 is an anion channel gene expressed in epidermal and cortical cells (Fig. 4.36) that, according to our results, regulates net Cl^- uptake in *A. thaliana* through the regulation of Cl^- release to the apoplast and the soil rhizosphere. It is noteworthy that *AtSLAH4* is not expressed in the root during the first days of the seedling establishment (Fig. 4.38), which is expected to strongly increase net Cl^- uptake at this developmental stage. In contrast, *AtSLAH1* is permanently expressed in the root since the first days after germination (Fig. 4.38). Therefore, The absence of SLAH4 and the presence of SLAH1 after germination under favourable conditions (Fig. 5.3) ensure abundant net uptake and efficient shoot translocation of Cl^-, providing an optimal Cl^- nutrition to the actively growing root and shoot organs.

5.3.2. Cl^- homeostasis in plants under favourable growth conditions

After seedling establishment and under favourable conditions, it is expected that the transcriptional induction of the *AtSLAH4* gene reduces net Cl^- uptake. Given that Cl^- is not assimilated, an adequate equilibrium between uptake and release must be reached to prevent an excessive accumulation of Cl^- in the shoot.

The aerial part of the plants requires a continuous supply of Cl^-, mainly during their vegetative development. In addition, the biggest reserves of Cl^- in the plant are found in the large vacuoles of leaf cells, so that efficient root-to-shoot xylem translocation of Cl^- is necessary in healthy growing plants. As discussed above (section 5.1.1.7), efficient xylem Cl^- translocation requires high transcriptional activity of *AtSLAH1* and *AtSLAH3* genes, as well as SLAH1/SLAH3 channel heteromerization in xylem-pole pericycle cells (Fig. 5.1).

Therefore, according to our model (Fig. 5.4), optimal growth of plants after seedling establishment under favourable conditions requires active expression of *AtSLAH4*, *AtSLAH1* and *AtSLAH3* genes for optimal modulation of Cl^- uptake and for root-to-shoot Cl^- translocation.

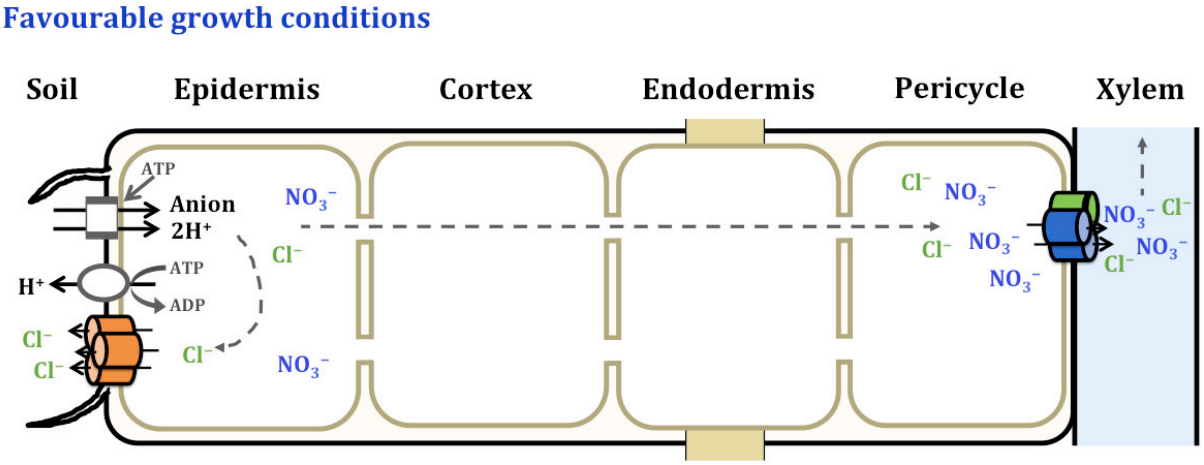

Figure 5.4. Model of SLAC/SLAH family channels activity within the root under favourable growth conditions. Under favourable conditions anion uptake is mediated by H^+/Cl^- symporters. In addition, SLAH4 channels (orange) mediate chloride (Cl^-) efflux from the root into the apoplast or the rhizosphere, while SLAH1/SLAH3 complex mediate Cl^- and nitrate (NO_3^-) translocation into the xylem.

5.3.3. The homeostatic model conforms to the phenotype of the *slah1* and *slah4* mutant lines grown under favourable conditions

The phenotypes associated with the lack of function of the *AtSLAH1* and *AtSLAH4* genes and their dependency on the level of Cl^- availability reinforce the function assigned to the SLAH1 and SLAH4 channels in the regulation of Cl^- nutrition (net uptake and root-to-shoot translocation of Cl^-, respectively), as well as the role of Cl^- on plant growth and development. While the *slah4-2* mutant line increased net Cl^- uptake, leading to plants with bigger root and shoot organs, the *slah1-2* mutant line reduced shoot Cl^- accumulation, resulting in a deficiency in development or in functions within aerial organs.

On the one side, hydroponically grown plants from the *slah4-2* mutant line presented significantly longer root length (Figs. 4.40 a-b and 4.41 a-b) and higher fresh (Fig. 4.40 e) and dry weight (Fig. 4.40 i) in comparison to the WT Col-0 line. The differences were more evident and significant in plants treated with low chloride (70 μM Cl^-) relative to the high chloride (5 mM Cl^-) treatment, indicating that suboptimal Cl^- nutrition magnify the differences between the mutant and the Col-0 line (Fig. 4.40 a-b, e-f, i-j). In potted plants grown with nutrient solutions containing different NO_3^-/Cl^- ratios, the *slah4-2* mutant also presented significantly higher shoot Cl^- content than the Col-0 line (Fig. 4.45), which correlates with bigger shoot organs (rosette diameter and number of leaves and inflorescences (Figs. 4.41 a-b; 4.42 a-b, e-f, i-j; 4.43 a-b, e-f, i-j and 4.44 a-b). Both *slah4-2* mutant and Col-0 lines exhibited a significantly higher number of rosette leaves when treated with the highest Cl^- treatment (Fig. 4.43 g-h).

On the other side, *slah1-2* mutant plants showed significantly lower development than the WT line of the root (Fig. 4.4 b), the rosette (diameter and number of leaves; Fig. 4.7 a, b) and of the floral stem (Fig. 4.8 a) principally under the high chloride (5 mM Cl^-) treatment. In addition, potted plants from the *slah1-2* mutant line presented significantly lower Cl^- content in the shoot than plants from the WT line (Figs. 4.9 and 4.10), and this finding correlates with the smaller shoot organs observed (Figs. 4.7 a, b and 4.8 a)._Moreover, Qiu and colleagues (2016) have recently published that the *slah1* knockdown mutant lines, generated by artificial microRNAs, with reduced *AtSLAH1* expression showed lower shoot Cl^- accumulation when growing with 2 mM NaCl treatment (with approximately 4 mM Cl^-). And the opposite phenotype was observed in lines overexpressing, constitutively or specifically in root stele cells, the *AtSLAH1* gene, i.e. these plants had chloride contents in the shoot significantly higher that those of the control line (Qiu *et al*., 2016).

According to the idea that the distinguishing phenotype was due to the differential amount of Cl^- transported to the shoot, which was lower in the *slah1-2* mutant than in the WT line, both lines exhibited bigger rosette development (diameter and number of leaves; Fig. 4.5 c, d, g, h) when treated with the highest Cl^- treatment under hydroponics conditions. The increase in the rosette development found in the *slah1-2* (Fig. 4.5 c, g) and *slah4-2* (Fig. 4.43 c, g) mutant lines and in the respective WT lines (Fig. 4.5 d and 4.43 d, h), which is related to the rise in Cl^- accumulation in the shoot, is in accordance with the fact that chloride is accumulated in leaves of plants under non-saline conditions (Brumós *et al.*, 2010; Franco-Navarro *et al.*, 2016a; Tadeo *et al.*, 2008).

5.3.4. Cl^- homeostasis in plants under abiotic stress conditions

In response to abiotic stresses (water deficit, **NO_3^- deficiency** and salinity), *AtSLAH1* and *AtSLAH4* genes expression is down-regulated by ABA and thus, the reduction of the respective protein abundance is expected with delay times of tens of minutes to a few hours. However, it must be considered that the *AtSLAH1* gene expression is significantly more sensitive than the *AtSLAH4* expression to the regulation by abiotic stress and ABA, i.e. *AtSLAH1* transcriptional repression is higher. The decrease of the SLAH1 and SLAH4 channels quantity in their respective cell types involves a diminution in the Cl^- outflow from the root to both the external medium and the shoot (Fig. 5.5). This result in an increased retention of Cl^- in the root, contributing to the reduction of the osmotic potential to generate water retention, turgor and cell expansion, as discussed previously. This will stimulate root growth, thus allowing efficiently exploring a bigger volume of soil in search of water or nutrients (Hsiao and Xu, 2000; Saab *et al.*, 1990; Sharp and Davies, 1979).

Under salt stress, reduced translocation of Cl^- into the xylem alleviates excessive Cl^- accumulation in the leaf and ion toxicity.

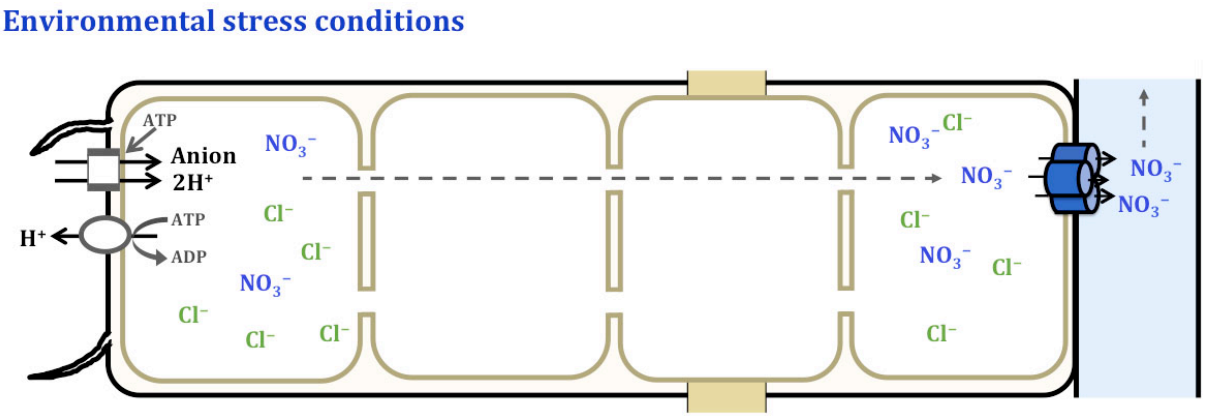

Figure 5.5. Model of SLAC/SLAH family channels activity within the root under abiotic stress conditions. Under water deficit, nitrate (NO_3^-) deficiency and salinity SLAH1 and SLAH4 channels abundance decrease and SLAH3 homomeric channels (blue) preferentially translocate NO_3^- than chloride (Cl^-) into the xylem, increasing the Cl^- accumulation within the root.

5.4. THE RELEVANCE OF SLAC/SLAH ANION CHANNELS *vs.* NPF TRANSPORTERS

Two members of the nitrate transporter 1/peptide transporter (NRT1/PTR) family (NPF) have recently been reported as plasma membrane transporters that mediate the efflux of Cl^- from plant cells. On the one hand, *AtNPF2.5* is predominantly expressed in root cortical cells and encodes a transporter that, similarly to *AtSLAH4*, has been proposed to be a pathway for Cl^- efflux from the root (Li *et al.*, 2017). On the other hand, its closest homolog of *AtNPF2.5*, sharing 83.2% identity at the amino acid level, is *AtNPF2.4* that has been identified as a gene encoding a anion transporter in the root stele that, similarly to the SLAH1/SLAH3 complex, has been suggested to facilitate the transfer of Cl^- into the root xylem (Li *et al.*, 2016).

It should be noted that, the inward currents elicited by SLAH1/SLAH3 (around −10,000 nA; Fig. 4.24 a-b) were significantly higher than those elicited by NPF transporters when the *Xenopus* oocyte plasma membrane was clamped at −100 mV, being 20 orders of magnitude

greater than the currents measured with *AtNPF2.5* (−100 nA; Li *et al*., 2017) and 100 orders of magnitude greater than those elicited by *AtNPF2.4* (−500 nA; Li *et al*., 2016).

Taking into account that the resting membrane potential of plant cells has usually values between –80 and –200 mV (Fromm and Lautner, 2007), S-type channels have a prominent role in mobilizing anions from plant cells in comparison with NPF transporters. The function of NPF transporters must be probably important at certain physiological conditions, but this hypothesis has to be further investigated.

CONCLUSIONS

6. CONCLUSIONS

1. The root-expressing *AtSLAH1* and *AtSLAH4* genes of *Arabidopsis thaliana* plants, encoding for slow(S)-type anion channels of the SLAC/SLAH family, have been characterized and their biological roles have been described in this work.

2. Homozygous knockout (KO) single mutant lines disrupted in the *AtSLAH1* or *AtSLAH4* genes, show developmental alterations according to the chloride (Cl^-) dose applied in the nutrient solution, proving that an interaction between Cl^- nutrition and SLAH1 and SLAH4 function exists.

3. In comparison to wild-type (WT) plants, the *slah1-2* KO single mutant accumulates less Cl^- in the shoot, while the *slah4-2* KO single mutant exhibits the opposite phenotype, showing more Cl^- accumulation in shoot organs and demonstrating that SLAH1 and SLAH4 channels are involved in Cl^- homeostasis at the whole plant level.

4. In xylem sap samples obtained from *slah1-2* mutant plants, the Cl^-, but not the nitrate (NO_3^-), content is reduced by 50% compared to the WT line, and this phenotype was reversed in the *slah1-2* mutant lines complemented with the native *AtSLAH1* gene, providing evidence of a role of SLAH1 in the regulation of root-to-shoot Cl^- translocation.

5. In the root, *AtSLAH1* is specifically expressed in pericycle cells facing xylem vessels, where this gene is co-expressed with *AtSLAH3*, other member of the SLAC/SLAH family of S-type anion channels. The *slah3-1* and *slah3-4* single mutant lines, as well as the *slah1-slah3* double mutant line, show the same phenotype as the *slah1-2* single mutant line, with similar reduction of the root-to-shoot Cl^- translocation degree, proving that a concerted activity of both SLAH1 and SLAH3 channels is required to properly regulate the Cl^- translocation into root xylem vessels.

6. Functional expression of WT SLAH1 channel in *Xenopus* oocytes, as well as the open-gated SLAH1 mutant F307A, remains electrically silent in the presence or absence of anion-channel-activating protein kinases, indicating that SLAH1 represents an anion channel that does not mediate transmembrane anion transport.

7. The silent SLAH1 and the anion-conducting SLAH3 channels physically interact when co-expressed in *Xenopus* oocytes, showing that they form heteromeric anion channels.

8. SLAH3 requires extracellular NO_3^- and Ca^{2+}-dependent kinases to conduct NO_3^- and Cl^- anions in *Xenopus* oocytes. However, macroscopic currents are measured when co-expressed with SLAH1 in the absence of both intracellular activating kinase and NO_3^-, proving that and the activity of the SLAH1/SLAH3 heteromer differs from that of the respective homomers.

9. Heteromers formed with pore-blocking mutants of SLAH1 (F307L and R47D) remain active, but heteromers formed with pore-blocking mutants of SLAH3 (F517L and G264D) do not elicit macroscopic currents, demonstrating two facts: (1) instead of the addition of a SLAH1 intrinsic Cl^- conductance, the activity of the heteromer is a consequence of a modification of the electrical properties of SLAH3. (2) SLAH1 substitutes for kinase and NO_3^--dependent activation of SLAH3.

10. As a consequence of the SLAH1/SLAH3 heteromer formation, Cl^- conductance increases seven times compared to that of the SLAH3/SLAH3 homomer, whereas de conductance for NO_3^- remains unaltered.

11. Abiotic stress (including water deficit and salinity) strongly down-regulates *AtSLAH1* expression through an ABA-dependent regulatory pathway.

12. It is proposed in this work that SLAH1 functions like a molecular switch that regulates Cl^- translocation according to environmental cues. Under optimal conditions, actively growing plants require the coordinated translocation of both Cl^- and NO_3^- nutrients by the SLAH1/SLAH3 heteromer. In contrast, abiotic stress favours the SLAH3/SLAH3 homomer through strong reduction of SLAH1 synthesis, greatly reducing root-to-shoot Cl^- translocation.

13. *AtSLAH1* is also actively expressed in flower organs, specifically in the anther filament and the stigmatic papillae, where the SLAH1 activity determines the optimal production of seeds.

14. *AtSLAH4* is expressed in root epidermal and cortical cells, indicating a role of the SLAH4 channel in the regulation of anion release to the root apoplast and/or the soil rizhosphere.

15. The loss of SLAH4 function leads to higher shoot Cl^- accumulation, proving that SLAH4 control net Cl^- uptake through the regulation of Cl^- release at the root or to the soil interface.

16. The high-Cl^- phenotype of the *slah4-2* KO mutant line is detectable during late developmental stages in plants treated with low NO_3^-, showing another level of interaction between the homeostasis of Cl^- and NO_3^- anions.

17. In contrast to *AtSLAH1*, *AtSLAH4* expression is developmentally down-regulated during early seedling establishment, indicating that optimal plant growth requires high Cl^- uptake after germination and during the first days of plant growth. Afterwards, proper Cl^- homeostasis requires the SLAH4 function to optimize the adequate balance between root Cl^- uptake and release, mainly during late developmental stages and senescence.

BIBLIOGRAPHY

BIBLIOGRAPHY

Abel GH (1969) Inheritance of the capacity for chloride inclusion and chloride exclusion by soybeans. *Crop Science* 9, 697–698.

Ache P, Becker D, Ivashikina N, Dietrich P, Roelfsema MR, Hedrich R (2000) GORK, a delayed outward rectifier expressed in guard cells of *Arabidopsis thaliana*, is a K^+-selective, K^+-sensing ion channel. *FEBS Letters* 486, 93–98.

Adler PR, Wilcox GE (1995) Ammonium increases the net rate of sodium influx and partitioning to the leaf of muskmelon. *Journal of Plant Nutrition* 18, 1951–1962.

Alboresi A, Gestin C, Leydecker MT, Bedu M. Meyer C, Truong HN (2005) Nitrate, a signal relieving seed dormancy in *Arabidopsis*. *Plant, Cell & Environment* 28, 500–512.

Albrecht V, Weinl S, Blazevic D, D'Angelo C, Batistic O, Kolukisaoglu Ü, Bock R, Schulz B, Harter K, Kudla J (2003) The calcium sensor CBL1 integrates plant responses to abiotic stresses. *The Plant Journal* 36, 457–470.

Allen GJ, Muir SR, Sanders D (1995) Release of Ca^{2+} from individual plant vacuoles by both InsP3 and cyclic ADPribose. *Science* 268, 735–737.

Allen S, Smith JAC (1986) Ammonium nutrition in *Ricinus communis*: Its effect on plant growth and the chemical composition of the whole plant, xylem and phloem saps. *Journal of Experimental Botany* 37, 1599–1610.

Almagro A, Lin SH, Tsay YF (2008) Characterization of the *Arabidopsis* nitrate transporter NRT1.6 reveals a role of nitrate in early embryo development. *The Plant Cell* 20, 3289–3299.

Aloni R (2001) Foliar and axial aspects of vascular differentiation: hypotheses and evidence. *Journal of Plant Growth Regulation* 20, 22–34.

Aloni R, Schwalm K, Langhans M, Ullrich CI (2003) Gradual shifts in sites of free-auxin production during leaf-primordium development and their role in vascular differentiation and leaf morphogenesis in *Arabidopsis*. *Planta* 216, 841–853.

Alscher RG, Donahue JL, Cramer CL (1997) Reactive oxygen species and antioxidants: relationships in green cells. *Physiologia Plantarum* 100, 224–233.

Altschul S, Madden T, Schaffer A, Zhang J, Zhang Z, Miller W, Lipman D (1997) Gapped BLAST and PSI-BLAST: a new generation of protein database search programs. *Nucleic Acids Research* 25, 3389–3402.

Antcliff AJ, Newman HP, Barret HC (1983) Variation in chloride accumulation in some American species of grapevine. *Vitis* 22, 357–362.

Apse MP, Blumwald E (2007) Na^+ transport in plants. *FEBS Letters* 581, 2247–2254.

Arteca RN, Arteca JM (2000) A novel method for growing *Arabidopsis thaliana* plants hydroponically. *Physiologia Plantarum* 108, 188–193.

Assmann SM, Shimazaki K (1999) The multisensory guard cell. Stomatal responses to blue light and abscisic acid. *Plant Physiology* 119, 809–816.

Assmann SM, Simoncini L, Schroeder JI (1985) Blue light activates electrogenic ion pumping in guard cell protoplasts of *Vicia faba*. *Nature* 318, 285–287.

Babourina O, Shabala S, Newman IAN (1998a) Auxin stimulates Cl^- uptake by oat coleoptiles. *Annals of Botany* 82, 331–336.

Babourina OK, Knowles AE, Newman IA (1998b) Chloride uptake by oat coleoptile parenchyma described by combined influx and efflux transport systems. *Australian Journal of Plant Physiology* 25, 929–936.

Baetz U, Eisenach C, Tohge T, Martinoia E, De Angeli A (2016) Vacuolar chloride fluxes impact ion content and distribution during early salinity stress. *Plant Physiology* 172, 1167–1181.

Bañuls JE, Legaz F, Primo-Millo E (1990) Effect of salinity on uptake and distribution of chloride and sodium in some citrus scion-rootstock combinations. *Journal of Horticultural Science* 65,715–724.

Bañuls J, Primo-Millo E (1992) Effects of chloride and sodium on gas exchange parameters and water relations of Citrus plants. *Physiologia Plantarum* 86, 115–123.

Bañuls JE, Serna MD, Legaz F, Talón M, Primo-Millo E (1997) Growth and gas exchange parameters of citrus plants stressed with different salts. *Journal of Plant Physiology* 150, 194–199.

Bar Y, Apelbaum A, Kafkafi U, Goren R (1997) Relationship between chloride and nitrate and its effect on growth and mineral composition of avocado and citrus plants. *Journal of Plant Nutrition* 20, 715–731.

Barbier-Brygoo H, De Angeli A, Filleur S, Frachisse JM, Gambale F, Thomine S, Wege S (2011) Anion channels/transporters in plants: from molecular bases to regulatory networks. *Annual Review of Plant Biology* 62, 25–51.

Barragán V, Leidi EO, Andrés Z, Rubio L, De Luca A, Fernández JA, Cubero B, Pardo, JM (2012) Ion exchangers NHX1 and NHX2 mediate active potassium uptake into vacuoles to regulate cell turgor and stomatal function in *Arabidopsis*. *Plant Cell* 24, 1127–1142.

Bassil E, Ohto MA, Esumi T, Tajima H, Zhu Z, Cagnac O, Belmonte M, Peleg Z, Yamaguchi T, Blumwald E (2011) The *Arabidopsis* intracellular Na^+/H^+ antiporters NHX5 and NHX6 are endosome associated and necessary for plant growth and development. *Plant Cell* 23, 224–239.

Bauer H, Ache P, Lautner S, Fromm J, Hartung W, Al-Rasheid KAS, Sonnewald S, Sonnewald U, Kneitz S, Lachmann N, Mendel Bittner F, Hetherington AM, Hedrich R (2013a) The stomatal response to reduced relative humidity requires guard cell-autonomous ABA synthesis. *Current Biology* 23, 53–57.

Bauer H, Ache P, Wohlfart F, Al-Rasheid KA, Sonnewald S, Sonnewald U, Kneitz S, Hetherington AM, Hedrich, R (2013b) How do stomata sense reductions in atmospheric relative humidity? *Molecular plant* 6, 1703–1706.

Bauerle WL, Whitlow TH, Setter TL, Bauerle TL, Vermeylen FM (2003) Ecophysiology of *Acer rubrum* seedlings from contrasting hydrologic habitats: growth, gas exchange, tissue water relations, abscisic acid and carbon isotope discrimination. *Tree Physiology* 23, 841–850.

Bauerle WL, Whitlow TH, Setter TL, Vermeylen FM (2004) Abscisic acid synthesis in *Acer rubrum* L. leaves — a vapor-pressure-deficit-mediated response. *Journal of the American Society for Horticultural Science* 129, 182–187.

Baylis T, Cierlik I, Sundberg E, Mattsson J (2013) SHORT INTERNODES/ STYLISH genes, regulators of auxin biosynthesis, are involved in leaf vein development in *Arabidopsis thaliana*. *New Phytologist* 197, 737–750.

Becker D, Dreyer I, Hoth S, Reid JD, Busch H, Lehnen M, Palme K, Hedrich R (1996) Changes in voltage activation, Cs^+ sensitivity, and ion permeability in H5 mutants of the plant K^+ channel KAT1. Proc Natl Acad Sci U S A 93, 8123–8128.

Beilby MJ, Walker NA (1981) Chloride transport in *Chara*. 1. Kinetics and current-voltage curves for a probable proton symport. *Journal of Experimental Botany* 32, 43–54.

Belin C, Thomine S, Scroeder JI (2010) Water balance and regulation of stomatal movements. *In*: Pareek A, Sopory SK, Bohnert J, Govindjee, eds. Abiotic stress adaptation in plants. Springer. 283–304.

Bemm F, Becker D, Larisch C, Kreuzer I, Escalante-Perez M, Schulze WX, Ankenbrand M, Van de Weyer AL, Krol E, Al-Rasheid KA, Mithöfer A, Weber A, Schultz J, Hedrich R (2016) Venus flytrap carnivorous lifestyle builds on herbivore defense strategies. *Genome research 26*, 812–825.

Bergsdorf EY, Zdebik AA, Jentsch TJ (2009) Residues important for nitrate/proton coupling in plant and mammalian CLC transporters. *Journal of Biological Chemistry* 284, 11184–11193.

Bernal CT, Bingham FT, Oertli J (1974) Salt tolerance of mexican wheat: II. Relation to variable sodium chloride and length of growing season. *Soil Science Society of America Journal* 38, 777–780.

Bernard P, Couturier M (1991) The 41 Carboxy-terminal residues of the mini-F plasmid CcdA protein are sufficient to antagonize the killer activity of the CcdB protein. *Molecular and General Genetics* 226, 297–304.

Bernstein L, Brown JW, Hayward HE (1956) The influence of rootstock on growth and salt accumulation in stone-fruit trees and almonds. *Proceedings of the American Society for Horticultural Sciences* 68, 86–95.

Bi YM, Wang RL, Zhu T, Rothstein SJ (2007) Global transcription profiling reveals differential responses to chronic nitrogen stress and putative nitrogen regulatory components in *Arabidopsis*. *BMC Genomics* 8, 281.

Binzel ML, Hess D, Bressan RA, Hasegawa PM (1988) Intracellular compartmentation of ions in salt-adapted tobacco cells. *Plant Physiology* 86, 607–614.

Blatt MR (2000) Cellular signaling and volume control in stomatal movements in plants. *Annual Review of Cell and Developmental Biology* 16, 221–241.

Blumwald E (2000) Sodium transport and salt tolerance in plants. *Current Opinion in Cell Biology* 12, 431–434.

Blumwald E, Aharon GS, Apse MP (2000) Sodium transport in plant cells. *Biochimica et Biophysica Acta-Biomembranes* 1465, 140–151.

Bock KW, Honys D, Ward JM, Padmanaban S, Nawrocki EP, Hirschi KD, Twell D, Sze H (2006) Integrating membrane transport with male gametophyte development and function through transcriptomics. *Plant Physiology* 140, 1151–1168.

Boudsocq M, Barbier-Brygoo H, Lauriere C (2004) Identification of nine sucrose nonfermenting 1-related protein kinases 2 activated by hyperosmotic and saline stresses in *Arabidopsis thaliana*. *Journal of Biological Chemistry* 279, 41758–41766.

Boyes DC, Zayed AM, Ascenzi R, McCaskill AJ, Hoffman NE, Davis KR, Görlach J (2001) Growth staged-base phenotypic analysis of *Arabidopsis*: a model for high throughput functional genomics in plants. *The Plant Cell* 13, 1499–1510.

Braconnier S, d'Azucac J (1990) Chloride and stomatal conductance in coconut. *Oleagineux* 45, 259–266.

Brandt B, Brodsky DE, Xue S, Negi J, Iba K, Kangasjärvi J, Ghassemian M, Stephan AB, Hu H, Schroeder JI (2012) Reconstitution of abscisic acid activation of SLAC1 anion channel by CPK6 and OST1 kinases and branched ABI1 PP2C phosphatase action. *Proceedings of the National Academy of Sciences of the United States of America* 109, 10593–10598.

Brini F, Masmoudi K (2012) Ion transporters and abiotic stress tolerance in plants. *International Scholarly Research Network Molecular Biology*, doi:10.5402/2012/927436.

Britto DT, Kronzucker HJ (2006) Futile cycling at the plasma membrane: a hallmark of low-affinity nutrient transport. *Trends in Plant Science* 11, 529–534.

Britto DT, Ruth TJ, Lapi S, Kronzucker HJ (2004) Cellular and whole-plant chloride dynamics in barley: insights into chloride-nitrogen interactions and salinity responses. *Planta* 218, 615–622.

Broadley M, Brown P, Cakmak I, Ma JF, Rengel Z, Zhao F, Marschner P (2012a) Beneficial elements. *In*: Marschner P, ed. Marschner's mineral nutrition of higher plants, 3rd edn. Academic Press. San Diego. 249–269.

LIBRO: Broadley M, Brown P, Cakmak I, Rengel Z, Zhao F (2012b) Function of nutrients: micronutrients. *In*: Marschner P, ed. Marschner's mineral nutrition of higher plants, 3rd edn. Academic Press. San Diego. 191–248.

Broyer T, Carlton A, Johnson A, Stout P (1954) Chlorine: A micronutrient element for higher plants. *Plant Physiology* 29, 526–532.

Brumós J, Colmenero-Flores J, Conesa A, Izquierdo P, Sánchez G, Iglesias D, López-Climent M, Gómez-Cadenas A, Talón M (2009) Membrane transporters and carbon metabolism implicated in chloride homeostasis differentiate salt stress responses in tolerant and sensitive Citrus rootstocks. *Functional & Integrative Genomics* 9, 293–309.

Brumós J, Talón M, Bouhlal R, Colmenero-Flores JM (2010) Cl^- homeostasis in includer and excluder citrus rootstocks: transport mechanisms and identification of candidate genes. *Plant, Cell & Environment* 33, 2012–2027.

Buwalda JG, Smith GS (1991) Influence of anions on the potassium status and productivity of kiwifruit (*Actinidia deliciosa*) vines. *Plant Soil* 133, 209–218.

Cakirlar H, Bowling DJF (1981) The effect of salinity on the membrane potential of sunflower roots. *Journal of Experimental Botany* 32, 479–485.

Cataldo DA, Maroon M, Schrader LE, Youngs VL (1975) Rapid colorimetric determination of nitrate in plant tissue by nitration of salicylic acid 1. *Communications in Soil Science and Plant Analysis* 6, 71–80.

Cerezo M, García-Agustín P, Serna MD, Primo-Millo E (1997) Kinetics of nitrate uptake by citrus seedlings and inhibitory effects of salinity. *Plant Science* 126, 105–112.

Champman HD, Liebig GF (1940) Nitrogen concentration and ion balance in relation to citrus nutrition. *Hilgardia* 13, 141–173.

Chandler PM, Robertson M (1994) Gene expression regulated by abscisic acid and its relation to stress tolerance. *Annual Review of Plant Biology* 45, 113–141.

Chen CZ, Lv XF, Li JY, Yi HY, Gong JM (2012) *Arabidopsis* NRT1.5 is another essential component in the regulation of nitrate reallocation and stress tolerance. *Plant Physiology* 159, 1582–1590.

Chen TY (2005) Structure and function of CLC channels. *Annual Review of Physiology* 67, 809–839.

Chen YH, Hu L, Punta M, Bruni R, Hillerich B, Kloss B, Rost B, Love J, Siegelbaum SA, Hendrickson WA (2010) Homologue structure of the SLAC1 anion channel for closing stomata in leaves. *Nature* 467, 1074–1080.

Chen ZC, Yamaji N, Fujii-Kashino M, Ma JF (2016) A cation-chloride cotransporter gene is required for cell elongation and osmoregulation in rice. *Plant physiology* 171, 494–507.

Cheong YH, Kim KN, Pandey GK, Gupta R, Grant JJ, Luan S (2003) CBL1, a calcium sensor that differentially regulates salt, drought, and cold responses in *Arabidopsis*. *Plant Cell* 15, 1833–1845.

Cheong YH, Pandey GK, Grant JJ, Batistic O, Li L, Kim BG, Lee SC, Kudla J, Luan S (2007) Two calcineurin B–like calcium sensors, interacting with protein kinase CIPK23, regulate leaf transpiration and root potassium uptake in *Arabidopsis*. *The Plant Journal* 52, 223–239.

Chiu CC, Lin CS, Hsia AP, Su RC, Lin HL, Tsay YF (2004) Mutation of a nitrate transporter, AtNRT1:4, results in a reduced petiole nitrate content and altered leaf development. *Plant and Cell Physiology* 45, 1139–1148.

Christmann A, Weiler EW, Steudle E, Grill E (2007) A hydraulic signal in root-to-shoot signalling of water shortage. *The Plant Journal* 52, 167-174.

Churchill KA, Sze H (1984) Anion-sensitive, H-pumping ATPase of oat roots: direct effects of Cl^-, NO_3^-, and a disulfonic stilbene. *Plant Physiology* 76, 490–497.

Clarkson DT (1993) Roots and the delivery of solutes to the xylem. Philosophical Transactions of the Royal Society (London) 341, 5–17.

Clough SJ, Bent AF (1998) Floral dip: a simplified method for *Agrobacterium* mediated transformation of *Arabidopsis thaliana*. *The Plant Journal* 16, 735–743.

Cole JP (1985) Chloride toxicity in citrus. *Irrigation Science* 6, 63–71.

Colmenero-Flores JM, Martinez G, Gamba G, Vazquez N, Iglesias DJ, Brumos J, Talon M (2007) Identification and functional characterization of cation-chloride cotransporters in plants. *The Plant Journal* 50, 278–292.

Conn SJ, Hocking B, Dayod M, Xu B, Athman A, Henderson S, Aukett K, Conn V, Shearer MK, Fuentes S, Tyerman SD, Gilliham M (2013) Protocol: optimising hydroponic growth

systems for nutritional and physiological analysis of *Arabidopsis thaliana* and other plants. *Plant Methods* 9, 4.

Craig Plett D, Møller IS (2010) Na^+ transport in glycophytic plants: what we know and would like to know. *Plant Cell and Environment* 33, 612–626

Cram WJ (1973) Chloride fluxes in cells of the isolated root cortex of *Zea mays*. *Australian Journal of Biological Sciences* 26, 757.

Cram W, Pitman M (1972) The action of abscisic acid on ion uptake and water flow in plant roots. *Australian Journal of Biological Science* 25, 1125–1132.

Crawford NM (1995) Nitrate: nutrient and signal for plant growth. *Plant Cell* 7, 859–868.

Cubero-Font P, Maierhofer T, Jaslan J, Rosales MA, Espartero J, Díaz-Rueda P, Müller HM, Hürter AL, Al-Rasheid KAS, Marten I, Hedrich R, Colmenero-Flores JM, Geiger D (2016) Silent S-Type anion channel subunit SLAH1 gates SLAH3 open for chloride root-to-shoot translocation. *Current Biology* 26, 2213–2220.

Cutler SR, Rodriguez PL, Finkelstein RR, Abrams SR (2010) Abscisic acid: emergence of a core signaling network. *Annual Review of Plant Biology* 61, 651–679.

Dadacz-Narloch B, Beyhl D, Larisch C, Lopez-Sanjurjo EJ, Reski R, Kuchitsu K, Muller TD, Becker D, Schonknecht G, Hedrich R (2011) A novel calcium binding site in the slow vacuolar cation channel TPC1 senses luminal calcium levels. *Plant Cell* 23, 2696–2707.

Davenport RJ, Muñoz-Mayor A, Jha D, Essah PA, Rus A, Tester M (2007) The Na^+ transporter AtHKT1;1 controls retrieval of Na^+ from the xylem in *Arabidopsis*. *Plant Cell and Environment* 30, 497–507.

De Angeli A, Monachello D, Ephritikhine G, Frachisse JM, Thomine S, Gambale F, Barbier-Brygoo H (2006) The nitrate/proton antiporter AtCLCa mediates nitrate accumulation in plant vacuoles. *Nature* 442, 939–942.

De Angeli A, Thomine S, Frachisse JM, Ephritikhine G, Gambale F, Barbier-Brygoo H (2007) Anion channels and transporters in plant cell membranes. *FEBS Letters* 581, 2367–2374.

De Angeli A, Zhang J, Meyer S, Martinoia E (2013) AtALMT9 is a malate-activatedvacuolar chloride channel required for stomatal opening in *Arabidopsis*. *Nature Communications* 4, 1804.

D'Angelo C, Weinl S, Batistic O, Pandey GK, Cheong YH, Schültke S, Albrecht V, Ehlert B, Schulz B, Harter K, Luan S, Bock R, Kudla J (2006) Alternative complex formation of the Ca^{2+}-regulated protein kinase CIPK1 controls abscisic acid-dependent and independent stress responses in *Arabidopsis*. *The Plant Journal* 48, 857–872.

Dechorgnat J, Nguyen CT, Armengaud P, Jossier M, Diatloff E, Filleur S, Daniel-Vedele F (2011) From the soil to the seeds: The long journey of nitrate in plants. *Journal of Experimental Botany* 62, 1349–1359.

Demir F, Horntrich C, Blachutzik JO, Scherzer S, Reinders Y, Kierszniowska S, Schulze WX, Harms GS, Hedrich R, Geiger D, Kreuzer I (2013) *Arabidopsis* nanodomain-delimited ABA signaling pathway regulates the anion channel SLAH3. *Proceedings of the National Academy of Sciences of the United States of America* 110, 8296–8301.

Díaz-Zorita M, Diarte FA, Barraco M (2004) Effects of chloride fertilization on wheat (*Tritticum aestivul* L.) productivity in the sandy Pampas region, Argentina. *Agronomy Journal* 96, 839–844.

Dietrich P, Hedrich R (1998) Anions permeate and gate GCAC1, a voltage-dependent guard cell anion channel. *The Plant Journal* 15, 479–487.

Dietrich P, Sanders D, Hedrich R (2001) The role of ion channels in light-dependent stomatal opening. *Journal of Experimental Botany* 52, 1959–1967.

Doyle DA, Cabral JM, Pfuetzner RA, Kuo A, Gulbis JM, Cohen SL, Chait BT, MacKinnon R (1998) The Structure of the Potassium Channel: Molecular Basis of K^+ Conduction and Selectivity. *Science,* 280, 69–77.

Drew M, Saker I, Ashley T (1973) Nutrient supply and the growth of the seminal root system in barley. I. The effect of nitrate concentration on the growth of axes and lateral. *Journal of Experimental Botany* 24, 1189–1220.

Drew MC, Saker IR (1975) Nutrient supply and the growth of the seminal root system in barley. II. Localized compensatory increases in lateral toot growth and rates of nitrate uptake when NO, is restricted to only part of the root system. *Journal of Experimental Botany* 26, 79–80.

Dreyer I, Gomez-Porras JL, Riaño Pachón DM, Hedrich R, Geiger D (2012) Molecular evolution of slow and quick anion channels (SLACs and QUACs/ALMTs). *Frontiers in Plant Science* 3, 1–12.

Dutzler R, Campbell EB, Cadene M, Chait BT, MacKinnon R (2002) X-ray structure of a ClC chloride channel at 3.0 A reveals the molecular basis of anion selectivity. *Nature* 415, 287–294.

Dutzler R, Campbell EB, MacKinnon R (2003) Gating the selectivity filter in ClC chloride channels. *Science* 300, 108–112.

Eaton FM (1966) Chlorine. *In*: Chapman HD, ed. Diagnostic criteria for plant and soils. Riverside: University of California Division of Agricultural Sciences. 98–135.

Eisenhut M, Hocken N, Weber AP (2015) Plastidial metabolite transporters integrate photorespiration with carbon, nitrogen, and sulphur metabolism. *Cell Calcium* 58, 98–104.

Epstein E (1972) Mineral Nutrition of Plants: *Principles and Perspectives*. John Wiley & Sons, New York, NY, USA.

Fan SC, Lin CS, Hsu PK, Lin SH, Tsay YF (2009) The *Arabidopsis* nitrate transporter NRT1.7, expressed in phloem, is responsible for source-to-sink remobilization of nitrate. *Plant Cell* 21, 2750–2761.

Fan LM, Zhao Z, Assmann SM (2004) Guard cells: a dynamic signaling model. *Current Opinion in Plant Biology* 7, 537–546.

Feigin A (1985) Gertilization management of crops irrigated with saline water. *Plant Soil* 89, 285–299.

Feigin A, Rylski I, Meiri A, Shalhvet J (1987) Response of melon and tomato plants to chloride-nitrate ratio in saline nutrient solutions. *Journal of Plant Nutrition* 10, 1787–1794.

Felle H (1994) The H^+/Cl^- symporter in root hair cells of *Sinapis alba*: an electrophysiological study using ion-selective microelectrodes. *Plant Physiology* 106, 1131–1136.

Filleur S, Dorbe M, Cerezo M, Orsel M, Granier F, Gojon A, Daniel-Vedele F (2001) An Arabidopsis T-DNA mutant affected in Nrt2 genes is impaired in nitrate uptake. *FEBS Letters* 489, 220–224.

Finazzi G, Petroutsos D, Tomizioli M, Flori S, Sautron E, Villanova V, Rolland N, Seigneurin-Berny D (2015) Ions channels/transporters and chloroplast regulation. *Cell Calcium* 58, 86–97.

Fischer RA (1968) Stomatal opening: role of potassium uptake by guard cells. *Science* 160, 784–785.

Fixen PE (1987) Chloride fertilization. *Crops and Soils Magazine* 39, 14–16.

Fixen PE (1993) Crop responses to chloride. *Advances in Agronomy* 50, 107–150.

Fixen PE, Gelderman RH, Gerwin J, Cholick FA (1986) Response of spring wheat, barley, and oats to chloride in potassium chloride fertilizers. *Agronomy Journal* 78, 664–668.

Fernández-Ballester G, García-Sánchez F, Cerdá A, Martínez V (2003) Tolerance of citrus rootstock seedlings to saline stress based on their ability to regulate ion uptake and transport. *Tree Physiology* 23, 265–271.

Flowers TJ (1988) Chloride as nutrient and as an osmoticum. *In*: Tinker B, Läuchli A, eds. Advances in plant nutrition. Praeger. New York. 55–78.

Flowers TJ, Colmer TD (2008) Salinity tolerance in halophytes. *New Phytologist* 179, 945–963.

Forde BG (2000) Nitrate transporters in plants: structure, function and regulation. *Biochimica et Biophysica Acta-Biomembranes* 1465, 219–235.

Forestier C, Bouteau F, Leonhardt N, Vavasseur A (1998) Pharmacological properties of slow anion currents in intact guard cells of *Arabidopsis*. Application of the discontinuous single-electrode voltage-clamp to different species. *European Journal of Physiology* 436, 920–927.

Fort KP, Lowe KM, Thomas WA, Walker MA (2013) Cultural conditions and propagule type influence relative chloride exclusion in grapevine rootstocks. *American Journal of Enology and Viticulture* 21, 147–155.

Franco-Navarro JD, Brumós J, Rosales MA, Cubero-Font P, Luque-González S, Vázquez-Rodríguez A, Talón M, Colmenero-Flores JM (2012) Chloride Nutrition: Impact in Plant Development and Water Relations. *In*: Bonilla I, Hernández LE, Lucena JJ, eds. La nutrición mineral de las plantas como base de una agricultura sostenible. Universidad Autónoma de Madrid. Madrid. 300–306.

Franco-Navarro JD, Brumós J, Rosales MA, Cubero-Font P, Talón M, Colmenero-Flores JM (2016a) Chloride regulates leaf cell size and water relations in tobacco plants. *Journal of Experimental Botany* 67, 873–891.

Franco-Navarro JD, Colmenero-Flores JM, Rosales MA (2016b) Chloride nutrition provides a more efficient use of nitrogen (NUE) in tobacco and tomato plants. *In*: XVI Simposio Hispano-Luso de Nutrición Mineral de las Plantas. Murcia, 82.

Franco-Navarro JD, Rosales MA, Díaz-Espejo A, Colmenero-Flores JM (2016c) Chloride nutrition increases mesophyll diffusion conductance to CO_2 in tobacco plants. *In:* XVI Simposio Hispano-Luso de Nutrición Mineral de las Plantas. Murcia, 19.

Frankenberger Jr WT, Tabatabai MA, Adriano DC, Doner H (1996) Bromine, chlorine, and fluorine. *Methods of soil analysis Part 3-chemical methods*, 833–867.

Freeman KW, Girma K, Mosali J, Teal RK, Martin KL, Raun WR (2006) Response of winter wheat to chloride fertilization in sandy loam soils. *Communications in Soil Science and Plant Analysis* 37, 1947–1955.

Fromm J, Eschrich W (1988) Transport processes in stimulated and non-stimulated leaves of *Mimosa pudica* III. Displacement of ions during seismonastic leaf movements. *Trees–Structure and Function* 2, 65–72.

Fromm J, Eschrich W (1989) Correlation of ionic movements with phloem unloading and loading in barley leaves. *Plant Physiology and Biochemistry* 27, 577–585.

Fromm J, Lautner S (2007) Electrical signals and their physiological significance in plants. *Plant, Cell and Environment* 30, 249–257.

Fu Y, Yi H, Bao J, Gong J (2015) LeNRT2. 3 functions in nitrate acquisition and long-distance transport in tomato. *FEBS letters* 589, 1072–1079.

Fujii H, Chinnusamy V, Rodrigues A, Rubio S, Antoni R, Park SY, Cutler SR, Sheen J, Rodriguez PL, Zhu JK (2009) *In vitro* reconstitution of an abscisic acid signalling pathway. *Nature* 462, 660–664.

Fujii H, Zhu JK (2009) Arabidopsis mutant deficient in three abscisic acid-activated protein kinases reveals critical roles in growth, reproduction and stress. *Proceedings of the National Academy of Sciences of the United States of America* 106, 8380–8385.

Fuqua BD, Sims JL, Leggett JE, Benner JF, Atkinson WO (1976) Nitrate and chloride fertilization effects on yield and chemical composition of Burley tobacco leaves and smoke. *Canadian Journal of Plant Science* 56, 893–899.

Furihata T, Maruyama K, Fujita Y, Umezawa T, Yoshida R, Shinozaki K, Yamaguchi-Shinozaki K (2006) ABA-dependent multisite phosphorylation regulates the activity of a transcription activator AREB1. *Proceedings of the National Academy of Sciences of the United States of America* 103, 1988–1993.

Gadsby DC (2009) Ion channels versus ion pumps: the principal difference, in principle. *Nature Reviews Molecular Cell Biology* 10, 344–352.

Garay-Arroyo A, Colmenero-Flores JM, Garciarrubio A, Covarrubias A (2000) Highly hydrophilic proteins in prokaryotes and eukaryotes are common during conditions of water eeficit. *The Journal of Biological Chemistry* 275, 5668–5674.

Garcia-Mata C, Lamattina L (2003) Abscisic acid, nitric oxide and stomatal closure – is nitrate reductase one of the missing links? *Trends in Plant Science* 8, 20–26.

Gaymard F, Pilot G, Lacombe B, Bouchez D, Bruneau D, Boucherez J, Michaux-Ferrière N, Thibaud JB, Sentenac H (1998) Identification and disruption of a plant shaker-like outward channel involved in K^+ release into the xylem sap. *Cell* 94, 647–655.

Geelen D, Lurin C, Bouchez D, Frachisse JM, Lelievre F, Courtial B, Barbier-Brygoo H, Maurel C (2000) Disruption of putative anion channel gene *AtCLC-a* in *Arabidopsis* suggests a role in the regulation of nitrate content. *The Plant Journal* 21, 259–267.

Geiger D, Becker D, Vosloh D, Gambale F, Palme K, Rehers M, Anschuetz U, Dreyer I, Judla J, Hedrich R (2009a) Heteromeric *At*KC1·AKT1 channels in *Arabidopsis* roots facilitate growth under K^+-limiting conditions. *Journal of Biological Chemistry* 284, 21288–21295.

Geiger D, Scherzer S, Mumm P, Marten I, Ache P, Matschi S, Liese A, Wellmann C, Al-Rasheid KA, Grill E, Romeis T, Hedrich R (2010) Guard cell anion channel SLAC1 is regulated by CDPK protein kinases with distinct Ca^{2+} affinities. *Proceedings of the National Academy of Sciences of the United States of America* 107, 8023–8028.

Geiger D, Scherzer S, Mumm P, Stange A, Marten I, Bauer H, Ache P, Matschi S, Liese A, Al-Rasheid KAS, Romeis T, Hedrich R (2009b) Activity of guard cell anion channel SLAC1 is controlled by drought stress signaling kinase-phosphatase pair. *Proceedings of the National Academy of Sciences of the United States of America* 106, 21425–21430.

Geiger D, Maierhofer T, Al-Rasheid KAS, Scherzer S, Mumm P, Liese A, Ache P, Wellmann C, Marten I, Grill E, Romeis T, Hedrich R (2011) Stomatal Closure by Fast Abscisic Acid Signaling Is Mediated by the Guard Cell Anion Channel SLAH3 and the Receptor RCAR1. *Science Signaling* 4, ra32-.

Geilfus CM, Mithofer A, Ludwig-Muller J, Zorb C, Muehling KH (2015) Chloride-inducible transient apoplastic alkalinizations induce stomata closure by controlling abscisic acid distribution between leaf apoplast and guard cells in salt-stressed *Vicia faba*. *New Phytologist* 208, 803–816.

Georgopoulou Z, Milborrow BV (2012) Initiation of the synthesis of 'stress' ABA by (+)-[$_2H6_6$] ABA infiltrated into leaves of *Commelina communis*. *Physiologia Plantarum* 146, 149–159.

Giaquinta R (1980) Mechanism and control of phloem loading of sucrose. *Plant Biology* 93, 187–201.

Gilliam JW (1971) Rapid measurement of chlorine in plant materials. *Soil Science Society of America Proceedings* 35, 512–513.

Gilliham M, Tester M (2005) The regulation of anion loading to the maize root xylem. *Plant Physiology* 137, 819–828.

Glass ADM, Shaff J, Kochian LV (1992) Studies of the uptake of nitrate in Barley. IV. Electrophysiology. *Plant Physiol* 99, 456–463.

Glass ADM, Siddiqi MY (1985) Nitrate inhibition of chloride influx in barley-implications for a proposed chloride homeostat. *Journal of Experimental Botany* 36, 556–566.

Glass ADM, Siddiqi MY (1995) Nitrogen absorption by plant roots. *In*: Srivastava HS, Singh RP, eds. Nitrogen nutrition in higher plants. Associated Publishing Company. 21–56.

Gobert A, Isayenkov S, Voelker C, Czempinski K, Maathuis FJ (2007) The two-pore channel TPK1 gene encodes the vacuolar K^+ conductance and plays a role in K^+ homeostasis. *Proceedings of the National Academy of Sciences of the United States of America* 104, 10726–10731.

Goldman DE (1943) Potential, impedance and rectification in membranes. *The Journal of General Physiology* 27, 37–60.

Gómez-Cadenas A, Iglesias DJ, Arbona V, Colmenero-Flores JM, Primo-Millo, E, Talón M (2003) Physiological and molecular responses of citrus to salinity. *Recent Research Developments in Plant Molecular Biology* 1, 281–298.

Gong H, Blackmore D, Clingeleffer P, Sykes S, Jha D, TesterM,Walker R (2011) Contrast in chloride exclusion between two grapevine genotypes and its variation in their hybrid progeny. *Journal of Experimental Botany* 62, 989–999.

Grant C, McLaren D, Johnston A (2001) Spring wheat cultivar response to potassium chloride fertilization. *Better Crops with Plant Food* 85, 20–23.

Greenway H, Munns R (1980) Mechanisms of salt tolerance in non-halophytes. *Annual Review of Plant Physiology* 31, 149–190.

Groen AJ, Sancho-Andrés G, Breckels LM, Gatto L, Aniento F, Lilley KS (2014) Identification of trans-golgi network proteins in *Arabidopsis thaliana* root tissue. *Journal of Proteome research* 13, 763–776.

Guan B, Chen X, Zhang H (2013) Two-electrode voltage clamp. *In*: Gamper N, ed. Ion channels. Methods and Protocols. 2nd edition. Springer Protocols. London. 79–89.

Guan R, Qu Y, Guo Y, Yu L, Liu Y, Jiang J, Chen J, Ren Y, Liu G, Tian L, Jin L, Liu Z, Hong H, Chang R, Gilliham M, Qiu L (2014) Salinity tolerance in soybean is modulated by natural variation in *GmSALT3*. *The Plant Journal* 80, 937–950.

Guo FQ, Wang R, Chen M, Crawford NM (2001) The *Arabidopsis* dual-affinity nitrate transporter gene AtNRT1.1 (CHL1) is activated and functions in nascent organ development during vegetative and reproductive growth. *Plant Cell* 13, 1761–1777.

Guo FQ, Young J, Crawford NM (2003) The nitrate transporter *At*NRT1.1 (CHL1) functions in stomatal opening and contributes to drought susceptibility in *Arabidopsis*. *Plant Cell* 15, 107–117.

Gutermuth T, Lassig R, Portes MT, Maierhofer T, Romeis T, Borst JW, Hedrich R, Feijó JA, Konrad KR (2013) Pollen tube growth regulation by free anions depends on the interaction between the anion channel SLAH3 and calcium-dependent protein kinases CPK2 and CPK20. *The Plant Cell* 25, 4525–4543.

Hamburger D, Rezzonico E, Petétot JMC, Somerville C, Poirier Y (2002) Identification and characterization of the *Arabidopsis PHO1* gene involved in phosphate loading to the xylem. *The Plant Cell* 14, 889–902.

Hafke JB, Hafke Y, Smith JA, Lüttge U, Thiel G (2003) Vacuolar malate uptake is mediated by an anionselective inward rectifier. *The Plant Journal* 35, 116–128.

Hamilton DWA, Hills A, Köhler B, Blatt MR (2000) Ca^{2+} channels at the plasma membrane of stomatal guard cells are activated by hyperpolarization and abscisic acid. *Proceedings of the National Academy of Sciences of the United States of America* 97, 4967–4972.

Hänsch R, Mendel RR (2009) Physiological functions of mineral micronutrients (Cu, Zn, Mn, Fe, Ni, Mo, B, Cl). *Current Opinion in Plant Biology* 12, 259–266.

Harada H, Kuromori T, Hirayama T, Shinozaki K, Leigh RA (2004) Quantitative trait loci analysis of nitrate storage in *Arabidopsis* leading to an investigation of the contribution of the anion channel gene, AtCLC-c, to variation in nitrate levels. *Journal of Experimental Botany* 55, 2005–2014.

Hartley JL, Temple GF, Brasch MA (2000) DNA cloning using *in vitro* site-specific recombination. *Genome Research* 10, 1788–1895.

Hawkesford M, Horst W, Kichey T, Lambers H, Schjoerring J, Møller IS, White P (2012) Functions of macronutrients. *In*: Marschner P, ed. Marschner's mineral nutrition of higher plants, 3rd edn. Academic Press. San Diego. 135–190.

Hayashi H, Chino M (1985) Nitrate and other anions in the rice phloem sap. *Plant and Cell Physiology* 26, 325–330.

Hayashi H, Chino M (1986) Collection of pure phloem sap from wheat and its chemical composition. *Plant and Cell Physiology* 27, 1387–1393.

Hechenberger M, Schwappach B, Fischer W, Frommer W, Jentsch T, Steinmeyer K (1996) A family of putative chloride channels from *Arabidopsis* and functional complementation of a yeast strain with a CLC gene disruption. *Journal of Biological Chemistry* 271, 33632–33638.

Hedrich R, Marten I, Lohse G, Dietrich P, Winter H, Lohaus G, Heldt HW (1994) Malate–sensitive anion channels enable guard cells to sense changes in the ambient CO_2 concentration. *The Plant Journal* 6, 741–748.

Hedrich R, Marten I (1993) Malate-induced feedback regulation of plasma membrane anion channels could provide a CO_2 sensor to guard cells. *Embo Journal* 12, 897–901.

Hetherington AM, Brownlee C (2004) The generation of Ca^{2+} signals in plants. *Annual Review of Plant Biology* 55, 401–427.

Hetherington AM, Woodward FI (2003) The role of stomata in sensing and driving environmental change. *Nature* 424, 901–908.

Henderson SW, Baumann U, Blackmore DH, Walker AR, Walker RR, Gilliham M (2014) Shoot chloride exclusion and salt tolerance in grapevine is associated with differential ion transporter expression in roots. *BMC Plant Biology* 14, 273.

Henderson SW, Wege S, Qiu J, Blackmore DH, Walker AR, Tyerman SD, Walker RR, Gilliham M (2015) Grapevine and *Arabidopsis* cation-chloride cotransporters localise to the Golgi and trans-Golgi network and indirectly influence long-distance ion homeostasis and salt tolerance. *Plant Physiology* 169, 2215–2229.

Heslop-Harrison JS (1990) Energy dispersive X-ray analysis. *In*: Linskens HF, Jackson JF, eds. Modern Methods in Plant Analysis New Series. Springer. Berlin. 244–277.

Heslop-Harrison JS, Heslop-Harrison Y, Reger BJ (1987) Anther-filament extension in *Lilium:* Potassium ion movement and some anatomical features. *Annals of Botany* 59, 505–515.

Heslop-Harrison JS, Reger BJ (1986) Chloride and potassium ions and turgidity in the grass stigma. *Journal of Plant Physiology* 124, 55–60.

Hille B (2001) Ion Channels of Excitable Membranes, 3rd edn. Sunderland, Massachusetts U.S.A. Sinauer Associates, Inc.

Himmelbach A, Yang Y, Grill E (2003) Relay and control of abscisic acid signaling. *Current Opinion in Plant Biology* 6, 470–479.

Hirayama T, Shinozaki K (2007) Perception and transduction of abscisic acid signals: keys to the function of the versatile plant hormone ABA. *Trends in Plant Science* 12, 343–351.

Hirsch RE, Lewis BD, Spalding EP, Sussman MR (1998) A role for the AKT1 potassium channel in plant nutrition. *Science* 280, 918–921.

Hirt H and Shinozaki K (2004) Plant Responses to abiotic Stress. *In*: Hohmann S, Francki MG, Xu S, eds. Topics in Current Genetics. Springer-Verlag Berlin Heidelberg.

Ho CH, Lin SH, Hu HC, Tsay YF (2009) CHL1 functions as a nitrate sensor in plants. *Cell* 138, 184–194.

Ho CH, Tsay YF (2010) Nitrate, ammonium and potassium sensing and signaling. *Current Opinion in Plant Biology* 13, 604–610.

Hodgkin AL, Huxley AF (1952) The components of membrane conductance in the giant axon of Loligo. *The Journal of Physiology* 116, 473–496.

Hodgkin AL, Huxley AF, Katz B (1952) Measurement of current-voltage relations in the membrane of the giant axon of Loligo. *The Journal of Physiology* 116, 424–448.

Hodgkin AL, Katz B (1949) The effect of sodium ions on the electrical activity of giant axon of the squid. *The Journal of Physiology* 108, 37–77.

Hoekenga OA, Maron LG, Pineros MA, Cancado GMA, Shaff J, Kobayashi Y, Ryan PR, Dong B, Delhaize E Sasaki T (2006) AtALMT1, which encodes a malate transporter, is identified as one of several genes critical for aluminum tolerance in *Arabidopsis*. *Proceedings of the National Academy of Sciences of the United States of America* 103, 9738–9743.

Horie T, Hauser F, Schroeder JI (2009) HKT transporter-mediated salinity resistance mechanisms in *Arabidopsis* and monocot crop plants. *Trends in Plant Science* 14, 660–668.

Hosy E, Vavasseur A, Mouline K, Dreyer I, Gaymard F, Poree F, Boucherez J, Lebaudy A, Bouchez D, Very AA, Simonneau T, Thibaud JB, Sentenac H (2003) The *Arabidopsis* outward K^+ channel GORK is involved in regulation of stomatal movements and plant transpiration. *Proceedings of the National Academy of Sciences of the United States of America* 100, 5549–5554.

Hoth S, Dreyer I, Dietrich P, Becker D, Müller-Röber B, Hedrich R (1997) Molecular basis of plant-specific acid activation of K+ uptake channels. *Proceedings of the National Academy of Sciences of the United States of America 94*, 4806–4810.

Hoth S, Morgante M, Sanchez JP, Hanafey MK, Tingey SV, Chua NH (2002) Genome-wide gene expression profiling in *Arabidopsis thaliana* reveals new targets of abscisic acid and largely impaired gene regulation in the *abi1-1* mutant. *Journal of Cell Science* 115, 4891–4900.

Hsiao TC, Xu LK (2000) Sensitivity of growth of roots versus leaves to water stress: biophysical analysis and relation to water transport. *Journal of Experimental Botany* 51, 1595–1616.

Hu CD, Chinenov Y, Kerppola TK (2002) Visualization of interactions among bZIP and Rel family proteins in living cells using bimolecular fluorescence complementation. *Molecular Cell* 9, 789–798.

Huang NC, Chiang CS, Crawford NM, Tsay YF (1996) CHL1 encodes a component of the low-affinity nitrate uptake system in *Arabidopsis* and shows cell type specific expression in roots. *The Plant Cell* 8, 2183–2191.

Huang NC, Liu KH, Lo HJ, Tsay YF (1999) Cloning and functional characterization of an *Arabidopsis* nitrate transporter gene that encodes a constitutive component of low-affinity uptake. *The Plant Cell* 11, 1381–1392.

Humble GD, Raschke K 1971 Stomatal opening quantitatively related to potassium transport: evidence from electron probe analysis. *Plant Physiology* 48, 447–453.

Iino M, Long C, Wang X (2001) Auxin-and abscisic acid-dependent osmoregulation in protoplasts of *Phaseolus vulgaris* pulvini. *Plant and Cell Physiology* 42, 1219–1227.

Imes D, Mumm P, Bohm J, Al-Rasheid KAS, Marten I, Geiger D, Hedrich R (2013) Open stomata 1 (OST1) kinase controls R-type anion channel QUAC1 in *Arabidopsis* guard cells. *The Plant Journal* 74, 372–382.

Isayenkov S, Isner JC, Maathuis FJ (2010) Vacuolar ion channels: roles in plant nutrition and signalling. *FEBS Letters* 584, 1982–1988.

Israelsson M, Siegel RS, Young J, Hashimoto M, Iba K, Schroeder JI (2006) Guard cell ABA and CO_2 signaling network updates and Ca2+ sensor priming hypothesis. *Current Opinion in Plant Biology* 9, 654–663.

James DW, Weaver WH, Reeder RL (1970) Chloride uptake by potatoes and the effects of potassium chloride, nitrogen and phosphorus fertilization. *Soil Science* 109, 48–53.

James RA, Munns R, von Caemmerer S, Trejo C, Miller C, Condon TA (2006) Photosynthetic capacity is related to the cellular and subcellular partitioning of Na^+, K^+ and Cl^- in salt-affected barley and durum wheat. *Plant Cell and Environment* 29, 2185–2197.

Jeanguenin L, Alcon C, Duby G, Boeglin M, Chérel I, Gaillard I, Zimmermann Sabine, Sentac H, Véry AA (2011) AtKC1 is a general modulator of *Arabidopsis* inward Shaker channel activity. *The Plant Journal* 67, 570–582.

Jefferson R (1987) Assaying chimeric genes in plants: The GUS gene fusion system. *Plant Molecular Biology Reports* 5, 387–405.

Johnson, CM, Stout, PR, Broyer, TC, Carlton, AB (1957) Comparative chlorine requirements of different plant species. *Plant and Soil* 8, 337–353.

Johnson RR, Wagner RL, Verhey SD, Walker Simmons MK (2002) The abscisic acid responsive kinase PKABA interacts with a seed-specific abscisic acid response elementbinding factor, TaABF, and phosphorylates TaABF peptide sequences. *Plant Physiology* 130, 837–846.

Jossier M, Kroniewicz L, Dalmas F, Le Thiec D, Ephritikhine G, Thomine S, Barbier-Brygoo H, Vavasseur A, Filleur S, Leonhardt N (2010) The *Arabidopsis* vacuolar anion transporter, AtCLCc, is involved in the regulation of stomatal movements and contributes to salt tolerance. *The Plant Journal* 64, 563–576.

Kafkafi U, Valoras N, Letey J (1982) Chloride interaction with nitrate and phosphate nutrition in tomato (*Lycopersicon esculentum* L). *Journal of Plant Nutrition* 5, 1369–1385.

Kang J, Hwang JU, Lee M, Kim YY, Assmann SM, Martinoia E, Lee Y (2010) PDR-type ABC transporter mediates cellular uptake of the phytohormone abscisic acid. *Proceedings of the National Academy of Sciences of the United States of America* 107, 2355–2360.

Kanno Kanno Y, Hanada A, Chiba Y , Ichikawa T, Nakazawa M, Matsui M, Koshiba T, Kamiya Y, Seo M (2012) Identification of an abscisic acid transporter by functional screening using the receptor complex as a sensor. *Proceedings of the National Academy of Sciences of the United States of America* 109, 9653–9658.

Kawashima CG, Yoshimoto, N, Maruyama-Nakashita A, Tsuchiya YN, Saito K, Takahashi H, Dalmay T (2009) Sulphur starvation induces the expression of microRNA-395 and one of its target genes but in different cell types. *The Plant Journal* 57, 313-321.

Kerppola TK (2006) Design and implementation of Bimolecular Fluorescence Complementation (BiFC) assays for the visualization of protein interactions in living cells. *Nat Protoc* 1, 1278–1286.

Kerppola TK (2008) Bimolecular Fluorescence Complementation (BiFC) analysis as a probe of protein interactions in living cells. *Annual Review of Biophysics* 37, 465–487.

Kiba T, Feria-Bourrellier AB, Lafouge F, Lezhneva L, Boutet-Mercey S, Orsel M, Bréhaut V, Miller A, Daniel-Vedele F, Sakakibara H, Krapp A (2012) The *Arabidopsis* nitrate transporter NRT2.4 plays a double role in roots and shoots of nitrogen-starved plants. *Plant Cell* 24, 245–258.

Kim TH, Bohmer M, Hu H, Nishimura N, Schroeder JI (2010) Guard cell signal transduction network: advances in understanding abscisic acid, CO_2, and Ca^{2+} signaling. *Annual Review of Plant Biology* 61, 561–591.

Kinoshita T, Nishimura M, Shimazaki K (1995) Cytosolic concentration of Ca^{2+} regulates the plasma membrane H^+-ATPase in guard cells of fava bean. *Plant Cell* 7, 1333–1342.

Kinoshita T, Shimazaki K (1999) Blue light activates the plasma membrane H^+-ATPase by phosphorylation of the C-terminus in stomatal guard cells. *The EMBO Journal* 18, 5548-5558.

Kjeldahl, J (1883) Neue Methode zur Bestimmung des Stickstoffs in organischen Körpern. *Zeitschrift für analytische Chemie* 22, 366–383.

Kline KG, Barrett-Wilt GA, Sussman MR (2010) In planta changes in protein phosphorylation induced by the plant hormone abscisic acid. *Proceedings of the National Academy of Sciences of the United States of America* 107, 15986–15991.

Kochian LV, Hoekenga OA, Pineros MA (2004) How do crop plants tolerate acid soils? Mechanisms of aluminum tolerance and phosphorous efficiency. *Annual Review of Plant Biology* 55, 459–493.

Köhler B, Blatt MR (2002) Protein phosphorylation activates the guard cell Ca^{2+} channel and it's a prerequisite for gating by abcisic acid. *The Plant Journal* 32, 185–194.

Köhler B, Hills A, Blatt MR (2003) Control of guard cell ion channels by hydrogen peroxide and abcisic acid indicates their action through alternate signalling pathway. *Plant Physiology* 131, 385–388.

Köhler B, Raschke K (2000) The delivery of salts to the xylem. Three types of anion conductance in the plasmalemma of the xylem parenchyma of roots of barley. *Plant Physiology* 122, 243–254.

Köhler B, Wegner LH, Osipov V, Raschke K (2002) Loading of nitrate into the xylem: apoplastic nitrate controls the voltage dependence of X-QUAC, the main anion conductance in xylem-parenchyma cells of barley roots. *The Plant Journal.* 30, 133–142.

Kolb HA, Marten I, Hedrich R (1995) Hodgkin-Huxley analysis of a GCAC1 anion channel in the plasma membrane of guard cells. *The Journal of Membrane Biology* 146, 273–282.

Kollist H, Jossier M, Laanemets K, Thomine S (2011) Anion channels in plant cells. *FEBS Journal* 278, 4277–4292.

Kotak S, Larkindale J, Lee U, von Koskull-Doering P, Vierling E, Scharf KD (2007) Complexity of the heat stress response in plants. *Current Opinion in Plant Biology*, 10, 310–316.

Kovermann P, Meyer S, Hortensteiner S, Picco C, Scholz-Starke J, Ravera S, Lee Y, Martinoia E (2007) The *Arabidopsis* vacuolar malate channel is a member of the ALMT family. *The Plant Journal* 52, 1169–1180.

Krapp A, David LC, Chardin C, Girin T, Marmagne A, Leprince A-S, Chaillou S, Ferrario-Méry S, Meyer C, Daniel-Vedele F (2014) Nitrate transport and signalling in *Arabidopsis*. *Journal of Expperimental Botany.* 65, 789–798.

Krebs M, Beyhl D, Görlich E, Al-Rasheid KA, Marten I, Stierhof YD, Hedrich R, Schumacher K (2010) *Arabidopsis* V-ATPase activity at the tonoplast is required for efficient nutrient storage but not for sodium accumulation. *Proceedings of the National Academy of Sciences of the United States of America* 107, 3251–3256.

Kronberg K, Vogel F, Rutten T, Hajirezaei MR, Sonnewald U, Hofius D (2007) The silver lining of a viral agent: increasing seed yield and harvest index in *Arabidopsis* by ectopic expression of the potato leaf roll virus movement protein. *Plant physiology*, 145, 905–918.

Krouk G, Crawford NM, Coruzzi GM, Tsay YF (2010a) Nitrate signalling: Adaptation to fluctuating environments. *Current Opinion in Plant Biology* 13, 266–273.

Krouk G, Lacombe B, Bielach A, Perrine-Walker F, Malinska K, Mounier E, Hoyerova K, Tillard P, Leon S, Ljung K, Zazimalova E, Benkova E, Nacry P, Gojon A. (2010b) Nitrate-regulated auxin transport by NRT1.1 defines a mechanism for nutrient sensing in plants. *Developmental Cell* 18, 927–937.

Krouk G, Ruffel S, Gutierrez RA, Gojon A, Crawford NM, Coruzzi GM, Lacombe B (2011) A framework integrating plant growth with hormones and nutrients. *Trends in Plant Science* 16, 178–182.

Kusunoki M (2007) Mono-manganese mechanism of the photosystem II water splitting reaction by a unique Mn_4Ca cluster. *Biochimica et Biophysica Acta-Biomembranes* 1767, 484–492.

Kwak JM, Mori IC, Pei ZM, Leonhardt N, Torres MA, Dangl JL, Bloom RE, Bodde S, Jones JDG, Schroeder JI (2003) NADPH oxidase *AtrbohD* and *AtrbohF* genes function in ROS-dependent ABA signaling in *Arabidopsis*. *The EMBO Journal* 22, 2623–2633.

Lagarde D, Basset M, Lepetit M, Conejero G, Gaymard F, Astruc S, Grignon C (1996) Tissue-specific expression of *Arabidopsis* AKT1 gene is consistent with a role in K^+ nutrition. *The Plant Journal* 9, 195–203.

Landy A (1989) Dynamic, structural and regulatory aspects of Lambda site-specific recombination. *Annual Review of Biochemistry* 58, 913–949.

Larkin MA, Blackshields G, Brown NP, Chenna R, McGettigan PA, McWilliam H, Valentin F, Wallace IM, Wilm A, Lopez R, Thompson JD, Gibson TJ, Higgins DG (2007) Clustal W and Clustal X version 2.0. *Bioinformatics* 23, 2947–2948.

Läuchli A, James RA, Huang CX, McCully M, Munns R (2008) Cell-specific localization of Na^+ in roots of durum wheat and possible control points for salt exclusion. *Plant Cell and Environment* 31, 1565–1574.

Lebaudy A, Very AA, Sentenac H (2007) K^+ channel activity in plants: Genes, regulations and functions. Febs Letters 581, 2357–2366.

Lee RB (1982) Selectivity and kinetics of ion uptake by barley plants following nutrient deficiency. *Annals of Botany* 50, 429–449.

Lee SC, Lan W, Buchanan BB, Luan S (2009) A protein kinase-phosphatase pair interacts with an ion channel to regulate ABA signaling in plant guard cells. *Proceedings of the National Academy of Sciences of the United States of America* 106, 21419–21424.

Leidi EO, Silberbush M, Soares MIM, Lips SH (1992) Salinity and nitrogen nutrition studies on peanut and cotton plants. *Journal of Plant Nutrition* 15, 591–604.

Leidi EO, Barragan V, Rubio L, El-Hamdaoui A, Ruiz MT, Cubero B, Fernandez JA, Bressan RA, Hasegawa PM, Quintero FJ, Pardo JM (2010) The *At*NHX1 exchanger mediates potassium compartmentation in vacuoles of transgenic tomato. *The Plant Journal* 61, 495–506.

Léran S, Muños S, Brachet C, Tillard P, Gojon A, Lacombe B (2013) *Arabidopsis* NRT1.1 is a bidirectional transporter involved in root-to-shoot nitrate translocation. *Molecular Plant* 6, 1984–1987.

Léran S, Varala K, Boyer JC, Chiurazzi M, Crawford N, Daniel-Vedele F, David L, Dickstein R, Fernandez E, Forde B, Gassmann W, Geiger D, Gojon A, Gong JM Halkier BA, Harris JM, Hedrich R, Limami AM, Rentsch D, Seo M, Tsay YF, Zhang M, Coruzzi G, Lacombe B (2014) A unified nomenclature of NITRATE TRANSPORTER 1/PEPTIDE TRANSPORTER family members in plants. *Trends in Plant Science* 19, 5–9.

Lessani H, Marschner H (1978) Relation between salt tolerance and long-distance transport of sodium and chloride in various crop species. *Australian Journal of Plant Physiology* 5, 27–37.

Leung J, Giraudat J (1998) Abscisic acid signal transduction. *Annual Review of Plant Biology* 49, 199–222.

Levchenko V, Konrad KR, Dietrich P, Roelfsema MR, Hedrich R (2005) Cytosolic abscisic acid activates guard cell anion channels without preceding Ca^{2+} signals. *Proceedings of the National Academy of Sciences of the United States of America* 102, 4203–4208.

Li B, Byrt C, Qiu J, Baumann U, Hrmova M, Evrard A, Johnson AAT, Birnbaum KD, Mayo GM, Jha D, Henderson SW, Tester M, Gilliham M, Roy SJ (2016) Identification of a stelar-localized transport protein that facilitates root-to-shoot transfer of chloride in *Arabidopsis*. *Plant Physiology* 170, 1014–1029.

Li B, Qiu J, Jayakannan M, Xu B, Li Y, Mayo GM, Tester M, Gilliham M, Roy SJ (2017) *AtNPF2.5* modulates chloride (Cl^-) efflux from roots of *Arabidopsis thaliana. Frontiers in Plant Science* 7:2013.

Li JY, Fu YL, Pike SM, Bao J, Tian W, Zhang Y, Chen CZ, Zhang Y, Li HM, Huang J, Li LG, Schroeder JI, Gassmann W, Gong JM (2010) The *Arabidopsis* nitrate transporter NRT1.8 functions in nitrate removal from the xylem sap and mediates cadmium tolerance. *The Plant Cell* 22, 1633–1646.

Li L, Kim BG, Cheong YH, Pandey GK, Luan S (2006) A Ca^{2+} signaling pathway regulates a K^+ channel for low-K response in *Arabidopsis*. *Proceedings of the National Academy of Sciences of the United States of America* 103, 12625–30.

Li W, Wang Y, Okamoto M, Crawford NM, Siddiqi MY, Glass AD (2007) Dissection of the AtNRT2.1:AtNRT2.2 inducible high-affinity nitrate transporter gene cluster. *Plant Physiology*. 143, 425–433.

Liesche J, Schulz A (2013) Symplasmic transport in phloem loading and unloading. *In*: Sokolowska K, Sowinski P, eds. Symplasmic transport in vascular plants. Spinger. New York. 133–163.

Lin SH, Kuo HF, Canivenc G, Lin CS, Lepetit M, Hsu PK, Tillard P, Lin HL, Wang YY, Tsai CB, Gojon A, Tsay YF (2008) Mutation of the *Arabidopsis* NRT1.5 nitrate transporter causes defective root-to-shoot nitrate transport. *Plant Cell* 20, 2514–2528.

Lind C, Dreyer I, López-Sanjurjo EJ, von Meyer K, Ishizaki K, Kohchi T, Lang D, Zhao Y, Kreuzer I, Al-Rasheid KAS, Ronne H, Reski R, Zhu JK, Geiger D, Hedrich R (2015) Stomatal guard cells co-opted an ancient ABA-dependent desiccation survival system to regulate stomatal closure. *Current Biology 25*, 928–935.

Linder B, Raschke K (1992) A slow anion channel in guard cells, activating at large hyperpolarization, may be principal for stomatal closing. *FEBS Letters* 313, 27–30.

Little DY, Rao H, Oliva S, Daniel-Vedele F, Krapp A, Malamy JE (2005) The putative high-affinity nitrate transporter NRT2.1 represses lateral root initiation in response to nutritional cues. *Proceedings of the National Academy of Sciences of the United States of America* 102, 13693–13698.

Liu KH, Huang CY, Tsay YF (1999) CHL1 is a dualaffinity nitrate transporter of *Arabidopsis* involving multiple phases of nitrate uptake. *Plant Cell* 11, 865–874.

Liu KH, Tsay YF (2003) Switching between the two action modes of the dual-affinity nitrate transporter CHL1 by phosphorylation. *EMBO Journal* 22, 1005–1013.

Liu L, Shelp BJ (1996) Impact of chloride on nitrate absorption and accumulation by broccoli (*Brassica oleracea* var. italic) *Canadian Journal of Plant Science* 76, 367–337.

Lohse G, Hedrich R (1995) Anions modify the response of guard cell anion channels to auxin. *Planta* 197, 546–552.

Lopez-Molina L, Mongrand S, Chua NH (2001) A postgermination developmental arrest checkpoint is mediated by abscisic acid and requires the ABI5 transcription factor in *Arabidopsis*. *Proceedings of the National Academy of Sciences of the United States of America* 98, 4782–4787.

Loqué D, Lalonde S, Looger LL, von Wirén N, Frommer WB (2007) A cytosolic *trans*-activation domain essential for ammonium uptake. *Nature* 446, 195–198.

Long C, Iino M (2001) Light-dependent osmoregulation in pea stem protoplasts. photoreceptors, tissue specificity, ion relationships, and physiological implications. *Plant Physiology* 125, 1854–1869.

Luo GZ, Wang HW, Huang J, Tian AG, Wang YJ, Zhang JS, Chen SY (2005) A putative plasma membrane cation/proton antiporter from soybean confers salt tolerance in *Arabidopsis*. *Plant Molecular Biology* 59, 809–820.

Lv QD, Tang RJ, Liu H, Gao XS, Li YZ, Zheng HQ, Zhang HX (2009) Cloning and molecular analyses of the *Arabidopsis thaliana* chloride channel gene family. *Plant Science* 176, 650–661.

Ma JF, Ryan PR, Delhaize E (2001) Aluminium tolerance in plants and the complexing role of organic acids. *Trends in Plant Science* 6, 273–278.

Ma Y, Szostkiewicz I, Korte A, Moes D, Yang Y, Christmann A, Grill E (2009) Regulators of PP2C phosphatase activity function as abscisic acid sensors. *Science* 324, 1064–1068.

Maas EV (1986) Physiological responses to chloride. *In:* Jackson TL, ed. Special Bulletin on Chloride and Crop Production. Atlanta. GA. 4-20.

Maas EV (1993) Salinity and citriculture. *Tree Physiology* 12, 195–216.

Maathuis FJM, Amtmann A (1999) K^+ nutrition and Na^+ toxicity: the basis of cellular K^+/Na^+ ratios. *Annals of Botany* 84, 123–133.

MacRobbie EA (1998) Signal transduction and ion channels in guard cells. *Philosophical Transactions of the Royal Society of London. Series B: Biological Sciences* 353, 1475–1488.

MacRobbie EAC (2000) ABA activates multiple Ca^{2+} fluxes in stomatal guard cells, triggering vacuolar $K^+(Rb^+)$ release. *Proceedings of the National Academy of Sciences of the United States of America* 97, 12361–12368.

MacRobbie EAC, Lettau J (1980) Ion content and aperture in 'isolated' guard cells of *Commelina communis* L. *The Journal of Membrane Biology* 53, 199–205.

Maierhofer T, Diekmann M, Offenborn JN, Lind C, Bauer H, Hashimoto K, Al-Rasheid KAS, Luan S, Kudla J, Geiger D, Hedrich R (2014a) Site- and kinase-specific phosphorylation-mediate activation of SLAC1, a guard cell anion channel stimulated by abcisic acid. *Science Signaling* 7, ra86.

Maierhofer T, Lind C, Hüttl S, Scherzer S, Papenfuß M, Simon J, Al-Rasheid KAS, Ache P, Rennenberg H, Hedrich R, Müller TD, Geiger D (2014b) A single-pore residue renders the *Arabidopsis* root anion channel SLAH2 highly nitrate selective. *Plant Cell* 26, 2554–2567.

Marin IC, Loef I, Bartetzko L, Searle I, Coupland G, Stitt M, Osuna D (2011) Nitrate regulates floral induction in *Arabidopsis*, acting independently of light, gibberellin and autonomous pathways. *Planta* 233, 539–552.

Marmagne A, Vinauger-Douard M, Monachello D, de Longevialle AF, Charon C, Allot M, Rappaport F, Wollman FA, Barbier-Brygoo H, Ephritikhine G (2007) Two members of the *Arabidopsis* CLC (chloride channel) family, AtCLCe and AtCLCf, are associated with thylakoid and Golgi membranes, respectively. *Journal of Experimental Botany* 58, 3385–3393.

Marschner H (1995) Mineral nutrition of higher plants, 2nd edn. London. Academic Press. London.

Marten H, Konrad KR, Dietrich P, Roelfsema MR, Hedrich R (2007) Ca^{2+}-dependent and -independent abscisic acid activation of plasma membrane anion channels in guard cells of *Nicotiana tabacum. Plant Physiology* 143, 28–37.

Martinoia E, Maeshima M, Neuhaus HE (2007) Vacuolar transporters and their essential role in plant metabolism. *Journal of Experimental Botany* 58, 83–102.

Martinoia E, Meyer S, De Angeli A, Nagy R (2012) Vacuolar transporters in their physiological context. *Annual Review of Plant Biology* 63, 183–213.

McAdam SA, Sussmilch FC, Brodribb TJ (2016) Stomatal responses to vapour pressure deficit are regulated by high speed gene expression in angiosperms. *Plant, Cell & Environment* 39, 485–491.

McAdam SAM, Brodribb TJ (2015) The evolution of mechanisms driving the stomatal response to vapour pressure deficit. *Plant Physiology* 167, 833–843.

Medici A, Krouk G (2014) The primary nitrate response: a multifaceted signalling pathway. *Journal of Experimental Botany* 65, 5567–5576.

Meinhard M, Grill E (2001) Hydrogen peroxide is a regulator of ABI1, a protein phosphatase 2C from *Arabidopsis*. *FEBS Letters* 508, 443–446.

Meinhard M, Rodriguez PL, Grill E (2002) The sensitivity of ABI2 to hydrogen peroxide links the abscisic acid-response regulator to redox signalling. *Planta* 214, 775–782.

Meyer S, Mumm P, Imes D, Endler A, Weder B, Al-Rasheid KAS, Geiger D, Marten I, Martinoia E, Hedrich R (2010) AtALMT12 represents an R-type anion channel required for stomatal movement in *Arabidopsis* guard cells. *The Plant Journal* 63, 1054–1062.

Meyer S, Schloz-Starke J, De Angeli A, Kovermann P, Burla B, Gambale F, Martinoia E (2011) Malate transport by the vacuolar AtALMT6 channel in guard cells is subject to multiple regulation. *The Plant Journal* 67, 247–257.

Mickelbart MV, Arpaia ML (2002) Rootstock influences changes in ion concentrations, growth, and photosynthesis of "Hass" avocado trees in response to salinity. *Journal of the American Society for Horticultural Science* 127, 649–655.

Miller AJ, Fan X, Orsel M, Smith SJ, Wells DM (2007) Nitrate transport and signalling. *Journal of Experimental Botany*, 58, 2297–2306.

Mishra G, Zhang W, Deng F, Zhao J, Wang X (2006) A bifurcating pathway directs abscisic acid effects on stomatal closure and opening in *Arabidopsis*. *Science* 312, 264–266.

Miyazono K, Miyakawa T, Sawano Y, Kubota K, Kang HJ, Asano A, Miyauchi Y, Takahashi M, Zhi Y, Fujita Y, Yoshida T, Kodaira KS, Yamaguchi-Shinozaki K, Tanokura M (2009) Structural basis of abscisic acid signalling. *Nature* 462, 609–614.

Møller IS, Tester M (2007) Salinity tolerance of *Arabidopsis*: a good model for cereals? *Trends in Plant Science* 12, 534–540.

Moran N (2007) Osmoregulation of leaf motor cells. *FEBS Letters* 581, 2337–2347.

Mori IC, Murata Y, Yang Y, Munemasa S, Wang YF, Andreoli S, Tiriac H, Alonso JM, Harper JF, Ecker JR, Kwak JM, Schroeder JI (2006) CDPKs CPK6 and CPK3 function in ABA regulation of guard cell S-type anion- and Ca^{2+}-permeable channels and stomatal closure. *PLOS Biology* 4, e327.

Moya JL, Tadeo FR, Gómez-Cadenas A, Primo-Millo E, Talon M (2002) Transmissible salt tolerance traits identified through reciprocal grafts between sensitive Carrizo and tolerant Cleopatra citrus genotypes. *Journal of Plant Physiology* 159, 991–998.

Moya JL, Gómez-Cadenas A, Primo-Millo E, Talon, M (2003) Chloride absorption in saltsensitive Carrizo citrange and salt tolerant Cleopatra mandarin citrus rootstocks is linked to water use. *Journal of Experimental Botany*, 54, 825–833.

Munns R (2002) Comparative physiology of salt and water stress. *Plant, Cell & Environment* 25, 239–250.

Munns R, James, RA Läuchli A (2006) Approaches to increasing the salt tolerance of wheat and other cereals. *Journal of Experimental Botany* 57, 1025–1043.

Munns R, James RA, Xu B, Athman A, Conn SJ, Jordans C, Byrt CS, Hare RA, Tyerman SD, Tester M, Plett D, Gilliham M (2012) Wheat grain yield on saline soils is improved by an ancestral Na^+ transporter gene. *Nature biotechnology* 30, 360–364.

Munns R, Tester M (2008) Mechanisms of salinity tolerance. *Annual Review of Plant Biology* 59, 651–681.

Murashige T, Skoog F (1962) A revised medium for rapid growth and bio assays with tobacco tissue cultures. *Physiologia Plantarum* 15, 473–497.

Murata Y, Pei ZM, Mori IC, Schroeder J (2001) Abscisic acid activation of plasma membrane Ca^{2+} channels in guard cells requires cytosolic NAD(P)H and is differentially disrupted upstream and downstream of reactive oxygen species production in abi1–1 and abi2–1 protein phosphatase 2C mutants. *Plant Cell* 13, 2513–2523.

Nazoa P, Videmar J, Tranbarger TJ, Mouline K, Damiani I, Tillard P, Glass ADM, Touraine B (2003) Regulation of the nitrate transporter gene *AtNRT2.1* in *Arabidopsis* thaliana, responses to nitrate, amino acids, and developmental stage. *Plant Molecular Biology* 52, 689–703.

Negi J, Matsuda O, Nagasawa T, Oba Y, Takahashi H, Kawai-Yamada M, Uchimiya H, Hashimoto M, Iba K (2008) CO_2 regulator SLAC1 and its homologues are essential for anion homeostasis in plant cells. *Nature* 452, 483–486.

Neill SJ, Desikan R, Hancock JT (2003) Nitric oxide signalling in plants. *New Phytologist* 159, 11–35.

Nguyen CT, Agorio A, Jossier M, Depré S, Thomine S, Filleur S (2016) Characterization of the chloride channel-like, AtCLCg, involved in chloride tolerance in *Arabidopsis* thaliana. *Plant and Cell Physiology* 57, 764–775.

Nishimura N, Hitomi K, Arvai AS, Rambo RP, Hitomi C, Cutler SR, Schroeder JI, Getzoff ED (2009) Structural mechanism of abscisic acid binding and signaling by dimeric PYR1. *Science* 326, 1373–1379.

Nishimura N, Sarkeshik A, Nito K, Park SY, Wang A, Carvalho PC, Lee S, Caddell D, Cutler SR, Chory J, Yates JR, Schroeder JI (2010) PYR/PYL/RCAR family members are major in-vivo ABI1 protein phosphatase 2C-interacting proteins in *Arabidopsis*. *The Plant Journal* 61, 290–299.

Noguero M, Lacombe B (2016) Transporters Involved in Root Nitrate Uptake and Sensing by *Arabidopsis. Frontiers in Plant Science* 7, 1391.

Nomura H, Komori T, Kobori M, Nakahira Y, Shiina T (2008) Evidence for chloroplast control of external Ca^{2+}-induced cytosolic Ca^{2+} transients and stomatal closure. *The Plant Journal* 53, 988–998.

Nørholm MH (2010) A mutant Pfu DNA polymerase designed for advanced uracil-excision DNA engineering. *BMC Biotechnology* 10, 21.

Nørholm MHH, Nour-Eldin HH, Brodersen P, Mundy J, Halkier BA (2006) Expression of the *Arabidopsis* high-affinity hexose transporter STP13 correlates with programmed cell death. *FEBS Lett*ers 580, 2381–2387.

Nour-Eldin HH, Hansen BG, Nørholm MH, Jensen JK, Halkier BA (2006) Advancing uracil-excision based cloning towards an ideal technique for cloning PCR fragments. *Nucleic Acids Research* 34, e122.

Oparka KJ, Turgeon R (1999) Sieve elements and companion cells—Traffic control centers of the phloem. *Plant Cell* 11, 739–750.

Orsel M, Chopin F, Leleu O, Smith SJ, Krapp A, Daniel-Vedele F, Miller T (2006) Characterization of a two-component high-affinity nitrate uptake system in *Arabidopsis*. Physiology and protein-protein interaction. *Plant Physiology* 142, 1304–1317.

Orsel M, Eulenburg K, Krapp A, Daniel-Vedele F (2004) Disruption of the nitrate transporter genes *AtNRT2.1* and *AtNRT2*.2 restricts growth at low external nitrate concentration. *Planta* 219, 714–721.

Orsel M, Filleur S, Fraisier V, Daniel-Vedele F (2002) Nitrate transport in plants: Which gene and which control? *Journal of Experimental Botany* 53, 825–833.

Ozanne PG, Woolley JT, Broyer TC (1957) Chloride and bromine in the nutrition of higher plants. *Australian Journal of Biological Science* 10, 66–79.

Pandey S, Zhang W, Assmann SM (2007) Roles of ion channels and transporters in guard cell signal transduction. *FEBS Lett*ers 581, 2325–2336.

Pardo JM (2010) Biotechnology of water and salinity stress tolerance. *Current Opinion in Biotechnology* 21, 185–196.

Park KY, Jung JY, Park J, Hwang JU, Kim YW, Hwang I, Lee Y (2003) A role for phosphatidylinositol 3-phosphate in abscisic acid-induced reactive oxygen species generation in guard cells. *Plant Physiology* 132, 92–98.

Park SY, Fung P, Nishimura N, Jensen DR, Fujii H, Zhao Y, Lumba S, Santiago J, Rodrigues A, Chow TF, Alfred SE, Bonetta D, Finkelstein R, Provart NJ, Desveaux D, Rodriguez PL, McCourt P, Zhu JK, Schroeder JI, Volkman BF, Cutler SR (2009) Abscisic acid inhibits type 2C protein phosphatases via the PYR/PYL family of START proteins. *Science* 324, 1068–1071.

Parker MB, Gascho GJ, Gaines TP (1983) Chloride toxicity of soybeans grown on Atlantic coast flatwoods soils. *Agronomy Journal* 75, 439–443.

Parker MB, Gaines TP, Gascho GJ (1985) Chloride effects on corn. *Communications in Soil Science and Plant Analysis* 16, 1319–1333.

Peel AJ, Rogers S (1982) Stimulation of sugar loading into sieve elements of willow by potassium and sodium salts. *Planta* 154, 94–96.

Peña-Cortés H, Fisahn J, Willmitzer L (1995) Signals involved in wound-induced proteinase inhibitor II gene expression in tomato and potato plants *Proceedings of the National Academy of Sciences of the United States of America* 92, 4106–4113.

Pilot G, Lacombe B, Gaymard F, Cherel I, Boucherez J, Thibaud JB, Sentenac H (2001) Guard cell inward K^+ channel activity in *Arabidopsis* involves expression of the twin channel subunits KAT1 and KAT2. *Journal of Biological Chemistry* 276, 3215–3221.

Patrick JW (1997) Phloem unloading: Sieve element unloading and post-sieve element transport. *Annual Review of Plant Physiology and Plant Molecular Biology* 48, 191–222.

Pei ZM, Ward JM, Harper JF, Schroeder JI (1996) A novel chloride channel in *Vicia faba* guard cell vacuoles activated by the serine/threonine kinase, CDPK. *EMBO Journal* 15, 6564– 6574.

Pei ZM, Murata Y, Benning G, Thomine S, Klusener B, Allen GJ, Grill E, Schroeder JI (2000) Calcium channels activated by hydrogen peroxide mediate abscisic acid signalling in guard cells. *Nature* 406, 731–734.

Peiter E (2011) The plant vacuole: emitter and receiver of calcium signals. *Cell Calcium* 50, 120–128.

Philippar K, Fuchs I, Lüthen H, Hoth S, Bauer CS, Haga K, Thiel G, Ljung K, Sandberg G, Böttger M, Becker D, Hedrich R (1999) Auxin-induced K^+ channel expression represents an essential step in coleoptile growth and gravitropism. *Proceedings of the National Academy of Sciences* 96, 12186–12191.

Pitman MG (1969) Simulation of Cl^- uptake by low-salt barley roots as a test of models of salt uptake. *Plant Physiology* 44, 1417–1427.

Pitman MG (1977) Ion transport into the xylem. *Annual Review of Plant Physiology* 28, 71–88.

Pitman MG (1982) Transport across plant roots. *Quarterly Reviews of Biophysics* 15, 481–554.

Pitman M, Luttge U, Lauchli A, Ball E (1974) Effect of previous water stress on ion uptake and transport in barley seedlings. *Functional Plant Biology* 1, 377–385.

Pitman MG, Wellfare D (1978) Inhibition of ion transport in excised barley roots by abscisic acid; relation to water permeability of the roots. *Journal of Experimental Botany* 29, 1123–1138.

Plant PJ, Gelli A, Blumwald E (1994) Vacuolar chloride regulation of an anion-selective tonoplast channel. *Journal of Membrane Biology* 140, 1–12.

Poffenroth M, Green DB, Tallman G (1992) Sugar concentrations in guard cells of *Vicia faba* illuminated with red or blue Light: analysis by high performance liquid chromatography. *Plant Physiology* 98, 1460–1471.

Ranf S, Wunnenberg P, Lee J, Becker D, Dunkel M, Hedrich R, Scheel D, Dietrich P (2008) Loss of the vacuolar cation channel, AtTPC1, does not impair Ca^{2+} signals induced by abiotic and biotic stresses. *The Plant Journal* 53, 287-299.

Raschkle K (1987) Action of abcisic acid on guard cells. *In*: Farquhar GD, Zeiger E, Cowan IR, eds. Stomatal Function. Stanford University Press. Stanford, CA. 253–279.

Raschke K, Shabahang M, Wolf R (2003) The slow and the quick anion conductance in whole guard cells: their voltage- dependent alternation, and the modulation of their activities by abscisic acid and CO_2. *Planta* 217, 639–650.

Raven JA (2017) Chloride: essential micronutrient and multifunctional beneficial ion. *Journal of Experimental Botany* 68, 359–367.

Reintanz B, Szyroki A, Ivashikina N, Ache P, Godde M, Becker D, Palme K, Hedrich R (2002) AtKC1, a silent *Arabidopsis* potassium channel α-subunit modulates root hair K^+ influx. *Proceedings of the National Academy of Sciences* 99, 4079–4084.

Remans T, Nacry P, Pervent M, Filleur S, Diatloff E, Mounier E, Tillard P, Forde BG, Gojon A (2006) The *Arabidopsis* NRT1.1 transporter participates in the signaling pathway triggering root colonization of nitrate-rich patches. *Proceedings of the National Academy of Sciences of the United States of America* 103, 19206–19211.

Rengasamy P (2010) Soil processes affecting crop production in salt-affected soils. *Functional Plant Biology* 37, 613–620.

Reyes JL, Chua NH (2007) ABA induction of miR159 controls transcript levels of two MYB factors during *Arabidopsis* seed germination. *The Plant Journal* 49, 592–606.

Roberts SK (1998) Regulation of K^+ channels in maize roots by water stress and abscisic acid. *Plant Physiology* 116, 145–153.

Roberts SK, Snowman BN (2000) The effects of ABA on channel-mediated K^+ transport across higher plant roots. *Journal of Experimental Botany* 51, 1585–1594.

Roberts SK (2006) Plasma membrane anion channels in higher plants and their putative functions in roots. *New Phytologist* 169, 647–666.

Roelfsema MR, Hedrich R (2005) In the light of stomatal opening: New insights into 'the Watergate'. *New Phytologist* 167, 665–691.

Roelfsema MRG, Hedrich R, Geiger D (2012) Anion channels: master switches of stress responses. *Trends in Plant Science* 17, 221–229.

Roelfsema MR, Levchenko V, Hedrich R (2004) ABA depolarizes guard cells in intact plants, through a transient activation of R- and S-type anion channels. *The Plant Journal* 37, 578–588.

Roelfsema MRG, Levchenko V, Hedrich R (2004) ABA depolarizes guard cells in intact plants, through a transient activation of R- and S-type anion channels. *The Plant Journal* 37, 578–588.

Romero MF, Kanai Y, Gunshin H Hediger MA (1998) Expression cloning using *Xenopus laevis* oocytes. *Methods in Enzymology* 296, 17–52.

Romero-Aranda R, Moya JL, Tadeo FR, Legaz F, Primo-Millo E, Talon M (1998) Physiological and anatomical disturbances induced by chloride salts in sensitive and tolerant citrus: beneficial and detrimental effects of cations. *Plant, Cell & Environment* 21, 1243–1253.

Roy SJ, Negrão S, Tester M (2014) Salt resistant crop plants. *Current Opinion Biotechnology* 26, 115–124.

Rozen S, Skaletsky H (2000) Primer3 on the WWW for general users and for biologist programmers. *Methods in Molecular Biology* 132, 365–386.

Ruffel S, Gojon A, Lejay L (2014) Signal interactions in the regulation of root nitrate uptake. *Journal of Experimental Botany* 65, 5509–5517.

Ruffel S, Krouk G, Ristova D, Shasha D, Birnbaum KD, Coruzzi GM (2011) Nitrogen economics of root foraging: transitive closure of the nitrate-cytokinin relay and distinct systemic signaling for N supply vs. demand. *Proceedings of the National Academy of Sciences of the United States of America* 108, 18524–18529.

Ruffel S, Poitout A, Krouk G, Coruzzi GM, Lacombe B (2016) Long-distance nitrate signaling displays cytokinin dependent and independent branches. *Journal of Integrative Plant Biology* 58, 226–229.

Ryan PR, Skerrett M, Findlay GP, Delhaize E, Tyerman SD (1997) Aluminum activates an anion channel in the apical cells of wheat roots. *Proceedings of the National Academy of Sciences of the United States of America* 94, 6547–6552.

Saab IN, Sharp RE, Pritchard J, Voetberg G (1990) Increased endogenous abscisic acid maintains primary root growth and inhibits shoot growth of maize seedlings at low water potentials. *Plant Physiology* 93, 1329–1336.

Saji S, Bathula S, Kubo A, Tamaoki M, Kanna M, Aono M, Nakajima N, Nakaji T, Takeda T, Asayama M, Saji H (2008) Disruption of a gene encoding C4-dicarboxylate transporter-like protein increases ozone sensitivity through deregulation of the stomatal response in *Arabidopsis thaliana*. *Plant and Cell Physiology* 49, 2–10.

Saez A, Apostolova N, González-Guzmán M, González-García MP, Nicolas C, Lorenzo O, Rodriguez PL (2004) Gain-of-function and loss-of-function phenotypes of the protein phosphatase 2C HAB1 reveal its role as a negative regulator of abscisic acid signalling. *The Plant Journal* 37, 354–369.

Saez, A. Robert N, Maktabi MH, Schroeder JI, Serrano R, Rodriguez PL (2006) Enhancement of abscisic acid sensitivity and reduction of water consumption in *Arabidopsis* by combined inactivation of the protein phosphatases type 2C ABI1 and HAB1. *Plant Physiology*. 141, 1389–1399.

Salon C, Avice JC, Larmure A, Ourry A, Prudent M, Voisin AS (2011) Plant N fluxes and nodulation by nitrogen, heat and water stresses: A review based on comparison of legumes and non legume plants. *In*: Shanker AK, Venkateswarlu BB, eds. Abiotic stress in plants. Mechanisms and adaptations. 79–118.

Sanders D (1980) The mechanism of Cl^- transport at the plasma membrane of *Chara corallina*. 1. Cotransport with H^+. *Journal of Membrane Biology* 53, 129–141.

Santiago J, Dupeux F, Round A, Antoni R, Park SY, Jamin M, Cutler SR, Rodriguez PL, Marquez JA (2009) The abscisic acid receptor PYR1 in complex with abscisic acid. *Nature* 462, 665–668.

Sano T, Becker D, Ivashikina N, Wegner LH, Zimmermann U, Roelfsema MRG, Nagata T, Hedrich R (2007) Plant cells must pass a K^+ threshold to re-enter the cell cycle. *The Plant Journal* 50, 401–413.

Sasaki T, Mori IC, Furuichi T, Munemasa S, Toyooka K, Matsuoka K, Murata Y, Yamamoto Y (2010) Closing plant stomata requires a homolog of an aluminum-activated malate transporter. *Plant Cell Physiology* 51, 354–365.

Sasaki T, Yamamoto Y, Ezaki B, Katsuhara M, Ahn SJ, Ryan PR, Delhaize E, Matsumoto H (2004) A wheat gene encoding an aluminium-activated malate transporter. *The Plant Journal* 37, 645–653.

Sato A, Sato Y, Fukao Y, Fujiwara M, Umezawa T, Shinozaki K, Hibi T, Taniguchi M, Miyake H, Goto DB, Uozumi N (2009) Threonine at position 306 of the KAT1 potassium channel is essential for channel activity and is a target site for ABA-activated SnRK2/OST1/SnRK2.6 protein kinase. *Biochemical Journal* 424, 439–448.

Sauter A, Davies WJ, Hartung W (2001) The long-distance abscisic acid signal in the droughted plant: the fate of the hormone on its way from root to shoot. *Journal of Experimental Botany* 52, 1991–1997.

Schachtman DP, Tyerman SD, Terry BR (1991) The K^+/Na^+ selectivity of a cation channel in the plasma-membrane of root-cells does not differ in salt-tolerant and salt-sensitive wheat species. *Plant Physiology* 97, 598–605.

Scherzer S, Maierhofer T, Al-Rasheid KAS, Geiger D, Hedrich R (2012) Multiple calcium-dependent kinases modulate ABA-activated guard cell anion Channels. *Molecular Plant* 5, 1409–1412.

Schmidt C, Schroeder JI (1994) Anion-selectivity of slow anion channels in *Vicia faba* guard cells: large nitrate permeability. *Plant Physiology* 106, 383-391.

Schroeder JI, Schmidt C, Sheaffer J (1993) Identification of high-affinity slow anion channel blockers and evidence for stomatal regulation by slow anion channels in guard-cells. *Plant Cell* 5, 1831–1841.

Schroeder J (1995) Anion channels as central mechanisms for signal transduction in guard cells and putative functions in roots for plant-soil interactions. *Plant Molecular Biology* 28, 353–361.

Schroeder JI, Allen GJ, Hugouvieux V, Kwak JM, Waner D. (2001**a**) Guard cell signal transduction. *Annual Review of Plant Physiology and Plant Molecular Biology* 52, 627–658.

Schroeder JI, Hagiwara S (1989) Cytosolic calcium regulates ion channels in the plasma membrane of *Vicia faba* guard cells. *Nature* 338, 427–430.

Schroeder JI, Keller BU (1992) Two types of anion channel currents in guard cells with distinct voltage regulation. *Proceedings of the National Academy of Sciences of the United States of America* 89, 5025–5029.

Schroeder JI, Kwak JM, Allen GJ (2001**b**) Guard cell abscisic acid signalling and engineering drought hardiness in plants. *Nature* 410, 327–330.

Schweighofer A, Hirt H, Meskiene I (2004) Plant PP2C phosphatases: emerging functions in stress signaling. *Trends in Plant Science*. 9, 236–243.

Schwenke GD, Simpfendorfer SR, Collard BCY (2015) Confirmation of chloride deficiency as the cause of leaf spotting in durum wheat grown in the Australian northern grains regions. *Crop and Pasture Science* 66, 122–134.

Segonzac C, Boyer JC, Ipotesi E, Szponarski W, Tillard P, Touraine B, Sommerer N, Rossignol M, Gibrat R (2007) Nitrate efflux at the root plasma membrane: identification of an *Arabidopsis* excretion transporter. *Plant Cell* 19, 3760–3777.

Shabala SN, Lew RR (2002) Turgor regulation in osmotically stressed *Arabidopsis* epidermal root cells. Direct support for the role of inorganic ion uptake as revealed by concurrent flux and cell turgor measurements. *Plant Physiology* 129, 290–299.

Sharp RE, Davies WJ (1979) Solute regulation and growth by roots and shoots in water-stressed maize plants. *Planta* 147, 43–49.

Shi H, Quintero FJ, Pardo JM, Zhu JK (2002) The putative plasma membrane Na^+/H^+ antiporter SOS1 controls long-distance Na^+ transport in plants. *The Plant Cell* 14, 465–477.

Shi H, Zhu JK (2002) Regulation of expression of the vacuolar Na^+/H^+ antiporter gene AtNHX1 by salt stress and abscisic acid. *Plant Molecular Biology* 50, 543–550.

Shimazaki K, Doi M, Assmann SM, Kinoshita T (2007) Light regulation of stomatal movement. *Annu Rev Plant Biol* 58, 219–247.

Shimazaki K, Iino M, Zeiger E (1986) Blue light-dependent proton extrusion by guard-cell protoplasts of *Vicia faba*. *Nature* 319, 324–326.

Silberbush M, Lips SH (1991) Potassium, nitrogen, ammonium/nitrate ratio, and sodium chloride effects on wheat growth. I. Shoot and root growth and mineral composition. *Journal of Plant Nutrition* 14, 751–764.

Sigel E (1990) Use of *Xenopus* oocytes for the functional expression of plasma membrane proteins. *The Journal of Membrane Biology* 117, 201–221.

Sirichandra C, Gu D, Ju HC, Davanture M, Lee S, Djaoui M, Valot B, Zivy M, Leung J, Merlot S, Kwak JM (2009) Phosphorilation of the *Arabidopsis* AtrbohF NADPH oxidase by OST1 protein kinase. *FEBS Letters* 583, 2982–2986.

Sjölund RD (1997) The phloem sieve element: a river runs through it. *Plant Cell* 9, 1137–1114.

Skerrett M, Tyerman SD (1994) A channel that allows inwardly directed fluxes of anions in protoplasts derived from wheat roots. *Planta* 192, 295–305.

Smart T G, Krishek BJ (1995) *Xenopus* oocyte microinjection and ion-channel expression. *Patch-Clamp Applications and Protocols*, 259–305.

Smith FA (1973) The internal control of nitrate uptake into excised barley roots with differing salt contents. *New Phytologist* 72, 769–782.

Smith GS, Clark CJ, Holland PT (1987) Chlorine requirement of kiwifruit (*Actinidia deliciosa*). *New Phytologist* 106, 71–80.

Smith JAC, Milburn JA (1980) Osmoregulation and the control of phloem-sap composition in *Ricinus communis* L. *Planta* 148, 28–34.

Somerville CR, Ogren, WL (1982) Mutants of the cruciferous plant *Arabidopsis thaliana* lacking glycine decarboxylase activity. *Biochemical Journal* 202, 373–380.

Stael S, Wurzinger B, Mair A, Mehlmer N, Vothknecht UC, Teige M (2012) Plant organellar calcium signalling: an emerging field. *Journal of Experimental Botany* 63, 1525–1242.

Staxen I, Pical C, Montgomery LT, Gray JE, Hetherington AM, McAinsh MR(1999) Abscisic acid induces oscillations in guard-cell cytosolic free calcium that involve phosphoinositide-specific phospholipase C. *Proceedings of the National Academy of Sciences of the United States of America* 96, 1779–1784.

Storey R, Walker RR (1999) Citrus and salinity. *Scientia Horticulturae* 78, 39–81.

Sunarpi, Horie T, Motoda J, Kubo M, Yang H, Yoda K, Horie R, Chan WY, Leung HY, Hattori K, Konomi M, Osumi M, Yamagami M, Schroeder JI, Uozumi N (2005) Enhanced salt tolerance mediated by AtHKT1 transporter-induced Na^+ unloading from xylem vessels to xylem parenchyma cells. *The Plant Journal* 44, 928–938.

Tadeo F, Cercos M, Colmenero-Flores JM, Iglesias DJ, Naranjo MA, Ríos G, Carrera E, Ruiz-Rivero O, Lliso I, Morillon R, Ollitrault P, Talon M (2008) Molecular physiology of development and quality of citrus. *Advances in Botanical Research: Incorporating Advances in Plant Pathology* 47, 147–223.

Takahashi H, Watanabe-Takahashi A, Smith FW, Blake-Kalff M, Hawkesford MJ, Saito K (2000) The roles of three functional sulphate transporters involved in uptake and translocation of sulphate in *Arabidopsis thaliana*. *The Plant Journal* 23, 171–182.

Taiz L, Zeiger E (2002) Plant physiology, 3rd ed. Sinauer Associates Inc., Sunderland, MA.

Takahashi S, Katagiri T, Hirayama T, Yamaguchi-Shinozaki K, Shinozaki K (2001) Hyperosmotic stress induces a rapid and transient increase in inositol 1, 4, 5-trisphosphate independent of abscisic acid in *Arabidopsis* cell culture. *Plant and Cell Physiology* 42, 214–222.

Talbott LD, Zeiger E (1998) The role of sucrose in guard cell osmoregulation. *Journal of Experimental Botany* 49, 329–337.

Tang RH, Han S, Zheng H, Cook CW, Choi CS, Woerner TE, Jackson RB, Pei ZM (2007) Coupling diurnal cytosolic Ca^{2+} oscillations to the CAS-IP_3 pathway in *Arabidopsis*. *Science* 315, 1423–1426.

Taochy C, Gaillard I, Ipotesi E, Oomen R, Leonhardt N, Zimmermann S, Peltier JB, Szponarski W, Simonneau T, Sentenac H, Gibrat R, Boyes JC (2015) The *Arabidopsis* root stele transporter NPF2.3 contributes to nitrate translocation to shoots under salt stress. *The Plant Journal* 83, 466–479.

Tardieu F, Davies WJ (1993) Integration of hydraulic and chemical signalling in the control of stomatal conductance and water status of droughted plants. *Plant, Cell & Environment* 16, 341–349.

Teakle NL, Tyerman SD (2010) Mechanisms of Cl^- transport contributing to salt tolerance. *Plant, Cell & Environment* 33, 566–589.

Teale WD, Paponov IA, Palme K (2006) Auxin in action: signalling, transport and the control of plant growth and development. *Nature Reviews Molecular Cell Biology 7*, 847–859.

Teardo E, Frare E, Segalla A, De Marco V, Giacometti GM, Szabo I (2005) Localization of a putative ClC chloride channel in spinach chloroplasts. *FEBS Letters* 579, 4991–4996.

Tester M, Davenport R (2003) Na^+ tolerance and Na^+ transport in higher plants. *Annals of Botany* 91, 503–527.

Theodoulou FL, Miller AJ (1995) *Xenopus* oocytes as a heterologous expression system for plant proteins. *Molecular Biotechnology* 3, 101–115.

Touraine B, Glass ADM (1997) NO_3^- and ClO_3^- fluxes in the *chl1-5* mutant of *Arabidopsis thaliana*: Does the *CHL1-5* gene encode a low-affinity NO_3^- transporter? *Plant Physiology* 114, 137–144.

Tregeagle JM, Tisdall JM, Tester M, Walker RR (2010) Cl^- uptake, transport and accumulation in grapevine rootstocks of differing capacity for Cl^- exclusion. *Functional Plant Biology* 37, 665–673.

Tsay YF, Chiu CC, Tsai CB, Ho CH, Hsu PK (2007) Nitrate transporters and peptide transporters. *FEBS Letters* 581, 2290–2300.

Tsay YF, Schroeder JI, Feldmann KA Crawford NM (1993) A herbicide sensitivity gene *CHL1* of *Arabidopsis* encodes a nitrate-inducible nitrate transporter. *Cell* 72, 705–713.

Tyerman SD, Findlay GP (1989) Current-voltage curves of single Cl^- channels which coexist with two types of K^+ channel in the tonoplast of *Chara corallina*. *Journal of Experimental Botany* 40, 105–117.

Ueno K, Kinoshita T, Inoue, S, Emi T, Shimazaki K (2005) Biochemical characterization of plasma membrane H^+-ATPase activation in guard cell protoplasts of *Arabidopsis thaliana* in response to blue light. *Plant and Cell Physiology* 46, 955–963.

Umezawa T, Sugiyama N, Mizoguchi M, Hayashi S, Myouga F, Yamaguchi-Shinozaki K, Ishihama Y, Hirayama T, Shinozaki K (2009) Type 2C protein phosphatases directly regulate abscisic acid-activated protein kinases in *Arabidopsis*. *Proceedings of the National Academy of Sciences of the United States of America* 106, 17588–17593.

Uno Y, Furihata T, Abe H, Yoshida R, Shinozaki K, Yamaguchi-Shinozaki K (2000) *Arabidopsis* basic leucine zipper transcription factors involved in an abscisic acid-dependent signal transduction pathway under drought and high-salinity conditions. *Proceedings of the National Academy of Sciences of the United States of America* 97, 11632–11637.

Uozumi, N, Nakamura T, Schroeder JI, Muto S (1998) Determination of transmembrane topology of an inward-rectifying potassium channel from *Arabidopsis thaliana* based on functional expression in *Escherichia coli. Proceedings of the National Academy of Sciences of the United States of America* 95, 9773–9778.

Vahisalu T, Kollist H, Wang YF, Nishimura N, Chan WY, Valerio G, Lamminmäki A, Brosché M, Moldau H, Desikan R, Schroeder JI, Kangasjarvi J (2008) SLAC1 is required for plant guard cell S-type anion channel function in stomatal signalling. *Nature* 452, 487–491.

Van Bel AJE (2003) The phloem, a miracle of ingenuity. *Plant, Cell & Environment* 26, 125–149.

Van der Weele CM, Spollen WG, Sharp RE, Baskin TI (2000) Growth of *Arabidopsis thaliana* seedlings under water deficit studied by control of water potential in nutrient-agar media. *Journal of Experimental Botany* 51, 1555–1562.

Van Kirk CA, Raschke K (1978) Presence of chloride reduces malate production in epidermis during stomatal opening. *Plant Physiology* 61, 361–364.

Vidal EA, Moyano TC, Canales J, Gutierrez RA (2014) Nitrogen control of developmental phase transitions in *Arabidopsis thaliana*. *Journal of Experimental Botany* 65, 5611–5618.

Vlad F, Rubio S, Rodrigues A, Sirichandra C, Belin C, Robert N, Leung J, Rodriguez PL, Laurière C, Merlot S (2009) Protein phosphatases 2C regulate the activation of the Snf1-related kinase OST1 by abscisic acid in *Arabidopsis*. *Plant Cell* 21, 3170–3184

Von der Fecht-Bartenbach J, Bogner M, Krebs M, Stierhof YD, Schumacher K, Ludewig U (2007) Function of the anion transporter *AtCLC-d* in the *trans*-Golgi network. *The Plant Journal* 50, 466–474.

Von der Fecht-Bartenbach J, Bogner M, Dynowski M, Ludewig U (2010) CLC-b mediated NO_3^-/H^+ exchange across the tonoplast of *Arabidopsis* vacuoles. *Plant Cell Physiology* 51, 960–968.

Walch-Liu P, Liu LH, Remans T, Tester M, Forde BG (2006) Evidence that L-glutamate can act as an exogenous signal to modulate root growth and branching in *Arabidopsis thaliana*. *Plant and Cell Physilogy* 47, 1045–1057.

Walker RR, Torokfalvy E, Downton WJS (1982) Photosynthetic responses of the citrus varieties Rangpur lime and Ertog citron to salt treatment. *Australian Journal of Plant Physiology* 9, 783–790.

Wang Y, He L, Li HD, Xu J, Wu WH (2010) Potassium channel α-subunit AtKC1 negatively regulates AKT1-mediated K^+ uptake in *Arabidopsis* roots under low-K^+ stress. *Cell Research* 20, 826-837.

Wang R, Guegler K, LaBrie ST, Crawford NM (2000) Genomic analysis of a nutrient response in *Arabidopsis* reveals diverse expression patterns and novel metabolic and potential regulatory genes induced by nitrate. *Plant Cell* 12, 1491–1510.

Wang R, Tischner R, Gutierrez RA, Hoffman M, Xing X, Chen M, Coruzzi G, Crawford NM (2004) Genomic analysis of the nitrate response using a nitrate reductase-null mutant of *Arabidopsis*. *Plant Physiology* 136, 2512–2522.

Wang R, Okamoto M, Xing X, Crawford NM (2003) Microarray analysis of the nitrate response in *Arabidopsis* roots and shoots reveals over 1,000 rapidly responding genes and new linkages to glucose, trehalose-6-phosphate, iron, and sulfate metabolism. *Plant Physiology* 132, 556–567.

Wang YF, Zhang A, Ren HM, Tan YQ, Qi GN, Yao FY, Wu GL, Yang LW, Hussain J, Sun SJ (2016) S-type anion channels SLAC1 and SLAH3 function as essential negativer regulators of inward K^+ Channels and stomatal opening in *Arabidopsis*. *The Plant Cell* 28, 949–965.

Wang YY, Hsu PK, Tsay YF (2012) Uptake, allocation and signaling of nitrate. *Trends in Plant Science* 17, 458–467.

Wang YY, Tsay YF (2011) *Arabidopsis* nitrate transporter NRT1.9 is important in phloem nitrate transport. *The Plant Cell* 23, 1945–1957.

Wang Y, Wu WH (2013) Potassium transport and signaling in higher plants. *Annual Review of Plant Biology* 64, 451–476.

Ward JM, Pei ZM, Schroeder JI (1995) Roles of ion channels in initiation of signal transduction in higher plants. *Plant Cell* 7, 833–844.

Ward JM, Schroeder JI (1994) Calcium-activated K^+ channels and calcium-induced calcium release by slow vacuolar ion channels in guard cell vacuoles implicated in the control of stomatal closure. *Plant Cell* 6, 669–683.

Weber AP, Linka N (2011) Connecting the plastid: transporters of the plastid envelope and their role in linking plastidial with cytosolic metabolism. *Annu Rev Plant Biol* 62, 53–77.

Weber WM (1999) Ion currents of *Xenopus laevis* oocytes: state of the art. *Biochimica et Biophysica Acta* 1421, 213–133.

Wege S, De Angeli A, Droillard MJ, Kroniewicz L, Merlot S, Cornu D, Gambale F, Martinoia E, Barbier-Brygoo H, Thomine S, Leonhardt N, Filleur S (2014) Phosphorylation of the vacuolar anion exchanger AtCLCa is required for the stomatal response to abscisic acid. *Science Signaling* 7, ra65.

Wege S, Gilliham M, Henderson SW (2017) Chloride: not simply a 'cheap osmoticum', but a beneficial plant macronutrient. *Journal of Experimental Botany*, doi:10.1093/jxb/erx050.

Wege S, Jossier M, Filleur S, Thomine S, Barbier-Brygoo H, Gambale F, De Angeli A (2010) The proline 160 in the selectivity filter of the *Arabidopsis* NO_3^-/H^+ exchanger AtCLCa is essential for nitrate accumulation in planta. *The Plant Journal* 63, 861–869.

Wei SQ, Zhou ZF, Liu C (1989) Effects of chloride on yield and quality of lettuce and its critical value of tolerance. *Chinese Journal of Soil Science* 30, 262–264.

White PJ, Broadley MR (2001) Chloride in soils and its uptake and movement within the plant: a review. *Annals of Botany* 88, 967–988.

Whitehead, DC (1985) Chlorine deficiency in red-clover grown in solution culture. *Journal of Plant Nutrition* 8, 193–198.

Wiesman, Z. (1995) Rootstock and nitrate involvement in Ettinger avocado response to chloride stress. *Scientia Horticulturae* 62, 33–43.

Wilkinson S, Bacon MA, Davies WJ (2007) Nitrate signalling to stomata and growing leaves: interactions with soil drying, ABA, and xylem sap pH in maize. *Journal of Experimental Botany* 58, 1705–1716.

Wilkinson S, Davies WJ (2002) ABA-based chemical signalling: the co-ordination of responses to stress in plants. *Plant, Cell & Environment* 25, 195–210.

Wille AC, Lucas WJ (1984) Ultrastructural and histochemical studies on guard cells. *Planta* 160, 129–142.

Xu G, Magen H, Tarchitzky J, Kafkafi U (2000) Advances in chloride nutrition of plants. *In*: Sparks D, ed. Advances in Agronomy 68. Academic Press. Amsterdam. 96–150.

Xu G, Fan X, Miller AJ (2012) Plant nitrogen assimilation and use efficiency. *Annual Review of Plant Biology* 63, 153–182.

Xu H, Martinoia E, Szabo I (2015) Organellar channels and transporters. *Cell Calcium* 58, 1–10.

Xu J, Li HD, Chen LQ, Wang Y, Liu LL, He L, Wu W (2006) A protein kinase, interacting with two calcineurin B–like proteins, regulates K^+ transporter AKT1 in *Arabidopsis*. *Cell* 125, 1347–60.

Yamagami M, Haga K, Napier RM, Iino M (2004) Two distinct signaling pathways participate in auxin-induced swelling of pea epidermal protoplasts. *Plant Physiology* 134, 735–747.

Yamashita A, Singh SK, Kawate T, Jin Y, Gouaux E (2005) Crystal structure of a bacterial homologue of Na^+/Cl^--dependent neurotransmitter transporters. *Nature* 437, 215–223.

Yancey PH (2005) Organic osmolytes as compatible, metabolic and counteracting cytoprotectants in high osmolarity and other stresses. *Journal of Experimental Biology* 208, 2819–2830.

Yin P, Fan H, Hao Q, Yuan XQ, Wu D, Pang YX, Yan CY, Li WQ, Wang JW, Yan N (2009) Structural insights into the mechanism of abscisic acid signaling by PYL proteins. *Nature Structural & Molecular Biology* 16, 1230–1236.

Yokosho K, Yamaji N, Ueno D, Mitani N, Ma JF (2009) OsFRDL1 is a citrate transporter required for efficient translocation of iron in rice. *Plant Physiology* 149, 297–305.

Zabala MDG (1984) Evaluation of chloride as a tool for studying nitrate assimilation in plants. *Dissertation Abstract International* 44, 2619.

Zampese E, Pizzo P (2012) Intracellular organelles in the saga of Ca2+ homeostasis: different molecules for different purposes? *Cellular and Molecular Life Sciences* 69, 1077–1104.

Zhang A, Jiang M, Zhang J, Tan M, Hu X (2006) Mitogen-activated protein kinase is involved in abscisic acid- induced antioxidant defense and acts downstream of reactive oxygen species production in leaves of maize plants. *Plant Physiology* 141, 475–487.

Zhang J (2013) Functional and structural characterization of the vacuolar anion channels *At*ALMT9 and *At*ALMT4 in *Arabidopsis thaliana*. Dissertation. Mathematical and natural sciences faculty, Zürich University, Switzerland, 136 pp.

Zhang J, Schurr U, Davies WJ (1987) Control of stomatal behaviour by abscisic acid which apparently originates in the roots. *Journal of experimental botany* 38, 1174–1181.

Zhang W, Qin C., Zhao J, Wang X (2004) Phospholipase D1-derived phosphatidic acid interacts with ABI1 phosphatase 2C and regulates abscisic acid signaling. *Proceedings of the National Academy of Sciences of the United States of America* 101, 9508–9513.

Zhao J, Wang X (2004) *Arabidopsis* phospholipase Dα1 interacts with the heterotrimeric G-protein a-subunit through a motif analogous to the DRY motif in G-protein-coupled receptors. *Journal of Biological Chemistry* 279, 1794–1800.

Zheng Z, He K, Kleist T, Chen F, Luan S (2015) Anion channel SLAH3 functions in nitrate-dependet alleviation of ammonium toxicity in *Arabidopsis*. *Plant, Cell & Environment* 38, 474–486.

Zhou BK, Zhang XY (1992) Effects of chloride on growth and development of sugar beet. *Soil Fertile* 3, 41–43.

Zhou M, Morais-Cabral JH, Mann S, MacKinnon R (2001) Potassium channel receptor site for the inactivation gate and quaternary amine inhibitors. *Nature* 411, 657–661.

Zhou Y, Morais-Cabral JH, Kaufman A, MacKinnon R (2001) Chemistry of ion coordination and hydration revealed by a K^+ channel–Fab complex at 2.0 Å resolution. *Nature* 414, 43–48.

Zhu JK (2001) Plant salt tolerance. *Trends in Plant Science* 6, 66–71.

Zhu JK(2002) Salt and drought stress signal transduction in plants. *Annual Review of Plant Biology* 53, 247–273.

Zifarelli G, Pusch M (2010) CLC transport proteins in plants. *FEBS Letters* 584, 2122–2127.

Zonia L, Cordeiro S, Tupý J, Feijó JA (2002) Oscillatory chloride efflux at the pollen tube apex has a role in growth and cell volume regulation and is targeted by inositol 3, 4, 5, 6-tetrakisphosphate. *The Plant Cell* 14, 2233–2249.